



HAL
open science

Evaluation of time-series SAR and optical images for the study of winter land-use

Julien Denize

► **To cite this version:**

Julien Denize. Evaluation of time-series SAR and optical images for the study of winter land-use. Electronics. Université de Rennes, 2019. English. NNT : 2019REN1S062 . tel-02510333

HAL Id: tel-02510333

<https://theses.hal.science/tel-02510333>

Submitted on 17 Mar 2020

HAL is a multi-disciplinary open access archive for the deposit and dissemination of scientific research documents, whether they are published or not. The documents may come from teaching and research institutions in France or abroad, or from public or private research centers.

L'archive ouverte pluridisciplinaire **HAL**, est destinée au dépôt et à la diffusion de documents scientifiques de niveau recherche, publiés ou non, émanant des établissements d'enseignement et de recherche français ou étrangers, des laboratoires publics ou privés.

THESE DE DOCTORAT DE

L'UNIVERSITE DE RENNES 1
COMUE UNIVERSITE BRETAGNE LOIRE

ECOLE DOCTORALE N° 601
*Mathématiques et Sciences et Technologies
de l'Information et de la Communication*

Spécialité : *Signal Image Vision & Géomatique*

Par

Julien Denize

**Evaluation of time-series SAR and optical images for the study of
winter land-use**

Thèse présentée et soutenue à Rennes, le 13 Novembre 2019

Unité de recherche : IETR

Thèse N° : -

Rapporteurs avant soutenance :

Nicolas Baghdadi	Directeur de Recherche, IRSTEA - UMR TETIS
Mehrez Zribi	Directeur de Recherche, CESBIO - UMR CNRS 5126

Composition du Jury :

Examineurs :	Jean-Louis Roujean	Directeur de Recherche, CESBIO - UMR CNRS 5126
	Julie Betbeder	Chargée de Recherche au CIRAD - Unité Forêts et Sociétés
	Thomas Corpetti	Directeur de Recherche, LETG - UMR CNRS 6554
	Laurent Ferro-Famil	Professeur, Université de Rennes 1, IETR - UMR CNRS 6164
Dir. de thèse :	Eric Pottier	Professeur, Université de Rennes 1, IETR - UMR CNRS 6164
Co-dir. de thèse :	Laurence Hubert-Moy	Professeure, Université de Rennes 2, LETG - UMR CNRS 6554

Invité(s)

Jacques Baudry	Directeur de Recherche, INRA - UMR BAGAP
----------------	--

Acknowledgements

L'aboutissement de ces trois années de thèse est pour moi une satisfaction immense que ce soit pour les connaissances et la détermination que j'ai pu acquérir afin de poursuivre mon parcours dans cette voie mais également pour toutes les personnes que j'ai pu côtoyé et sans qui de près ou de loin cette thèse n'aurait pas aboutie.

Avant tout, je tiens à adresser mes remerciements à mes directeurs de thèse, Éric Pottier et Laurence Hubert-Moy. Je les remercie de m'avoir donné l'opportunité de réaliser cette thèse, de l'avoir encadrée dans toutes les circonstances et de m'avoir soutenu pendant ces trois années. Éric un grand merci tout d'abord de m'avoir choisi pour cette première bourse de thèse après plusieurs années. Je suis sincèrement reconnaissant pour votre constante sympathie, votre présence, les conseils et les connaissances que vous avez pu m'apporter sur ma thèse et à côté durant ces trois années. Laurence, je tiens à vous remercier d'avoir accepté de co-encadrer cette thèse. Un grand merci également pour tous les conseils, les connaissances, la rigueur scientifiques et les valeurs que vous avez pu me transmettre pendant ces années de thèse. Je remercie également Jacques Baudry, directeur de recherche à l'INRA, pour le temps qu'il a investi pour me transmettre ces connaissances agronomiques mais également pour le temps passé sur le terrain. J'y associe Julie Betbeder, Chercheuse au CIRAD et ancienne post-doctorante du LETG sans qui mes travaux de thèse et les campagnes terrain n'aurait pas été les mêmes, un grand merci pour la bonne humeur, le temps investi et les conseils prodigués.

Je remercie Mehrez Zribi, Nicolas Baghdadi, Jean-Louis Roujean, Julie Betbeder, Thomas Corpetti, Laurent Ferro-Famil et Jacques Baudry d'avoir accepté de participer à mon jury de thèse et d'évaluer mon travail.

Durant mon parcours universitaire, certaines personnes mon permis d'avancer et d'orienter mes choix et décisions effectués jusqu'à ce jour permettant à l'étudiant de devenir un jeune chercheur. C'est pourquoi je tiens à remercier trois personnes en particulier. Samuel Corgne, sans qui rien cette thèse ne serait arrivée, un grand merci pour votre pédagogie à tout épreuve qui m'a fait découvrir et aimer la télédétection, traçant ainsi mon parcours. Un grand merci également d'avoir pensé à moi pour effectuer dès le master 1 un superbe stage à la Réunion puis une nouvelle fois lors de ce projet de thèse. Thibault Catry, maître de stage lors de ma première année de master, m'ayant transmis une partie de sa connaissance dans le domaine de la télédétection radar, m'apportant l'envie de poursuivre et d'effectuer des recherches dans cette voie, pour cela un grand merci. Pierre Todoroff, mon tuteur de stage lors de ma première et deuxième année de master, il n'est cessé de motivé et de me transmettre ses connaissances pour continuer d'en la voie que j'avais entrepris, merci à lui et aux membres de son équipe au CIRAD l'a Réunion pour leurs connaissances et leur joie de vivre.

Je tiens à remercier fortement Jean Nabucet, Ingénieur-docteur au LETG, pour tous ces conseils, ta bonne humeur et les heures passées sur le terrain et les chantiers qui m'ont permis de me changer les idées et oublier la thèse l'espace de quelques heures. J'y associe Charlotte Vincent pour son soutien sans faille avant, pendant et surement après la thèse, les heures passées derrière un appareil ou sur un chantier à se vider la tête et oublier les problèmes, les soirées inoubliables ... Un grand merci.

Je remercie également, Thomas Houet pour ses conseils, sa bonne humeur parfois tranchante mais également les nombreuses sorties terrain et les chantiers toujours aussi sympa. Damien Arvor pour ses précieux conseils en R et sa bonne humeur sans faille en soirée. J'y associe Antoine Lefebvre ancien membre du LETG dont les conseils passés et futurs mon permis et me permettront d'avancer.

Un grand merci à mes collègues de bureau passés et actuels, pour leur aide, leur conseil et leur humeur sans qui je n'aurais réussi à finir cette thèse. Merci à Perrine, Adeline, Véronique, Amit et Thibault sans qui le bureau des gens cools n'aurait pas été aussi cool. Mais aussi à Fanny, Audrey et Florent pour cette dernière passée à vos côtés. Petit dédicace à Audrey dont les idées éclairées m'ont permis d'avancer, #Style word, #Bocage.

Je n'oublie pas l'ensemble des collègues et amis actuels ou passés, doctorants, contractuels, stagiaires sans qui les journées au laboratoire et les soirées autour d'un verre aurait été interminables. Merci à Carole, Enzo, Marianne, Solen, Renan, Edwige, Igor, Gwen, Emilien, Alexandre, Damien, Clémence, Elodie, Jeanne. Un grand merci à eux pour leur sympathie, gentillesse, professionnalisme lorsqu'il le faut et leur soutien sans faille pendant les derniers mois. Avec une dédicace toute particulière à Pauline et Xavier dont les enseignements en tant qu'étudiant de Licence puis leurs conseils avisés lors de mon parcours professionnel qui m'ont permis d'avancer un peu plus dans le monde de la recherche. Mais aussi à Arthur et Olivier collègues et amis du LETG dont nos soirées mémorables resteront à jamais gravées !

Merci aussi aux stagiaires : Marianne Balaesque (L3 Physique-Chimie), Napo N'Bohn (M2 Géographie et télédétection), Maxime Dubrul (M2 Telenvie) ; Et à Jean-Luc Roger (Assistant Ingénieur à l'IRA) pour le passer temps et le soutien durant les campagnes terrain. Merci également à Guy Grunfelder et Paul Leroy de l'INSA et l'IETR sans qui les campagnes terrain n'aurait pu avoir lieu.

Je tiens à remercier tout le personnel administratif de l'IETR et du LETG qui prennent en charge des formalités toujours plus contraignantes et chronophages. Un merci tout particulier pour Noëlle Le Ber pour sa bonne humeur, sa gentillesse et le temps accordé à mes démarches administratives. J'y associe les membres du LETG qui de près ou de loin ont su faire avancer mes travaux de thèse. Merci à Hervé, Alban, Solène, Adeline C., Simon, Anne-Julia, Vincent...

Puis, un grand merci à mes parents, ma famille (Morgane, Wesley, Mathieu, Aurélie) pour leur soutien infaillible, leur affection et les nombreuses heures à rigoles durant ces trois années qui m'ont permis d'avancer sans encombre. Mais également à tous mes amis. Je commencerais évidemment par Alan et Alex avec les voyages de l'Irlande à l'Allemagne en passant par la Pologne m'ont permis de rencontrer des gens formidables, de voir des paysages inoubliables et de m'évader pendant plusieurs jours. Je remercierais également Maël et Clément pour leur aide et leur bonne humeur de la deuxième année du master à aujourd'hui et ceux malgré la distance qui nous séparent. Il est important pour moi de remercier aussi Alan, Mathilde, Valentin, Gaëtan, Anaïs, Thomas, Marion, Enora, William, Adelaïde, avec qui les nombreuses soirées passées à Vitré ou en Mayenne m'ont permis de me changer les idées et de faire des rencontres toujours plus plaisantes. Je tiens également à remercier l'ensemble des membres de mon association sportive qui pendant deux ans m'a permis de me défouler et d'oublier l'espace de quelques heures mes travaux de thèse.

Enfin, je n'ai pas assez de mots pour remercier Mathilde d'avoir été à mes côtés pendant cette troisième année de thèse, me permettant d'avancer et d'oublier les problèmes et déboires afin d'arriver au bout de cette thèse.

Acronyms

AIS	Areas of Ecological Interest
ALOS	Advanced Land Observing Satellite
CAP	Common Agricultural PolicyERS
CESBIO	Centre d'Etudes Spatiales de la BIOsphère
CIPAN	Culture Intermédiaire Pièges A Nitrates
CIRAD	Centre de coopération Internationale en Recherche Agronomique pour le Développement
CNES	Centre National d'Etudes Spatiales
CNRS	National Centre for Scientific Research
Db	Decibels
DN	Digital Number
DTW	Dynamic Time Wrapping
EPSG	European Petroleum Survey Group
ESA	European Space Agency
FAPAR	Fraction of photosynthetically active radiation
Fcover	Fractional vegetation cover
FEDER	Fonds Européen de DEveloppement Régional
GAEC	Good Agricultural and Environmental Conditions
GIS Bretel	Groupement Bretagne Télédétection
IETR	Institut d'Electronique et de Télécommunication de Rennes
IGN	National Institute for Geographic and Forest Information
ILTER	International Long Term Ecological Research Network
INRA	Institut National de Recherche Agronomique
JAXA	Japanese Space Agency
LAI	Leaf Area Index
LETG	Littoral - Environnement - Télédétection - Géomatique
LTER	Long Term Ecological Research Network

LULC	Land Use and Land Cover
MAJA	MACCS ATCOR Joint Algorithm
Maxlike	Maximum Likelihood Classification
MDA	MacDonald, Dettwiler, and Associates
MESR	Ministry of Higher Education and Research of France
MIR	Mid-infrared
MODIS	Moderate Resolution Imaging Spectroradiometer
NAP	National action program
NASA	National Aeronautics and Space Administration
NDVI	Normalized Difference Vegetation Index
NDWI	Normalized difference water index
NIR	Near-infrared
OA	Overall Accuracy
PALSAR	Phased Array L-band Synthetic Aperture Radar
PCA	Principal Component Analysis
RADAR	RAdio Detection And Ranging
RF	Random Forest
RGA	Raygrass Anglais
RGB	Red Green Blue
RGE	Référentiel géographique à Grande Échelle
RGF	Réseau Géodésique Français
RGI	Raygrass Italien
RPG	Registre Parcellaire Graphique
RVI	RADAR Vegetation Index
SAR	Synthetic Aperture RADAR
SAVI	Soil Adjusted Vegetation Index
SE	Shannon Entropy
SE_i	Shannon Entropy Intensity

SE_p	Shannon Entropy Polarized
SLC	Single Look Complex
SNAP	Sentinel Application Platform
SPOT	Satellite Pour l'Observation de la Terre
SRTM	Shuttle Radar Topography Mission
SVM	Support Vector Machine
SWIR	ShortWave InfraRed
TWDTW	Time-Weighted Dynamic Time Wrapping
UAA	Utile Agricultural Area
UMR	Unité Mixte de Recherche
UTM	Universal Transverse Mercator
VHSR	Very high spatial resolution
ZAA	Zone Atelier Armorique

Table of contents

GENERAL INTRODUCTION	1
PART 1: WINTER LAND-USE: CONCEPTS, DATA AND METHODS	7
INTRODUCTION OF THE FIRST PART	9
CHAPTER 1: WINTER LAND-USE	11
I.1. INTRODUCTION	13
I.2. THEMATIC FRAMEWORK	13
I.3. LEGAL MEASURES	15
I.4. FUNCTION AND INTEGRATION OF WINTER LAND-USE IN THE AGRICULTURAL LANDSCAPE	21
CHAPTER 2: SPATIAL REMOTE SENSING FOR THE STUDY OF WINTER LAND-USE	25
II.1. INTRODUCTION	27
II.2. CHARACTERISTICS OF REMOTE SENSING DATA	27
II.3. IDENTIFICATION AND CHARACTERIZATION OF WINTER LAND-USE USING REMOTE SENSING DATA	45
CHAPTER 3: STUDY SITES AND DATA	49
III.1. INTRODUCTION	51
III.2. STUDY SITES	51
III.3. REMOTE SENSING DATA	55
III.4. FIELD MEASUREMENTS	61
CHAPTER 4: METHODOLOGICAL PROCEDURE	67
IV.1. INTRODUCTION	69
IV.2. FIRST AXIS: DETERMINATION OF AN EFFICIENT CLASSIFICATION PROCEDURE FOR THE IDENTIFICATION AND CHARACTERIZATION OF WINTER LAND-USE AT A LOCAL SCALE	71

IV.3. SECOND AXIS: POLARIMETRIC SAR TIME-SERIES FOR WINTER LAND-USE IDENTIFICATION	78
IV.4. THIRD AXIS: IDENTIFICATION OF WINTER LAND-USE AT A REGIONAL SCALE	78
CONCLUSION OF THE FIRST PART	81
PART 2: CLASSIFICATION PROCEDURE FOR THE WINTER LAND-USE STUDY AT A LOCAL SCALE	85
INTRODUCTION OF THE SECOND PART	87
CHAPTER 5: DETERMINATION OF THE MOST EFFICIENT CLASSIFICATION PROCEDURE AND SENTINEL TIME-SERIES FOR THE STUDY OF WINTER LAND-USE	89
V.1. INTRODUCTION	91
V.2. STUDY SITE AND DATA	93
V.3. METHODS	96
V.4. RESULTS AND DISCUSSION	102
V.5. CONCLUSIONS	120
CONCLUSION OF THE SECOND PART	125
PART 3: SAR CONFIGURATION FOR THE STUDY OF WINTER LAND-USE AT A LOCAL SCALE	127
INTRODUCTION OF PART THREE	129
CHAPTER 6: IDENTIFICATION OF WINTER LAND-USE USING POLARIMETRIC SAR TIME-SERIES	131
VI.1. INTRODUCTION	134
VI.2. MATERIALS AND METHODS	136
VI.3. RESULTS	144
VI.4. DISCUSSION	152
VI.5. CONCLUSIONS	154
CONCLUSION OF THE THIRD PART	161
PART 4: THE STUDY OF WINTER LAND-USE AT A REGIONAL SCALE	163
INTRODUCTION OF THE FOURTH PART	165
CHAPTER 7: IDENTIFICATION OF WINTER LAND-USE AT A REGIONAL SCALE	167
VII.1. INTRODUCTION	170
VII.2. STUDY SITE AND DATA	171

VII.3. METHODOLOGY	174
VII.4. RESULTS AND DISCUSSION	176
VII.6. CONCLUSIONS	181
CONCLUSION OF THE FOURTH PART	185
GENERAL CONCLUSION AND PERSPECTIVES	187
REFERENCES	193
RÉSUMÉ ÉTENDU	249

General introduction

Agricultural land currently occupies more than a third of the world's land and is expected to feed more than 8.5 billion people by 2030. Faced with the constant increase in the world's population and in the context of global warming, one of the major challenges of this century lies in our ability to produce enough food in a sustainable manner, while preserving natural resources and limiting the pressures exerted by our societies on the environment. In this context, many scientific studies have shown the negative impacts of intensification and changes in land use (increase in monoculture, removal of hedgerows, development of the use of inputs such as nitrogen, pesticides and phosphorus, etc.) on the environment through the observation of degradation of water, soil, air quality and population health (Lambin and Meyfroidt, 2011; Newbold et al., 2015). This is particularly visible in regions such as Brittany where intensive agriculture dominates, and where changes in agricultural practices, landscape fragmentation, and land-use changes that have occurred over the past several decades have led to profound environmental disruptions. To mitigate these impacts, national and local European legislation and programs were developed from the 1990s onwards, leading to the implementation of spatial planning operations and actions to change agricultural practices. Thus, a new series of environmental measures was initiated in the early 2000s by the European authorities requiring the presence of vegetation cover and seeding of catch crops during the winter period, which is crucial for the transfer of pollutant flows ("Nitrates Directive," 2019).

Monitoring vegetation cover in winter is a major environmental and scientific challenge in agricultural areas. From an environmental perspective, the presence and type of vegetation cover in winter influences the transport of pollutants to watercourses by reducing the loss of nitrates, nutrients, pesticides or sediment from agricultural fields (Galloway et al., 2008; Withers et al., 2014). The lack of vegetation cover acts as an accelerator when soils are stripped after a main crop (maize, rapeseed, etc.), while catch crops act as an obstacle to flow and material transfers (Dabney, 1998). In this context, the identification and characterization of winter land-use is a major component of restoring water quality and sustainable management in agricultural landscapes (Corgne, 2004).

However, knowledge of the spatio-temporal dynamics associated with winter land-use remains a challenge for the scientific community today. Indeed, from a methodological point of view, the characterization of the spatio-temporal dynamics of land use and land cover (LULC) at the scale of the agricultural plot is difficult because of the diversity of agricultural strategies and practices in winter. Identifying winter land-use remains a major scientific challenge for the remote sensing community.

In this context, spatial remote sensing has emerged as a key tool for setting up methods land-for use monitoring on large areas. In the early 2000s, a number of scientific studies showed the value of optical remote sensing with medium spatial resolution (from 250 m to 1 km) to meet this challenge. The works of Clark et al., (2010) and Zhang et al., (2003) have thus made it possible to develop the first methods of discrimination of large crop units on large areas. Nevertheless, the limits of these medium-resolution optical sensors were quickly reached to study land use during the winter period, particularly in areas where the plots are small, with only patches dominated by bare soils being identified (Lecerf et al., 2005). Subsequently, very high resolution optical spatial remote sensing data were evaluated to perform annual land-use mapping integrating winter crops. However, the limitation of this type of data lies in the small number of images that can be used during the winter period during which cloud cover may be frequent (Guerschman et al., 2015; Lillesand et al., 2015; Xu and Guo, 2014). In this context, active spatial remote sensing makes it possible to remove this constraint insofar as it makes it possible to avoid meteorological, atmospheric and lighting conditions. The development, over the past twenty years, of SAR sensors such as Radarsat-2, which allow the acquisition of denser time-series with high spatial resolution, has confirmed their interest in identifying and characterizing land use in the winter period. Jiao et al., (2010); McNairn et al., (2001) and Skriver, (2011) have thus highlighted the value of these data for land-use classification through the use of dielectric properties of soil, surface roughness, and land cover structure. The launch of the Sentinel-1 and -2 SAR and optical satellites from 2014-2015 onwards opens up new possibilities for studying winter land-use. Thus, Belgiu and Csillik, (2018) and Vuolo et al., (2018) demonstrated the potential of Sentinel-2 images to map land use during the vegetative period. Bargiel, (2017) and Veloso et al., (2017) illustrated the value of Sentinel-1 data for the study and classification of annual crops. However, to date, very little research has demonstrated the value of SAR imagery in identifying and characterizing winter land-use, the main work done being to determine vegetation cover rates (Minh et al., 2018).

In this context, the main objective of this thesis was to evaluate high spatial resolution SAR and optical time-series to identify winter land use at local and regional scales. More precisely, it consists in developing methods using these time series to (1) determine the most suitable classification method to identify land use in winter, both at the level of the classifier itself and the classification approach (pixel or object-oriented); (2) compare Sentinel-1 SAR images and Sentinel-2 optics; and (3) define the most suitable SAR configuration by comparing three image time-series (Alos-2, Radarsat-2 and Sentinel-1).

To achieve this objective, a general approach divided into 5 parts has been implemented:

- ✓ The first part of this manuscript presents the thematic and methodological framework of this thesis in analysing first the challenges of winter land-use in intensive agricultural areas and their study, and, second, material and methods used in this thesis in exposing in details the study site, the data including field and remote sensing data and the methodology implemented.
- ✓ The second part of this thesis, based on the thematic and methodological framework carried out in the first part, is mainly focused on the determination of the most appropriate classification procedure for the identification and characterization of winter land-use. This approach includes the evaluation of several classification algorithms, the determination of an optimal nomenclature and the assessment of optical (Sentinel-2) and SAR (Sentinel-1) time-series potential for this study.
- ✓ The third part focuses on the evaluation of SAR imagery for the identification and fine characterization of winter land-use. It aims to determine the most appropriate SAR configuration for this purpose.
- ✓ Finally, the objective of the last part is to evaluate the reproducibility of the classification method selected for the identification and characterization of winter land-use. One of the objectives of this approach is to extend the classification method implemented at a local scale to a regional one.

1

Winter land-use: concepts, data and methods

Contents

INTRODUCTION OF THE FIRST PART	9
CHAPTER 1: WINTER LAND-USE	11
CHAPTER 2: SPATIAL REMOTE SENSING FOR THE STUDY OF WINTER LAND-USE	25
CHAPTER 3: STUDY SITES AND DATA	49
CHAPTER 4: METHODOLOGICAL PROCEDURE	67
CONCLUSION OF THE FIRST PART	81

Introduction of the first part

The first part of this manuscript presents the thematic and methodological framework of this thesis through the formalization of the issues related to the study of winter land-use in an intensive agricultural area and the approach required for its identification and characterization.

The objective of this part is to implement a reflection based on the scientific literature, to improve understanding of winter land-use concepts and associated practices but also to define the methodological decisions that will be implemented in order to identify and characterize this land use during the winter period.

In the first chapter, we will define the winter land-use concept. We also describe the elements of winter land-use in an agricultural landscape through an overview of legal measures implemented to regulate land-use during winter at the European scale. Finally, we will conclude this chapter with a part presenting the functional role of land use and its components.

In the second chapter, first, we will provide a review of the characteristics and benefits of optical and SAR spatial imagery. In a second step, we will present state-of-the-art of the data and methods used in the scientific literature to identify and characterize land-use during winter. In order to accomplish these objectives, we will concentrate more particularly on the identification and characterization of winter land-use classes using remote sensing data (optical, SAR and the fusion of both sources).

In the third chapter, we will present the study sites selected for this thesis. First, the Zone Atelier Armorique (ZAA) which is referenced in the ecology research networks (LTER and ILTER) as a privileged area ranging from a hedged agricultural landscape to an open field landscape, and secondly the Brittany region as an intensive agricultural area. Then we will describe the satellite data used during this thesis, the field data collected during these 3 years and the pre-processing applied to them.

Finally, in the fourth chapter, we will discuss about the general methodology developed for this thesis. We will discuss the implemented approaches, including optical and SAR remote sensing data, but also field data used in these methodological processes.

Chapter 1

Winter land-use

Contents

I.1. INTRODUCTION	13
I.2. THEMATIC FRAMEWORK	13
I.3. LEGAL MEASURES	15
I.4. FUNCTION AND INTEGRATION OF WINTER LAND-USE IN THE AGRICULTURAL LANDSCAPE	21

I.1. Introduction

In this chapter, we will first define the notions, concepts of land use and land cover in order to provide a framework for the thematic approach. Then we will focus on the winter land-use classes framed by European legal measures. Finally, we will present the functions and constraints of land use in biogeochemical and environmental processes globally and with a focus on the winter cover components.

I.2. Thematic framework

The agronomic function of soils was discovered less than 10,000 years ago by our prehistoric ancestors and was, until recently, with all plant and animal production, the only recognized function or service provided by the soil. Half a century ago, new definitions and functions of soil emerged. Its major involvement in the functioning of terrestrial biogeochemical cycles and ecosystems, the support of urbanization or land-use planning have made the soil, in collective imagery, essential and stable support for agronomic production, renewable resource production and the development of societies.

To optimize the use of these services and limit negative effects, the definition, and understanding of hazards and risks of physical, chemical and biological degradation in order to suggest sustainable soil protection and management measures have been a longstanding and crucial issue. More recently, the management of environmental, economic and soil policy issues have become a subject of concern and questioning at an international level to ensure the food security of a growing world population and to alleviate the ever-increasing environmental problems. In this context, the understanding of the transversal functions and processes affecting soils and their use is still a major challenge for several communities: scientific, decision-making and others (Girard et al., 2011). To achieve this understanding, it is essential to identify the main concepts such as land use and land cover as support for processes influencing soil dynamics. However, even today, a precise and explicit definition of these concepts is still complicated by the ensuing interactions and are therefore still the subject of divergence.

Land cover was frequently defined as the biophysical characteristics of a landscape or an environment (Meyer and Turner, 1992). However, new approaches have highlighted land cover as vegetation (natural or planted) or artificial constructions (buildings, etc.) on the ground surface. Water, ice, bare rock, sand, and other similar surfaces also count as land cover ("Michigan state university," 2019; US Department of Commerce, 2019). Conversely, land use has often been represented by several concepts defined according to a common denominator, the human factor's impact. For example, Brown and Duh, (2004) and Foley et al., (2005) define land use as human activity on land and their intention for land. Nevertheless, a new perspective has emerged from recent research that defines it as a set of land operations carried out by humans with the intention of obtaining products and/or benefits through the use of land resources ("Michigan state university," 2019; US Department of Commerce, 2019).

The diversity of definitions and concepts surrounding land use and land cover exists since several decades now bringing many confusions. In recent years, a significant number of studies have been carried out on this issue, highlighting the debates that have occurred regarding the designation and definition of these concepts, which remain inherently linked (Comber et al., 2005, 2003; Veldkamp and Verburg, 2004). Indeed, as Meyer and Turner (1992) have presented, the establishment of a relationship between both is an immediate cause of

change. Human activities (“land use”) modify directly the physical environment that is often described as “land cover”. These activities reflect human objectives shaped by underlying social drivers, which can change the land cover and lead to environmental consequences that can ultimately affect land use. In this context, it becomes difficult to consider only one narrow definition, as pointed out by Comber (2008), for whom the common approach to overcome this confusion is to transform land cover classes into land use, as shown in **Figure I.1** (Hu et al., 2016).

A method is then established in place to identify aspects of land use and land cover. For example, the economic and social value in urban contexts and food production in rural areas. Each class is scored in each dimension. The combination of scores determines the degree of land use or land cover. Thus, the approach separates the concepts of land cover and land use from the task at hand, and results show the degree of land use, land cover and the locations where the concepts of land use and land cover are confused (Comber, 2008). In other words, the definition of these two concepts is related to each person's perception in a specific context, according to their own approach. This means that both concepts may be used as long as a framework is established in order to define the subject of the developed thematic approach. **In this thesis, a thematic scoping defined winter "land use" as the object studied and as a sub-segment of winter agriculture a land-cover class.** Concept defined by legal measures establishing an institutional framework that we will present in the next section.

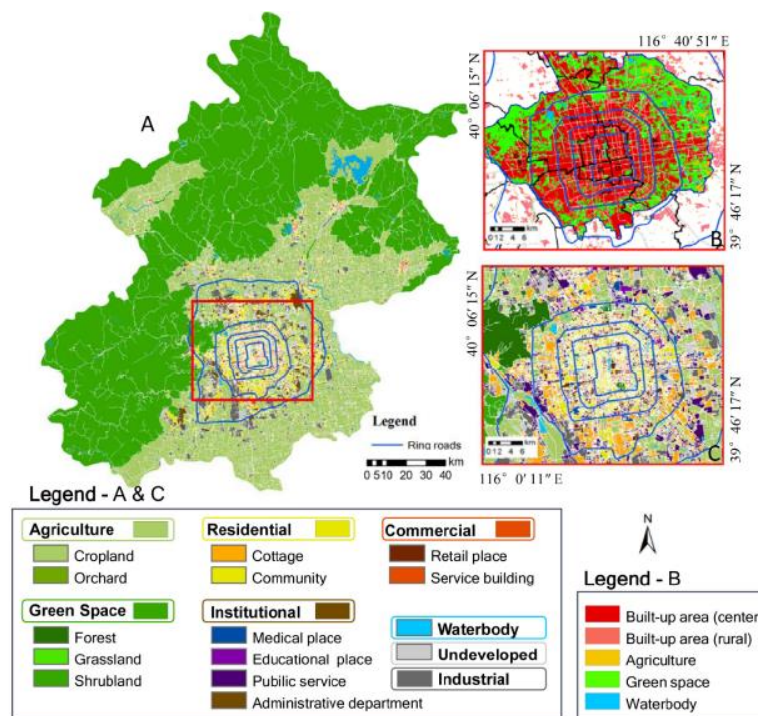


Figure I.1: Mapping demonstrating the confusion between land use and land cover (Hu et al., 2016).

I.3. Legal measures

Pressures related to land-use, whether environmental, economic or human, have always been major issues for the scientific community but also for decision-makers. From this perspectives, for decades many policies have been implemented to establish a legislative framework structuring land use. In this context, the policies relative to winter land-use are an important part of it. To meet these issues, since the early 1990s, national and international policies have been instituted to contextualize authorized land-use practices during the winter season. Two of these policies are now recognized as reference texts structuring winter land-use practices.

I.3.1. The European Directive 91/676/EEC

The European Directive 91/676/EEC, also known as the "Nitrates Directive", was introduced in December 1991 in response to non-compliance with the environmental standards set by Directive 75/440/EEC of 1975 on the quality required for surface waters used for drinking water production ("Nitrates Directive," 2019). This directive aims to supervise and organize the installation of winter land-use. In France, this directive is enshrined in legislation through two action programs.

- ✓ A national action program (NAP) that establishes the framework for all French vulnerable areas.
- ✓ Regional action programs (RAPs), which specify in a proportionate and adapted way for each territory, the additional measures and reinforcements necessary to achieve the objectives of improving water quality in relation to agricultural nitrate pollution.

To prevent pollution, five action programs of the "Nitrates Directive" were successively implemented between 1996 and 2018. These programs have established a set of measures in order to restore and/or preserve the quality of surface and ground waters in areas where the quality has been degraded. Since August 2018, a 6th action plan has been implemented. It takes up and extends the measures introduced in the previous action programs. One of the most important measures and the subject of this thesis, is the obligation to establish land use during winter season ("Nitrates Directive," 2019). This obligation has been intensified with the implementation of national and international policies "Areas of Ecological Interest (AIS)" resulting from the Common Agricultural Policy (CAP) and the nitrate directives, which require the establishment of vegetation covering during the critical period in order to prevent pollutant transfers to the environment. In an intensive agricultural region such as Brittany, it is reflected in the establishment of a four winter land-use categories:

I.3.1.1. Winter Crops

Considered as one of the winter land-use types, winter crops are main crops sown between October to November and harvested during the following summer (between June and July). This category includes winter wheat, winter barley, and rapeseed (**Fig. I.2**), which are the three predominant winter crops in the French agricultural system. These crops are harvested to provide grain and fodder for livestock.



Figure I.2: illustration of two types of winter crops. A) Winter wheat, B) Winter barley and C) Rapeseed.

I.3.1.2. Grasslands

Considered as a permanent cover with major importance in the preservation of the environment and biogeochemical processes, grasslands have been the subject of a large amount of research over the past decades. The term "grassland" is a concept with very contrasting realities (**Fig. I.3**), represented by a wide diversity of cover ranging according to the environments and human activities (Sanderson et al., 2009). To date, several categories have been used to describe grasslands in agricultural environments, the simplest of which was established in 1998 by the Central Service for Studies and Statistical Surveys of the Ministry of Agriculture, based on their botanical composition, their duration and their management method. This typology distinguishes three main categories of grasslands (Dusseux et al., 2014):

- ✓ Surfaces always grassy or permanent grasslands.
- ✓ Temporary grasslands that must be replaced every 5 years.
- ✓ Artificial grasslands.

Present on the field during a year without interruption, grasslands are considered to be the most suitable cover in order to reduce erosion and prevent pollutant transfers towards the environment. However, they remain an agricultural cover used for its forage quality with various management methods (such as grazing or mowing), with diverse impacts on the environment and biogeochemical cycles. Management variations and continuous presence all year round make grasslands a land-use class with a specific phenological profile that changes from each year and from each field (Gibson, 2009).



Figure I.3: Illustration of grassland types.

I.3.1.3. Catch crops

The concept of intercropping refers to several agricultural practices depending on the country. For most of them, intercropping is considered as the process of sow two or more crops at the same time in the same field. The most common purpose of intercropping is to achieve higher yield using resources that would not be used in a single crop (Ouma and Jeruto, 2010). In the French agricultural system, the concept of intercropping represents primarily the period between the harvest of the main crop and the sowing of the next. Its length depends on the harvest and sowing dates of the main crops, ranging from a few days to several months (up to 9 months) in the case of a spring crop ("INRA - Catch crops," 2012). During this period, an intermediate crop, also called "intercrop", was established, in order to provide ecosystem services (agronomic and ecological) through agro-ecological functions such as reducing runoff, erosion or leaching (transferring nitrates to the environment).

In the scope of the thesis, this winter land-use class will be mentioned under the name "catch crops" in order to avoid any confusion with the concept of intercropping that is highlighted in the scientific literature. We distinguish 2 types of "Catch crops":

- ✓ Catch crops no used (intermediate cultures nitrate trap, CIPAN in French, (Fig. I.4), present on the fields during the winter period only, they have for aim to stock nitrogen and to prevent leaching toward the environment. They are destroyed during the spring in order to sow the next main crop without specific valorization. However, they provide an agronomic value by facilitating tillage in particular. In the framework of the European Directive 91/676/CEE, a list of catch crops no used has been defined by European authorities to keep the most optimal varieties in order to prevent pollutant transfers (Table I.1).

Table I.1: Catch crops no use authorized during the winter season.

Crops	Frosty species
Oat	X
Bromine	
Garden cress	X
Orchard grass	
Fescue	
Timothy grass	
Moha	
Mustard	X
Fodder turnips	
Nyger	X
Rough bluegrass	
Phacelia	X
Fodder radish	X
Rye-grass	
Sorghum	X
Buckwheat	X
Rye	
Sunflower	X

**Figure I.4:** Illustration of catch crops no used. A) Phacelia; B) Mustard.

- ✓ Catch crops used (Dérobées in French, **Fig. I.5**), present on the fields during the winter period too, have for aim to prevent pollutant transfers and to provide a supplementary yield in a short time (forage). Contrary to the catch crops no used, they provide less effective protection against agricultural pollutant transfers due to the farming practices. In this land-use class, we find crops such as ryegrass or fodder cabbage.



Figure I.5: Illustration of catch crops used. A) Ryegrass; B) Fodder cabbage.

The establishment of catch crops has been made mandatory with the European Directive 91/676/CEE previously mentioned. It also determines the efficiency conditions of these covers, particularly in an intensive region such as Brittany, where nitrogen production per hectare between November 1st and March 1st is important. During this period, all sowing conditions must be performed in order to absorb nitrogen, to limit erosion and to prevent leaching towards water bodies (“Nitrates Directive,” 2019). To this end, it’s necessary to:

- ✓ Sow early, by sowing directly after harvest, the catch crop can develop to her maximum extent.
- ✓ Choose the crop species according to the previous main crop.
- ✓ Sow the catch crop properly, with prior tillage and adapted seeding.
- ✓ Adapt the destruction methods according to the crop species.

I.3.1.4. Crop residues and temporary bare soil

The two last winter land-use classes represent crop residues and temporary bare soils. The European Directive 91/676/CEE mentioned above, requires the establishment of winter land-use to prevent pollutant transfers. However, under certain conditions, farmers can leave the residues of the main crop (globally maize, **Fig. I.6**) in the field without sowing a catch crop. This practice is however regulated by strict conditions. First of all, it applies only to fields where the harvest was realized after the November 1st, i.e. mainly for maize crops. Then, soil cover can be obtained by finely grinding and burying the maize residues within 15 days of the harvest (“Nitrates Directive,” 2019).



Figure I.6: Illustration of a crop residues parcel.

Finally, to conclude the “legal measures” section, it is important to mention the bare soils, which is probably the most difficult class to determine. The definition of the term is still complicated, it refers to the soil without crops or vegetation cover. However, the main difficulty lies in determining the minimum length of time we can consider soil as a part bare soil class (i.e. long-term bare soil). During the winter period, there is still a moment when parcels can be categorized as bare soil from the end of the main crop harvest (Fig. I.7) until the emergence of a catch crop or a next main crop. However, the designation bare soil, as a class must be assigned when its presence persists over time and thus involves a risk to the environment. But today in an intensive agricultural region such as ZAA with high nitrate concentrations, the European Directive 91/676/EEC being restrictive, it remains difficult to find long-term bare soils except in some exceptions (“Nitrates Directive,” 2019). In this situation, European Directive 91/676/EEC requires these parcels to be declared before September 1st, through the elaboration of a document explaining the reasons for this non-coverage (*Appendix 1*). In this thesis, we first attempted to identify temporary bare soils as a winter land-use class (*Part 2*). However, the results showed that this class could not be considered and thus would be excluded in Part 3 to 5.



Figure I.7: Illustration of a temporary bare soil.

I.3.2. The rules of Good Agricultural and Environmental Conditions (GAEC)

The second European measure corresponds to the Good Agricultural and Environmental Conditions (GAEC) rules. They are part of a wider framework relating to the conditionality of subsidies granted by the CAP to farmers. This concept was introduced in 2003 by the reform of Council Regulation No 1782/2003 of the CAP. Under the new CAP 2015-2020, the rules of conditionality have been simplified, but not significantly modified. In this context, France has chosen to rationalize the conditionality requirements, especially with the implementation of the new green payment. Conditionality involves requirements relating to compliance with regulatory provisions in the environment, animal protection, animal production health, crop production health, and Good Agricultural and Environmental Conditions ("GAEC"), that the farmer must respect on the areas, animals and elements over which he has control ("GAEC," 2019). These rules, divided into 7 norms, stipulate the establishment of ecological interest areas maintained by farmers up to 5% of their arable land surface. These areas are divided into two groups, agricultural covers, and landscape elements, their functions are to limit pollutant transfer and preserve biodiversity by promoting the implementation of green corridors (*Appendix 2*). **In this thesis, we will focus on the fourth norm relating to the vegetative cover of soils in winter period whose primary objective is to promote carbon storage.**

I.4. Function and integration of winter land-use in the agricultural landscape

Contemporary society needs appropriate information regarding many aspects of its activities to establish sustainable measures. Winter land-use is only one of these issues but has become more significant as States consider overcoming environmental degradation, loss of agricultural land quality, wetland destruction, and loss of fish and wildlife habitat (Anderson, 1976).

Knowledge of winter land-use is essential for analyzing the environmental processes and problems in order to improve or maintain living conditions. In this situation, actualize, precise and meaningful data on winter land-use are essential for public and private organizations in order to establish optimal scenarios for future actions. However, the acquisition of this information regarding winter land-use is based on the understanding of the primary functions of the agricultural landscape. To date, a large number of studies have demonstrated the significant contribution of winter land-use to biogeochemical and environmental processes, in particular on the water cycle, biodiversity, health and broader climate scales, which are considered as the primary functions of an agricultural area (Foley et al., 2005; Galloway et al., 2004). **The functional role of winter land-use is part of multidisciplinary approaches. During this thesis project, we focused on the agronomic and ecological functions of winter land-use.** In other words, on its contribution to the water cycle processes, but also on the involvement in the preservation and conservation of biodiversity.

I.4.1 Biogeochemical cycles

As the main mechanism for transporting particles and sediments to drainage channels such as rivers, water is considered to be the most important element in biogeochemical cycles. Understanding integrated flows within the water cycle has become crucial to predict and

manage transfers of nutrients, sediments, and contaminants in agricultural watersheds (Haygarth and Jarvis, 2002). In this context, water plays an essential part as a major element of land-atmosphere exchanges, but especially biogeochemical exchanges that are increasing of interest. Nitrogen exchanges are one example among others, nitrogen is a fundamental element of any living being. Once in the soil, Nitrogen will undergo chemical transformations to form nitrates. Nitrate is a highly volatile chemical element that can cause nutritional disorders leading to eutrophication and environmental degradation. This issue is particularly true in an environment where the intensive agriculture has become a significant issue to satisfy a constantly growing population, which is recognized today as one of the main factors in the disruption of major biogeochemical cycles (water, carbon, nitrogen, phosphorus) for the degradation of terrestrial and aquatic ecosystems.

In this context, the winter land-use has a special place. Indeed, numerous studies have demonstrated the importance of winter land-use elements as a limiter of agricultural flow transfers (pollutants, sediments, etc.). The works of Decau and Pujol, (1992) and Soussana and Lüscher, (2007) are consistent with this approach by emphasizing the significant contribution of winter crops (wheat, barley, etc.) and grasslands to regulate agricultural flows into the environment. Along these lines, many studies have also demonstrated the important function of catch crops in reducing agricultural pollutant transfers (nitrogen, pesticides, etc.) to the environment (Dabney et al., 2009; Wagger et al., 1998). Moreover, research has proven that inappropriate management of winter land-use represents a potential risk of agricultural pollutants being transferred to the environment. (Lacroix, 1995) thus demonstrated the incapacity of cereal crops (wheat, barley, oats, etc.) to catch the nitrogen excess, increasing the risk of transfer to the environment.

From this perspective, the establishment of winter land-use has become essential for regulating the transfer of nutrients, sediments and agricultural pollutants to the environment. Furthermore, despite the potential of winter land-use, it is important to be aware of the diversity and inequality of land-use classes as regards their involvement and contribution to the optimal management of flow transfers into the environment.

I.4.2. Biodiversity

In recent decades, land-use changes related to climate change have led to a significant decrease in distribution areas and the extinction of hundreds of species. Even more dramatic changes are expected in this century. The acceleration of these changes and the destruction of natural habitats caused by land-use changes are recognized as the two greatest threats to biodiversity (Jetz et al., 2007). In this context, understanding the functional role of winter land-use in biodiversity preservation is still a significant issue. For several years, numerous studies have shown that specific winter land-use classes, promote the preservation and development of biodiversity. Nicholls and Altieri, (2013) and Peeters, (2009) thus highlighted the major contribution of grasslands but also of catch crops such as phacelia or mustard as support for biodiversity. In France, a significant amount of research conducted by government departments and research institutes (e. g. the Institut National de Recherche Agronomique (INRA) has contributed to the understanding and demonstrating the importance of catch crops in the preservation of biodiversity. These researches conducted by INRA ("CIPAN," 2008) have presented the ecological functions of catch crops, such as the attractiveness of the parcel for insects and small wildlife, as a key factor in the preservation of biodiversity in agricultural environments.

Thus, the understanding of biodiversity/winter land-use interactions has become a significant interdisciplinary issue. Defined as a set of interconnected elements that create a functional environment, the comprehension of these interactions has been the subject of several studies to date, enabling us to identify their interests and limits. However, despite the implementation of some research programs, few questions remain outstanding, in particular concerning the manner of monitoring the evolution of agricultural fields during the winter period in order to improve our understanding of land-use and biodiversity interaction dynamics. **This is the context of this thesis, which aims to identify and characterize winter land-use elements required by European regulations relating to the vegetative cover of soils in winter period in order to protect the environment and limit agricultural pollutant transfers to populations. To this end, the methodological approach of this thesis aims to determine whether spatial remote sensing can be considered as an interesting instrument for the identification and characterization of winter land-use in order to realize an adapted monitoring of these areas.**

Chapter 2

Spatial remote sensing for the study of winter land-use

Contents

II.1. INTRODUCTION	27
II.2. CHARACTERISTICS OF REMOTE SENSING DATA	27
II.3. IDENTIFICATION AND CHARACTERIZATION OF WINTER LAND-USE USING REMOTE SENSING DATA	45

II.1. Introduction

Monitoring winter land-use has become a global environmental issue in recent decades, particularly in regions where intensive agriculture is prevalent. To overcome this issue, spatial remote sensing that is now considered as an essential tool for identifying and characterizing land use, could provide valuable information.

Remote sensing is a concept that has evolved over the decades. It is currently recognized as a tool to derive information from land and water surfaces through the use of images acquired from an aerial perspective (without contact with the target), using electromagnetic radiation, from one or more regions of the electromagnetic spectrum, reflected or emitted by the land surface (Campbell and Wynne, 2011). One of the main benefits of remote sensing is the ability to conduct a land-use study at different scales of analysis. However, the quality of monitoring and its spatiotemporal accuracy inherently depend on the nature of the imagery and methods used to process it.

The main purpose of this chapter is first to present the characteristics of remote sensing data that can be used to identify and characterize agricultural winter land-use. Secondly, to present a state of the art of works dealing with the study of winter land-use based on remote sensing data.

II.2. Characteristics of remote sensing data

Remote sensing provides information on the physical and biological characteristics of an object based on information derived from electromagnetic radiation (representing a disturbance of the electric and magnetic field), emitted or reflected by the Earth's surface. The decomposition of this radiation according to its components such as wavelength, energy or frequency represents the electromagnetic spectrum (Fig. I.8). The decomposition of the spectrum wavelengths provided by airborne or spaceborne sensors provides a broader range of information. Nowadays, remote sensing offers an increasingly wide variety of data, allowing information to be collected from the optical (visible) to microwave and infrared wavelengths (Cracknell, 2007).

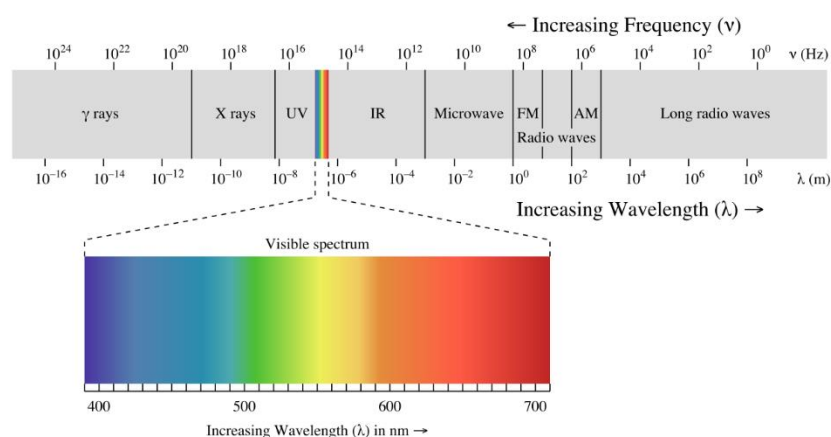


Figure I.8: Electromagnetic spectrum (“Electromagnetic Spectrum,” 2016).

However, it is essential to distinguish two types of acquisitions related to remote sensing data. The passive mode, which corresponds to the acquisition by a sensor of the electromagnetic radiation from a natural energy source (such as the sun) reflecting or emitting

from the Earth's surface. For this kind of acquisition, we find the optical and infrared data. Depending on the natural energy source, these sensors are sensitive to climatic conditions such as cloudiness or the lighting conditions, making it impossible the acquisition of night images due to the absence of a light source.

Conversely, the active mode, which represents the acquisition of electromagnetic radiations from an artificial source that emits and acquires the backscattered signal from the Earth's surface, such as microwave sensors or SAR (Synthetic Aperture Radar). As a result, they are often unaffected by atmospheric climatic conditions (according to the frequency) (Lusch, 1999).

As a consequence, active or passive sensors are privileged tools, for the observation of the Earth's surface. Passive sensors are characterized by their spatial, spectral and temporal resolution, which depends on the spectral domain (Caloz and Collet, 2001). SAR active sensors are characterized by their spatial and temporal resolution, but also by their frequency, polarization, and angle of incidence.

II.2.1. Optical and infrared data

Passive remote sensing has become an adapted instrument for monitoring global land surface conditions through the acquisition of land use and land cover information. In recent decades, the evolution of multispectral and hyperspectral satellites (optical and infrared) has led to new opportunities for land-use monitoring during winter season. Nevertheless, the achievement of these opportunities is related to the use of appropriate data to identify and characterize winter land-use. The determination of the suitable data to meet a thematic issue is based on the sensors' characteristics:

The spatial resolution of a sensor designates the minimum size of an object that can be detected in an image. In remote sensing, the spatial resolution represents the pixel size, which is defined from the product of angular resolution and the distance between the sensor and the object to be discerned (Campbell and Wynne, 2011; Forshaw et al., 1983). It can range from one kilometer for sensors with low spatial resolution (such as MODIS, Proba-V,...); to one centimeter for very high spatial resolution (VHSR) sensors (such as Ikonos, Pléiades,...)(Duveiller and Defourny, 2010).

The temporal resolution or revisit time corresponds to the time that the satellite will spend in order to achieve a complete orbital cycle, i.e. the time required to observe the same area. Temporal and spatial resolutions of sensors are intrinsically linked and depend directly on the sensor field of view. For a reduced field of view, a high spatial resolution and a low temporal resolution are obtained. Conversely, for an extended field of view, a low spatial resolution for a high temporal resolution (one to few days) are obtained (Canada, 2008). The time factor is consequently important in remote sensing, especially when:

- ✓ Cloud cover is persistent (e. g. in the tropics), which limits the time of Earth's surface observation.
- ✓ We want to monitor short-term phenomena (floods, oil spills, etc.).
- ✓ Multi-temporal images are needed (for example, to study over several years the extent of crop diseases).
- ✓ Temporal changes are used to distinguish two elements of the Earth's surface.

The spectral resolution is the ability of a sensor to distinguish two adjacent wavelengths. In other words, his ability to differentiate the spectral emissivity curves that characterize a target or surface for a set of wavelengths. This resolution is expressed as a function of the number of available spectral bands. It can consequently range from a few bands as for multispectral sensors to several tens in the case of hyperspectral sensors (Cracknell, 2007).

These optical and infrared data are now widely used for land-use and land-cover observation at a given time (Immitzer et al., 2016). These observations are made possible through the development of descriptors, either by using empirical or semi-empirical methods. These descriptors can be presented as vegetation indices or biophysical variables by applying inverse modeling of radiative transfer (Jacquemoud et al., 2009).

First, vegetation indices are arithmetic combinations of reflectances in the Visible and Near-Infrared (**Fig. I.9**). To date, a wide range of indices has been developed from simple ratios to more complex relationships. The most widely used remains the Normalized Difference Vegetation Index (NDVI), which corresponds to the ratio between the Near-infrared and Red spectral bands (Rouse Jr et al., 1974) (**Eq. I.1**).

$$NDVI = \frac{PIR-R}{PIR+R} \quad (\text{Eq. I.1}).$$

In several publications, many of these vegetation indices were quickly considered unsuitable for the study of specific environments because of the lack of consideration of sensor spectral characteristics as well as soil and atmospheric effects. Therefore, some indices were developed taking these limits into account. The Soil Adjusted Vegetation Index (SAVI) developed in the 1980s is one of the indices developed following the limitations encountered by conventional vegetation indices. It also uses the ratio between Red and Near-infrared while applying a soil coefficient (Huete, 1988) (**Eq. I.2**).

$$SAVI = \frac{PIR-R}{PIR+R+L} * (1 + L) \quad (\text{Eq. I.2}).$$

In this continuity, the development in the 1990s of indexes based on the Near and Mid-infrared ratio, the normalized difference water index (NDWI) to highlight the water content of plants has become essential to study agriculture and forest areas (Gao, 1996) (**Eq. I.3**).

$$NDWI = \frac{PIR-MIR}{PIR+MIR} \quad (\text{Eq. I.3}).$$

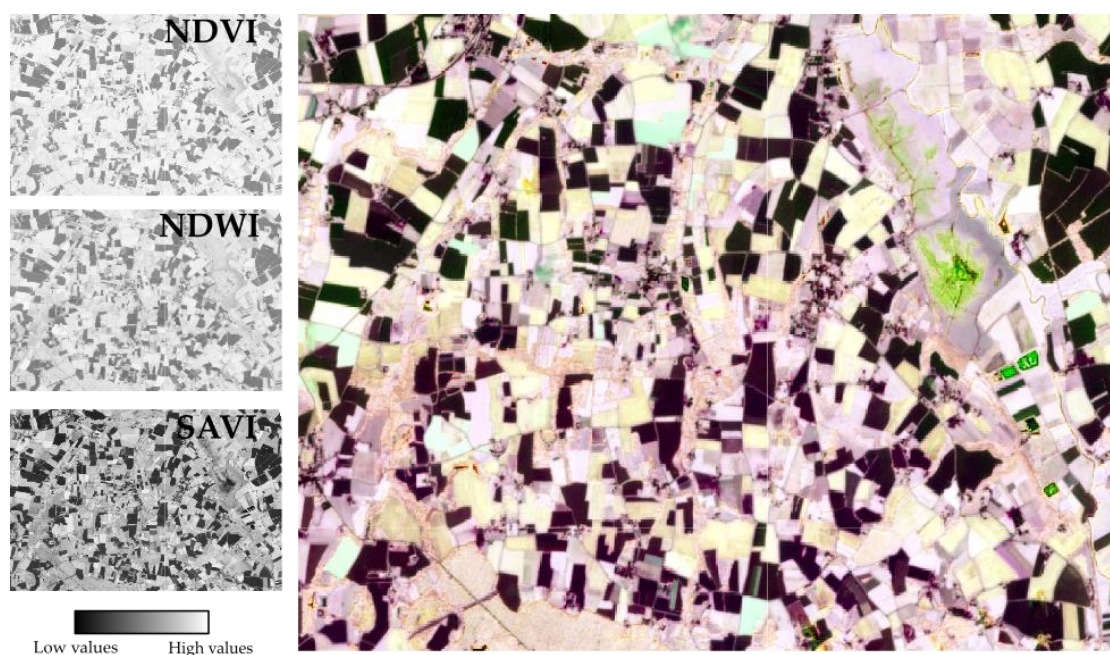


Figure I.9: Illustration of vegetation indexes derived from a Sentinel-2 image from May 2017 using a Red Green Blue (RGB) color composition. NDVI in Red (R); NDWI in Green (G); SAVI in Blue (B).

Secondly, biophysical variables that use the optical properties of vegetation cover. For this thesis, 3 types were computed:

- ✓ The Leaf Area Index (LAI), which is derived from leaf area density and canopy height, corresponding to the rate of land cover by the leaf area.
- ✓ The FAPAR (Fraction of photosynthetically active radiation), which is the direct result of the canopy radiative transfer model. It is dependent on the canopy structure, the optical properties of the vegetation elements and the illumination conditions.
- ✓ The FCover, which is the fraction of the soil covered by vegetation. It is mainly used to separate soil and vegetation in energy transfer processes, including temperature and evapotranspiration.

These descriptors have already proved their potential to identify, characterize cultural practices, conduct inter-annual crop monitoring or to identify information on crop conditions and thus detect potential problems such as water stress, diseases... Nevertheless, its use is still restricted to periods when weather and atmospheric conditions remain favorable, which makes intra-annual monitoring and the identification and characterization of winter land-use difficult, particularly in temperate regions. In addition, despite the relevance of indexes and spectral variables derived from optical data, the information provided by these descriptors is confined to the canopy surface study. Thus, the characterization of the canopy internal structure remains quite limited (Betbeder, 2015). In this context, many scientists have considered the use active remote sensing (SAR) data for intra-annual monitoring to identify and characterize land use.

II.2.2. SAR data

Developed in the 1970s, the Synthetic Aperture Radar (SAR) system is a technology generating and receiving signals in the microwave wavelength. Microwave detection includes both the active and passive forms of remote sensing. They are located in a larger domain of the electromagnetic spectrum. According to the frequency, they are less impacted by atmospheric conditions, and can thus cross the cloud cover, while being less affected by weather conditions such as drizzle, dust and light rain.

II.2.2.1. Principle of SAR systems in remote sensing

A SAR is an active sensor operating in the microwave region of the electromagnetic spectrum (**Fig. I.10**). The first SAR sensor installed for Earth's observation dates in the late 1970s, SEASAT. Despite the rapid end to this sensor, its efficiency has made SAR imagery an essential source of information for observing the Earth's surface. Installed on a moving platform, a SAR system operates in 3 essential steps. i) A transmitter generates short microwave pulses at a regular interval that are concentrated into a beam by an antenna. ii) The beam illuminates laterally, with a defined incidence angle, the surface. iii) The signal is then backscattered by various illuminated objects to the receiver. Then, a SAR processes the signal to synthesize a high spatial resolution 2-D image (Lee and Pottier, 2009).

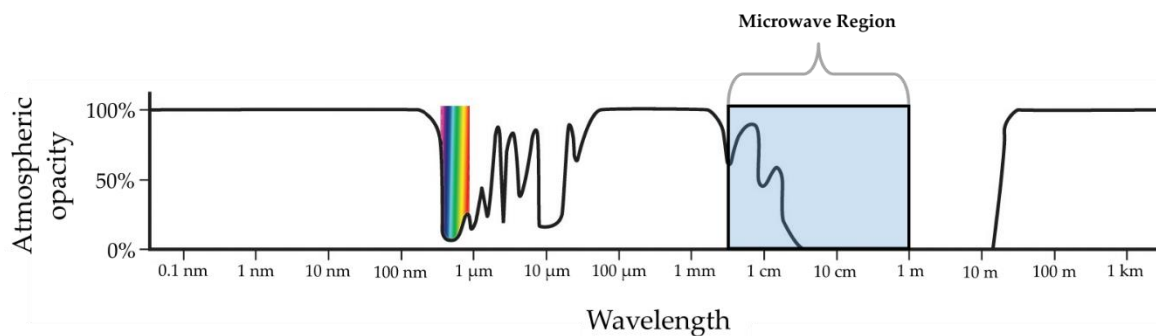


Figure I.10: Atmospheric absorption bands in relation to radar wavelengths (“HUMBOLDT State university,” 2019).

This system makes sensors independent of solar illumination (acquires days and nights), but also of cloud, fog or smoke conditions... The transmitted signal sent by SAR systems use wavelengths ranging from 0.75 cm to 1 m designated by letters (**Table I.2**), following:

Table I.2: Microwave frequency of SAR sensors.

Frequency (GHz ($\times 10^9$))	Band name	Wavelength (cm)
40 - 26.5	Ka	0.75 – 1.1
26.5 - 18	K	1.1 – 1.67
18 - 12.5	Ku	1.67 – 2.4
12.5 - 8	X	2.4 – 3.75
8 - 4	C	3.75 – 7.5
4 - 2	S	7.5 – 15
2 - 1	L	15 – 30
1 - 0.3	P	30 – 100

Subsequently, to provide information on a specific surface, measurements are performed by SAR systems comparing the received signal with the transmitted signal in terms of time and energy. Similar to optical sensors, the effectiveness of measurements performed by a SAR system depends on the specific characteristics and properties of the system, such as spatial resolution. This resolution is one of the most important criteria in SAR imagery. However, the pixel size should not be confused with the spatial resolution of an image. Spatial resolution is the minimum distance required between two targets to be discriminated. The pixel size is always smaller than the resolution.

II.2.2.2. SAR Image Properties

The synthesized SAR image is a 2-D, where an element (pixel) is associated to a small area of the Earth's surface whose size is determined by the SAR system's characteristics. Thus, each pixel provides complex information, represented by an amplitude and a phase, associated with the reflectivity of all the scattering contained in a SAR cell (Lee and Pottier, 2009). It is important to note that surface reflectivity, also called SAR backscatter, is dependent on SAR system parameters (frequency, polarization, incidence angle) and surface parameters (topography, local incidence angle, roughness, humidity, dielectric constant...) (Richards, 2009).

SAR images represent a specific acquisition geometry. SAR sensors are positioned on a moving platform (**Fig. I.11**) with a velocity (V_{SAR}) and a height (H). During the displacement of the platform along the flight line also called "azimuth" (y), the sensor with a fixed antenna transmits a signal to the ground with a defined angle of incidence (θ_0). Then this signal illuminates the Earth's surface and the backscattered waves are received and recorded by the receptor. The surface x and y axis represent respectively "ground range" and "azimuth" directions (Lee and Pottier, 2009).

The number of columns in the SAR image is determined by the sampling frequency acquisition of the backscattered wave. The higher the frequency, the more columns are and thus the greater the sharpness of the image. The first column corresponds to the illuminated surface closest to the sensor ("proximal range" or "near range"), the last to the furthest surface ("distal range" or "far range"). In addition, it is important to note that the beam width is inversely proportional to the length of the antenna (also called aperture), so a long antenna will produce a thinner beam and a better resolution.

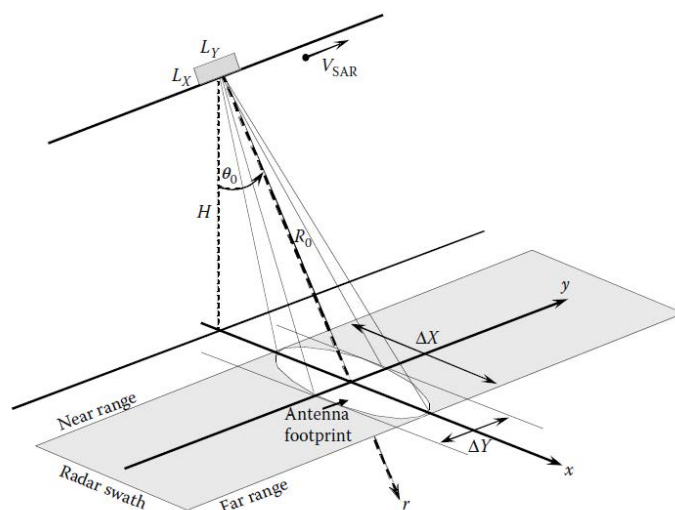


Figure I.11: SAR image property (Lee and Pottier, 2009).

Through this specific geometric acquisition, targets located in the near range appear compressed compared to those in the far range, these distortions being related to the oblique scale. Thus, the pixel size in the azimuthal direction depends on the wavelength emitted, the size of the antenna and the ground-radar distance. Moreover, in the range direction a SAR image represents a measurement of the time required for the signal to interact with targets and be backscattered on the antenna. The complexity of image acquisition generates geometric distortions due to the difference between azimuth and ground distance. There are 3 types of distortions:

- ✓ *Layover* occurs when the SAR signal reaches the top of a target before reaching its base, i.e. the difference (in distance) between the signal backscatter from the top and bottom of an object. It depends on the depression angle. To the greater the angle, the stronger the layover is and conversely the weaker it is the more limited the layover is (Lusch, 1999). As a result, the order of the surface elements on the SAR image is the opposite of reality (**Fig. I.12**).
- ✓ *Foreshortening* is undoubtedly the most significant distortion of SAR images. It is the dominant effect for images of mountainous areas, especially when the sensor has a high inclination. It occurs when the SAR signal reaches the base of a structure before reaching the top. This leads to cross-compression of backscattered radiometric information on slope areas (Lee and Pottier, 2009). In this case, as shown in **Figure I.12**, the slope of the object is shortened (smaller than reality).
- ✓ *The Radar shadow* is dependent on the relationship between the angle of depression, the inclination and the orientation of the object's slope. It occurs when the beam is not able to illuminate the ground surface. Shadow areas appear as dark areas in the SAR image, corresponding to a zero signal (**Fig. I.12**).

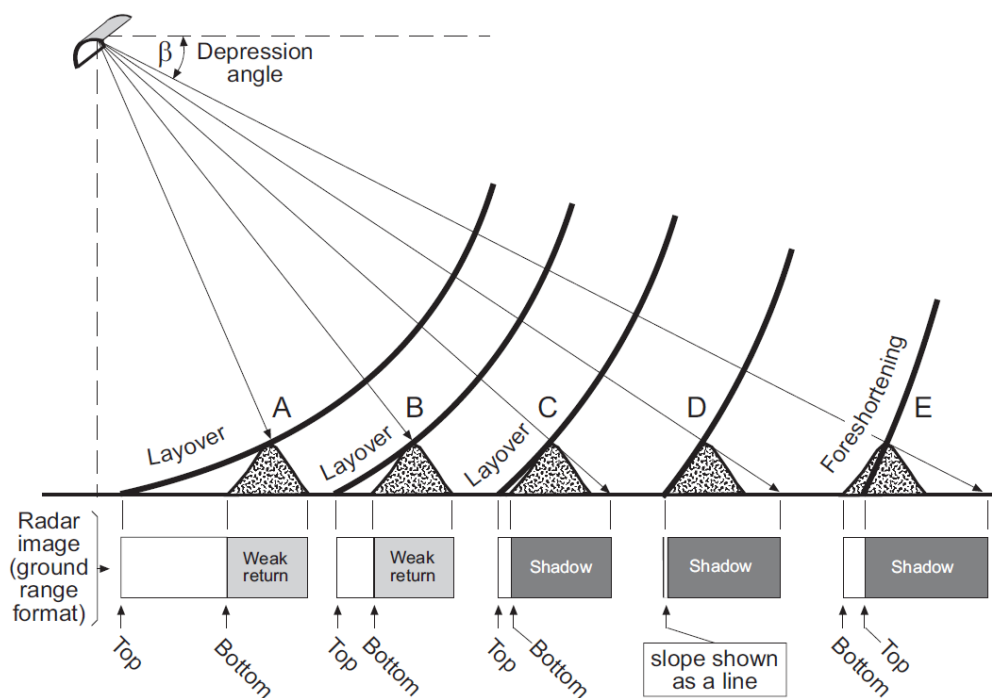


Figure I.12: SAR images geometric distortions (Lusch, 1999).

In addition to these geometric distortions, other specific effects occur for these SAR images. Speckle is one such example, it appears as a pepper and salt texture on the image and is a consequence of the principle of consistent acquisition of SAR data. A SAR image consists of several resolution cells. Within each resolution cell, several diffusers can coexist. Thus, the response of a resolution cell is the coherent sum of the scatterers present in the cell. The interference of these phase-shifted waves causes a pepper and salt effect on the image known as speckle. It causes a variation in pixel-by-pixel intensity that is manifested by this particular texture. It then complicates the interpretation and analysis of the image and reduces the effectiveness of the image segmentation and classification. There are 2 methods to limit these noise effects (Lee and Pottier, 2009; Mott, 2006) :

- ✓ *Multi-look processing* which consists in acquiring several distinct images of the same scene, then by averaging all the images we obtain a final image where the effect of the speckle is reduced.
- ✓ *Spatial filtering* consists in extracting a window of a few pixels, filtering is then performed by applying a calculation using the value of the window's pixels and replacing the corresponding pixel of the resulting image with the result of the operation.

In the specific context of SAR images, the development of an approach based on time series requires first of all the correction of the intrinsic effects of SAR images. To do this, a series of preprocessing is required to correct the distortions but also to reduce speckle effects. Then, the information provided by the SAR images can then be extracted from various methods based on the principles of SAR imaging. We find there (Lee and Pottier, 2009):

- ✓ The use of SAR signal intensity.
- ✓ The use of SAR polarimetry, to study the transformations of the polarization behavior of an electromagnetic wave in contact with a surface.
- ✓ The use of SAR interferometry to exploit the difference in phase between SAR images.
- ✓ The use of SAR tomography to obtain information on the physical properties of an environment.

In this thesis, according to the scientific literature, the choice of using SAR signal intensity and SAR polarimetry has been established according to their aptitude to identify and characterize vegetation cover as demonstrated in several studies (Jackson and Schmugge, 1991; McNairn and Brisco, 2004).

II.2.2.3. SAR signal intensity

SAR signal intensity is one of the most commonly used source of information in SAR imagery. The intensity often called "Sigma nought" or " backscattering coefficient " or σ^0 is proportional to the ratio between the received power and the power transmitted by the antenna (Lusch, 1999). As a function of the physical and electrical target properties, it also depends on the frequency and polarization of the SAR system, as well as the projected incidence angle (modified by the relief effect, **Fig. I.13**).

The intensity is expressed in natural values (m^2/m^2) (Eq. I.4) or on a logarithmic basis, in decibels ($\text{dB m}^2/\text{m}^2$) (Eq. I.5):

$$\sigma^0 = \frac{\langle \sigma \rangle}{A_L} = \frac{4\pi r^2 \langle |\vec{E}_S|^2 \rangle}{A_L |\vec{E}_I|^2} \quad (\text{Eq. I.4}).$$

$$\sigma^0 = 10 \cdot \log_{10}(\sigma^0) \quad (\text{Eq. I.5}).$$

With A_L , the illumination area, \vec{E}_I the incident electromagnetic field and \vec{E}_S the scattered electromagnetic field (corresponding respectively to the transmitted and received power).

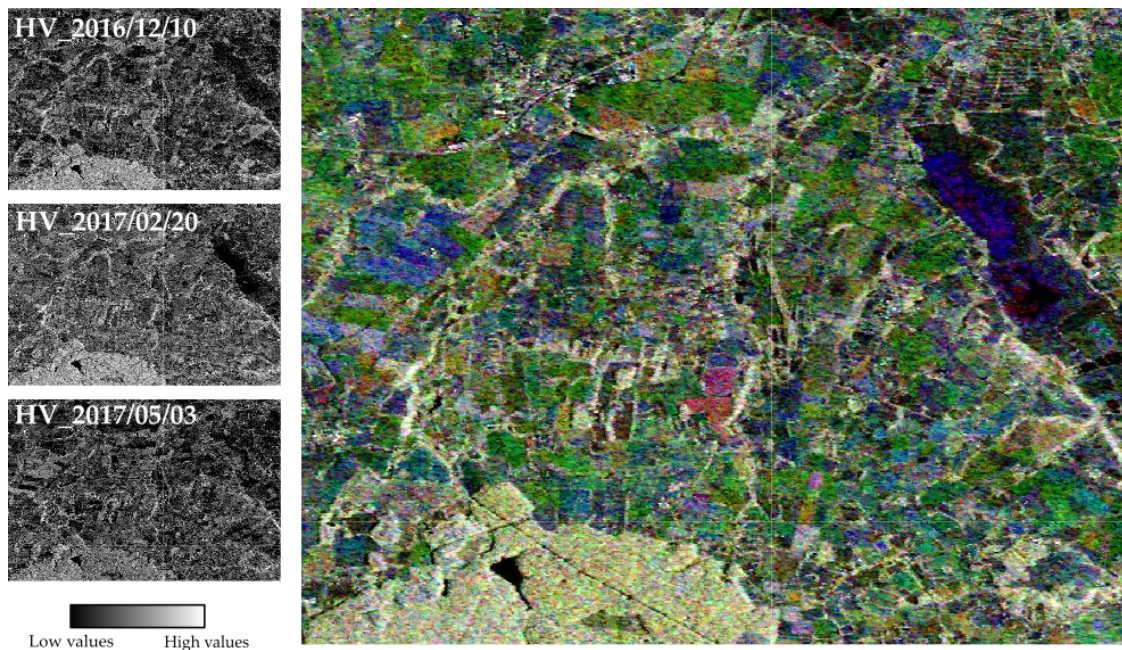


Figure I.13: Illustration of HV backscattering coefficient parameter derived from a Radarsat-2 images using a RGB color composition. HV from 10 December 2016 in Red (R); HV from 20 February 2017 in Green (G); HV from 03 May 2017 in Blue (B).

II.2.2.4. SAR polarimetry

SAR polarimetry consists in studying the transformations of the electromagnetic wave polarization behavior after an interaction with a surface (Lee and Pottier, 2009). These polarization changes are mainly related to the geometric, physical and biophysical structure of the illuminated target. The polarimetric information contained in a SAR image can, therefore, be used to characterize the observed object using the knowledge acquired on electromagnetic behavior (Betbeder, 2015).

II.2.2.4.1. SAR polarization basics

A polarized electromagnetic wave traveling through time and space can reach and interact with a particular target. This interaction can generate the absorption by the target of a portion of the incident wave while the rest is backscattered as a new electromagnetic wave. This interaction can, therefore, lead to a change in the polarimetric properties of the wave (Lee and Pottier, 2009).

The modification of polarimetric properties of a wave can be modeled as a complex 2×2 matrix called coherent scattering matrix or "Scattering matrix" $[S]$. It can be used to connect the incident wave and the backscattered wave. In this context, Jones' formalism mentioned above is relevant. Based on the latter, the matrix $[S]$ links the Jones vector incident E^i to the Jones vector broadcast E^s and can be written as follows (Eq. I.6):

$$\begin{bmatrix} E_h^s \\ E_v^s \end{bmatrix} = \begin{bmatrix} S_{hh} & S_{hv} \\ S_{vh} & S_{vv} \end{bmatrix} \begin{bmatrix} E_h^i \\ E_v^i \end{bmatrix} \quad (\text{Eq. I.6}).$$

The 4 components of the matrix are complex numbers (amplitude and phase). The diagonal elements of the Sinclair matrix S_{hh} and S_{vv} are the co-polarized elements, S_{vh} and S_{hv} are called cross-polarized elements.

In a thematic approach, these co-polarized elements will be very sensitive to the physical characteristics of the soil. On the other hand, cross-polarized elements will be very sensitive to the volume of the objects (Baghdadi et al., 2008; Baghdadi and Zribi, 2016; Betbeder, 2015; Haldar et al., 2012; Lee et al., 2001; McNairn et al., 2009; McNairn and Brisco, 2004; Skriver, 2011; Skriver et al., 1999).

In monostatic mode, the transmitter and receiver are positioned on the same antenna, so the S_{hv} and S_{vh} elements are considered equal. This is the reciprocity hypothesis, commonly verified for artificial targets. So the matrix can be summarized into 5 independent parameters, representing 3 amplitudes $\{|S_{vv}|, |S_{hv}|, |S_{hh}|\}$ and the two related phases ϕ_c and ϕ_x where $\phi_c = (\varphi_{vv} - \varphi_{hh})$ and $\phi_x = (\varphi_{hv} - \varphi_{hh})$. The Sinclair matrix $[S]$ can then be represented by a complex target vector composed of 4 elements (Eq. I.7).

$$\vec{k} = [k_0, k_1, k_2, k_3]^T \quad k_i = \frac{1}{\sqrt{2}} \text{tr}([S]\phi_i) \quad (\text{Eq. I.7}).$$

With $\text{tr}(\cdot)$ which represents the sum of the diagonal elements of a matrix and ϕ_i is a set of matrices that define the projection base. The two most commonly used bases are the lexicographic base (Φ_L) (Eq. I.8) and the Pauli base (Φ_P) (Eq. I.9). Pauli base tends to value the scattering matrix according to a physical interpretation of the backscattering mechanisms of a target (Betbeder, 2015).

$$\{\Phi_L\} = \left\{ 2 \begin{bmatrix} 1 & 0 \\ 0 & 0 \end{bmatrix}, 2 \begin{bmatrix} 0 & 1 \\ 0 & 0 \end{bmatrix}, 2 \begin{bmatrix} 0 & 0 \\ 1 & 0 \end{bmatrix}, 2 \begin{bmatrix} 0 & 0 \\ 0 & 1 \end{bmatrix} \right\} \quad (\text{Eq. I.8}).$$

$$\{\Phi_P\} = \left\{ \sqrt{2} \begin{bmatrix} 1 & 0 \\ 0 & 1 \end{bmatrix}, \sqrt{2} \begin{bmatrix} 1 & 0 \\ 0 & -1 \end{bmatrix}, \sqrt{2} \begin{bmatrix} 0 & 1 \\ 1 & 0 \end{bmatrix}, \sqrt{2} \begin{bmatrix} 0 & -j \\ j & 1 \end{bmatrix} \right\} \quad (\text{Eq. I.9}).$$

In a monostatic configuration, where the reciprocity hypothesis holds, the lexicographic target k_L (Eq. I.10) and Pauli k_P (Eq. I.11) vectors contain only three elements :

$$k_L = \begin{bmatrix} S_{hh} \\ \sqrt{2}S_{hv} \\ S_{vv} \end{bmatrix} \quad (\text{Eq. I.10}). \quad k_P = \frac{1}{\sqrt{2}} \begin{bmatrix} S_{hh} + S_{vv} \\ S_{hh} - S_{vv} \\ 2S_{hv} \end{bmatrix} \quad (\text{Eq. I.11}).$$

The two vectors are coherent representations of the scattering matrix. The vector norm is the SPAN of a target (Fig. I.14), which corresponds to the total power scattered by the target and is given by (Eq. I.12):

$$SPAN = |S_{hh}|^2 + 2|S_{hv}|^2 + |S_{vv}|^2 \quad (\text{Eq. I.12}).$$

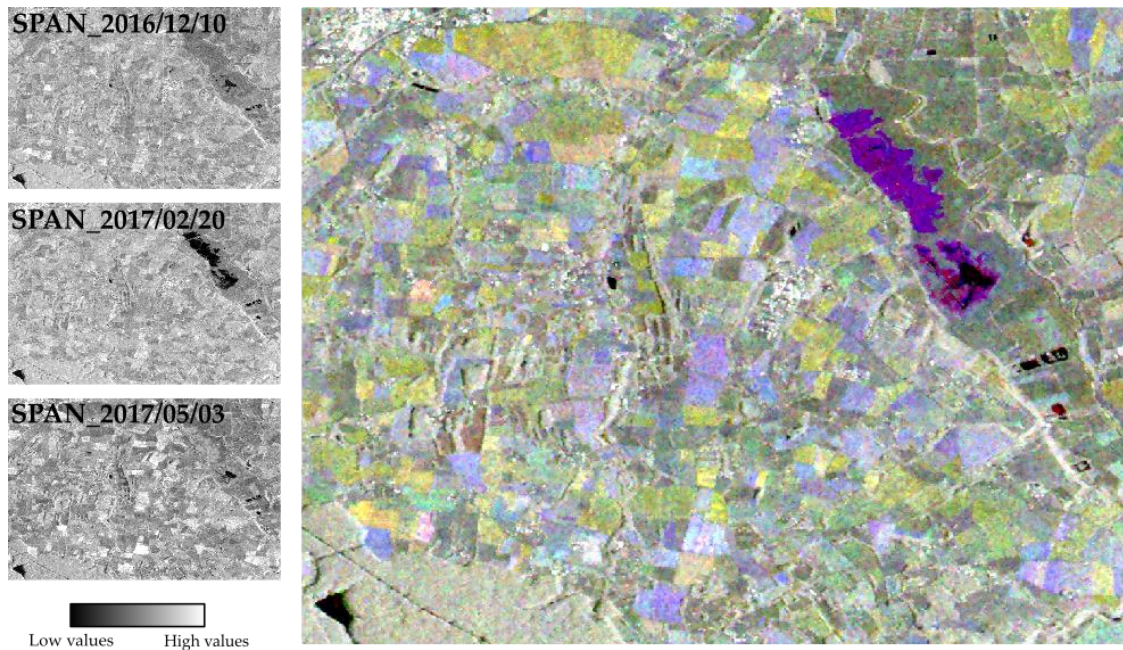


Figure I.14: Illustration of SPAN parameter derived from a Radarsat-2 images using a RGB color composition. SPAN from 10 December 2016 in Red (R); SPAN from 20 February 2017 in Green (G); SPAN from 03 May 2017 in Blue (B).

II.2.2.4.1.1. Dominant vs. non-dominant scattering mechanisms

A resolution cell in a SAR image is formed by the coherent addition of the responses of the elementary scattering. Two situations are then possible: i) if there is no dominant mechanism, the signal response is given by the Gaussian complex diffusion model, which is at the origin of speckle; ii) The resolution cell contains an identifiable target, which dominates the cell, then the backscatter is the result of a coherent combination of 2 components: The dominant scattering mechanism and the coherent combination due to congestion. The response is then dominated by a strong contribution from the dominant mechanism.

However, in SAR remote sensing, the resolution cell is larger than the transmitted wavelength, it then contains a set of scattering mechanisms represented by the matrix $[S]$. A coherent representation of the scattering matrix is then necessary in order to simplify and carry out a complete analysis of the connected effects of the scattering mechanisms. With the application of target vectors and more precisely of the Pauli base, the matrix $[S]$ can be used to study coherent targets. This representation expresses the terms of the Sinclair matrix for a target as a combination of simpler responses and thus establishes a physical interpretation of the interaction between the signal and the target (Betbeder, 2015) (**Fig. I.15**).

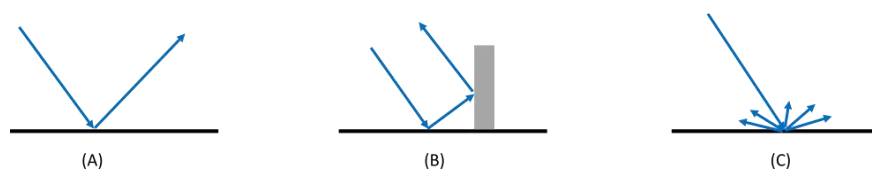


Figure I.15: The dominant scattering mechanisms (a) single bounce, (b) double bounce and (c) diffuse scattering (Lee and Pottier, 2009).

From the target vectors, complex polarimetric coherence and covariance matrices can be defined according to:

- ✓ The covariance matrix $[C_3]$ (Eq. I.13) is constructed from the target lexicographic vector k_L^{T*} .

$$C_3 = \langle k_L k_L^{T*} \rangle = \begin{bmatrix} \langle |S_{hh}|^2 \rangle & \sqrt{2} \langle S_{hh} S_{hv}^* \rangle & \langle S_{hh} S_{vv}^* \rangle \\ \sqrt{2} \langle S_{hv} S_{hh}^* \rangle & 2 \langle |S_{hv}|^2 \rangle & \sqrt{2} \langle S_{hv} S_{vv}^* \rangle \\ \langle S_{vv} S_{hh}^* \rangle & \sqrt{2} \langle S_{vv} S_{hh}^* \rangle & \langle |S_{vv}|^2 \rangle \end{bmatrix} \quad (\text{Eq. I.13}).$$

- ✓ The coherency matrix $[T_3]$ (Eq. I.14) constructed from the Pauli target vector k_p^{T*} :

$$T_3 = \langle k_p k_p^{T*} \rangle = \frac{1}{2} \begin{bmatrix} \langle |S_{hh} + S_{vv}|^2 \rangle & \langle (S_{hh} + S_{vv})(S_{hh} + S_{vv})^* \rangle & 2 \langle (S_{hh} + S_{vv}) S_{hv}^* \rangle \\ \langle (S_{hh} - S_{vv})(S_{hh} - S_{vv})^* \rangle & \langle |S_{hh} - S_{vv}|^2 \rangle & 2 \langle (S_{hh} - S_{vv}) S_{hv}^* \rangle \\ 2 \langle S_{hv} (S_{hh} + S_{vv})^* \rangle & 2 \langle S_{hv} (S_{hh} - S_{vv})^* \rangle & 4 \langle |S_{hv}|^2 \rangle \end{bmatrix} \quad (\text{Eq. I.14}).$$






They both have the same positive or null eigenvalues but have different eigenvectors. The trace of these 2 matrices is equal to the SPAN, while the off-diagonal terms represent the complex correlations between the polarizations channels.

II.2.2.4.1.2. Polarimetric decompositions

To retrieve information on a target from these complex matrices $[C_3]$ and $[T_3]$, the implementation of polarimetric decomposition models is necessary to extract the scattering mechanisms of a target. Resulting from Chandrasekhar's work, and first formalized by Huynen (Huynen, 1970), polarimetric decompositions search to express the global mean matrix to a sum of independent matrices representing the scattering mechanisms of a target, thus facilitating their interpretation.

The scattering mechanisms are also translated into canonical targets (Table I.3) corresponding to simple geometric shapes whose physical interpretation is known. These targets differ according to the number of interactions of the backscattered signal with a target. An odd number of interactions will produce a zero phase difference (Betbeder, 2015).

Table I.3: Geometric and matrix representations of canonical targets adapted from (Lee and Pottier, 2009).

Geometric representation	Canonical target	Matrix $[S]$
	Sphere	$S = \frac{1}{\sqrt{2}} \begin{bmatrix} 1 & 0 \\ 0 & 1 \end{bmatrix}$
	trihedron	$S = \frac{1}{\sqrt{2}} \begin{bmatrix} 1 & 0 \\ 0 & 1 \end{bmatrix}$
	vertical dipole	$S = \begin{bmatrix} 0 & 0 \\ 0 & 1 \end{bmatrix}$
	horizontal dipole	$S = \begin{bmatrix} 1 & 0 \\ 0 & 0 \end{bmatrix}$
	Dihedral oriented according to an angle Θ	$S = \frac{1}{\sqrt{2}} \begin{bmatrix} \cos 2\theta & \sin 2\theta \\ \sin 2\theta & -\cos 2\theta \end{bmatrix}$

To further explore, **Figure I.16** presents the main scattering mechanisms that can interact with an incoherent target. There are 3 mechanisms: (i) more or less simple surface diffusion (sphere, horizontal or vertical dipole); (ii) volume diffusion from the foliage of a tree, for example (collection of randomly oriented dipoles) and (iii) double-bounce diffusion (dihedral).

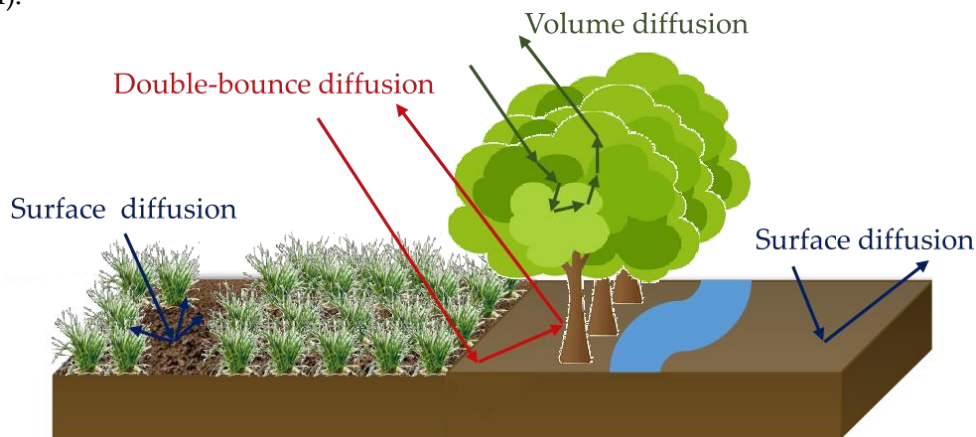


Figure I.16: The three main scattering mechanisms.

The decompositions are then classified into 2 types, coherent decompositions of the Sinclair matrix and incoherent decompositions of the covariance C_3 or coherency T_3 matrices. In this thesis, we will consider only two coherent decompositions: The Cloude and Pottier and the Freeman and Durden decompositions that have already proven their effectiveness in the scientific literature.

II.2.2.4.1.2.1. Cloude and Pottier decomposition

Cloude and Pottier decomposition (Fig. I.17) is based on the eigenvalue decomposition of the coherency matrix $[T_3]$ (Cloude and Pottier, 1996). The complex information retrieved from this decomposition is simplified by the expression of 3 secondary parameters which are defined as a function of the eigenvalues and eigenvectors of the matrix $[T_3]$.

- ✓ Entropy H (Eq. I.15) which corresponds to the degree of randomness of the target. H is computed from the target's eigenvalues according to the following formula:

$$H = \sum_{i=1}^3 -P_i \log_3(P_i) \quad (\text{Eq. I.15}).$$

$$P_i = \frac{\lambda_i}{\sum_{k=1}^3 \lambda_k}$$

Ranging between 0 and 1, H defines the number of diffusion mechanism present on a target. When it is 0, only one scattering mechanism is present, which corresponds to a pure target. On the other hand, when it is 1, several mechanisms are present (Betbeder, 2015).

- ✓ Anisotropy A , a complementary parameter of entropy, characterizes the importance of secondary mechanisms in relation to the main one. It is also derived from the eigenvalues of the coherency matrix and is interesting for high H values. If its value is 0 then the secondary mechanisms are mixed, whereas if it is 1, the 2nd mechanism dominates.
- ✓ The alpha angle α , ranging from 0 to 90°, enables to retrieve information on the dominant scattering mechanism. If $\alpha = 0^\circ$, then the dominant mechanism is surface scattering or simple bounce scattering mechanism. If $\alpha = 45^\circ$, there is a multiple or volume scattering mechanism. And finally, if $\alpha = 90^\circ$, there is a double bounce diffusion.

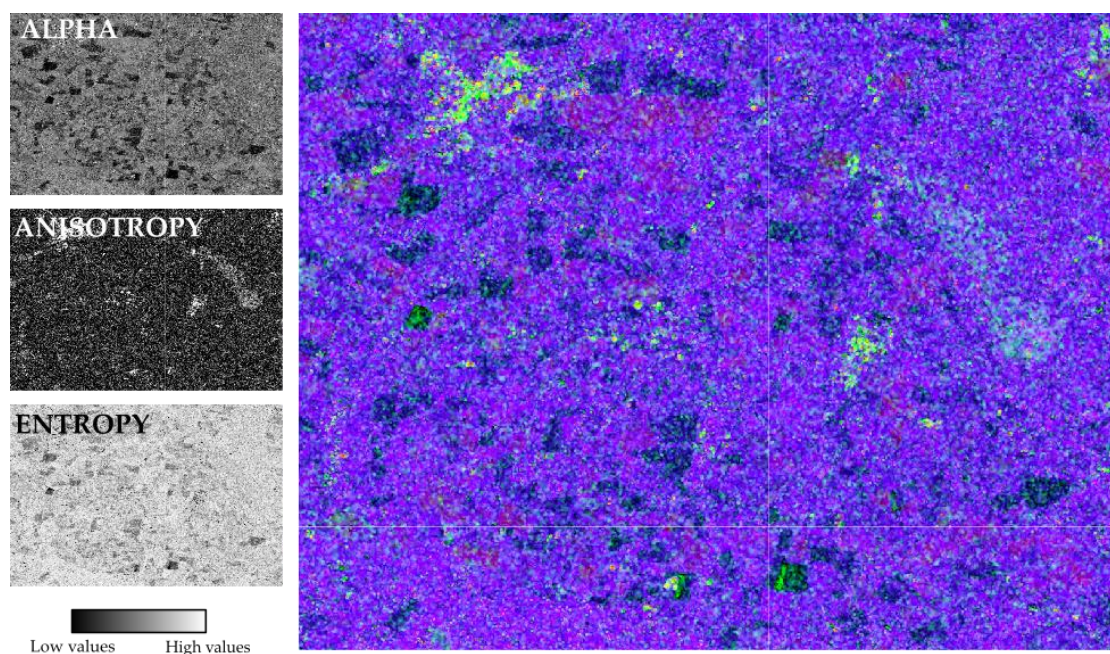


Figure I.17: Illustration of Cloude and Pottier decomposition derived from a Radarsat-2 image of April 2017 using a RGB color composition. Alpha in Red (R); Anisotropy in Green (G); Entropy in Blue (B).

II.2.2.4.1.2.2. Freeman-Durden decomposition

The Freeman-Durden decomposition (**Fig. I.18**) attempts to separate the dominant scattering mechanisms from a physical model based on the covariance matrix $[C_3]$ (Freeman and Durden, 1998). Three scattering mechanisms are highlighted by this model:

- ✓ *The surface scattering* that refers to flat surfaces such as bare soils.
- ✓ *The double bounce scattering* that represents the interaction of the incident signal between a flat object and a vertical object such as a building.
- ✓ *The volume scattering* or canopy that represents multiple or random scattering mechanism.

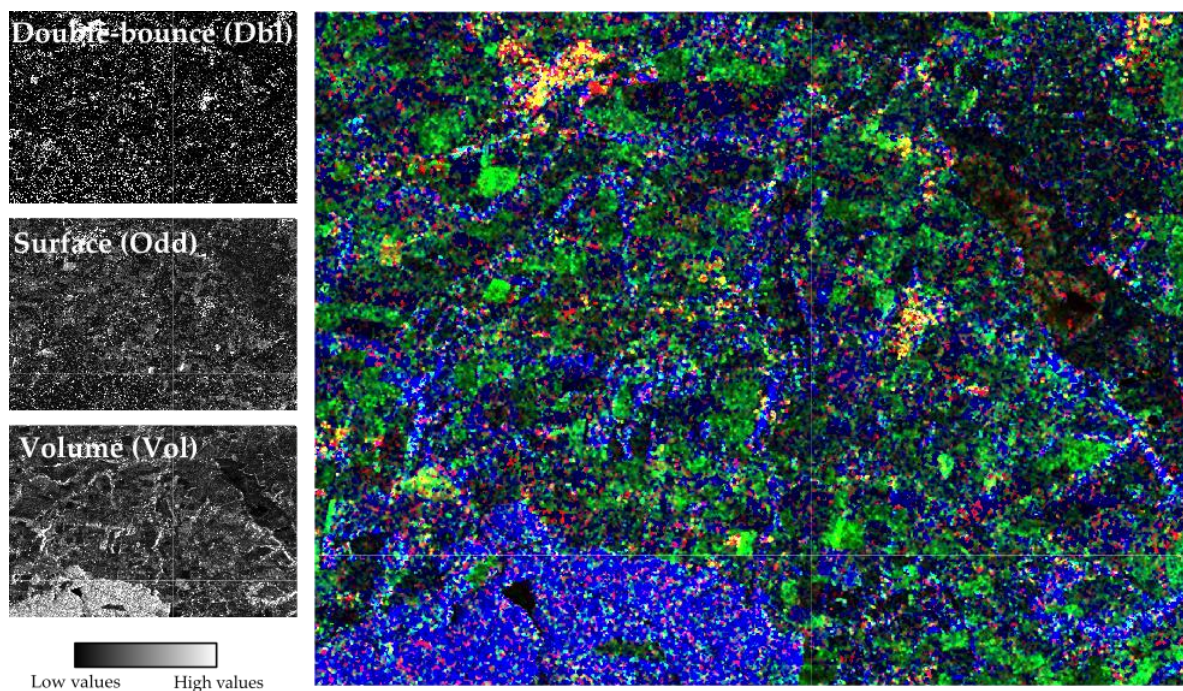


Figure I.18: Illustration of Freeman and Durden decomposition derived from a Radarsat-2 image of April 2017 using a RGB color composition. Double-bounce in Red (R); Surface in Green (G); Volume in Blue (B).

In addition to these parameters resulting from the decompositions, a number of polarimetric discriminators can be extracted in order to characterize the studied surface.

II.2.2.4.1.3. Polarimetric discriminators

II.2.2.4.1.3.1. Shannon Entropy

It corresponds to the sum of two contributions relating to intensity (SE_I) and degree of polarization (SE_P) (Fig. I.19). Shannon Entropy (SE) can be calculated from the coherency matrix [T_3] or the covariance matrix [C_3] (Lee and Pottier, 2009) according to (Eq. I.16) :

$$SE = \log(\pi^2 e^3 |C_3|) = SE_I + SE_P \quad (\text{Eq. I.16}).$$

where

$$SE_I = 3 \log\left(\frac{\pi e T_r(C_3)}{3}\right)$$

$$SE_P = \log\left(27 \frac{|C_3|}{T_r(C_3)^3}\right)$$

Where $|\cdot|$ represents the determination of a matrix, and $T_r(\cdot)$, the trace of a matrix.

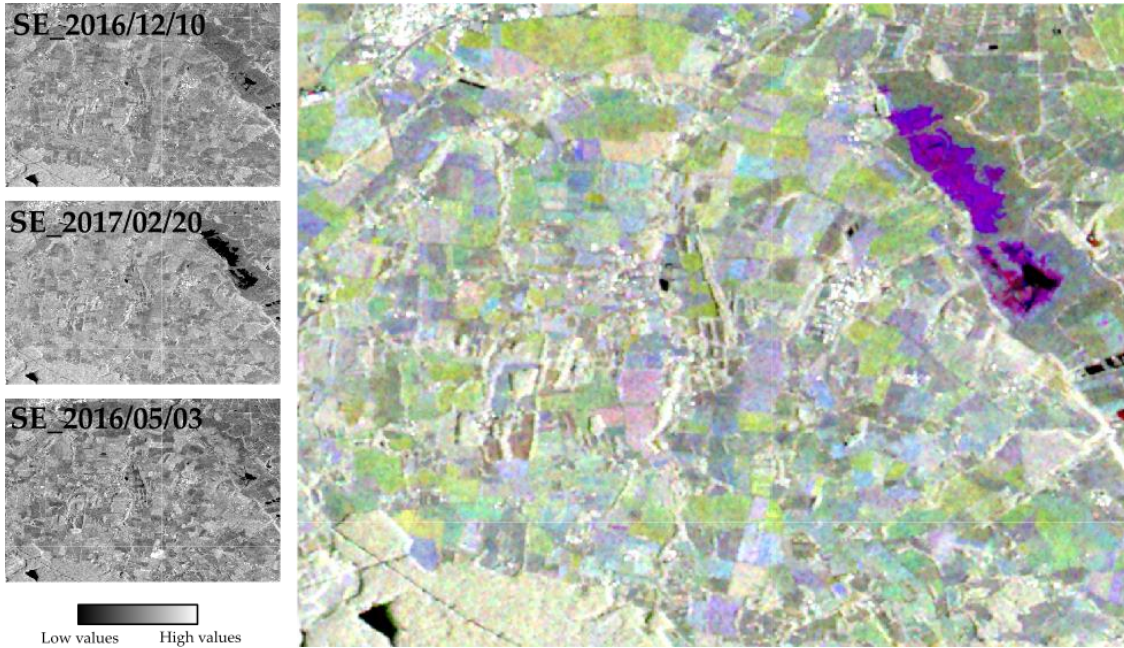


Figure I.19: Illustration of Shannon Entropy (SE) parameter derived from a Radarsat-2 images using a RGB color composition. SE from 10 December 2016 in Red (R); SE from 20 February 2017 in Green (G); SE from 03 May 2017 in Blue (B).

II.2.2.4.1.3.2. Radar Vegetation Index (RVI)

Computed from the coherency matrix T_3 , the radar vegetation index (RVI) is a function between the incidence angle and the path length of the SAR signal in a vegetation canopy (Kim et al., 2011). Represented by an index ranging from 0 to 1, the RVI corresponds to a measure of the randomness of the scattering (Fig. I.20) and is given by the following equation (Eq. I.17):

$$RVI = \frac{8\sigma_{HV}^0}{\sigma_{HH}^0 + \sigma_{VV}^0 + 2\sigma_{HV}^0} \quad (\text{Eq. I.17}).$$

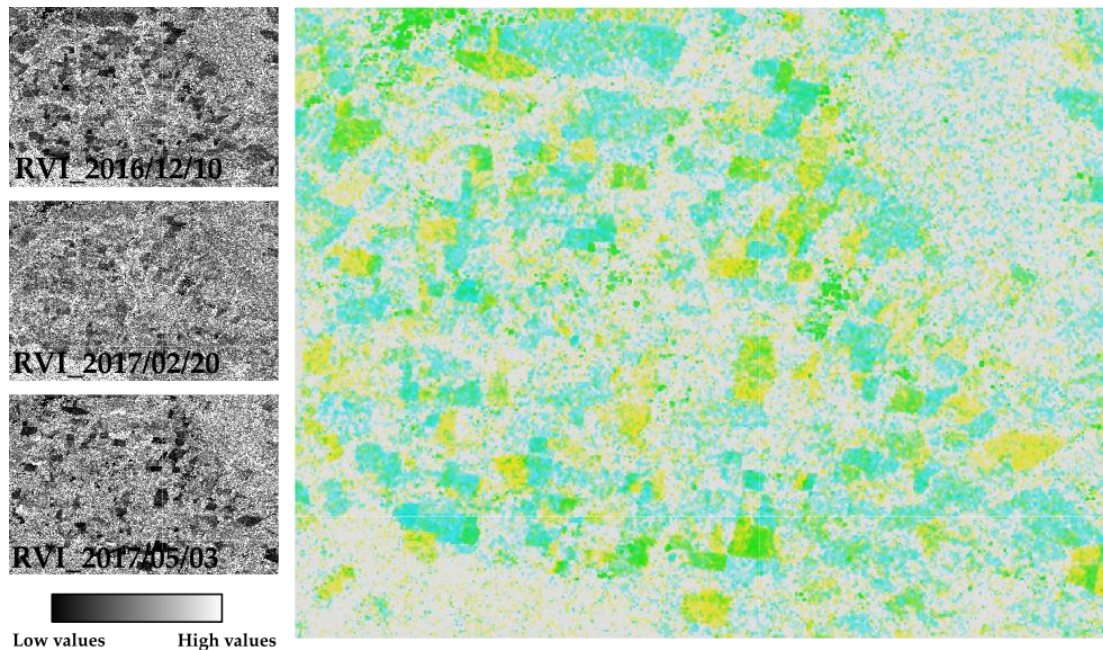


Figure I.20: Illustration of Radar Vegetation Index (RVI) parameter derived from a Radarsat-2 images using a RGB color composition. RVI from 10 December 2016 in Red (R); RVI from 20 February 2017 in Green (G); RVI from 03 May 2017 in Blue (B).

II.2.2.4.1.3.3. Pedestal Height (Pedestal)

The pedestal height also derived from the coherency matrix T_3 represents the ratio between the maximum and minimum intensity received by a target (**Fig. I.21**). The pedestal height is an indicator of the presence of a not polarized scattering component, and therefore of the degree of polarization of a scattered wave (McNairn et al., 2004).

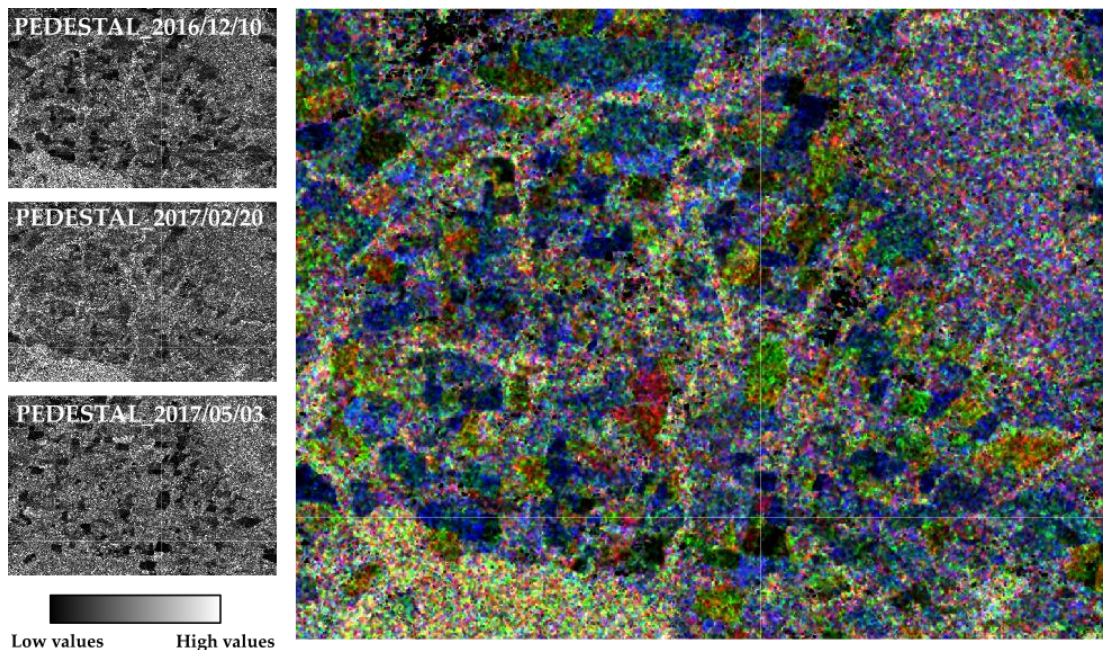


Figure I.21: Illustration of Pedestal Height (PED) parameter derived from a Radarsat-2 images using a RGB color composition. PED from 10 December 2016 in Red (R); PED from 20 February 2017 in Green (G); PED from 03 May 2017 in Blue (B).

The interpretation of the polarimetric parameters depends on several factors, including the roughness and humidity of the targets. Roughness is a function of wavelength and angle of incidence. Thus, a surface will be considered rough if the variations in height of the illuminated surface are greater than the wavelength used. Humidity directly influences the intensity of the backscattered signals. Thus, the more humid a surface is, the more reflectivity will increase (Ulaby and Elachi, 1990).

II.3. Identification and characterization of winter land-use using remote sensing data

II.3.1. Introduction

The identification and characterization of winter land-use is still a major environmental and scientific challenge. From an environmental perspective, the presence and type of vegetation is a decisive factor in biogeochemical and ecological processes (*Section I.4*). From a scientific viewpoint, the spatial and temporal characterization of winter land-use dynamics at field scale remains a considerable challenge for the scientific community. In this context, the contributions of remote sensing images have an important function in monitoring winter land-use. While optical remote sensing data have already shown interest in studying land use, several questions arise about their effectiveness in winter when meteorological conditions may affect the acquisition of optical images. On the other hand, SAR remote sensing, which is known to overcome most meteorological conditions, has still faced very few problems in identifying and characterizing land-use in winter. The purpose of this section is to provide an overview of the research carried out using remote sensing data for the identification and characterization of winter land-use.

II.3.2. Study of winter land-use based on optical data

The development in the 1970s of the first optical Earth observation satellites opened the era of modern remote sensing. The constant development of sensors and methods for processing digital data has broadened the application scope of remote sensing, which has become, in the space of a few decades, an essential tool for the inter and intra-annual study and monitoring of land use at different scales. A scientific milestone was marked in particular by the improvement of sensors, whose spatial, temporal and spectral resolutions have continued to increase, allowing new opportunities to meet this issue.

At the end of the 1990s, the emergence of new efficient optical sensors with medium spatial resolution such as MODIS or SPOT-Vegetation (250m and 1km respectively) quickly became valuable instruments to study the evolution of vegetation on a global scale. In this context, a large number of research works have been carried out on the interest of these new satellites for the identification and characterization of land use or land cover. Jakubauskas et al., (2002); Sakamoto et al., (2005); Tottrup and Rasmussen, (2004); Wardlow and Egbert, (2008) and Zhang et al., (2003) demonstrated the potential of the MODIS satellite to identify and characterize crop areas and their long-term evolution on large scales. Similarly, Khan et al., (2010) were able to present the capacities of the SPOT-Vegetation satellite, in order to identify and map crops with an accuracy of around 90%. However, the spatial resolution of such sensors quickly became a constraint to a detailed study of land use and land cover. Despite the development of new methodologies using medium-resolution pixel unmixing to classify crop areas more accurately (Ozdogan, 2010; Verbeiren et al., 2008), the accuracy obtained by these methods is still insufficient to meet the expectations of scientists and decision-makers. For this reason, very few studies have so far focused on monitoring winter land-use using these data, whose spatial resolution remains insufficient, as highlighted in the work of (Lecerf et al., 2005), who consider that the low number of studies carried out is mainly due to an insufficient spatial resolution to observe only patches, thus limiting the identification of winter land-use classes.

With the evolution of spatial technologies, the deployment of high spatial resolution sensors with ever-increasing performance has allowed new opportunities for the identification and characterization of winter land-use. High-resolution data have quickly emerged as a reliable source of information for inter-annual land-use monitoring. The works of Guerschman et al., (2015) and Xu and Guo, (2014) in this way demonstrate the potential of Landsat-8 time series (30 meters of spatial resolution) for inter-annual monitoring of land use and land cover at the regional scale. From 2010, the launch by the European Space Agency (ESA) of a new series of sensors (Sentinel Constellation) with a high spatial resolution (10m) and very high temporal resolution (6 days), has allowed more accurate land-use monitoring to be carried out. The research of Immitzer et al., (2016) and Vuolo et al., (2018) are some examples. These studies show the potential of the Sentinel-2 optical time-series for annual crop mapping, with overall accuracies ranging from 76% to 96% depending on the land-use classes. However, despite numerous research studies on summer crop mapping and inter-annual evolution, only a few studies have highlighted the potential of high spatial resolution time series for intra-annual land-use monitoring (especially in winter). Martínez-Casasnovas et al., (2005) and Radoux et al., (2016) are among the first works to highlight the potential of optical data for studying intra-annual changes in land use and land cover. In their approaches, they present the advantages of the Landsat-8, Sentinel-2 and Spot-5 time-series for detecting changes in land use and land cover during the growing season with an overall accuracy of around 90%. However, to date, no work has been conducted to identify precisely winter land-use using optical time-series, particularly due to weather conditions during the winter period.

On a fine scale, the use of very high spatial resolution optical data is currently employed by a large community to develop land-use maps. Gressin et al., (2014); Kuenzer et al., (2015) and Vaudour et al., (2015) have thus shown the potential of very high spatial resolution data Pleiades for 1) crop identification; 2) studying land-use changes at fixed dates; 3) identifying cultural practices in the summer season. Nevertheless, the characterization of surface variations such as soil surface condition and vegetation growth conditions are phenomena that evolve daily and whose mechanisms remain essential for the study of winter land-use but remain unexplored (Pacheco and McNairn, 2010). Indeed, the characteristics of very high spatial resolution sensors complicate the implementation of intra-annual land-use monitoring due to a low temporal resolution (with a revisit time of several tens of days).

Thus, time-series obtained from optical satellites with medium, high or very high spatial resolution have already demonstrated their potential to identify and characterize the inter-annual evolution of agricultural areas. However, they are still under-exploited in order to study intra-annual evolution and changes in land use in winter mainly due to weather and atmospheric conditions but also sensors characteristics. This absence of information represents the main issue for scientists and decision-makers in order to establish strategies to limit the negative impact of our societies on the environment. However, the development in the 1990s of SAR satellites allowed new possibilities in order to overcome the lack of information.

II.3.3. Study of winter land-use based on SAR data

The launch in the 1990s of improved SAR sensors has opened up new opportunities for monitoring, identifying and characterizing land use, particularly in winter. Opportunities enhanced by SAR sensors' insensitivity to illumination and weather conditions, and their ability to obtain information on the physical properties of a target (dielectric constant, size, shape or distribution) (Skriver, 2011) as mentioned in *Section II.2.2.* which may facilitate a more effective discrimination of land use (Hosseini et al., 2015; Ulaby et al., 1986).

The potential of SAR imagery has been quickly demonstrated by several studies, which are highlighted the importance of SAR parameters (such as backscatter coefficients or polarimetric variables) for land-use classification. The works of Jiao et al., (2014); Larrañaga and Álvarez-Mozos, (2016) and Liu et al., (2012) are perfect examples. These studies have presented the potential of SAR parameters (backscatter coefficients, polarimetric indicators, etc.), extracts from Radarsat-2 C-Band images for mapping and monitoring land use, with an overall classification accuracy of over 85%.

In addition, the physical characteristics of SAR sensors such as frequency or incidence angle have also been the subject of extensive investigations. This enthusiasm for the use of physical properties is related to their importance in the discrimination of vegetation cover by the SAR signal. For example, wavelength penetration into the vegetation canopy remains more important using the L-Band (~20 cm) than C-Band (~5.5 cm). Conversely, C-Band will interact more with the upper canopy, while L-Band will generate greater interaction with the ground below the canopy (Ulaby et al., 1986). Thus, these allow us to set up appropriate monitoring and discrimination according to the vegetation cover and the areas studied. In this context, numerous studies have been undertaken in order to determine the potential of frequency bands for the study of agricultural areas. Abdikan et al., (2016); Bargiel, (2017) and Hong et al., (2015) have thus presented the interest of the C-Band for the identification and classification of land cover and land use using Sentinel-1 or Radarsat-2 data with overall accuracies ranging from 78% to 93%. Wiseman et al., (2014) and Yang et al., (2017) have highlighted the value of C-Band SAR imaging for determining phenological stages and estimating crop biomass using RADARSAT-2 polarimetric images with accuracy better than 80%. Similarly, several studies have also demonstrated the interest of other frequency bands, such as the X or L-Band for monitoring, identifying and classifying land use. Haldar et al., (2012) and Zhang and Wu, (2011) have thus demonstrated the potential of L-Band for land-use classification based on supervised approaches (Deep learning and Maxlike) with overall accuracies above 90%. Kemp and Burns, (2016) presented new methods based on X-Band radar interferometry to detect plowing and crop planting periods in South Africa for agricultural monitoring purposes.

In this context, highlighting the interest of the various frequency bands for the identification, characterization, and monitoring of agricultural practices, studies have focused on the complementarity of these frequency bands for these thematic approaches. Thus, McNairn et al., (2009); Paloscia et al., (2015) and Skriver, (2011) have shown the benefits of combining SAR data from X and C-Bands but also from C and L-Bands to monitor and map agricultural areas with overall accuracy ranging from 84 to 95%.

Nevertheless, despite a demonstrated potential for land-use classification and monitoring, to date, only a few researches have highlighted the potential of SAR imagery for the fine identification and characterization of land use during the winter season. The works of Baghdadi et al., (2008) McNairn et al., (2004) and Wang et al., (2016), are the main demonstrators. Based on different wavelengths (L, C and X-Bands), they highlighted the

relevance of the SAR signal in order to characterize bare soils and crop residues. In a similar context, El Hajj et al., (2009) and Hong et al., (2015) also highlighted the interest of these data for monitoring and discriminating grasslands by using time-series or single date data with an overall accuracy of over 70%. However, the monitoring, identification, or characterization of winter land-use remain mainly limited to these three classes. More recently, the works of (Minh et al., 2018) have demonstrated the ability of C-Band SAR sensors to map field coverage rates during the winter period, an essential factor to reduce environmental risks, but without defining land-use classes, which is also a key factor (*Section I.4*). Thus, to date, no information is available to finely identify and characterize winter land-use classes (mentioned in *Section I.3*), such as catch crops that play a key role in regulating agricultural pollutant transfers to the environment.

Thus, SAR imagery has demonstrated its potential to implement monitoring and mapping of land-use at different scales. Nevertheless, in a current context where fine and detailed information on winter land-use is needed to help decision-makers, only a few studies using SAR imagery have put in place to obtain such information. However, the use of new Sentinel sensors (Constellation Sentinel) with similar physical characteristics (spatial and temporal resolution) in the optical and radar wavelengths has opened up opportunities for the detailed identification and characterization of winter land-use from data fusion methods.

II.3.4. Study of winter land-use based on merged optical and SAR data

Optical imagery is currently considered to be a robust and suitable tool to discriminate land-use patterns. SAR imagery, for its part, through the acquisition of information on the physical properties of a target (roughness, humidity, shape, size, etc.), allows a detailed characterization of land-use changes but remains limited regarding the fine discrimination of land-use types. In this sense, the complementarity of these two types of data is assumed to provide optimal information for land-use identification and characterization (Joshi et al., 2016). In this context, the data fusion was the subject of a few studies. Inglada et al., (2016); Steinhausen et al., (2018) and Van Tricht et al., (2018) have highlighted the synergy of Sentinel sensors for inter-annual analysis and mapping of land cover and land use. These studies shown in particular that the combined use of optical ("Sentinel-2") and SAR ("Sentinel-1") sensors increase the overall accuracy of classifications from 5 to 10%. Several studies have also shown the benefits of the Radarsat-2 and optical data synergy. For example, the works of Pereira et al., (2013) and Skakun et al., (2015) have demonstrated the potential of Radarsat-2 imagery combined with optical data, such as Landsat-8 for crop classification and monitoring with an accuracy of over 80%.

However, despite the proven complementarity of optical and SAR images for land-use identification and characterization, their effectiveness for studying winter land-use remains unexplored. Nevertheless, some studies have shown the value of combining this type of data in order to analyze and characterize specific land-use classes such as grasslands Dusseux et al., (2014) and Fieuzal et al., (2013). However, no scientific studies have so far highlighted the potential of optical and SAR data fusion for the detailed identification and characterization of winter land-use classes. In this context, this thesis attempts to evaluate the potential of optical and SAR time series alone or in complementarity for the study of winter land-use at a local and regional scale.

Chapter 3

Study sites and data

Contents

III.1. INTRODUCTION	51
III.2. STUDY SITES	51
III.3. REMOTE SENSING DATA	55
III.4. FIELD MEASUREMENTS	61

III.1. Introduction

The identification and characterization of winter land-use realized in this thesis and based on multi-scale approaches were carried out over two study areas: i) the Zone Atelier Armorique, (ZAA) (at the local scale); ii) Brittany (at the regional scale). This chapter presents, in a first step, the study sites selected to identify and characterize winter land-use. In a second step, it describes the data used during this thesis, remote sensing data but also field campaigns data.

III.2. Study sites

III.2.1. « Zone Atelier Armorique »

A “Zone Atelier” represents a research system accredited by the National Center for Scientific Research (CNRS) whose the main objective is the implementation of interdisciplinary research on the environment and anthropo-systems in relation to societal issues (“ZAA,” 2019). Research carried out over the long term who’s a partnership with local actors, allowing collaborations in order to support the decisions and actions of decision-makers.

The French territory counts 14 “Zone Atelier” extending from Brittany to Antarctica representing a range of contrasting and complementary areas from the perspective of social environments and systems (“Zone Atelier,” 2019). These areas are structured through European (Long-Term Ecological Research, LTER-Europe) and global (International Long-Term Ecological Research, ILTER networks) networks. These networks make it possible to study the complex relationships between human activities and ecosystem functioning over different territories.

The “Armorique” zone, included in the department of Ille-et-Vilaine (Brittany, France), is divided in three territories representing distinct landscape entities in which interdisciplinary researches on the environment and anthropo-systems are carried out: i) The city; ii) the alluvial plain (part of the study area); iii) the hedgerow network landscape.

The city is represented by Rennes Metropole (France), which has been regularly monitored since 2011. It refers mainly to an urban observatory set up on the Saint-Martin meadows site, to rehabilitate a former industrial site into an urban park.

The alluvial plain represents a marsh zone located in the south of Mont-Saint-Michel (France), she uses as a grazing area for herds from spring to autumn. This area has been monitored since 2006 as a wetland of high heritage with fauna and flora interest. In this thesis, this area is referred to as grazed grassland in the land-use nomenclature.

Finally, the hedgerow network landscape, the subject to this thesis, is represented by the Pleine-Fougères agricultural area located in the southern part of the Bay of Mont-Saint-Michel (N 48°31'0", W 1°31'30"), in France (**Fig. I.22**). This area, referenced within the LTER and ILTER networks, has been monitored since 1993, mainly for land-use studies. It is characterized by a landscape gradient ranging from a dense hedgerow network in the south, with small fields, to a loose hedgerow network in the north. With a temperate climate, an average annual temperature above 12°C (minimum average above 8°C, maximum average 16 °C) and average annual rainfall ranging from 600 to 700 mm, this site of 9,400 ha includes approximately 7,000 agricultural parcels, who’s the size varies from 0.1 to 65 ha, with an average of 2.1 ha. The

agricultural landscape, dominated by "polyculture-livestock" production systems, is characterized by structural variability (plot size, hedge density) due to soil and subsoil characteristics. In summer, vegetable crops are grown on the northeastern part of the site, which is characterized by alluvial soil; in the northwest and south half of the site, many grasslands and field crops are cultivated because of granitic and schistous subsoils.

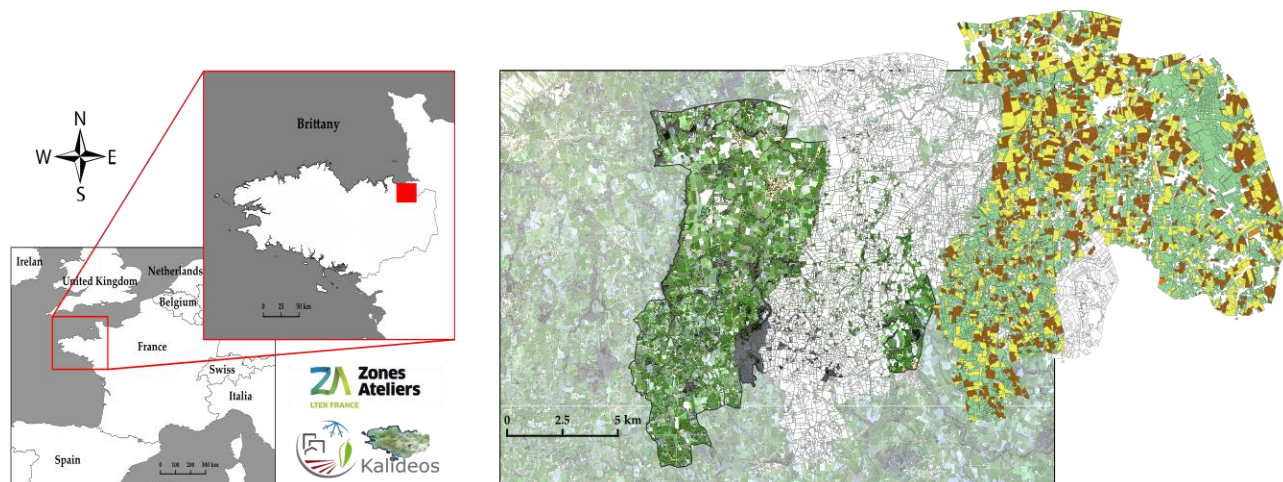


Figure I.22: Location of the « Zone Atelier Armorique », sub-site of « Pleine Fougères ».

In winter, the agricultural system is characterized by the establishment of winter land-use required and regulated by the "Nitrates directive" (*Section I.3.1*) ("Nitrates Directive," 2019), in order to reduce the agricultural pollutants transfers to the environment. This winter land-use is represented through a 5-class classification: winter crops, catch crops, grasslands as a permanent crop, crop residues and temporary bare soils. Nevertheless, the research conducted in this thesis, have demonstrated that bare soil class referred (for the Brittany region) to a temporary surface state between the harvest and the growth of a main crop. As a result, it could not be defined as a winter land-use class (**Table I.4**).

Table I.4: Winter land-use classification.

Winter land-use types	Main Crops
Winter Crops	Winter wheat Winter barley Rapeseed
Grasslands	Mown grasslands Grazed grasslands
Catch crops	Oat Fodder cabbage Ray-grass and clover Phacelia Phacelia and mustard Phacelia and oat
Crop residues	Maize stalks
<i>Temporary Bare soils</i>	<i>None</i>

These winter land-use types are spread over the entire Utile Agricultural Area (UAA) of the "Zone Atelier Armorique" (ZAA) with fluctuating proportions:

- ✓ Winter crops, which represent 44% of the UAA. They refer to winter wheat, winter barley, and rapeseed. Wheat and barley, sown from October onwards, are characterized by similar phenology and structures. The differentiation is made during the harvest period, in June for barley and in July for wheat. The rapeseed is sown in September to be harvested in July the following year. It is characterized by a vertical structure without a defined shape but a large height (up to 2m).
- ✓ Grasslands, which can be grazed or mowed, represent about 30% of the UAA and play a main role in regulating agricultural pollutants transfers.
- ✓ Catch crops, sown from August to October, they cover 25% of the UAA. They are quite diverse in terms of structure and phenology but also in terms of utility.
- ✓ Crop residues, which represent 1% of the UAA. They correspond to the maize stalks left in the fields after a harvest.

III.2.2. Brittany

Brittany, located in the far west of France (**Fig. I.23**), is a 27,209 km² area characterized by an oceanic climate with an annual average temperature above 12°C, a minimum average for the coldest year above 8°C, a maximum average above 16°C and an average of annual rainfall between 600 and 700mm. With a UAA of 1,699,363 hectares divided into 4 departments, representing 53% of its territory, Brittany is the second agricultural region in France ("CCI Bretagne," 2017). With 2% of its population (1% in France) working in the primary sector, and 6% in the agri-food sector (2% in France), Brittany is the leading production region in several sectors such as tomatoes, pigs and poultry production ("Agreste," 2017). In summary, with about 30,000 farms recorded, the wealth generated by agriculture and agri-food represent about 8% of regional GDP in 2015 ("Agreste," 2017).

In summer, Brittany's agricultural system is divided into four crop production sectors:

- ✓ Cereal production, which represents in 2015 about 20% of the UAA, is dominated by the production of soft wheat, barley, and triticale.
- ✓ Vegetable production, which represents approximately 10% of the UAA, is mainly composed of Tomatoes, cauliflower, and Artichokes and makes Brittany the leading French region in the vegetable sector.
- ✓ Oilseeds-Protein crops production, which is mainly limited to the production of rapeseed (88% of the surface area associated with this production). It includes less than 3% of the UAA.
- ✓ Fodder production, the largest production sector in Brittany with nearly 63% of the regional UAA (against 49% at the French level). It is mainly composed of forage corn, temporary or permanent grassland but also fodder rapeseed or Ryegrass.

In winter, with 98% of its territory subject to a Nitrogen flow declaration, Brittany is one of the most affected French regions to environmental risks such as agricultural pollutants transfers (nitrates, phosphorus...). The establishment of winter land-use is therefore highly regulated and controlled by the European authorities (*Section I.3*).

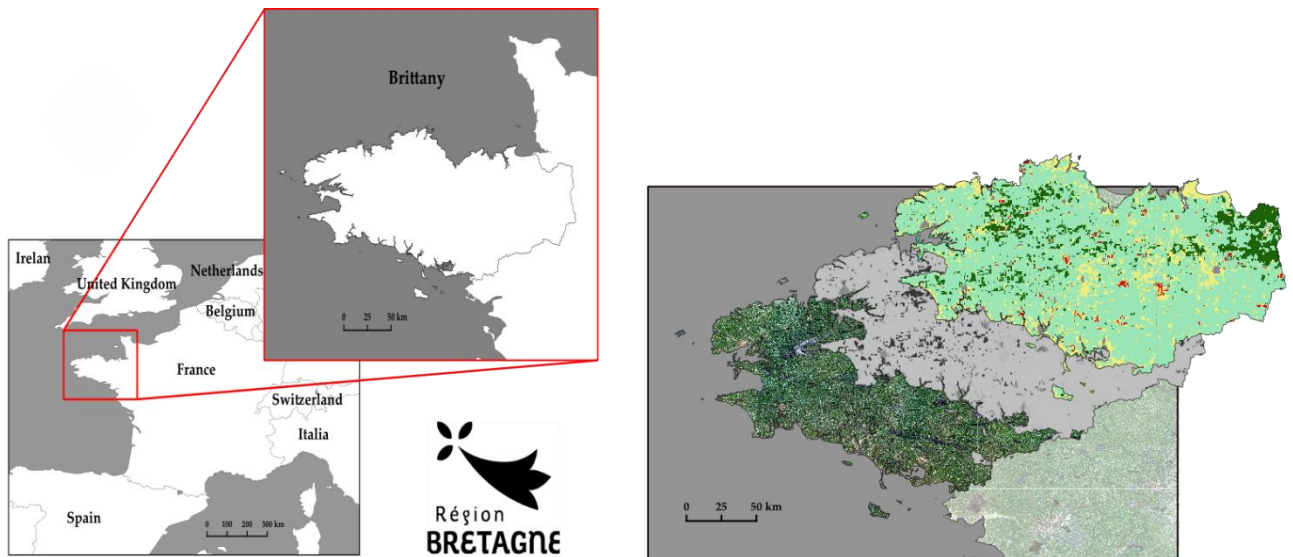


Figure I.23: Location of the regional study site, Brittany.

III.3. Remote sensing data

III.3.1. Images

A set of 6 optical and SAR time-series images was acquired in this thesis. These time-series include Sentinel-2 (S2) images for optical data, and Sentinel-1 (S1), Radarsat-2 (RST-2) and Alos-2 (AL-2) images for SAR data. They were acquired through collaborations with scientific programs and institutions (“Gis Bretel,” 2017; “Kalideos,” 2019; “VIGISAT,” 2019).

III.3.1.1. Optical images

III.3.1.1.1. Local-scale

At the local scale, a time series of 9 Sentinel-2 optical images was acquired between August 2016 and May 2017 by the European Space Agency (ESA) and provided by the Copernicus scientific hub (“Open Access Hub,” 2019). These images obtained at level 1C (i.e. corrected for geometric effects) were acquired with a spatial resolution ranging from 10 to 60 meters and a spectral resolution of 13 bands. Their characteristics are summarized in **Table I.5** below.

Table I.5: Sentinel-2 images. NIR: Near-infrared, SWIR: Shortwave-infrared.

	SENTINEL-2
Spatial resolution	10 m to 60 m
Spectral resolution- central wavelength (μm)	Band 1 (Coastal) – 0.443μm Band 2 (Blue) – 0.490μm Band 3 (Green) – 0.560μm Band 4 (Red) – 0.665μm Band 5 (Red Edge) – 0.705μm Band 6 (Red Edge) – 0.740μm Band 7 (Red Edge) – 0.783μm Band 8 (NIR) – 0.842μm Band 8A (NIR) – 0.865μm Band 9 (Water) – 0.940 μm Band 10 (SWIR) – 1.375 μm Band 11 (SWIR) – 1.610μm Band 12 (SWIR) – 2.190μm
Coverage	290 km
Dates (M-D-Y)	08-22-2016 10-31-2016 11-30-2016 12-20-2016 01-19-2017 02-18-2017 04-09-2017 05-09-2017

III.3.1.1.2. Regional-scale

At the regional scale, a time series of 51 Sentinel-2 optical tiles was acquired between September 2016 and May 2017 by the European Space Agency (ESA) and provided by Theia continental surface and services cluster data hub ("Theia," 2019). This hub has three objectives:

- ✓ Build a common system capable of producing spatial data (from local to global scale) with added value for the scientific community and provide services in line with users' needs.
- ✓ Encourage the sharing of experience and the capitalization of methods.
- ✓ Make national achievements visible at European and international level.

These images acquired at level-2A (i.e. corrected for geometric and atmospheric effects) were obtained with a spatial resolution ranging from 10 to 20 meters and a spectral resolution of 10 bands. The atmospheric corrections made in order to obtain the 2A-level were performed using the MACCS ATCOR Joint Algorithm (MAJA) preprocessing chain developed by the Centre d'Etudes Spatiales de la BIOSphère (CESBIO). MAJA is a chain for cloud detection, atmospheric correction and adapted for processing time-series of high-spatial-resolution images acquired from constant or almost constant angles of view ("MAJA," 2019).

III.3.1.2. SAR images

At the local scale, three SAR time-series images have been acquired, with the corresponding characteristics are summarized in **Table I.6**:

III.3.1.2.1. Sentinel-1 time-series

A time series of 22 Sentinel-1 (S1) images was acquired from August 2016 to May 2017 by the European Space Agency (ESA) and provided by the data hub ("Open Access Hub," 2019). S1 images were obtained in Single Look Complex (SLC) mode (delivered in dual-polarization mode with VH and VV polarization channels) with an incidence angle ranging from 31° to 46°. The range and azimuth spatial resolutions are respectively equal to 2.3 and 13.9 m.

III.3.1.2.2. Radarsat-2 time-series

A time series of 10 Radarsat-2 images was acquired between October 2016 and May 2017 by MacDonald, Dettwiler, and Associates (MDA) and provided in the frame of the "Groupement Bretagne Télédétection" (GIS Bretel) by the VIGISAT ground station managed by CLS. These images were obtained in SLC mode (delivered in quad-polarization mode with HH, HV, VH and VV polarization channels) with an incidence angle of 35°, and range and azimuth resolution are 8.2 and 4.7 meters respectively.

III.3.1.2.3. Alos-2 time-series

A time series of 6 Alos-2 (AL-2) images was acquired from January 2017 to June 2017 by the Japanese Space Agency (JAXA) and made available by the Kalidéos program ("Kalideos," 2019). The AL-2 images were obtained in SLC format (delivered in dual-polarization mode with HH and HV polarization channels) with an incidence angle of 40°, and range and azimuth resolution are 1.4 and 1.9 meters respectively.

Table I.6: Characteristics of the RADARSAT-2, Alos-2, and Sentinel-1 SAR images.

	Radarsat-2	Sentinel-1		Alos-2
Dates (M-D-Y)	10-23-2016	08-25-2016	01-16-2017	01-04-2017
	11-16-2016	09-18-2016	01-28-2017	02-04-2017
	12-10-2016	09-30-2016	02-09-2017	03-06-2017
	01-03-2017	10-12-2016	02-21-2017	04-15-2017
	01-27-2017	10-24-2016	03-05-2017	05-13-2017
	02-20-2017	11-05-2016	03-17-2017	06-10-2017
	03-16-2017	11-17-2016	03-29-2017	
	04-09-2017	11-29-2016	04-10-2017	
	05-03-2017	12-11-2016	04-22-2017	
	05-27-2017	12-23-2016	05-04-2017	
			01-04-2017	05-16-2017
Ground resolution	8.2 m	2.3 m	1.4 m	
Azimuth resolution	4.7 m	13.9 m	1.9 m	
Frequency	C-Band	C-Band	L-Band	
Polarization	Quad (HH-VV-HV-VH)	Dual (VV-VH)	Dual (HH-HV)	
Mode	Fine Quad Polarization (SLC)	Interferometric wide (SLC)	Spotlight (SLC)	
Incidence angle	35° (right descending)	31°-46° (right descending)	40° (Left ascending)	
Coverage	18 km x 25 km	> 250 km x 100 km	25 km x 25 km	

III.3.2. Time-series pre-processing

Pre-processing were then performed on the recovered optical and SAR time-series images. These pre-processing differ according to the thematic approaches studied. In this section, we present only the basic and common pre-processing for Optical and SAR time-series.

III.3.2.1. Pre-processing of optical time-series

III.3.2.1.1. Local-scale

Sentinel-2 optical images obtained from the Copernicus Scientific Data Hub in level-1C were orthorectified and georeferenced based on the Universal Transverse Mercator (UTM, area 30N) reference system. The first step of pre-processing was to assess the accuracy of the corrected images. Then, Sentinel-2 images were corrected from atmospheric effects using Sen2Cor toolbox from the Sentinel Application Platform (SNAP) software v6.0.

Sen2Cor is a Level-2A (L2A) processor that corrects single-date Level-1C Sentinel-2 products from atmospheric effects to provide a L2A surface reflectance product (Louis et al., 2016). Afterward, Sentinel-2 images were resampled to 10 meters' resolution based on the blue band (Band 2) in order to derived optical descriptors. Two vegetation indices were then derived from the Near-infrared (NIR) and Red (R) bands using SNAP v6.0 software: The NDVI and the SAVI. The NDWI was also calculated from the Near-infrared (NIR) and Mid-infrared (MIR) bands. These 3 indices were chosen due to their ability to highlight different processes related to vegetation such as water stress, growth peak, or phenological stage (Gu et al., 2008; Panda et al., 2010; Veloso et al., 2017).

III.3.2.1.2. Regional-scale

Sentinel-2 optical images retrieved from the Theia hub in L2A were orthorectified, geo-referenced based on the UTM (area 30N) reference system but also atmospherically corrected from the MAJA chain. Similarly, to the local scale, an assessment of corrected images accuracy was performed. Then, a single vegetation index was calculated, the NDVI using SNAP v6.0 software. Finally, the NDWI was derived from the Near-infrared (NIR) and Mid-infrared (MIR) bands.

III.3.2.2. Pre-processing of SAR images

III.3.2.2.1. Local-scale

SAR images have been pre-processed using SNAP v6.0 or v5.0 and PolSARpro v5.1.3 or v6.0 software (Pottier et al., 2018) and according to the adopted thematic approaches. These approaches will be detailed in the next chapter.

III.3.2.2.1.1. Backscattering coefficients

- i. The first step was to radiometrically calibrate SAR time-series from the appropriate equations for each time-series using SNAP v6.0 software:

Sentinel-1 (Miranda and Meadows, 2015) :

$$values(i) = \frac{DN_i I_i^2}{A_i^2} \quad (\text{Eq. I.18}).$$

where DN is the digital number of each pixel (i) (amplitude of backscattering signal) and A is the information required to convert SAR reflectivity into physical units provided in the Calibration Annotation Data Set in the image metadata. The equation transforms the DN of each pixel into a backscattering coefficient on a linear scale (Eq. I.18).

Radarsat-2 ("Radarsat Products," 2019) :

$$\sigma_j^o = \beta_j^o + 10 * \log_{10}(\sin I_j) \quad (\text{Eq. I.19}).$$

Where β is the radar brightness and I_j is the incidence angle at the j^{th} range pixel. The formula assumes that Earth is a smooth ellipsoid at sea level (Eq. I.19).

Alos-2 (Lavalley and Wright, 2009) :

$$\sigma_{ij}^0 = K \cdot DN_{ij}^2 \quad (\text{Eq. I.20}).$$

Where K is an absolute calibration constant and DN is the intensity value of a pixel in the i line and j column (Eq. I.20).

- ii. The second step was to apply a spectral filter on the calibrated images in order to reduce speckle effects. Following the thematic approach, two filter types were applied:
 - ✓ A Lee refined 7×7 filter applied with SNAP v5.0 software (Lee, 1981).
 - ✓ A Lee Sigma 7×7 filter with a sigma value of 0.7 or 0.8 applied with SNAP v6.0 (Lee et al., 2008).

The selection of a filter was first made based on the scientific literature. The Lee Refined filter was retained as a baseline filter in many studies using SAR data. In a second time, a set of tests was performed to improve the filter selection (Fig. I.24). The Lee Sigma filter was then selected for its ability to maintain target information and variability.

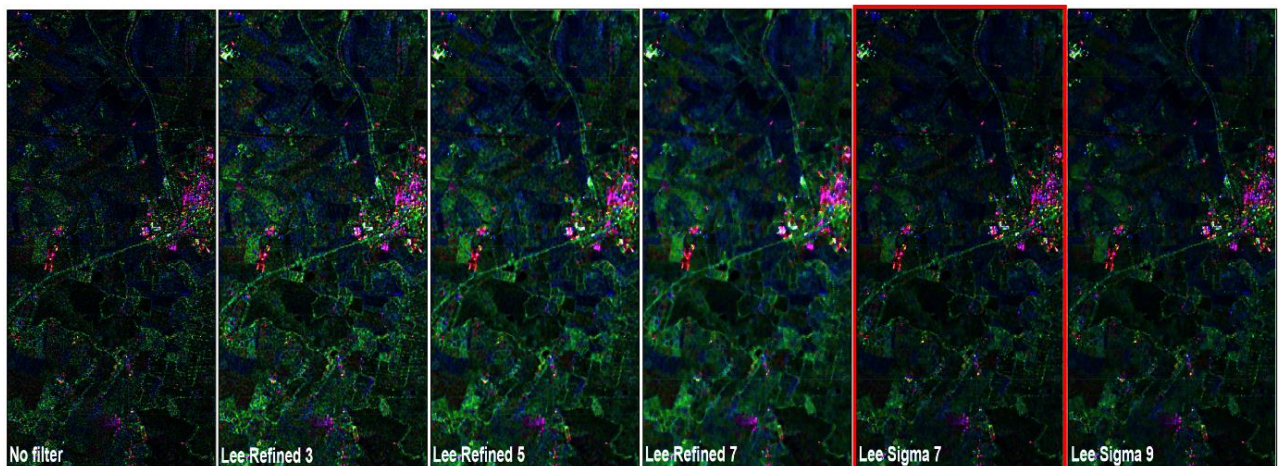


Figure I.24: Test results performed on Radarsat-2 images with different filters and window sizes.

Regarding the window sizes, a size of 7×7 was chosen in order to optimize the reduction of speckle noise while preserving an appropriate spatial scale necessary to ensure the identification and characterization of winter land-use.

- iii. The third step was to correct the images of the topographical deformations using a digital Terrain model "Shuttle Radar Topography Mission 3s (SRTM)". Image resolution was then modified to fit with the thematic approaches and will be detailed in the following chapters. These images were also geometrically corrected and geo-referenced in a suitable projection system.
- iv. Finally, the last step consisted to perform ratios and/or differences (adapted to the studies) from the corrected backscatter coefficients and to convert all the indicators (backscatter coefficients, backscatter coefficients ratios, and backscatter coefficients differences) into decibels using the following equation (Eq. I.21):

$$\sigma^0(\text{db}) = 10 \times \log_{10}(\sigma^0) \quad (\text{Eq. I.21}).$$

III.3.2.2.1.2. Polarimetric parameters

Similar to the backscatter coefficients, the polarimetric parameters were extracted according to the thematic requirements. We will introduce here only the pre-processing general framework carried out to extract the polarimetric indicators, the whole pre-processing will be detailed in the following chapters.

Quad-polarization mode

Pre-processing performed for full-polarization mode time-series can be summarized in 4 steps:

- ✓ Extraction of a 3×3 coherency matrix T_3 from the scattering matrix (S) using PolSARpro v5.1.3 software.
- ✓ Application of a Lee sigma filter with a window size of 7×7 and a sigma value of 0.8.
- ✓ Correction of T_3 matrix elements of topographic deformations and orthorectification using SNAP v6.0 software with a SRTM digital terrain model.
- ✓ Extraction of polarimetric parameters, which are the following:
 - i. Cloude-Pottier decomposition, computed from the matrix T_3 , is the eigen-decomposition of the coherency matrix T_3 into three independent coherent elements: (i) the entropy (H), which expresses the randomness of the scatter; (ii) the alpha angle (α), which describes the dominant scattering mechanism; and (iii) the anisotropy (A), which represents the relative power of the second mechanism. In addition, 4 parameters based on Cloude and Pottier decomposition entropy (H) and anisotropy (A) were calculated: $H * A$; $H * (1 - A)$; $(1 - H) * A$; $(1 - H)(1 - A)$.
 - ii. Freeman-Durden decomposition is used to modeling the covariance matrix 3×3 (C_3) into three scattering mechanisms: The volume diffusion (Freeman VOL), double bounce diffusion (Freeman DB) and surface or single bounce diffusion (Freeman SB).
 - iii. The SPAN, which corresponds to the total scattered power.
 - iv. The Shannon Entropy (SE), which corresponds to the sum of two contributions related to the intensity (SE_i) and the degree of polarization (SE_p), see (Eq. I.16).
 - v. The Radar Vegetation Index (RVI), see (Eq. I.17).
 - vi. The Pedestal height, a ratio of the maximum received intensity to the minimum received intensity.

Dual-polarization mode

In dual-polarization the pre-processing also involves 4 steps:

- ✓ Extraction of a 2×2 covariance matrix (C_2), computed using PolSARpro v5.1.3 software.
- ✓ Application of a Lee Refined or Lee sigma filter (according to the thematic studies) with a window size of 7×7 and a sigma value of 0.8.
- ✓ Correction of C_2 , matrix elements from topographic deformations and orthorectification using SNAP v6.0 software with a SRTM digital terrain model.
- ✓ Extraction of the following polarimetric parameters: SPAN, Shannon Entropy and its intensity and polarization derivatives.

III.4. Field measurements

III.4.1. Data

As part of this thesis, a set of field campaigns framed by a predefined protocol was conducted in correlation with the optical and SAR time-series acquisition between October 2016 and May 2017. These campaigns have been set up to obtain precise and spatialized information on the winter land-use and their practices in the ZAA of Pleine-Fougères. Two types of surveys were carried out during the field campaigns. Land-use records on the one hand and detailed surveys with farmers on the other hand.

III.4.1.1. Measurement protocol

To achieve the objectives mentioned in *Section II.3*, a field protocol was implemented to evaluate the optical and SAR time-series for the identification and characterization of winter land-use at the Pleine-Fougères site. This protocol consists of the development of 2 field campaigns in order to obtain precise and spatialized information on land use during winter 2016-2017. It was developed in collaboration with “INRA UMR SAD paysages”, as an upstream part of the European project BIODIVERSA WOODNET, which aims to characterize the internal heterogeneity of landscape elements in an ecologically or agronomically relevant manner.

III.4.1.2. 1st campaign: Land-use records

In order to identify and finely characterize the winter land-use classes using time-series images, land-use records were conducted from October 2016 to November 2016 on a set of 415 parcels heterogeneously distributed throughout the ZAA, shown in **Figure I.25**. For each parcel surveyed, a crop code and land use were defined.

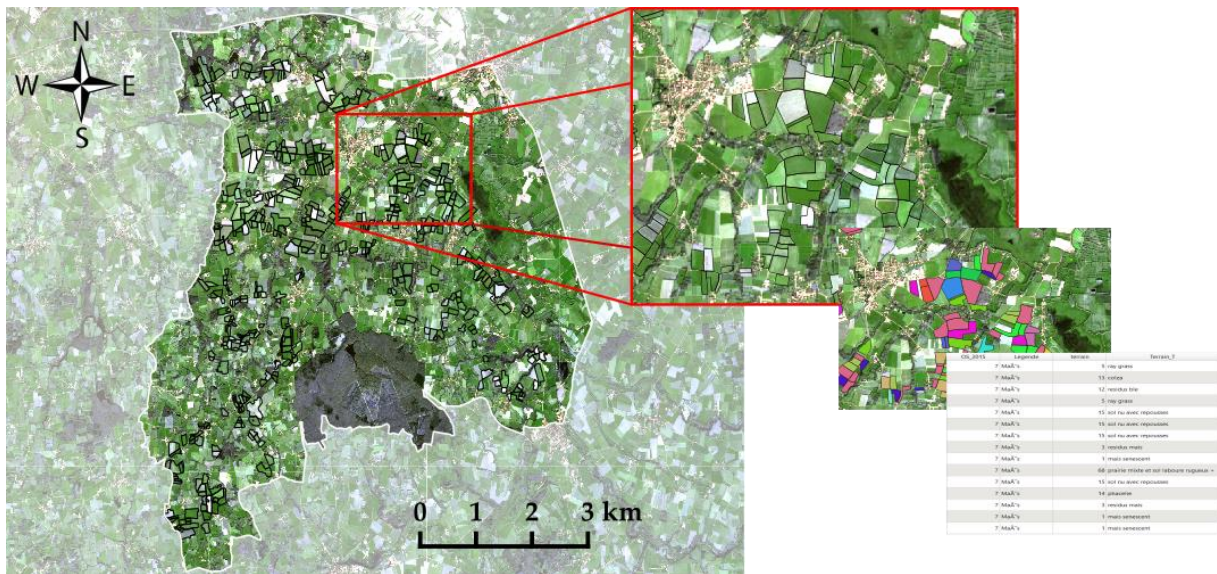


Figure I.25: Localization and illustration of land-use records.

III.4.1.3. 2nd campaign: Land-use surveys

To obtain more detailed information about winter land-use and the associated practices during the October 2016 to May 2017 period, surveys were conducted with farmers. First, a farmers' pre-selection was carried out using a database referencing all ZAA farmers provided by "INRA SAD paysages". This pre-selection allowed us to keep 30 farmers who might be relevant according to their exploitation (hectares cultivated in particular) and their previous collaborations in research projects. Among these 30 farmers, 10 were retained to conduct field surveys due to their availability (lack of time, cessation of activity, closed farm) and denial of participation.

These 10 surveys provided us accurate and spatialized information about 231 parcels spread over the entire ZAA (Fig. I.26). The information retrieved was as follows (An example is given in *Appendix 3*):

- ✓ Farm data:
 - Name of the farm and personal information (name of the farmer, address, phone number).
 - Year of installation.
 - Total area exploited (hectares).
 - Part of the farm in UAA.
 - The surface of the spreadable UAA.
 - Livestock farming.
 - If so, what type of livestock?
 - Their opinion on the contribution of effluents and winter land-use.
- ✓ Field data:
 - Crops 2015-2016
 - Harvest date
 - Crops 2016-2017
 - Sowing date

- Catch crops
- Date and method of catch crops establishment
- Date and method of catch crops destruction or harvest
- Other practices

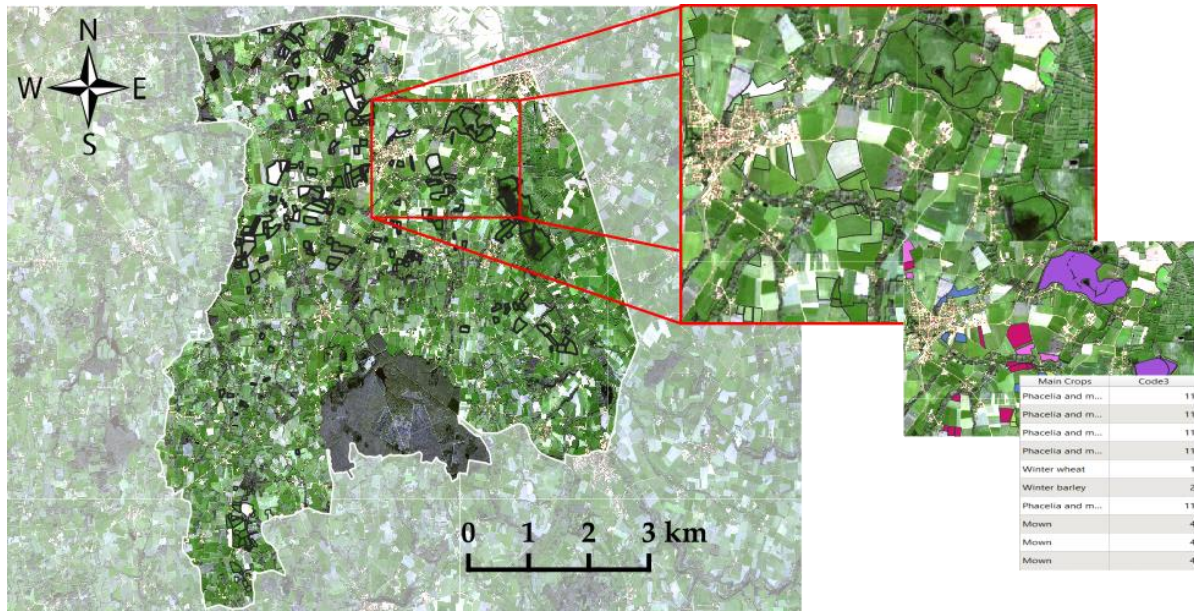


Figure I.26: Localization and illustration of land-use surveys.

III.4.1.4. Additional data: meteorological records

A set of meteorological records was also retrieved between September 2016 and May 2017. Meteorological data and more precisely rainfall and temperature data are essential for a fine understanding of the SAR signal. These data were acquired from a network of 5 Campbell BWS 200 weather stations located in the ZAA (Fig. I.27). These stations are composed of different sensors including a CS215 hygrometer thermometer and an Arg100 Rain Gauge.

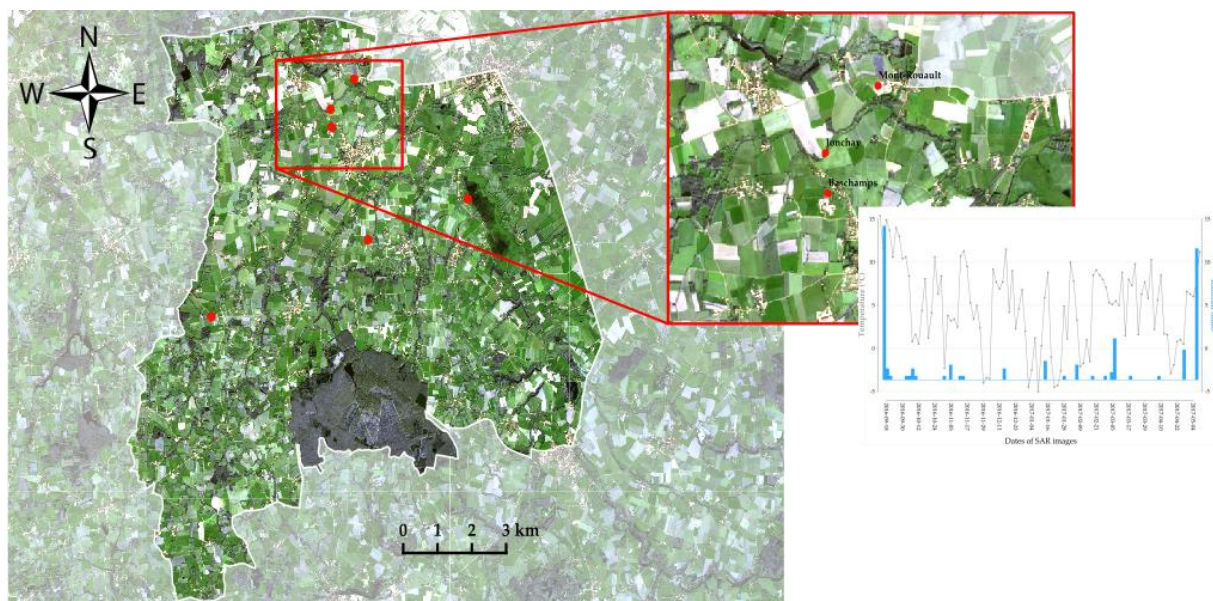


Figure I.27: Localization of weather stations and illustration of weather records.

III.4.2. Field measurements Pre-processing

III.4.2.1. Pre-processing of land-use records

Spatialized records of winter land-use collected between October 2016 and November 2016 underwent two levels of pre-processing. The first step was to integrate them into a database summarizing all land-use data (records and farmers' surveys). The second step consisted in cross-checking the information from these records with the land-use surveys results conducted with farmers in order to remove the parcels identified as inconsistent (misuse, problem identified with the farmer...). The corrected and preprocessed records were used as calibration and validation data in the classification models implemented in this thesis.

III.4.2.2. Pre-processing of land-use surveys

Information collected during the field surveys was spatialized, integrated and synchronized in the land-use database mentioned above. The spatialization of information concerned a set of information collected from the field's surveys:

- ✓ Crops 2015-2016
- ✓ Harvest date
- ✓ Crops 2016-2017
- ✓ Sowing date
- ✓ Catch crops
- ✓ Date and method of catch crops establishment
- ✓ Date and method of catch crops destruction or harvest
- ✓ Other practices

A cross-analysis of spatialized data integrated into the land-use database (land-use records and field surveys), allowed: (i) a better understanding of the agricultural context; (ii) the establishment of a crop successions calendar for the ZAA during Winter 2016-2017. The agricultural context was then summarized in three points in order to understand the agricultural situation during this period:

- ✓ The analysis of the main crops established in summer 2016 and summer 2017 shows an agricultural system based on 4 main crops and a permanent culture (corn, winter wheat, winter barley, rapeseed and grasslands). However, a predominance is observed for corn (35% in 2016 and 30% in 2017), winter wheat (26% in 2016 and 27% in 2017) and grassland (24% in 2016 and 27% in 2017) in the years 2016 to 2017 (**Fig. I.28**).

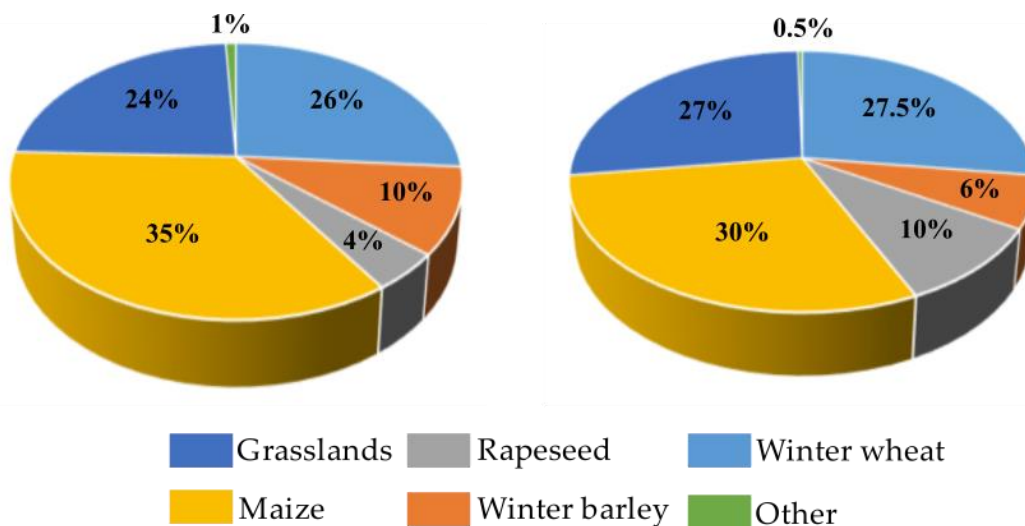


Figure I.28: Main crops in A) summer 2016, B) summer 2017.

- ✓ The second point sought to identify the winter land-use on the ZAA for winter 2016-2017 (Fig. I.29). This approach showed a predominance of 3 winter land-use types, winter crops (~38% of the fields surveyed), catch crops (~30%) and grasslands (~26%). This highlights the necessity for farmers to produce a quantity of forage due to changing weather conditions. This result is supported by the last point.

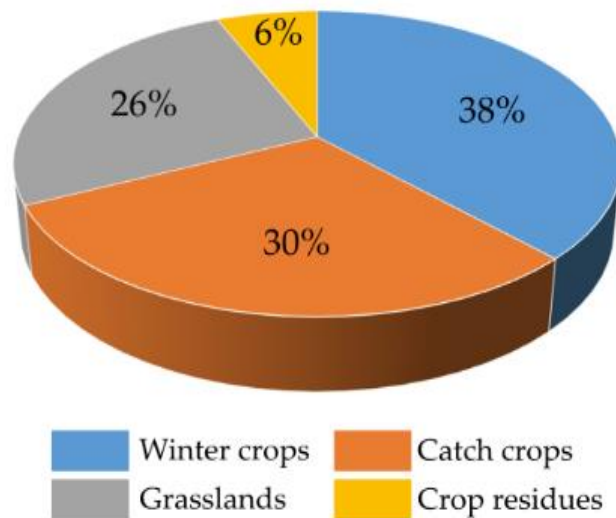


Figure I.29: Winter land-use established during winter 2016-2017.

- ✓ The last point focused on determining the proportion of catch crops in the ZAA during winter 2016-2017. This analysis reflects farmers' willingness to produce more forage due to weather conditions and lower yields during summer 2016. Figure I.30 illustrates the dominance of catch crops used, particularly RGI, in order to provide additional forage.

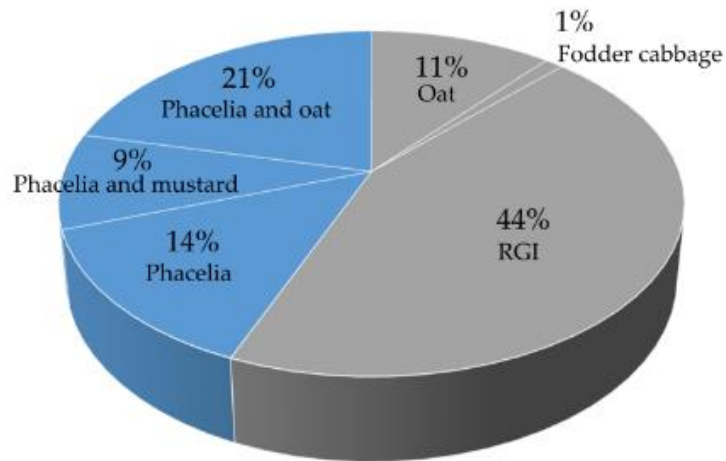


Figure I.30: Catch crops established during winter 2016-2017, with catch crops no used in blue and catch crops used in grey. RGI: Italian Ryegrass.

Finally, this spatialized information was used in the different thematic approaches presented in the thesis.

III.4.2.3. Pre-processing of meteorological data

Hourly meteorological data were acquired by the ZAA weather stations between September 2016 and July 2017 and synthesized in order to preserve the key periods to evaluate the SAR signal. Regarding the rainfall data, a summary of the 6 hours before the satellite passage was made by summing up the rainfall values. For temperature data, a 6-hour synthesis was implemented by retrieving the data 3 hours before and after the satellite's time. An average was then performed to obtain a single value. An ombrothermal diagram was drawn up to model the climatic situation for the period between September 2016 and July 2017 (**Fig. I.31**).

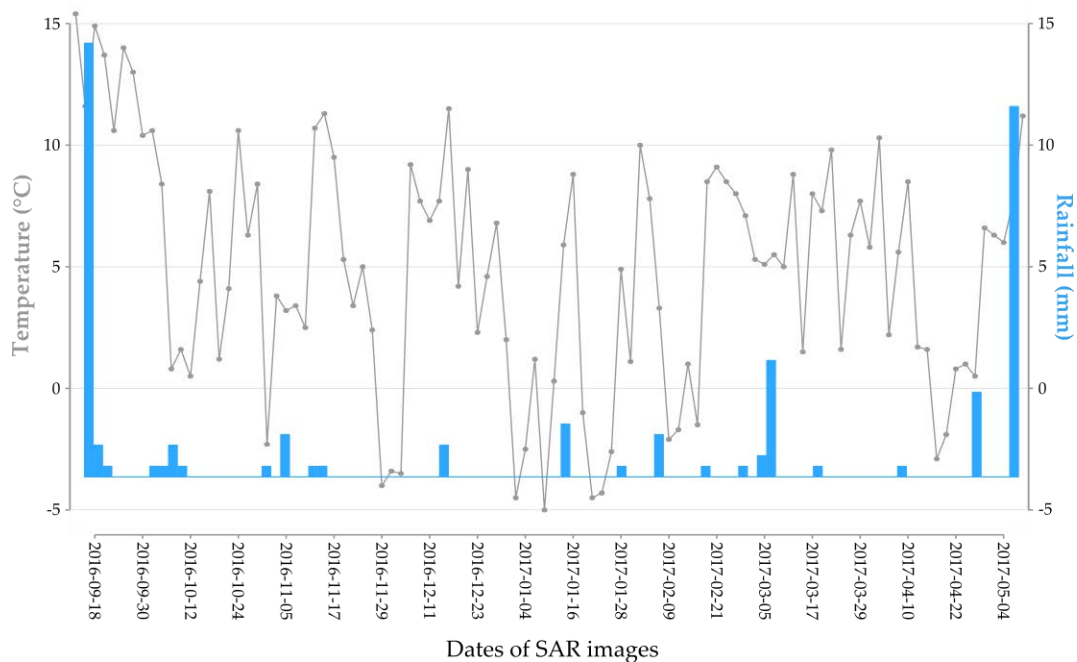


Figure I.31: Umbrothermal diagram over the period September 2016 - July 2017.

Chapter 4

Methodological procedure

Contents

IV.1. INTRODUCTION	69
IV.1. FIRST AXIS: DETERMINATION OF AN EFFICIENT CLASSIFICATION PROCEDURE FOR THE IDENTIFICATION AND CHARACTERIZATION OF WINTER LAND-USE AT A LOCAL SCALE	ERREUR ! SIGNET NON DEFINI.
IV.2. SECOND AXIS: POLARIMETRIC SAR TIME-SERIES FOR WINTER LAND-USE IDENTIFICATION	ERREUR ! SIGNET NON DEFINI.
IV.3. THIRD AXIS: IDENTIFICATION OF WINTER LAND-USE AT A REGIONAL SCALE	ERREUR ! SIGNET NON DEFINI.

IV.1. Introduction

The comprehension of inter-relationships between winter land-use and bio-geophysical processes is still a major environmental, decision-making and societal issue for scientific and decision-makers. In this context, spatial remote sensing has quickly emerged as a fundamental tool to identify and understand the concepts and processes resulting from these interactions (Joshi et al., 2016). The identification, characterization, and mapping of land use have therefore become a main objective for a large number of scientific studies (Verburg et al., 2011; Zaks and Kucharik, 2011). In general, these studies have sought to identify the most optimal methods for identifying land-use classes based on conventional or non-conventional classification procedures. In this context, several studies have highlighted the importance of methods such as the Maximum Likelihood Classification (Maxlike) or the Principal Component Analysis (PCA) in order to discriminate land-use classes and to carry out detailed mapping (Erb et al., 2013; Joshi et al., 2015). For a few decades, a new trend has emerged with the extensive use of classification methods based on machine learning principles, such as Support Vector Machine (SVM) or Random Forest (RF). Methods that have already demonstrated their full potential for land-use identification and characterization (DeFries et al., 1999; Herrmann and Tappan, 2013). Finally, more recently, a small number of studies have tried to highlight the value of time-series classification methods, initially developed for language-related functionalities but well known in remote sensing (Dynamic Time Wrapping (DTW)), for land-use discrimination and monitoring (Maus et al., 2016). Nevertheless, despite the development of a large number of methodological approaches for the identification, characterization or monitoring of land use, only a few studies as mentioned above (*Section II.3.3*) have been able to highlight an adapted approach for the identification and characterization of winter land-use.

In this context, the general methodology developed for this thesis aims to identify and characterize winter land-use at a local and regional scale. To this end, this methodology will be based on the classification approaches mentioned above, while adapting them to meet the thematic expectations (**Fig. I.32**). The implementation of these approaches will be carried out in 3 steps:

- ✓ Determination of the most efficient classification procedure for the identification and characterization of winter land-use. The approach will consist of (i) the evaluation of several classification approaches; ii) the establishment of an optimal winter land-use nomenclature and iii) Assessment of optical (S2) et SAR (S1) time-series potential for winter land-use classification at a local scale.
- ✓ Assessment of SAR time-series potential for the identification of winter land-use at a local scale. The purpose of this approach will be to determine the most appropriate SAR configuration.
- ✓ Evaluation of the best identified classification procedure for the identification of winter land-use at a regional scale. This approach will consist in extending the developed methodology to the Brittany region.

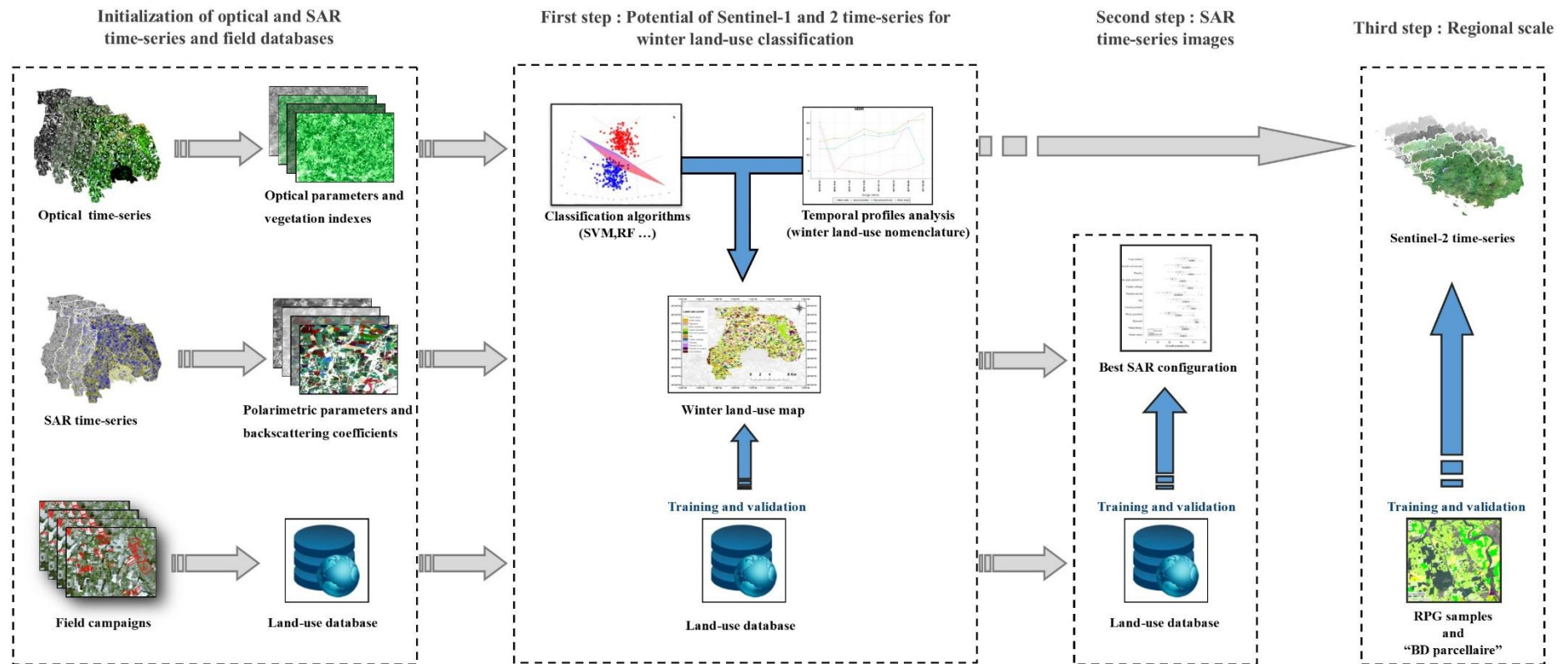


Figure I.32: General methodology implemented in this thesis.

IV.2. First axis: Determination of an efficient classification procedure for the identification and characterization of winter land-use at a local scale

The first axis of the thesis will aim to define the most efficient classification procedure (which methodology and data) in order to identify and characterize winter land-use. The development of three steps will be implemented in this framework. They will be carried out using the Sentinel-1 and Sentinel-2 time-series images acquired between September 2016 and May 2017 as presented in *Section III.3.1*. In addition, they will be implemented on a general and detailed nomenclature elaborated from the field data (*Section III.4.1*) summarizing the ZAA's winter land-use in 5 and 12 classes respectively. The procedure with the best results will be then preserved in order to carry out the next approaches conducted for this thesis.

IV.2.1 Determination of the most efficient classification algorithm for the winter land-use study at a local scale

The first step of this methodological approach aims to evaluate several classification procedures for the identification and characterization of winter land-use using optical and SAR time-series. In remote sensing, a classification process is performed to convert images into meaningful information, such as assigning a class to pixels or groups of pixels in an image. The implementation of classification processes based on remotely sensed time-series image has already been the subject of extensive studies in various application fields (Davranche et al., 2010; Gómez et al., 2016; Wardlow et al., 2007). However, as (Chi et al., 2008) point out, the classification of remote sensing images is not a trivial task. Indeed, the majority of the models developed to date require a sufficient number of samples to learn and validate. However, the definition and acquisition of reference data is often a critical issue (Mountrakis et al., 2011) for some areas of application, such as winter land-use. In addition, the particular phenologies and physiognomies of the crops during the winter period, increase the complexity of crops discrimination. It becomes logical that the success of any image classification depends on various factors, including the choice of an appropriate classification procedure (Lu and Weng, 2007).

In this context, the first step will focus on determining the most efficient algorithm for this issue. In this section, we will attempt to define the different models and approaches that will be used after in this thesis.

IV.2.1.1. Maximum Likelihood (Maxlike)

Maximum likelihood classification developed by (Yang, 1993), remains one of the most widely used classification techniques for a wide range of applications in remote sensing (Comber et al., 2012; Soria-Ruiz et al., 2010). Based on the theory of multivariate normal distribution (Abkar, 1999), it aims to set up a statistical analysis of a spectral vector distribution of learning samples in order to define probability zones around class centers. A probability of belonging is then calculated for each of the undefined pixels and assigned an affection to the class for which the probability of belonging is highest (**Fig. I.33**).

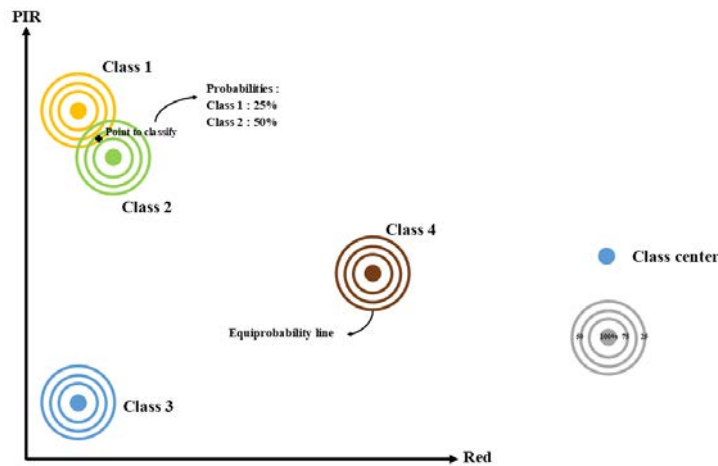


Figure I.33: Maximum Likelihood conceptual example.

This method offers several advantages such as providing for each pixel, as well as the allocation to a class, an index of certainty related to this allocation. This Bayesian feature of the classification algorithm separates the statistical weight of each class based on the data set. Classes with a low variance may be defined by a higher weight than other classes due to a higher probability of belonging of unaffected and spectrally close pixels. However, this classification technique is subject to certain limitations, particularly in cases where input data are multimodal due to the exclusive application of a normal distribution and when it concerns the classification of remote sensing time-series images (Liu et al., 2011).

In this context, the continuous emergence of new classification algorithms opens up new possibilities. To date, the two most commonly used algorithms in remote sensing remain the Support Vector Machines and the Random Forest.

IV.2.1.2. Support Vector Machines (SVM)

Support vector machines (SVMs) is a supervised non-parametric statistical learning technique, therefore there is no assumption made on the underlying data distribution (Mountrakis et al., 2011). Developed by (Vapnik, 1979) and then expanded by (Cortes and Vapnik, 1995), it aims, based on a set of labeled data, to find a hyperplane that separates the dataset into a discrete predefined number of classes in a fashion consistent.

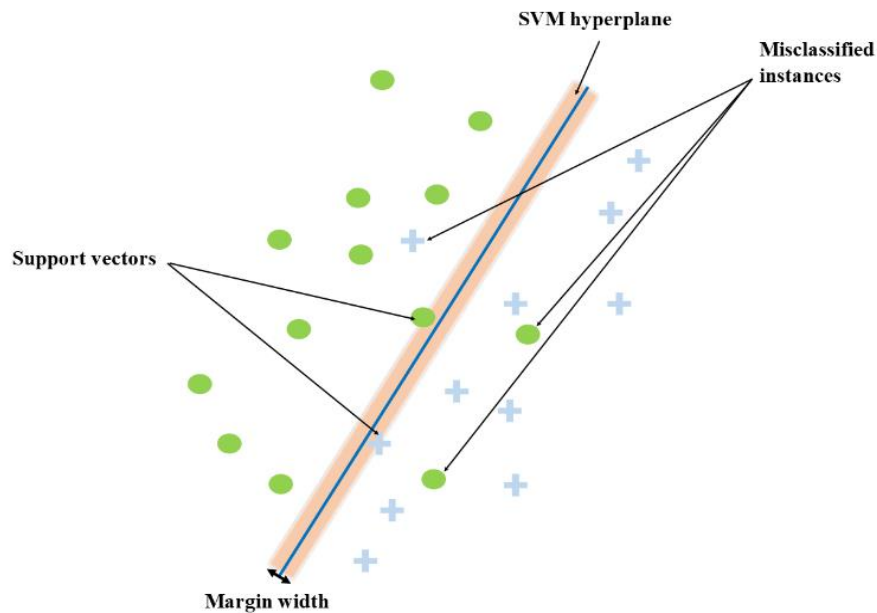


Figure I.34: Mechanism of Support Vectors Machines adapted of (Burges, 1998).

The notion of the optimal separator (adapted hyperplane) represents the decision limit to minimize classification errors. During its learning process, the classifier tries to find an optimal partition to separate the simulation data according to the same configurations (dimensions) (Zhu and Blumberg, 2002). In its simplest form, an SVM is a linear classifier that assigns a defined class to a given sample. In remote sensing, a sample to be labeled is usually represented by a set of individuals' pixels of an image. These pixels are then defined as a vector for each band of the image and consists of a set of digital measurements. **Figure I.34** illustrates a simple classification scenario, where the classifier tries to separate two classes in two-dimensional input space. The subsets of points located on the margin (called support vectors) are the only ones defining the hyperplane of the maximum margin. The implementation of a linear SVM requires that remote sensing data be linearly separable. In practice, the class data points overlap, which makes linear separability difficult. The definition of an adapted nucleus (polynomial, Gaussian, etc.) is therefore essential and often has an impact on the results (Mountrakis et al., 2011).

SVMs are therefore a very interesting algorithm in remote sensing because of their ability to successfully process small data sets, often generating more accurate results than more conventional methods such as Maxlike (Mantero et al., 2005). In addition, they minimize classification errors on "invisible" data without prior assumptions about the distribution of these data.

IV.2.1.3. Random Forest (RF)

A majority of classifiers do not make assumptions about frequency distribution and have thus become increasingly popular for remote sensing data classifications, which are rarely normally distributed (Belgiu and Drăguț, 2016). Furthermore, such approaches are facilitated by the implicit assumption that reality has a coherent spectral response. However, the latter becomes inaccurate when factors.

In this context, the RF algorithm has been developed. The RF is a classification method, consisting of a combination of classifier trees (**Fig. I.35**) where each classifier is generated using

a random vector sampled independently of the input vector and each tree gives a unit vote for the most popular class to classify the input vector (Breiman, 2001; Pal, 2005). Thus, it consists of using selected entities (pixels for example) at random or a combination of entities at each node to grow a tree. Based on the "Bagging" approach, this method allows the RF to generate a set of training data by drawing lots with N replacement examples, where N is the size of the original training set (Breiman, 1996).

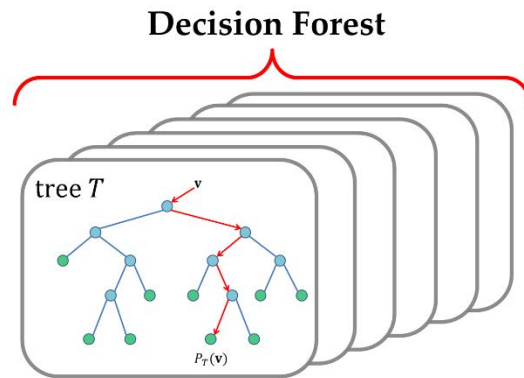


Figure I.35: Random forest algorithm example.

The pixels of an image are thus classified into a class defined according to the number of votes they are assigned by all the predictor trees of the forest. One of the major advantages of RF is the use of the Gini index as an attribute selection measure, which measures the impurity of an attribute in relation to classes (Pal, 2005), thus allowing predictive variables to be ranked according to their importance in the classification performed. This function of RF has been of great interest in recent years in remote sensing (Corcoran et al., 2013; Pedergrana et al., 2013) in order to optimize the space of elements by measuring the correlation between them in a large dataset.

Classifiers based on data mining approaches have demonstrated their potential to implement classification methods based on remote sensing data. However, (Petitjean et al., 2012) have shown that the use of such classifiers for crop mapping based on time series can become very complicated due to 3 points: (i) The lack of samples used to form the supervised algorithm; (ii) lack of temporal data due to cloud cover; (iii) annual changes in phenological cycles due to weather or agricultural practices variations. To overcome this problem since the 1970s, new types of classifiers have emerged.

IV.2.1.4. Time-Weighted Dynamic Time Wrapping (TWDTW)

Sakoe and Chiba, (1978) developed in the 1970s a time-series classification algorithm called Dynamic Time Warping (DTW). This algorithm is a well-known method for determining an optimal alignment between two given sequences (time-dependent) under certain restrictions (Müller, 2007). Originally developed to compare speech models in automatic speech recognition, it has proven to be useful in data mining and information retrieval, particularly for the automatic management of time-dependent data deformations such as time series. Despite this potential, some studies have shown its inadequacy in processing satellite image time series (Ratanamahatana and Keogh, 2004). In this context, (Maus et al., 2016) proposed a time-weighted version of the DTW (TWDTW) method capable of classifying crops with diverse plant dynamics using remote sensing time series. The

TWDTW method (**Fig. I.36**) introduces a time constraint, making the DTW more suitable for noisy and out of phase time series.

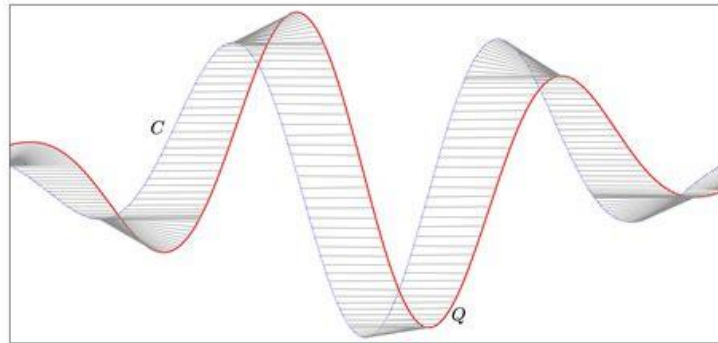


Figure I.36: Time-Weighted Dynamic Time Wrapping conceptual example.

These algorithms based on various statistical approaches have already demonstrated their potential for remote sensing data classification. For this reason, they have been selected to identify and characterize winter land use for this thesis.

IV.2.2. Establishment of an optimal winter land-use nomenclature

In a second step, we will evaluate the potential of the Sentinel-1 and 2 time-series to improve the classification level (nomenclature). Indeed, the classifications implemented in the first step of this methodological approach (*Section IV.2.1.*) were based on a general winter land-use nomenclature divided into 5 classes (winter crops, catch crops, grasslands, crop residues, and bare soils). However, the results obtained, have showed strong confusions between the "bare soil" class and the other winter land-use classes, suggesting approximations in the implemented nomenclature. Consequently, a readjustment of the nomenclature is required.

In this context, the second step of the first axis will evaluate the potential of the Sentinel-1 and 2 time-series to identify and characterize precisely winter land-use, in order to readjust winter land-use nomenclature. This process will be performed according two steps:

- ✓ Understand and analyze the interactions between remote sensing signal and winter land-use.

As mentioned previously, in remote sensing, a classification process is performed to convert images into meaningful information. However, this process does not remain a trivial task. In this context, the development of a detailed winter land-use classification for operational monitoring requires, among other things, an understanding of the temporal variations of the remote sensing signal according to the different types of crops in a given region (Veloso et al., 2017). From this perspective, the use optical and SAR remote sensing data, is an opportunity to study the temporal variations. However, up to now, the monitoring of crop dynamics has been hampered by the unavailability of satellite time-series with high temporal and spatial resolution. The launch in the mid-2010 of the first Sentinel satellites presented in *Section III.3.1* provided a significant and unprecedented amount of free data to consider new opportunities for identifying and characterizing winter land-use. Based on these new Earth observation satellites, the first step will analyze the temporal trajectory of remote

sensing data for the different winter land-use classes summarized in the "main crop" column of **Table I.4** in order to re-adjust the nomenclature implemented in the first step (*Section IV.2.1.*).

- ✓ Readjustment of the winter land-use nomenclature

The readjustment of the general nomenclature used in the first step will be based on the results of (i) the interactions analysis between remote sensing signals (optical and SAR) and winter land-use classes, and (ii) the classification results developed in the first step. These results highlighted, in particular, a significant confusion between the bare soil class and the other classes. Considering all this information, the land-use nomenclature will be readjusted, detailed and summarized in **Table I.4**.

IV.2.3. Assessment of Sentinel-2 (optical) and Sentinel-1 (SAR) time-series potential for the classification of winter land-use at a local scale

The third step of this first axis will consist of setting up a global and detailed classification in order to determine the best Sentinel time-series to identify and characterize winter land-use. The development of these classifications will be performed in 3 steps:

- ✓ Elaboration of a global winter land-use classification

The global winter land-use classification will be carried out using the procedure determined in the first step, based on Sentinel-1 and Sentinel-2 time-series acquired between September 2016 and May 2017 on the ZAA (presented in *Section III.3.1*) and applied on the nomenclature presented in the **Table I.4** and summarized in five global winter land-use classes.

This global classification will be performed according two classification approaches, pixel-based or object-based, in order to evaluate the best approach for the winter land-use study. Many studies have already shown the value of these two approaches for identifying and characterizing land use (Araya and Hergarten, 2008; Jianya et al., 2008). In particular, they highlighted some critical points to be considered for this thesis:

- Pixel-based approach

The pixel remains the basic unit for image analysis and techniques using remote sensing data. Indeed, in remote sensing in classification procedures, one pixel remains the atomic analysis unit of the procedures where spectral characteristics are used to detect and measure changes without considering the spatial context. In most cases, statistical operators are used to evaluate individual pixel. In this context, researchers have further investigated pixel-based approaches associated with classification methods such as SVM (Hussain et al., 2013) to demonstrate their potential for classifying remotely sensed images. These studies have highlighted that one of the advantages of the pixel approach lies in its ability to maintain the variability of a target. However, this advantage can also be a disadvantage and depends intrinsically on the relationship between the spatial resolution of the sensor and the size of the objects. For example, it is necessary to carry out a pixel approach from MODIS images because of its spatial resolution, unlike SPOT imaging, or the question may arise.

- Object-based approach

Remote sensing communities have soon recognized the pixel to be not a real geographical object but rather a cellular representation of spectral values in a grid whose boundaries do not reflect the real world (Fisher, 1997). The work of Addink et al., (2012) supported the fact that one pixel is not the optimal spatial unit for landscape mapping. This approach is now supported by the evolution of remote sensing and the launch of new sensors for which, the high variability of reflectance within individual characteristics and the number of classes present in high spatial resolution images have limited traditional pixel analysis (Johansen et al., 2010). However, the increase in spatial resolution accuracy has resulted in an increase in mixed pixels in objects, which are considered to be one of the main sources of error and uncertainty in land use and land cover studies (Boyd and Foody, 2011). In addition, the implementation of an object approach is known to generate image smoothing, reducing the variability of an object which is an important part of the classification process.

- ✓ Elaboration of a detailed winter land-use classification

This classification will be carried out using the procedure determined in the first step, based on Sentinel-1 and Sentinel-2 time-series acquired between September 2016 and May 2017 on the ZAA (presented in *Section III.3.1*) and applied for the new nomenclature of 12 winter land-use classes determined in step 2 of this axis.

- ✓ Comparison of Sentinel-1 and -2 time-series potential

Finally, a comparative analysis will be carried out to determine the potential of the Sentinel-1 and -2 time-series.

IV.3. Second axis: Polarimetric SAR time-series for winter land-use identification

The second axis, based on the findings and prospects of the first axis, will attempt to evaluate the relevance of SAR time-series (Alos-2, Radarsat-2, and Sentinel-1) for the identification of winter land-use. Indeed, although the potential of high spatial resolution SAR images has been developing steadily over, no studies have so far demonstrated its potential for the detailed identification, characterization of land use during the winter season. In this context, based on SAR time-series images acquired between August 2016 and May 2017 on the ZAA (presented in *Section III.3.1*), it will try to determine the most appropriate SAR configuration (polarization, frequency, time series density) for detailed winter land-use classification. The classification procedure determined in the first axis will be reused and applied to the detailed nomenclature (12 classes) defined in the second axis.

IV.4. Third axis: Identification of winter land-use at a regional scale

Finally, the last axis will aim to assess the reproducibility, at a regional scale, of the method considered as the most efficient for the identification and characterization of winter land-use at a local scale. To this end, based on the adaptation of the best classification procedure and remote sensing time-series (Sentinel-2) a 2-steps pre-processing methodology will be first implemented at Brittany scale:

- ✓ Acquisition of a denser time-series where meteorological conditions will be restrictive. An appropriate method should be implemented:
 - ❖ For atmospheric corrections.
 - ❖ For the storage and computation, volumes to be devoted to the processing of these data.
- ✓ Adjustment of calibration and validation data to perform classification models:
 - ❖ Acquisition of new learning database at Brittany scale, the “Registre Parcellaire Graphique” (RPG), which is a geographical database used as a reference for the appraisal of Common Agricultural Policy (CAP) aids. Nevertheless, as these data are provided by farmers to government services, pre-processing are required to avoid any errors.
 - ❖ Acquisition of validation data and Parcellaire Database developed by the “Institut national de l’information géographique et forestière” (IGN), which provides digital, geo-referenced and continuous cadastral information throughout France. The Cross-referencing of the RPG and Parcellaire Database will enable to obtain a database referencing parcels not declared to the CAP (for various reasons), which represents a major challenge for many communities (scientists, decision-makers, etc.).
 - ❖ Then, a processing methodology will be implemented in order to develop a classification model based on RPG data and a dense Sentinel-2 time-series. This

model will be then reproduced on the "BD Parcellaire" at Brittany regional scale in order to identify the winter land-use of the parcels not declared under the RPG and evaluate the reproducibility of the best classification procedure identified in this thesis. Thus, this axis will aim to provide a technical support to decision-makers in order to assist the implementation of environmental measures in a sustainable development context of agricultural areas.

Conclusion of the first part

The state of the art implemented in this first part has defined the concepts, functions and issues related to winter land-use in an intensive agricultural area but also how they can be identified and characterized.

Globally, land use can be defined according to a plurality of concepts framed by a common denominator, the impact of the human factor. In this sense, many studies have attempted to establish a limited definition of land use, which has become a source of important confusions and disagreement, especially since land use is still intrinsically linked to the notion of land cover. In this context, the work of (Comber, 2008) have provided a new perspective for defining this concept. He considers that it is impossible to focus on a limited definition of the land-use concept, but rather that its definition can be contextualized by the people' perception in a specific thematic context. Following this approach, the subject of this thesis was therefore defined as "land-use" during the winter season ("winter land-use"), a sub-unit of the object "agriculture", a land-cover element. The perception of the land-use concept remains all the more important because it involves a wide range of interconnected processes and functions. In this context, understanding the pressures and interactions, including environmental, economic and human interactions, is a major challenge.

To meet these challenges, international institutions have decided over several decades now to implement a legislative framework to regulate the practices and actions that might generate these pressures. Framework represented by two major European policies on land-use practices, particularly in winter, a crucial period for land use/environment interactions.

I) The European Directive 91/676/EEC, also known as the "Nitrates Directives". Established in December 1991 in response to non-compliance with the environmental standards set by Directive 75/440/EEC of 1975 on the required quality of surface water used for drinking water production. The purpose of this directive is to provide a framework and structure for the establishment of agricultural covers during the winter period. Under French law, it is expressed in the implementation of action programs allowing the implementation of measures to restore and/or preserve a better quality of surface and groundwater in sectors where this quality has been degraded. Since August 2018, a 6th action plan has been in force, requiring the establishment of a ground cover in winter ("Nitrates Directive," 2019) divided into 5 main land-use classes, (i) winter crops; (ii) grasslands; (iii) catch crops and (iv) crop residues and (v) bare soils.

II) The Rules on Good Agricultural and Environmental Conditions (GAEC). As part of a more general framework and integrated into the conditionality of CAP support to farmers, these rules include requirements for regulatory compliance in the environment, animal protection, animal production health, crop production health and in particular the conservation of areas known as " ecological interest " on at least 5% of the arable land surface (Tarn, 2015).

In this context, the impact of winter land-use on the environment has emerged as a major issue for the scientific community. (Galloway et al., 2004; i Canals et al., 2007; Withers et al., 2014) have thus demonstrated the essential role of winter land-use on biogeochemical and environmental processes, particularly on the water cycle, biodiversity, health or even on a broader scale on climate. The understanding of processes, and interactions resulting from

winter land-use have therefore become essential in order to address the environmental issues having a significant impact on our societies.

From these perspectives, it has become essential to obtain updated and accurate data on winter land-use, its processes and interactions. To this end, remote sensing data have appeared to be a privileged tool for the spatiotemporal identification and characterization of the winter land-use dynamics. However, although optical remote sensing data have already shown their potential in studying land use, several questions arise as to their effectiveness during the winter period where meteorological conditions can affect the behavior of the optical signal. Similarly, although SAR remote sensing is well known to overcome a part of the meteorological conditions, its capacity to obtain information on the physical characteristics and structure of crop is still unknown for the identification and characterization in detail of winter land-use patterns.

Thus, this thesis attempt to evaluate the potential of optical and SAR time-series images for the study of winter land-use. To this end, a 3-steps general methodology will be developed in order to identify and characterize winter land-use: (i) Define the most appropriate classification procedure and satellite time-series images for this issue at a local scale; (ii) Determine the most efficient SAR configuration for this issue at a local scale; (iii) Evaluate the reproducibility of the best classification procedure and remote sensing data for the identification of winter land-use at a regional scale.

2

Classification procedure for the winter land-use study at a local scale

Contents

INTRODUCTION OF THE SECOND PART	87
CHAPTER 5: DETERMINATION OF THE MOST EFFICIENT CLASSIFICATION PROCEDURE AND SENTINEL TIME-SERIES FOR THE STUDY OF WINTER LAND-USE	ERREUR ! SIGNET NON DEFINI.9
CONCLUSION OF THE SECOND PART	ERREUR ! SIGNET NON DEFINI.

Introduction of the second part

The second part of this manuscript presents the studies conducted to determine an adapted classification procedure and to evaluate the potential of Sentinel-1 and Sentinel-2 time-series images for the identification and characterization of winter land-use. The general framework of this methodology has been developed in *Section IV.1* and will be presented in details below.

This part is divided according to three purposes: *i)* Determination of the most efficient algorithm for winter land-use classification; *ii)* Analysis of SAR and optical multi-temporal signal behavior to establish an optimal winter land-use nomenclature; *iii)* Assessment of optical (S2) et SAR (S1) time-series potential for the classification of winter land-use at a local scale.

In the fifth chapter, winter land-use will be analyzed at the local level from optical (Sentinel-2) and SAR (Sentinel-1) time-series presented in *Section III.3.1*. An approach will be first conducted to determine the most appropriate classification algorithm (*Section IV.1*) to identify and characterize winter land-use. A comparative approach will be performed based on the classifications accuracies obtained using four classification algorithms. Then, using temporal profiles extracted from Sentinel time-series images, an analysis will be computed to interpret Sentinel-1 (SAR) and Sentinel-2 (optical) signal behavior in order to establish an adapted nomenclature and identify the best Sentinel parameters for the winter land-use study. Finally, using the best Sentinel dataset parameters and classification algorithm, a global and detailed winter land-use classification will be performed over the ZAA.

Chapter 5

Determination of the most efficient classification procedure and Sentinel time-series for the study of winter land-use

Contents

V.1. INTRODUCTION	91
V.2. STUDY SITE AND DATA	93
V.3. METHODS	96
V.4. RESULTS AND DISCUSSION	102
V.5. CONCLUSIONS	120



A part of this chapter was published in a peer-reviewed journal



Denize, J., Hubert-Moy, L., Betbeder, J., Corgne, S., Baudry, J., & Pottier, E. (2019). Evaluation of Using Sentinel-1 and-2 Time-Series to Identify Winter Land Use in Agricultural Landscapes. *Remote Sensing*, 11(1), 37.



A part of this chapter was accepted with revisions in a peer-reviewed journal

Remote Sensing and Environment, 2020



and presented in two international conferences

Conference IGARSS (IEEE Geoscience and Remote Sensing Society), Valence (Spain), 22-27 July 2018, Title: Identification of winter land use in temperate agricultural landscapes based on Sentinel-1 and 2 times-series.

Conference ESA Living Planet Symposium, Milan (Italia), 13-17 May 2019, Title: Sentinel-1 and Sentinel-2 time-series analysis of winter land-use temporal behavior in agricultural areas

V.1. Introduction

The world population is predicted to reach 8.7 billion by 2030, which will increase and intensify pressure on the environment and increasingly require considering socio-economic conditions and environmental impacts of agricultural systems (Belgiu and Csillik, 2018). In addition, farmers will have to alter their farming practices according to climate change and given conditions (Veloso et al., 2017). Information about land use is essential for estimating effects of farming practices on the environment, not only for mapping annual crops and pastures, but also for identifying land-surface conditions during winter. Winter crop-management practices such as intercropping and land-management practices, such as minimum tillage were developed to reduce runoff and the soil erosion it causes, increase nitrogen fixation, and increase carbon sequestration (Galloway et al., 2004). The great diversity in agricultural practices and variability in climatic conditions result in a wide variety of land-use patterns in winter, each of which has specific environmental impacts (Dabney et al., 2009). Hence, it is of great importance to identify detailed land-use classes during the intercropping season.

However, finely discriminating winter land-use classes over large areas remains challenging. While most studies that monitored land use in winter using remote sensing data focused on detecting vegetation cover on the surface (Minh et al., 2018), only a few identified land-use classes, and those classes have been broad. In contrast, it is important to describe land surfaces in detail and discriminate finely between land-use classes. High spatial resolution time-series from satellite images can help map land-use classes accurately during the intercropping season. The wide variety of land-use types in winter also complicates detection of individual crop patterns. Although they are widely used to identify annual crops (Fieuzal et al., 2013), optical images have several limitations for determining land use in winter due to meteorological conditions such as frost or rain (Su et al., 2011). The wide variety of land-use types in winter also complicates detection of individual crop patterns.

However, several studies have demonstrated the ability of optical medium-resolution time-series to map crops that cover large areas and long-term changes in crop areas (Wardlow and Egbert, 2008) and to identify and characterize crop phenology over large areas (Jakubauskas et al., 2002). However, these data can only detect winter land-use in small field areas due to their broad spatial resolution (Lecerf et al., 2005). Optical very-high resolution time-series have also been used to map cropping patterns. For example, (Kuenzer et al., 2015) showed the potential of Pleiades images for identifying crops and land-surface dynamics, as well as farming practices in summer. However, identification of winter land-use types implies the detection of soil surface and vegetation growth dynamics that vary daily, seasonally, and from one field to another (Pacheco and McNairn, 2010) requires several satellite images in winter (Denize et al., 2019). However, high-resolution optical time-series are underused, because only few cloudless images are available in winter.

Due to shorter revisiting intervals and acquisition abilities that are not influenced by weather, synthetic aperture radar (SAR) time-series data are well suited to characterize winter land-use dynamics when mapping crops (Bargiel, 2017). High-resolution SAR images have been widely used to identify bare soils and tillage practices during winter season (Ulaby et al., 1986). Several studies have demonstrated the potential of radar data for mapping crop residues (McNairn and Brisco, 2004; Smith and Major, 1996) and crop types in summer (Bargiel, 2017). Despite this ability to overcome meteorological conditions, only a few studies have highlighted the capacity of SAR time-series data to identify winter land-use. (Haldar et al.,

2016) presented the ability of polarimetric C-band SAR time-series data for mapping wheat and mustard. Similarly, while optical and SAR data should be complementary, few studies have evaluated their combined use for mapping land use in summer (Fieuzal et al., 2013; Skakun et al., 2015) and, to our knowledge, only one identified broad land-use classes in winter (Denize et al., 2019). The launch of the Sentinel-1 and Sentinel-2 sensors that provide optical and SAR data with high spatial and temporal resolution, offers interesting possibilities to study the temporal dynamics of winter land-use. Several studies have highlighted the Sentinel-1 and -2 potential to characterize and classify land use, either separately or combined (Inglada et al., 2016; Veloso et al., 2017). Among these studies, a few have demonstrated the potential of Sentinel-2 time-series data for identifying intra-annual land-use changes. (Forkuor et al., 2018) obtained better land-use maps with Sentinel-2 time-series than Landsat-8 time-series. Similarly, (Belgiu and Csillik, 2018) and (Vuolo et al., 2018) presented the potential of Sentinel-2 data for land use mapping during the growing season with high accuracy (overall accuracy (OA) > 90%). A few studies have shown the potential of Sentinel-1 for identifying and characterizing land-cover and land-use dynamics (Minh et al., 2018; Torbick et al., 2017). (Bargiel, 2017) and (Veloso et al., 2017) illustrated the benefits of Sentinel-1 time-series for understanding crop behavior and dynamics to classify land use. Minh et al., (2018) produced a winter vegetation map in five quality classes (from “bare soil” to “high quality”) with a high overall accuracy (98%) using Sentinel-1 data and a deep-learning classification procedure. The potential of combined Sentinel SAR and optical data to map land cover have been highlighted by only few studies (Mercier et al., 2019; Sun et al., 2019). (Carrasco et al., 2019) have shown that use of combined Sentinel-1 and -2 images improved the accuracy of land use classifications by 5-10%. Nonetheless, the use of Sentinel-1 and -2 images to identify and characterize detailed winter land-use remains unexplored.

In this context, this chapter try to evaluate the potential of free Sentinel-1 and Sentinel-2 time-series for the identification and characterization of winter land-use. To this end, two datasets of optical (Sentinel-2) and SAR (Sentinel-1) time-series images acquired on the ZAA between September 2016 and May 2017. A three-steps procedure was then developed. i) A classification procedure was established to identify the most adapted algorithm; ii) Then, after analyzing temporal profiles of SAR and optical Sentinel parameters, we estimated the best nomenclature and parameters for winter land-use study; iii) Finally, the most important Sentinel-1 and 2 parameters were used to perform global and detailed winter land-use map with the best classification algorithm.

V.2. Study site and Data

V.2.1. Study Site

The study site on a ca. 130 km² agricultural area located to the south of the Bay of Mont-Saint-Michel (48°31'0" N, 1°31'30" W), western France, the "ZAA of Pleine-Fougères" presented in *Section III.3.2*. This area, which is a Long-Term Ecological Research (LTER) site, has a temperate climate with a mean annual temperature > 12°C, a minimum mean annual temperature > 8°C, a maximum mean annual temperature of 16°C, and mean annual precipitation of 600-700 mm. It contains ca. 7000 agricultural plots ranging in size from 0.1-65 ha (mean of 2.1 ha) and is surrounded by a hedgerow network. Farming systems are oriented mainly toward dairy cattle and some crop production. Grasslands and fodder crops cover a high percentage of the Utilized Agricultural Area (UAA). The crop system is characterized by sowing of secondary annual crops, hereafter "winter crops" (winter wheat, winter barley, and rapeseed), or intermediate crops, hereafter "catch crops", in autumn, after harvest of the main annual crops (maize, wheat, rapeseed. and barley).

The winter land-use types considered in this study are presented in **Figure II.1.** and **Table II.1.** Winter crops cover 40% of the UAA. Wheat and barley that are sown in October have a comparable plant morphology and growth stages (Denize et al., 2019). Wheat is harvested mainly in mid-July and barley in late June or early July. Rapeseed, sown mostly in September, is harvested in early July. At full development, rapeseed plants are taller than wheat and barley, and their stems are intertwined with no clear vertical structure (Veloso et al., 2017). Sowing of catch crops, which is required under the European Union Nitrates Directive, reduces nitrate leaching, application of mineral fertilizers, and the risk of erosion. Catch crops are destroyed at the end of winter and are sown after the main crops from August-October and cover 25% of the UAA. They are very varied (e.g. oat, phacelia, mustard), and have different plant structures and phenologies. In most areas where the main annual crops are harvested after November, crop residues (cereal stubble such as maize stalks) are left on the soil surface to prevent leaching (5% of the UAA). Grasslands that influence nitrogen cycle as well as soil water and carbone storage, cover ca. 30% of the UAA. Because they can be mown or grazed, grasslands have similar plant structure but different phenologies. Finally, although bare soils have been banned for several years to avoid soil erosion and water pollutant, some of them were identified during the first field measurement campaign. So, we decided to include a bare soil class that will be reconsidered during these works.

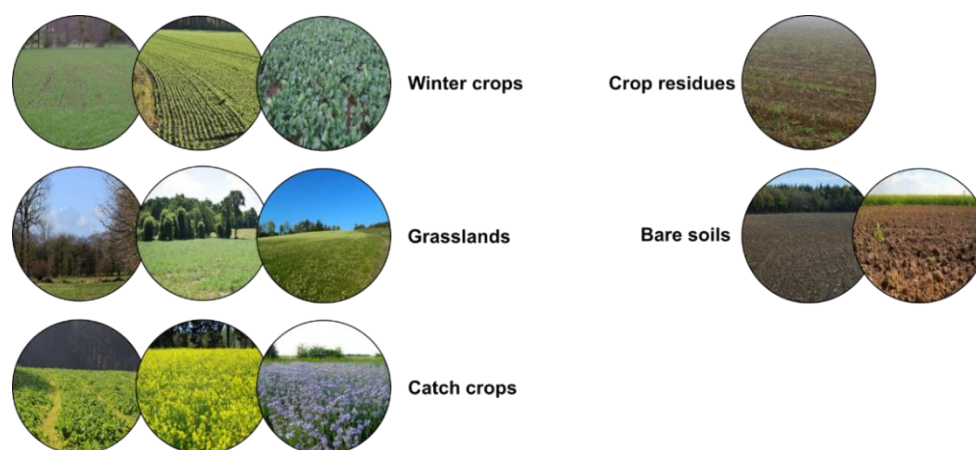


Figure II.1. The five main winter land-use types in the study area.

Table II.1. Types and sub-types of winter land-use classified in the study.

Land-use type	Land-use sub-types
Winter crops	Winter wheat Rapeseed Winter barley
Catch crops	Ryegrass and clover Phacelia Oat Fodder cabbage Phacelia and mustard Phacelia and oat
Crop residues	Maize stalks
Grasslands	Grazed grasslands Mown grasslands
Bare soil	None

V.2.2. Land-Use

The land-use classification used for this methodological approach was realized from two field campaigns presented in *Sections III.4.1.2 and III.4.1.3*. It is divided into two levels of classification gathering the winter land-use classes observed during these campaigns and summarized in **Table II.1**.

V.2.3. Meteorological data

As presented in *section III.4.2.3*, meteorological records were collected from five weather stations in the study area that record air temperature and rainfall each hour. Only the temperatures closest to the Sentinel-1 overpass time recorded from August 2016 to September 2017 were used. Rainfall data were summed over 6-hour periods by retrieving the data three hours before and after the Sentinel-1 overpass time during the same period. These data were collected to analyze the scattering behavior of the SAR signal for each type of land use, since weather conditions influence it greatly.

V.2.4. Satellite time-series images

V.2.4.1. Sentinel-2 time-series

A time-series of nine Sentinel-2 images presented in the Section III.3.1 was downloaded from the Copernicus Open Access Hub between August 2016 and May 2017 at the local scale of the ZAA. These Sentinel-2 Level-1C images (i.e., corrected for geometric and atmospheric effects) were acquired with a spatial resolution of 10-20 m and 10 spectral bands (bands with 60 m resolution were not considered) (**Table II.2**).

V.2.4.2. Sentinel-1 time-series

Two series of nine (sparse) and twenty (dense) S-1 SAR images presented in the *Section III.3.1* were downloaded from the Copernicus Open Access Hub between August 2016 and May 2017 at the local scale of the ZAA. S-1 images were obtained in Single Look Complex (SLC) mode

(delivered in dual-pol mode: VH and VV) with an incidence angle of 31°-46°. The range and azimuth spatial resolutions were 2.3 and 13.9 m, respectively (**Table II.2**).

Table II.2. Characteristics of Sentinel-1 and Sentinel-2 images. Dates in bold text for Sentinel-1 images indicate those with sparse time-series, while asterisks indicate those with dense time-series.

Characteristic	Sentinel-1	Characteristic	Sentinel-2
Ground resolution (m)	2.3	Spatial resolution (m)	10-20
Azimuth resolution (m)	13.9		
Polarization	Dual (VV-VH)	Spectral resolution-central wavelength (µm)	Band 2 (Blue) – 0.490
Frequency	C-band		Band 3 (Green) – 0.560
Mode	Interferometric wide (SLC)		Band 4 (Red) – 0.665
			Band 5 (Red Edge) – 0.705
Incidence angle (°)	31°-46°(right descending)		Band 6 (Red Edge) – 0.740
			Band 7 (Red Edge) – 0.783
			Band 8 (NIR) – 0.842
			Band 8A (NIR) – 0.865
			Band 11 (SWIR) – 1.610
			Band 12 (SWIR) – 2.190
Coverage (km)	> 250 × 100	Coverage (km)	> 250 × 100
Dates (m-d-y)	08-25-2016	01-16-2017*	
	09-18-2016*	01-28-2017*	08-25-2016
	09-30-2016*	02-09-2017*	11-05-2016
	10-12-2016*	02-21-2017*	11-29-2016
	10-24-2016*	03-05-2017*	12-29-2016
	11-05-2016*	03-17-2017*	01-16-2017
	11-17-2016*	03-29-2017*	02-21-2017
	11-29-2016*	04-10-2017*	03-29-2017
	12-11-2016*	04-22-2017*	04-10-2017
	12-23-2016*	05-04-2017*	05-10-2017
	01-04-2017*	05-16-2017	

V.3. Methods

Several parameters were derived from the Sentinel-1 and Sentinel-2 time-series. The method developed to analyze winter land-use from these parameters had two steps: (1) pre-process the optical and SAR image time-series to generate parameter datasets (*section V.3.1*) and (2) process the optical and SAR parameters by identifying the best classification algorithms, extracting temporal profiles of winter land-use classes, and classifying Sentinel parameters (*section V.3.2*).

V.3.1 Pre-processing of Sentinel time-series images

V.3.1.1 Sentinel-1 SAR images

V.3.1.1.1 SAR parameter selection

Backscattering coefficients and polarimetric parameters were selected to monitor winter land-use. Backscattering coefficients (VV and VH polarizations) are usually used to monitor vegetation because the vertically (V) and horizontally (H) polarized microwaves react differently to vegetation in the C-band (McNairn and Brisco, 2004). The predominant vertical structure of most agricultural crops creates destructive interference with V microwaves, which decreases their penetration through the canopy (i.e. attenuates the microwave signal). In contrast, H microwaves tend to penetrate the canopy more than V microwaves. Many studies have demonstrated the value of VV polarization for identifying changes in growth stages of vegetation (Jackson and Schmugge, 1991). VH polarization, which results from multiple scattering from rough surfaces and multiple volume scattering from within the vegetation-soil volume, is sensitive to plant structure within the total canopy volume, and thus provides information that is complementary to VV polarization (McNairn and Brisco, 2004). However, some studies have shown that Sentinel-1 VH and VV polarizations can contain mixed interactions between vegetation and the ground due to the double-bounce effect and to attenuation of ground backscattering by the canopy in the C-band, which includes simple and multiple scattering (Ulaby et al., 1986). The VH:VV ratio is used to address this issue (Velooso et al., 2017) because it can reduce the double-bounce effect, as well as errors associated with the acquisition system or environmental factors. Thus, the VH:VV ratio is more stable than VV or VH polarization considered independently. Other parameters derived from SAR data are useful for studying cropping systems, such as Shannon Entropy (SE), which highlights the order and disorder of an object and can discriminate soil from specific crops, such as wheat and rapeseed (Betbeder et al., 2015). Another parameter is SPAN, which characterizes the total backscattering power that is reflected; it helps discriminate crops by highlighting the main backscattering mechanisms.

V.3.1.1.2 Backscattering coefficients

First, Sentinel-1 time-series were radiometrically calibrated with SNAP v6.0 software to transform radar signals into backscattering coefficients. To reduce the speckle noise inherent in SAR imaging, a Lee sigma filter (Lee et al., 2008) was applied with a window of 7×7 pixels and a sigma value of 0.7 using SNAP v6.0 software for dense Sentinel-1 time-series and a Lee Refined filter (Lee, 1981) was applied with a window of 7×7 pixels using SNAP v6.0 software

for sparse Sentinel-1 time-series. Shuttle Radar Topography Mission 3s data were then used to correct the topographic effects and geocoded SAR images. The geometric correction accuracy was 10 m for each pixel. A backscattering ratio, which highlights the scattering mechanisms of each target (McNairn and Brisco, 2004), was calculated by dividing backscattering coefficient σ^0_{VH} by σ^0_{VV} . This ratio, σ^0_{VH} and σ^0_{VV} were then converted into decibels (db) using the following equation (Eq.II.1):

$$\sigma^0(db) = 10 \cdot \log_{10}(\sigma^0) \quad (\text{Eq. II.1})$$

V.3.1.1.3. Polarimetric parameters

First, a 2x2 covariance matrix (C_2) was computed from the scattering matrix S of each SLC image using PolSARpro v5.1.3 software (Pottier and Ferro-Famil, 2012). The geocoding process was performed to the elements of the (C_2) matrix (Lusch, 1999), using SNAP v6.0 software. A Lee sigma filter with a window of 7x7 pixels and a sigma value of 0.7 or a Lee Refined with a window of 7x7 pixels were then applied to reduce speckle noise (For dense and sparse time-series respectively). SPAN and SE, which equal the sum of the intensity (SE_i) and degree of polarization (SE_p) (Réfrégier, P., and Morio, J., 2006), were then calculated from the (C_2) matrix (Eq. II.2). SE measured the disorder in the polarimetric SAR images as follows:

$$SE = \log(\pi^2 e^2 |C_2|) = SE_i + SE_p \quad (\text{Eq. II.2})$$

V.3.1.2. Sentinel-2 optical images

All Sentinel-2 spectral bands at 10 and 20 m resolution, as well as some indices, were chosen to monitor winter land-use. Three indices were selected based on their ability to highlight different processes related to vegetation, such as water stress, growth peak, and phenological stage (Gu et al., 2008; Veloso et al., 2017). The Normalized Difference Vegetation Index (NDVI) was selected because it is the vegetation index used most to study vegetation at multiple scales and environmental changes (Bannari et al., 1995). It leads to a reduction in spectral noise generated by environmental conditions. The Soil-Adjusted Vegetation Index (SAVI) was used for its ability to highlight vegetation growth peak and phenological stage (Gu et al., 2008). The Normalized Difference Water Index (NDWI) was selected for its ability to highlight water in plants and water stress. Sentinel-2 optical images retrieved from the Copernicus Open Access Hub in Level-1C were already orthorectified and georeferenced based on the UTM (area 30N) reference system. The first step of Sentinel-2 pre-processing was to assess the accuracy of the corrected images. Sentinel-2 images were then corrected for atmospheric effects to deliver a Level-2A surface-reflectance product using the Sen2Cor toolbox of SNAP v6.0 software. Sentinel-2 images were resampled at 10 m resolution. NDVI, NDWI, and SAVI were calculated using SNAP v6.0 software. Biophysical parameters (Leaf Area Index, fraction of photosynthetically active radiation and fractional vegetation cover) were finally calculated using the PROSAIL radiative transfer model (Weiss et al., 2004; Jacquemoud et al., 2009) implemented in SNAP v6.0 software. These parameters describe the state of the vegetation cover and provide information on the density of green vegetation (Dusseux et al., 2014).

A total of 10 SAR parameters were derived from Sentinel-1 time-series (2 backscattering coefficients and 1 ratio based on the backscattering coefficients, 1 SPAN, 2 SE, 2 SE_i and 2 SE_p), and 16 optical parameters (10 bands, 3 vegetation indices, 3 Biophysical parameters) were calculated from Sentinel-2 time-series. Thus, 200 parameters for Sentinel-1 dense time-series

(10 parameters \times 20 dates), 90 parameters for Sentinel-1 sparse time-series (10 parameters \times 9 dates) and 144 parameters for Sentinel-2 data (16 parameters \times 9 dates) were extracted.

V.3.2. Processing of Sentinel time-series images

V.3.2.1 Feature extraction

In this fifth chapter three parameters datasets (one Sentinel-2 dataset and two Sentinel-1 datasets (dense and sparse)) derived from Sentinel time-series were used to process two classification approaches: an object-based and a pixel-based approach. Hedgerows, which are considered noisy features when mapping land use, were removed from the images by applying a 5 m negative buffer around the boundaries of the field boundaries observed on the study site. Then, two feature extraction sequences were performed: (i) for the object-based approach, the mean and median values of optical and SAR parameters were calculated at the field scale; (ii) for the pixel-based approach, 100 pixels were randomly selected from the ground surveys for each winter land-use class, yielding 500 pixels (5 classes \times 100 pixels) for the global winter land-use classification, and 1 200 pixels (12 classes \times 100 pixels) for the detailed winter land-use classification.

V.3.2.2. Determination of the most efficient classification algorithm

To determine the most efficient algorithm for the identification and characterization of winter land-use a set of classifications using four classifiers and based on the global pixel feature extraction (500 pixels (5 classes \times 100 pixels)) was implemented.

V.3.2.2.1. MAXLIKE

First, the MAXLIKE supervised classification algorithm presented in *Section IV.2* was performed using the `classifyRasclass` function integrated into the `Rasclass` package (v.0.2.2.2) implemented in the R software (v3.5 and above) ("R Core Team, 2019," 2019). The package developed by Daniel Wiesmann (Wiseman et al., 2014) allows the implementation of a supervised pixel-oriented classification set from a single function (`ClassifyRasclass`). The classification results are then validated using the same package that provides information on the accuracy related to these classifications from a set of indices such as "overall accuracy".

V.3.2.2.2. SVM

A set of classification was realized using the Support Vectors Machine (SVM). This classifier, presented in *Section IV.2*, aims to define the most optimal margin (hyperplane) to separate two datasets. Initially developed to separate two datasets linearly, it currently allows by selecting an adapted kernel (Polynomial, Gaussian...) to separate optimally two datasets. SVM algorithm integrated into the `e1071` package (v 1.7-0) developed by (Dimitriadou et al., 2008) and implemented in R (v3.5) software was used in this second part. First, four SVM parameters (gamma, cost, degree, and nu) were randomly adjusted using the "tune" function implemented in the package. Then, several tests were carried out to determine the most optimal kernel for the classification of winter land-use. The "polynomial" kernel was then conserved.

V.3.2.2.3. Random Forest

In a third time, the RF classifier presented in *Section IV.2* was employed using the randomForest package (v 4.6) developed by (Liaw and Wiener, 2002) and implemented in R (v3.5) software. Two RF parameters were then determined for this approach. *i*) The number of trees (ntree), determined by a random selection of samples extracted from the Sentinel-1 and 2 time-series images. This parameter has been set at 1,000, which is considered as the optimal number to minimize the classification errors (Lawrence et al., 2006); *ii*) The number of variables used for the tree node division (mtry) determined from the "tune" function integrated into the package.

V.3.2.2.4. TWDTW algorithm

Finally, a set of classifications was calculated using the TWDTW algorithm (Maus et al., 2016) presented in *Section IV.2*. The main function of this algorithm is to find an optimal alignment between two given sequences (time-series) by imposing a time constraint allowing better separation of the winter land-use classes time profiles. The dtwSat package (v.0.2.1) developed by (Maus et al., 2016) and implemented in R (v3.5) software was used for this approach. This package consists of applying the DTW algorithm to each time-series with a time constraint. The DTW algorithm matches each pattern to the input time-series independently of the others. Then, the land-use classification is created using the model with the shortest distance DTW. To implement this algorithm on the Sentinel-1 and -2 datasets, a three-step process was performed: 1) the creation of time models for each winter land use classes based on Sentinel-1 and Sentinel-2 parameters datasets; 2) the application of TWDTW analysis using the dtwSat::twdtwApply function with $\alpha = -0.1$ or -0.2 for Sentinel-2 and -1 and $\beta = 40$ or 50 for Sentinel-2 and -1 respectively 3) the classification of raster time-series .

The classifications assessments were carried out through a validation procedure, 100 pixels were randomly selected by minimizing spatial autocorrelation among the fields contained in the land-use type database presented in *Section III.4.1* and representing the 5 main winter land-use classes (in total, 500 pixels). The four classifiers were then applied in turn from two-thirds of the 500 pixels randomly selected (i.e. 332 pixels). The One-third of the remaining samples (168 pixels) was used to validate the classifications. This process was then replicated 100 times by changing the training and validation subset samples. The accuracy of the classification was then assessed using the overall accuracy (OA).

V.3.2.3. Analysis of SAR and optical multi-temporal signal behavior

The evaluation of the potential of the Sentinel-1 and 2 time-series to improve the classification level (nomenclature) was performed according to the first observations obtained with classification algorithms based on a general winter land-use nomenclature composed of 5 classes (winter crops, catch crops, grasslands, crop residues, and bare soils). The results showed strong confusion between the "bare soil" class and the other winter land-use classes, suggesting approximations in the implemented nomenclature. Consequently, a readjustment of the nomenclature is required. For that, Median and mean temporal profiles for Sentinel-1 and Sentinel-2, respectively, were calculated for the 12 winter land-use classes (without bare

soils) from the best SAR and optical parameters generated from 10 m Sentinel-1 and -2 time-series using R software v3.5.1.

V.3.2.4. Assessment of optical (S2) et SAR (S1) time-series potential

V.3.2.4.1 Evaluation of Sentinel parameters importance for winter land-use classification

The importance of each Sentinel parameter was analysed to (1) identify the most important parameters for mapping winter land-use and (2) reduce the number of parameters to be classified in order to assess the influence of fewer parameters on classification accuracy. This process was performed according the two classification approaches (pixel-based or object-based) presented above and using the RF significance function. A measure of variable importance was provided for each candidate predictor using this heuristic method based on the Gini Index (Breiman, 2001; Kostelich and Schreiber, 1993; Pal, 2005). A break in each histogram was used as the threshold for selecting the most important parameters.

V.3.2.4.2. Global winter land-use classification

The RF and SVM algorithms, which are supervised classification methods, were used to classify land use during winter 2016–2017. These algorithms were chosen for their consistently strong performance and the accuracy with which they classify LULC (Belgui and Dragut, 2016; Mountrakis et al., 2011) and as identified previously (*Section V.3.2.2.*). The RF algorithm is an ensemble algorithm that uses a set of classification and regression trees to make a prediction (Breiman, 2001). The package `randomForest` developed by (Liaw and Weiner, 2002) and implemented in R (v.3.3.2) was used to perform winter land-use classifications. Two Random Forest parameters, namely the number of trees (`ntree`), which was created by randomly selecting samples from the training dataset (Belgui and Csillik, 2017) and the number of variables used for tree nodes splitting (`mtry`) were tuned and randomly determined using the `tune` function implemented in the `randomForest` package. For this study, the `ntree` parameter was set at 1.000, as mentioned previously (*section V.3.2.2.3*). The SVM algorithm is based on statistical learning theory that aims to determine the location of decision boundaries that produce an optimal separation of classes (Cortes and Vapnik, 1995). In a two-class pattern-recognition problem in which classes can be separated linearly, the SVM selects the linear decision boundary that creates the greatest margin between the two classes. The margin is the sum of distances to the hyperplane from the closest points of the two classes. Thus, it initially extracts the best linear boundary between two classes of the training set; however, it is not restricted to linear discrimination, since one of its main advantages is its extension to nonlinear discrimination via the kernel trick (Betbeder et al., 2015). The package `e1071` (v 1.7-0) developed by (Dimitriadou et al., 2008) and implemented in R (v.3.3.2) was used to perform SVM classifications. A set of four SVM parameters (`gamma`, `cost`, `degree`, `nu`) was randomly tuned using the `tune` function integrated in the `e1071` package. Then, several tests were carried out to determine the optimal kernel for winter use classification. At the end of the selection process the polynomial kernel was selected. Results obtained with RF and SVM algorithm were compared to evaluate their suitability for classifying vegetation cover into land use classes. Classification performance was estimated using a cross-validation test. The

classification was applied to a varying subset of 257 fields (500 pixels): two-thirds (171 fields or 332 pixels) were used for training, one-third (86 fields or 168 pixels) for validation. This process was repeated by changing the training/validation subsamples. Classification accuracy was assessed using OA and the Kappa index, which expresses the proportional decrease in error generated by the classification compared to the error of a completely random classification (Congalton, 1991). Finally, the vegetation cover used to map land use was classified using the algorithm with the highest OA. The classification process was tested for the two approaches: object-based and pixel-based. Sentinel-1 and Sentinel-2 parameters were classified separately and by combining optical and SAR data in the same dataset, that is, we realized a fusion at the lowest processing level (pixels level) referring to the merging of measured physical parameters (Pohl and Van Genderen, 1998). The combination of Sentinel-1 and -2 parameters were then classified.

V.3.2.4.3. Detailed winter land-use classification

For this second classification process, only the best classification approach (pixel) and algorithm (Random Forest) was used. Thus, for the detailed winter land-use classification, half of the 1 200 samples (600 “in-bag” samples) were used to train the trees, while the other half (600 “out-of-bag” samples) were used in an internal cross-validation technique to estimate the accuracy of the RF model (Belgiu and Drăguț, 2016). The *randomForest* package (v 4.6-14) (Liaw and Wiener, 2002) of R was used to perform classifications. Two RF parameters were also tuned using the “name” function of the package. The first one, the number of trees (*ntree*) randomly created from the training dataset, was set to 1 000. The second one, the number of variables used to split tree nodes (*mtry*), was set randomly.

Similarly to the global winter land-use classification, a cross-validation procedure was used to assess the classification. The RF classifier was applied to a subset of 600 training samples chosen at random, and the remaining 600 samples were used for validation. This process was repeated 100 times by changing the training and validation subsamples. Classification accuracy was assessed using OA and the Kappa index. Sentinel-1 and Sentinel-2 parameter time-series were first classified separately using the RF classifiers. Finally, the Sentinel-1 and -2 parameter time-series were combined into a single dataset using a simple integrated-stack approach (Joshi et al., 2016) and were classified using the RF classifiers.

V.4. Results and discussion

V4.1. Determination of the most efficient classification algorithm

The assessment of classification algorithm performance for the identification and characterization of winter land use is based on 100 classification models performed for each algorithm. These models were developed from 144 parameters (16 parameters X 9 dates) extracted from the Sentinel-2 time-series and 90 parameters (10 parameters X 9 dates) extracted from the Sentinel-1 sparse time-series presented in *Section III.3.1*.

Results presented in **Figure II.2** highlight significant variations between algorithms accuracies, with higher OA obtained using Sentinel-2 data than Sentinel-1 data (mean OA of 71.6 and 59.4% respectively). For Sentinel-2 data, the RF algorithm achieves the best results (mean OA of 71.6%). Conversely, the lowest accuracies are obtained with the TWDTW with a mean OA that hardly reaching 40%. The SVM and MAXLIKE obtain slightly similar results but lower than the RF algorithm (OA of 64.9% and 64.4% respectively). Moreover, a high variability can be observed for the results performed using the MAXLIKE algorithm (standard deviation of 57%).

For Sentinel-1 data, the lowest accuracy is obtained for the MAXLIKE algorithm (mean accuracy of 29%) with high variance (OA ranging from 17 to 38%). Conversely, the highest accuracies are obtained for the SVM algorithm with a mean accuracy of 59.4%. However, RF remains very similar with a mean accuracy of 57.7%. Finally, the TWDTW algorithm obtains a low accuracy with a mean accuracy of 43.5%.

These results highlight the potential of RF classifier for winter land-use identification using both optical (Sentinel-2) or SAR (Sentinel-1) data. Nevertheless, it is important to note that SVM models remain very close to the RF classification and even slightly higher for the Sentinel-1 data. In addition, we can observe the ability of MAXLIKE algorithm for classifying winter land-use based using Sentinel-2 data. However, its instability and poor results using Sentinel-1 data require us to exclude this algorithm for further work. Finally, the TWDTW obtains very low results for the classification performed with both datasets, which also require us to exclude this algorithm.

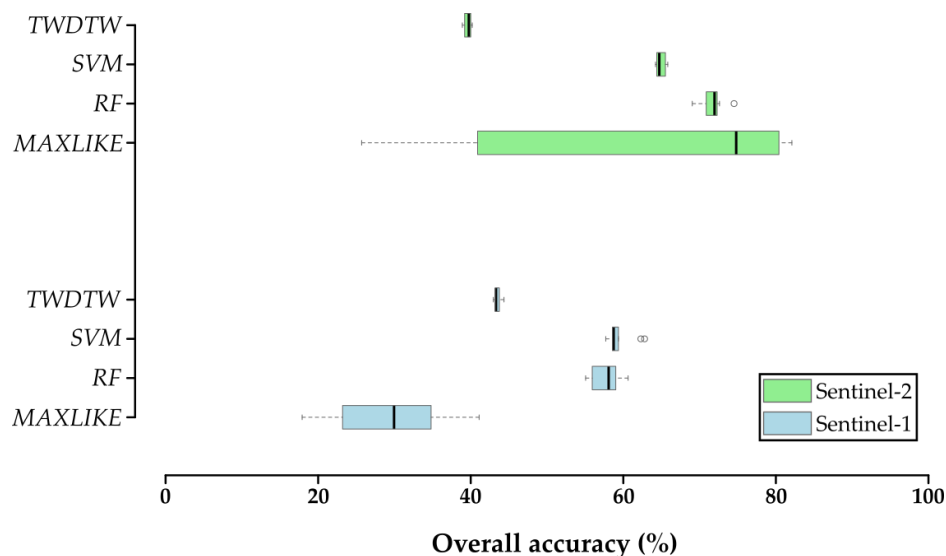


Figure II.2: Winter land-use classification accuracy according to classification algorithms. Box-and-whisker plots represent the variation in classification accuracy based on 100 iterations.

V.4.2. Analysis of temporal profiles of winter land-use

V.4.2.1. Winter crops

Examining the two most important SAR (VH and VV backscattering coefficients) and optical parameters (NDWI and NDVI) for the three winter-crop sub-types (winter barley, winter wheat, and rapeseed) (**Fig. II.3**), a strong and abrupt decrease in VV and VH on 12 October 2016 (observed in all fields regardless of sub-type) was caused by rainfall the previous day that increased humidity during the Sentinel-1 passage. Strong and abrupt decreases in VV and VH on 29 November 2016, 4 January 2017, and 9 February 2017 were caused by frost, as confirmed by the temperature records (mean temperature of -4°C , -2°C , and 2°C , respectively). Generally, the optical parameters (NDWI and NDVI) appeared more stable over time and more sensitive to winter-crop growth cycles than the SAR parameters (VV and VH), improving discrimination of the three winter crops. Although the VH and VV profiles appear complex, their variations have a physical explanation. The trends in VV and VH profiles for rapeseed (from -19 to -15 db) were similar to those for barley and wheat (from -21 to -16 db), despite having different ranges. The trends in NDWI and NDVI profiles were similar to those for the VV and VH profiles, except for April images, in which the SAR and optical profiles responded differently to crop activity. Specifically, a decrease in VV and VH from August-October for barley and wheat was due to backscatter from the soil (after harvest in July) attenuated by the growing grass and especially by progressive smoothing of the soil until 12 October 2016. This effect was confirmed by NDWI and NDVI, which decreased due to harvesting of main crops. A strong increase in VV and VH from 10-24 October 2016, which corresponded to the sowing period, was caused by strong soil backscatter due to tillage. From November-February, VV and VH remained stable or slightly decreased due to backscatter attenuated by growing grass. This growth was also identified by NDWI and NDVI, which were low in November (0.2 and 0.4 respectively) and progressively increased until February. VV decreased strongly from early March to early May, probably due to interactions between the SAR signal and the canopy and vertical structures. For VH profiles, the backscatter of soil attenuated by wheat growth is related to the high incidence angles ($> 45^{\circ}$), which are not adapted to crop monitoring (Satalino et al., 2009) and thus decrease the SAR signal. This is highlighted by the large increase in NDWI and NDVI generated by peak vegetation (in May).

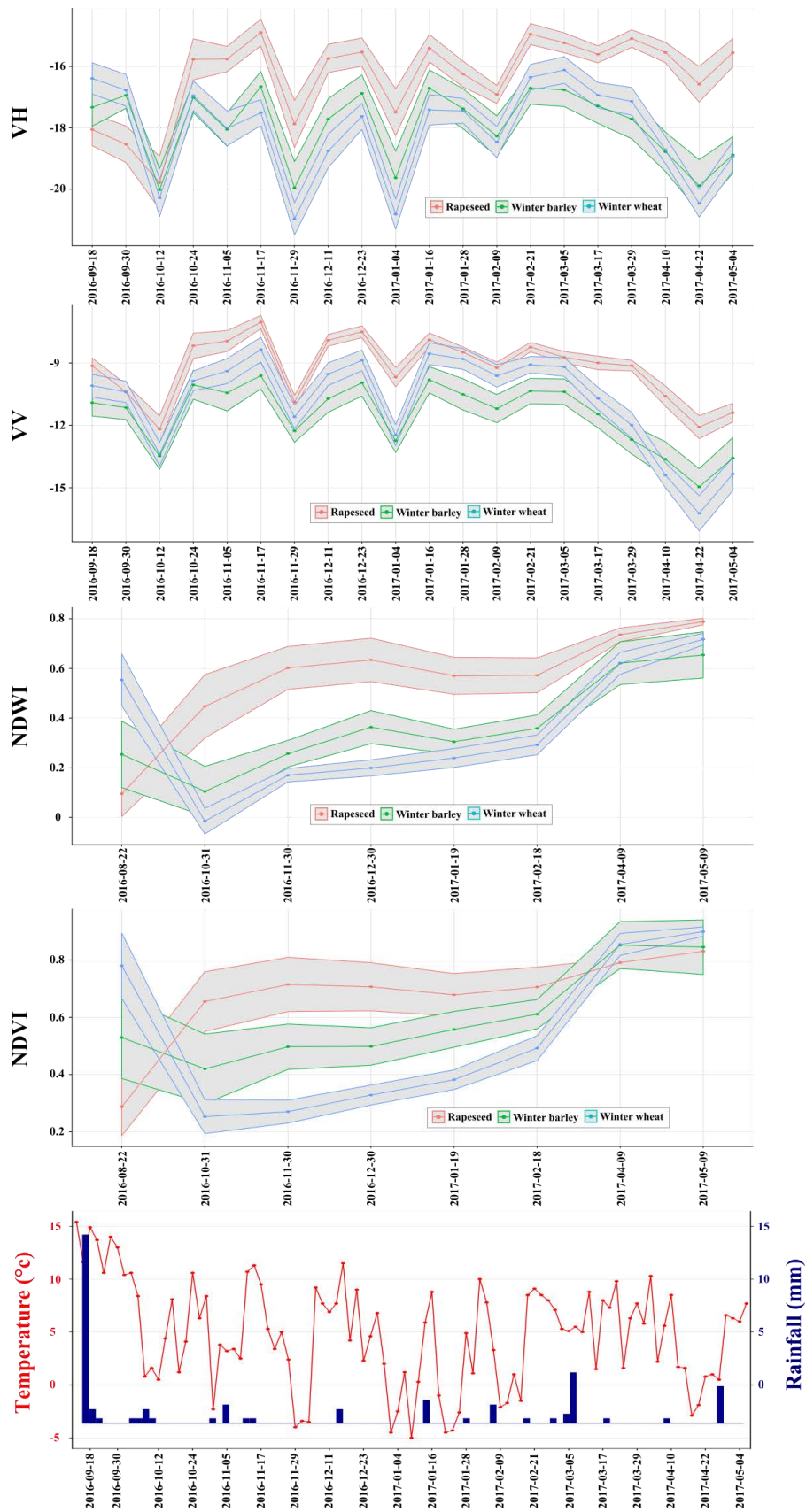


Figure II.3. Temporal profiles of SAR parameters VH and VV, optical parameters NDWI and NDVI (the central line corresponds to the median of each class and the profile limits correspond to the interquartile, 1st (lower) and 3rd (upper)), rainfall, and temperature for winter crops at the study site from September 2016 to May 2017.

V.4.2.2. Catch crops

Examining the same four parameters for the six catch-crop sub-types (fodder cabbage, oat, phacelia, phacelia and mustard, phacelia and oat, and ryegrass and clover) (**Fig. II.4**), the same sharp and abrupt decreases in VV and VH were observed (in all fields regardless of sub-type). The optical parameters (NDWI and NDVI) were also more stable over time than the SAR parameters (VV and VH) and were more sensitive to catch-crop growth cycles. The dynamics of VH and VV profiles can be explained by catch-crop characteristics. Catch crops, sown mainly after the main crops in August, have high diversity and different plant structures. From September 2016 to March 2017, catch crops grew continually, resulting in a slight increase in VV and VH. VH, which was dominated by volume-scattering mechanisms, increased due to interaction of the SAR signal with the vertical structure of the catch crops. VH was low (-15 to -21 db), however, due to the strong dominance of canopy backscatter during this period. In this context, VV, which was dominated by direct influence of the ground and canopy, also increased due to the dominance of canopy backscatter. From March to late April, which corresponded to the tilling period for catch crops, VV and VH decreased significantly due to the backscatter of vegetation blooms attenuated by soil. From April to late May, which corresponded to the sowing period for the main crops, VV and VH increased sharply due to strong soil backscatter after tillage.

NDWI and NDVI profiles differed slightly. An increase from August 2016 to early January 2017 corresponded to the catch-crop growth period, with vegetation peaks in December. NDWI and NDVI decreased gradually from January 2016 to April 2017, which corresponded to the progressive flowering of the catch crops, but increased afterwards, corresponding to the sowing and growth of the main crops. In contrast, due to continuous growth, NDWI and NDVI of the ryegrass and clover sub-type increased progressively from August 2016 to April 2017, when it was destroyed to sow the main crops.

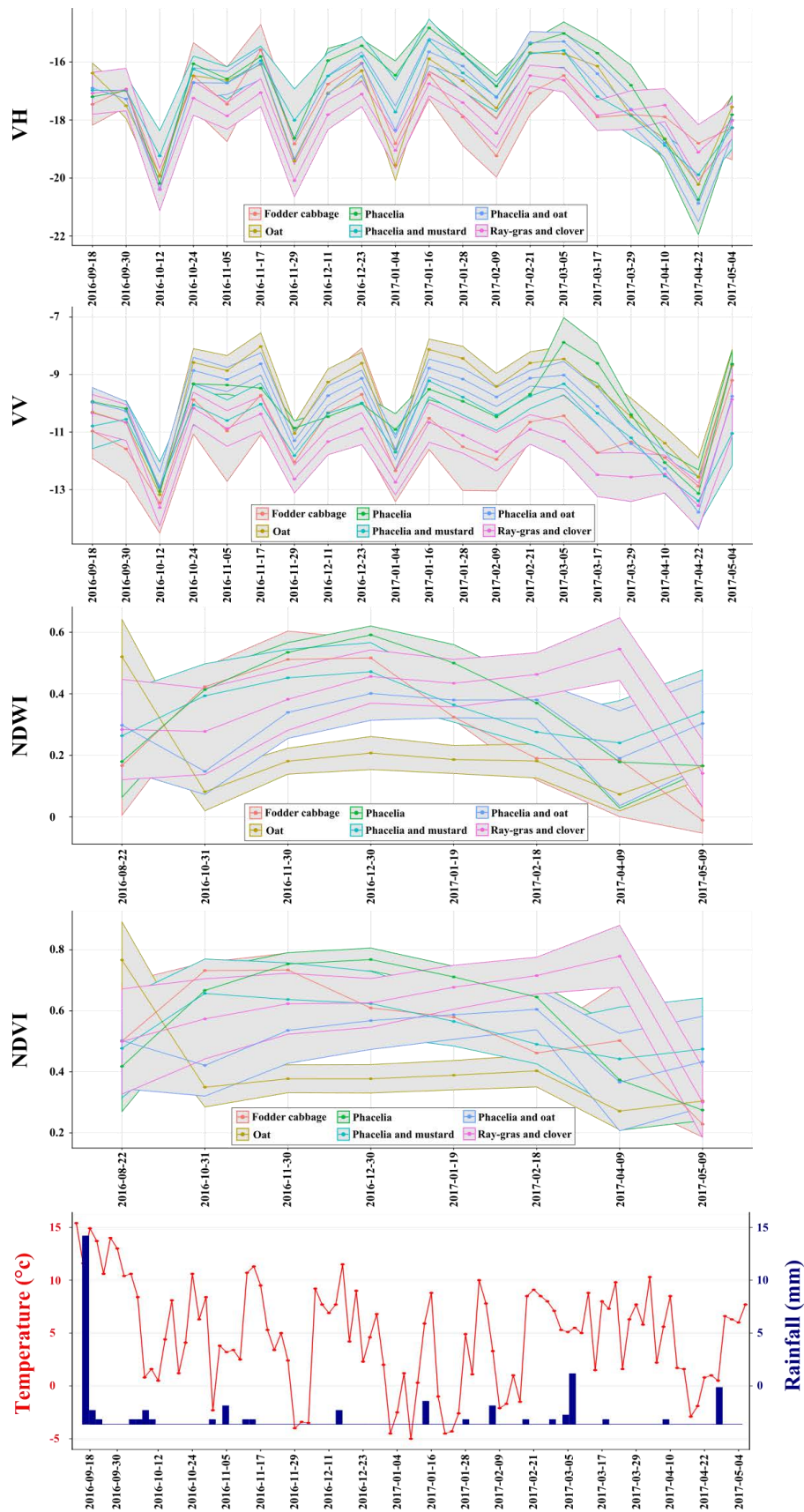


Figure II.4. Temporal profiles of SAR parameters VH and VV, optical parameters NDWI and NDVI (the central line corresponds to the median of each class and the profile limits correspond to the interquartile, 1st (lower) and 3rd (upper)), rainfall, and temperature for catch crops at the study site from September 2016 to May 2017.

V.4.2.3. Crop residues

Examining the same four parameters for crop residues (maize stalks) (**Fig. II.5**), the same strong and abrupt decreases in VV and VH were observed, while NDWI and NDVI profiles were more stable over time and more sensitive to the crop-residue cycle. VV and VH remained stable from September 2016 to March 2017 due to stabilization of soil surface conditions, after which they decreased until April, probably due to backscatter of soil resulting from growing grass. Finally, like for the other winter land-use types, VV and VH increased after April, which corresponded to sowing and growth of the main crops. The crop-residue pattern was more obvious from the optical profiles: from August-October, NDWI and NDVI decreased due to harvesting, while from November-May, they remained stable due to stabilization of soil surface conditions.

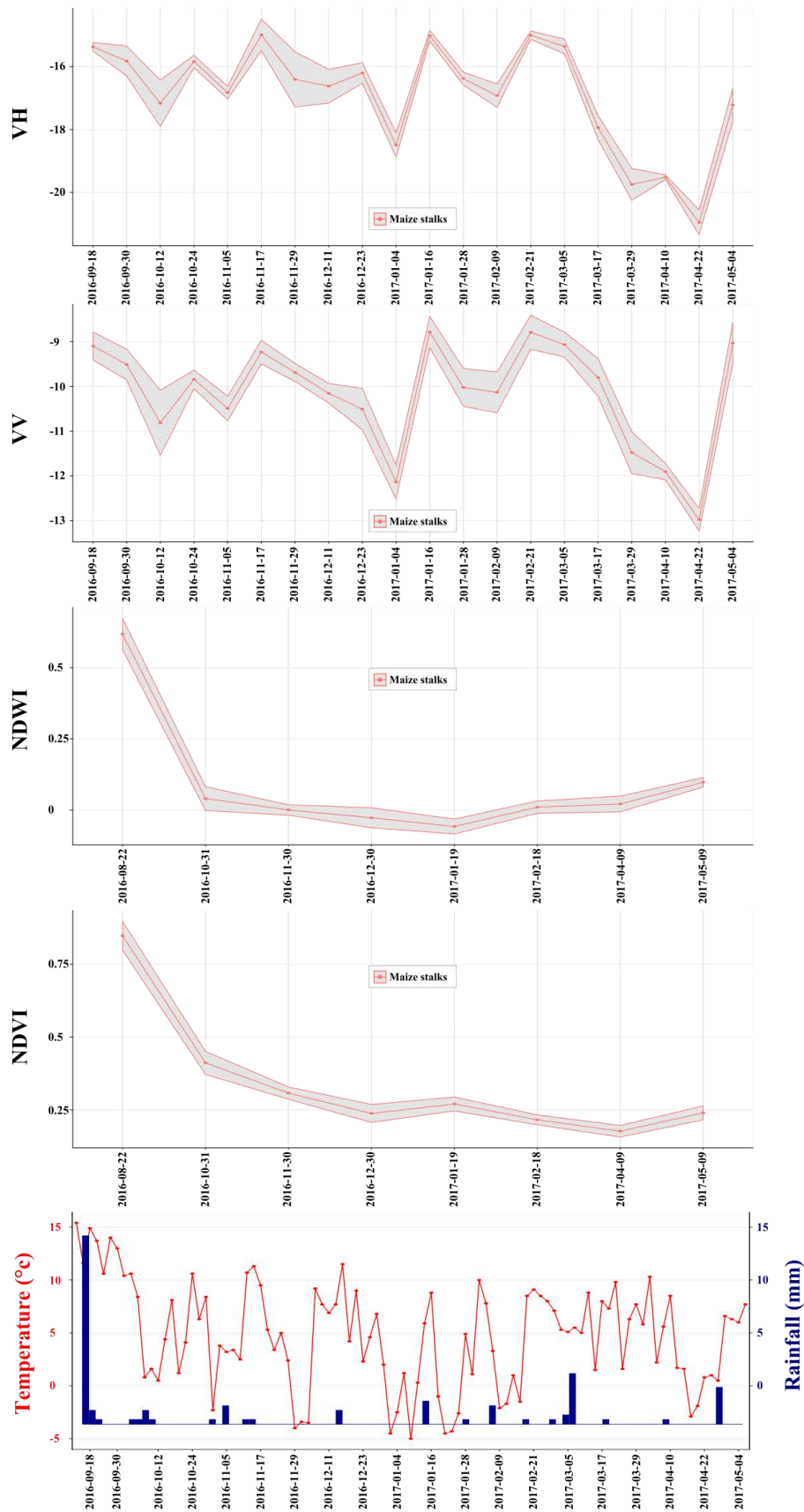


Figure II.5. Temporal profiles of SAR parameters VH and VV, optical parameters NDWI and NDVI (the central line corresponds to the median of each class and the profile limits correspond to the interquartile, 1st (lower) and 3rd (upper)), rainfall, and temperature for crop residue at the study site from September 2016 to May 2017.

V.4.2.4. Grasslands

Examining the same four parameters for the two grassland sub-types (grazed and mown) (**Fig. II.6**), the same strong and abrupt decreases in VV and VH were observed. Both SAR and optical parameters provided information useful for discriminating these sub-types: SAR parameters had lower values for grazed grasslands than mown grasslands, while the opposite was observed for optical parameters. From August 2016 to February 2017, VH increased slightly, VV decreased slightly, and NDWI and NDVI remained stable due to gradual growth. From February-May, NDWI and NDVI increased due to increasing growth of grasslands in late winter, while VV decreased slightly and VH remained stable, probably due to interactions between the vertical structure of the grasslands and the high incidence angle ($> 45^\circ$).

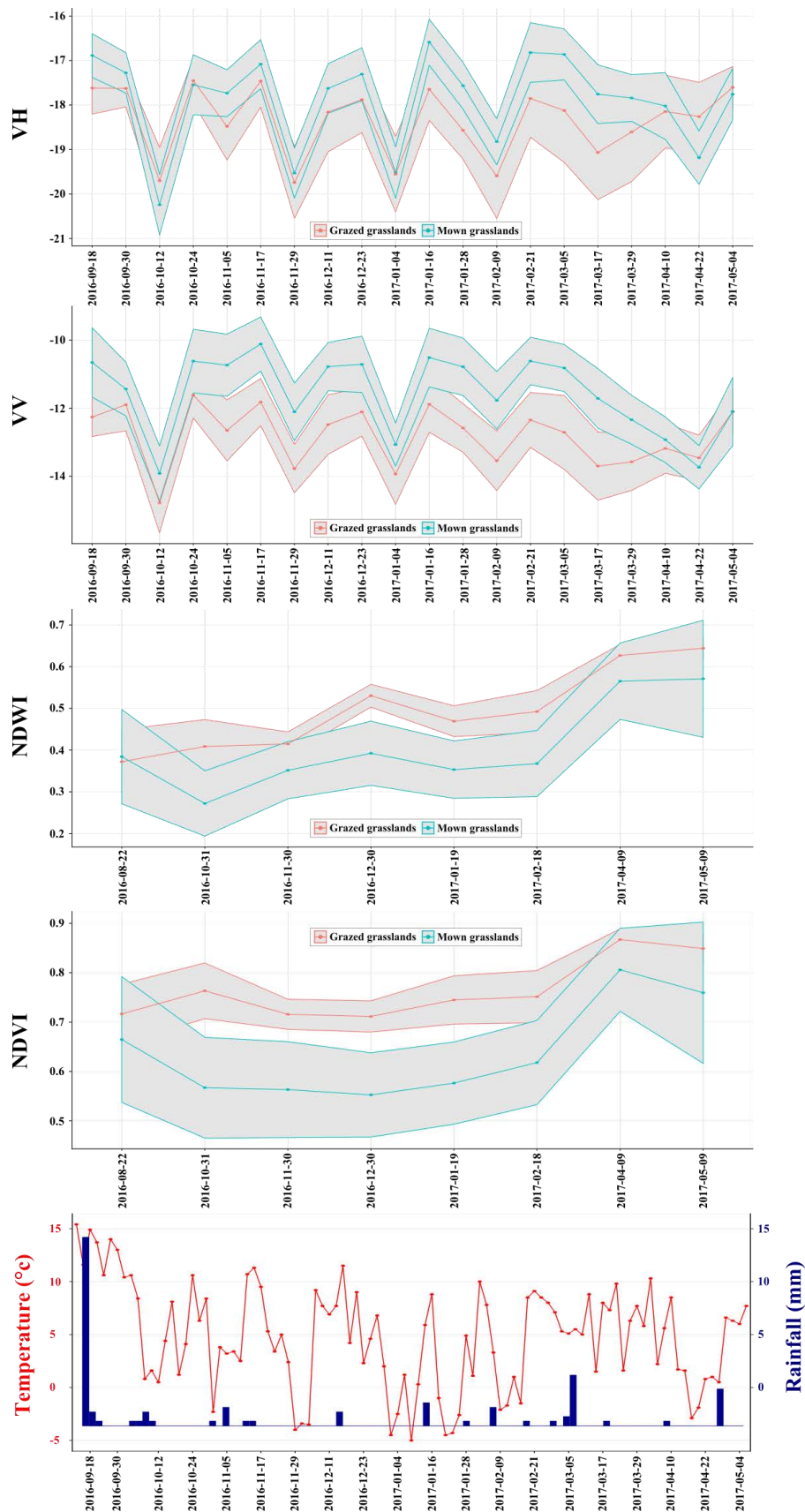


Figure II.6. Temporal profiles of SAR parameters VH and VV, optical parameters NDWI and NDVI (the central line corresponds to the median of each class and the profile limits correspond to the interquartile, 1st (lower) and 3rd (upper)), rainfall, and temperature for grasslands at the study site from September 2016 to May 2017.

V.4.3. Assessment of optical (S2) et SAR (S1) time-series potential

Approaches performed in order to evaluate the potential of optical (S2) et SAR (S1) time-series were realized according to level of classification to validate the hypothesis mentioned previously (*section V.4.2*): A global classification with 5 winter land-use classes and a detailed classification with 12 winter land-use classes.

V.4.3.1. Evaluation of Sentinel parameters importance for winter land-use classification

V.4.3.1.1. Global winter land-use classification

An analysis of the parameter relevance was performed using the RF significance function to further reduce the number of parameters to be classified. A measure of variable importance was provided for each candidate predictor using this heuristic method based on the Gini Index as mentioned in *Section V.3.2.4.1*. Thus, **Figure II.7** shows the parameter contribution to land use classifications, ranked by importance for optical and Synthetic-Aperture Radar image time-series. The break in the histogram (after band 5 in May for Sentinel-2; after polarized Shannon Entropy in April for Sentinel-1) was used as the threshold for selecting the most relevant parameters, that is, 15 optical and 15 SAR parameters. These 30 parameters were used for winter land use classifications.

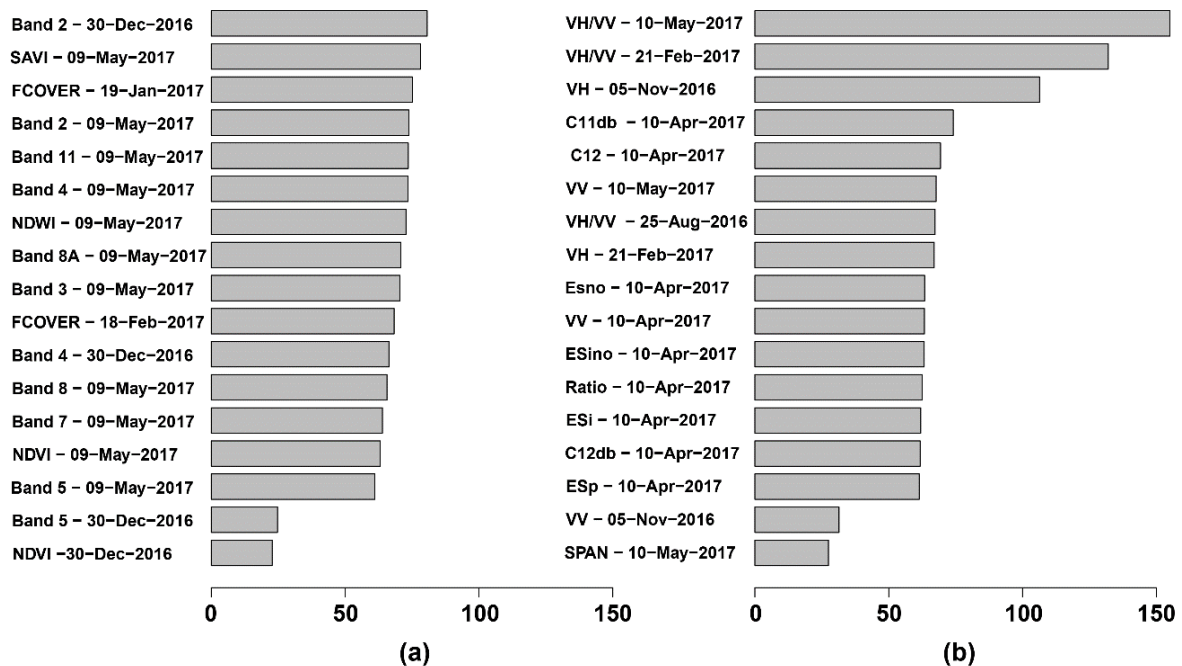


Figure II.7. Parameters that contributed the most to land use classifications, ranked by importance for (a) optical and (b) Synthetic-Aperture Radar image time-series from August 2016 to May 2017. See Table 3 for the definition of abbreviations.

The most important SAR parameter was the ratio VH/VV in May, which highlights crop growth, especially of winter crops (Veloso et al., 2017). Similarly, the backscattering coefficients were also important. Results show the importance of parameters derived from the May and April images due to their sensitivity to variations in double-bounce and volume-

scattering mechanisms (Wiseman et al., 2014). The backscattering coefficient VH calculated from the November image was also important due to its sensitivity to direct contributions from the ground and the canopy (Brown et al., 2003). These parameters highlight the difference between bare soils and crops.

Concerning optical parameters, the two most important parameters were band 2 in December 2016 and SAVI in May 2017 with a Gini index above 70. One can notice that the best NDVI parameter came in 14th position, which is not in accordance with the current literature (Yengoh et al., 2014). Results also show the importance of parameters derived from the May image, 11 parameters out of the 15 most important parameters being derived from this image. This is due to the fact that this period is the main phase of highly dynamic plant growth: vegetation peaks in May (the end of spring), when grasslands are easily detected (Fig. II.7). The spectral distributions of two of the most pertinent parameters, that is, SAVI in May 2017 and VH/VV ratio in May 2017, were computed for the five classes of winter land use (Fig. II.8). SAVI was selected over Band 2 based on the current literature, which demonstrated the potential of this vegetation index to discriminate and characterize crop dynamics (Belgiu and Csillik, 2017; Clay et al., 2006; Bargiel, 2017).

The Figure II.8.a shows the potential of SAVI to discriminate winter crops and grasslands from catch crops and crop residues in May -when the phenological stages and land use changes are most pronounced. Conversely, results highlight the difficulty to discriminate bare soils from the other classes, due to a high intra-class variance. To a lesser extent, Figure II.8.b shows the potential of the VH/VV ratio to further separate winter crops and grasslands from catch crops and crop residues. However, like the SAVI parameter, the VH/VV ratio is not sufficient to separate bare soils from other classes due to a very high intra-class variance. These results are consistent with the existing literature, which demonstrated the importance of using backscattering coefficients alone (σ_{VH}^0 or σ_{VV}^0) or in combination (VH/VV) to identify land use (Beck et al., 2006).

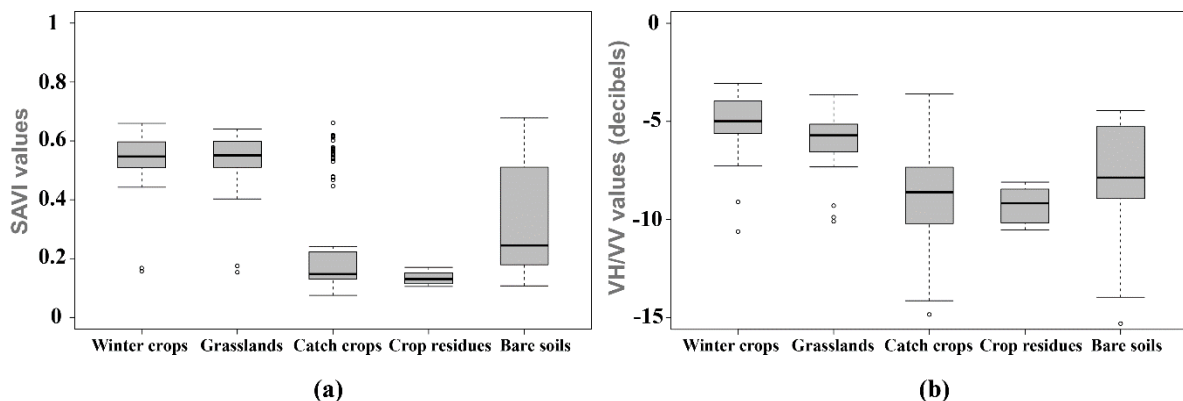


Figure II.8. Distribution of (a) the Soil Adjusted Vegetation Index (SAVI) and (b) the ratio VH/VV parameters for winter land use classes calculated from May 2017 images.

V.4.3.1.2. Detailed winter land-use classification

For SAR parameters, based on an analysis of the parameter relevance was performed using the RF significance function, 43 of the 200 parameters were selected for classification (Fig. II.9.a). Of these 43 parameters, the most important (i.e. the most frequent with a normalized Gini index > 0.13) were the VH and VV backscattering coefficients, the VH:VV ratio, and SE (Fig. II.9.a). Results revealed the importance of parameters derived from the May and April

images, from which 16 of these 43 parameters were derived. The importance of VH:VV in May and VH in April (normalized Gini index > 0.35) highlights crop growth, especially for winter crops, due to these parameters' ability to characterize plant structure and characteristics. Results also revealed the importance of October and November images, from which 8 of these 43 parameters were derived, which highlights differences between ground and canopy contributions and thus the difference between temporarily bare soils and crops.

For optical parameters, 39 of the 104 parameters were selected for classification. Of these 39 parameters, the most important (i.e. the most frequent with a normalized Gini index > 0.12) were NDWI, NDVI, Band 5 (red edge), and Band 8 (near infrared) (**Fig. II.9.b**). Results again revealed the importance of parameters derived from the May and April images (25 of the 39 parameters) due to their ability to identify the main phase of highly dynamic plant growth (vegetation peaks). The importance of Band 2 (blue) in May and NDWI in May (normalized Gini index > 0.5) enabled land-use sub-types to be discriminated.

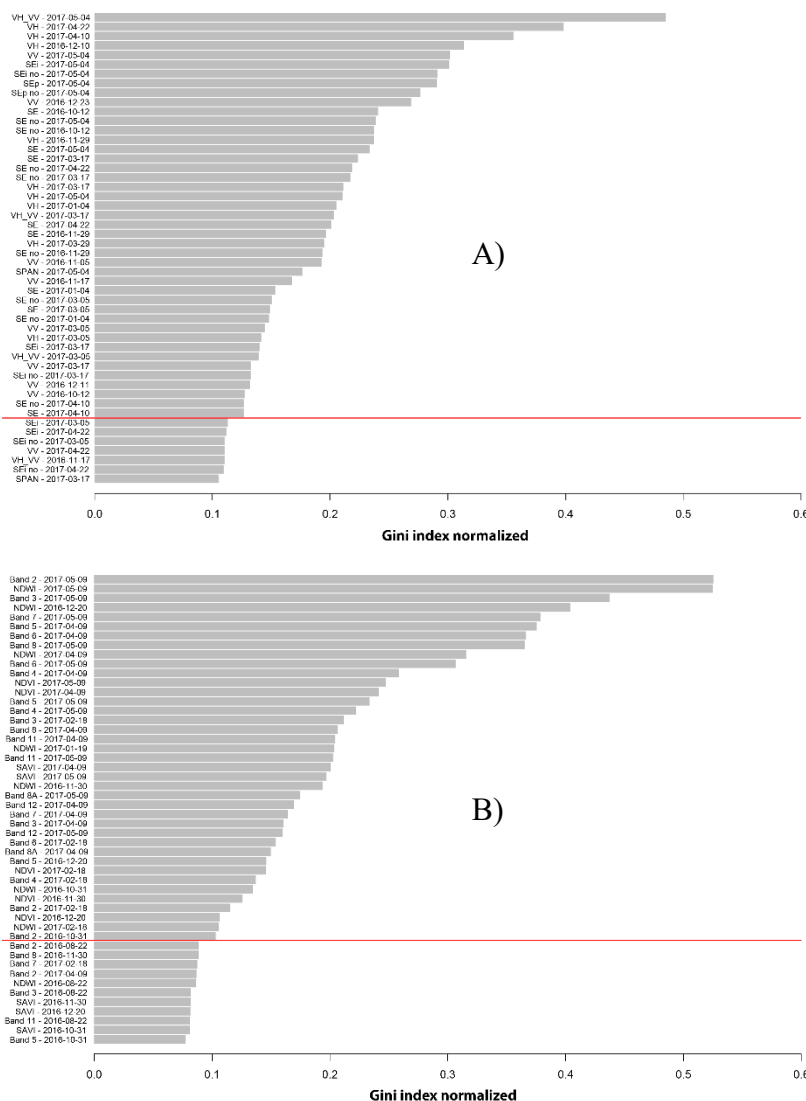


Figure II.9. Most contributing parameters to land-use classifications, ranked by importance for (a) SAR and (b) optical image time-series from August 2016 to May 2017. The most important parameters are in bold. The red lines indicate the break in each histogram used as the threshold for selecting the most important parameters.

V.4.3.2. Winter Land-Use classification

V.4.3.2.1. Global winter land-use classification

Accuracy of the winter land use classification obtained from optical and SAR parameters varied significantly depending on (i) the classification approach (i.e., pixel-based or object-based), (ii) the classification algorithm (i.e., RF or SVM) and (iii) the time-series dataset (i.e., Sentinel-1, Sentinel-2 or a combination of both).

Results of the pixel-based and object-based approaches to identifying winter land use had similar accuracy for the Sentinel-2 dataset and the combined Sentinel-1 and -2 dataset. The object-based approach had a slightly higher OA (68–83%, Kappa = 0.64–0.77) than the pixel-based approach (55–81%, Kappa = 0.51–0.77) (**Fig. II.10**). Although this is consistent with other studies of LULC (Duro et al., 2012), few studies have presented advantages of using the object-based approach instead of the pixel-based approach to identify and characterize LULC (Myint et al., 2011; Yan et al., 2006). In contrast, results obtained with the Sentinel-1 data showed the superiority of the object-based approach, due to the heterogeneity of SAR values within fields in winter.

Concerning the classification techniques, the RF algorithm had higher OA than the SVM algorithm (median OA = 81% and 79%, respectively). The RF algorithm also had less variation in OA than SVM (72–83% (Kappa = 0.67–0.77) and 68–80% (Kappa = 0.64–0.76), respectively). The potential of SVM and RF algorithms for remote sensing studies has been widely demonstrated (Pal, 2005; Mountrakis et al., 2011. Belgiu and Dragut, 2016). Our results show that the RF algorithm is slightly more accurate effective than the SVM algorithm, which is consistent with results of other studies (Gislason et al., 2006).

This study evaluated the respective advantages of Sentinel optical and SAR time-series to identify winter land use. Classification was better using a combination of Sentinel-1 and -2 parameters (median OA = 81%, Kappa = 0.77) (**Table II.3**), with OA ranging from 75-82% (Kappa = 0.68–0.77). Conversely, classifications based on either Sentinel-1 or Sentinel-2 parameters alone had OAs of 68–78% and 74–80%, respectively (**Fig. II.10**). While the results highlight the utility of Sentinel-1 and Sentinel-2 individually, they also emphasize that classification using the Sentinel-2 dataset always outperformed that using the Sentinel-1 dataset. The classification results highlight the advantages of using the combined Sentinel-1 and -2 datasets, with OA ranging from 68-83% (Kappa = 0.64–0.77). Therefore, our study confirms the effectiveness of Sentinel-1 and -2 time-series for identifying land use, as previous studies have demonstrated (Inglada et al., 2016; Veloso et al., 2017) and also shows the potential of using the combined Sentinel-1 and -2 datasets for this purpose. Additionally, the originality of this study is the identification of land use in winter.

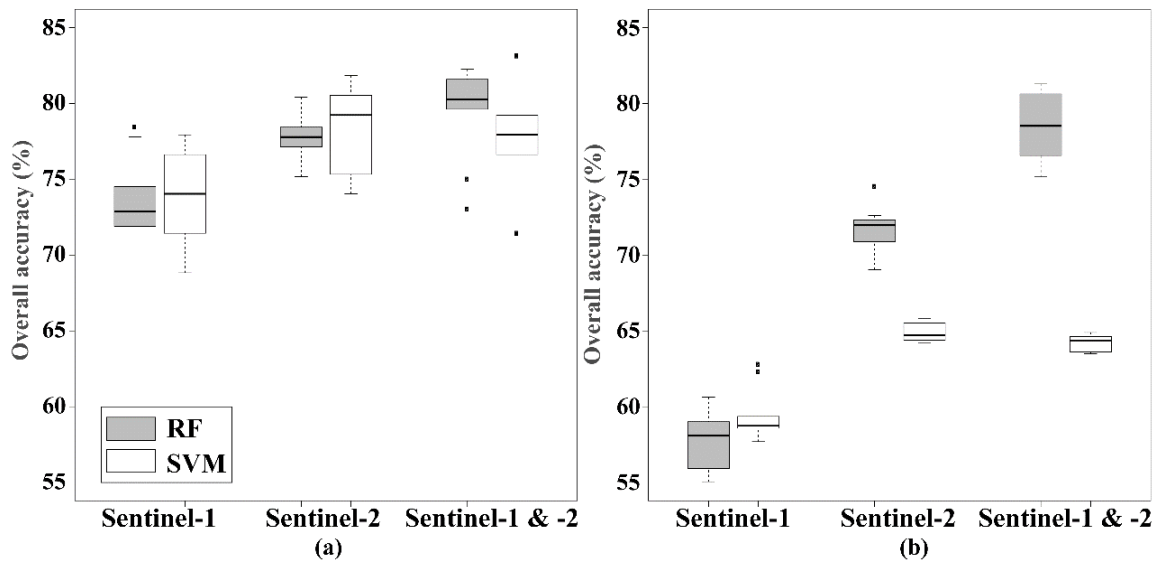


Figure II.10. Overall accuracy of (a) object-based and (b) pixel-based image classifications of winter land use, for the best Sentinel-1, Sentinel-2 and combined Sentinel-1 and -2 parameters using the Random Forest (RF) and Support Vector Machine (SVM) algorithms.

Table II.3. Median accuracy of winter land use classifications obtained for the best Sentinel-1, Sentinel-2 and combined Sentinel-1 and -2 parameters using the Random Forest (RF) and Support Vector Machine (SVM) algorithms. OA: overall accuracy, Kappa: Kappa index.

Algorithms	Datasets	Object-based Approach		Pixel-based Approach	
		OA	Kappa	OA	Kappa
RF	Sentinel-1	72%	0.67	58%	0.52
	Sentinel-2	78%	0.75	72%	0.67
	Sentinel-1 & -2	81%	0.77	79%	0.76
SVM	Sentinel-1	73%	0.67	59%	0.53
	Sentinel-2	79%	0.76	65%	0.54
	Sentinel-1 & -2	78%	0.75	64%	0.54

The best classification, with OA of 81% and Kappa of 0.77, used an object-based approach and 30 parameters derived from a combination of Sentinel-1 and -2 parameters. Misclassification errors were observed between bare soils (under- and over-estimation rates of 64% and 94%, respectively) and the other classes (**Table II.4**). This agrees with the study's difficulty in discriminating bare soils from the other classes (**Fig. II.10**).

Table II.4. Confusion matrix of the best winter land use classification obtained using a parameter dataset derived from a combination of Sentinel-1 and -2 time-series. Overall accuracy = 81%, Kappa index = 0.77.

	Catch Crops	Winter Crops	Grasslands	Crop Residues	Bare Soils	Commission Errors
Catch crops	310	42	19	0	83	68.3 %
Winter crops	1	410	20	0	23	90.3 %
Grasslands	20	56	310	0	68	68.3 %
Crop residues	0	3	0	389	62	85.7 %
Bare soils	16	7	5	0	426	93.8 %
Omission errors	89.3 %	79.2 %	87.6 %	100 %	64.4 %	81 %

The spatial distribution of winter land uses mapped at the 1:100,000 scale from the best classification (**Fig. II.11**) shows that bare soils and crop residues covered less than 5% of the UAA, while a high percentage was covered with grasslands (30%) or winter crops (35%). In general, catch crops and winter crops were located on the largest fields, while bare soils and grasslands were located on the smallest fields.

The distribution of membership probabilities associated with this classification indicates that accuracy decreased at the edges of the study site (**Fig. II.12**). Fields smaller than 1 ha had the lowest membership probability (0.47), while those larger than 10 ha had the highest (0.84), indicating that classification accuracy increased with field size. These results agree with the confusion matrix (**Table II.4**), in which misclassification was greatest for bare soils.

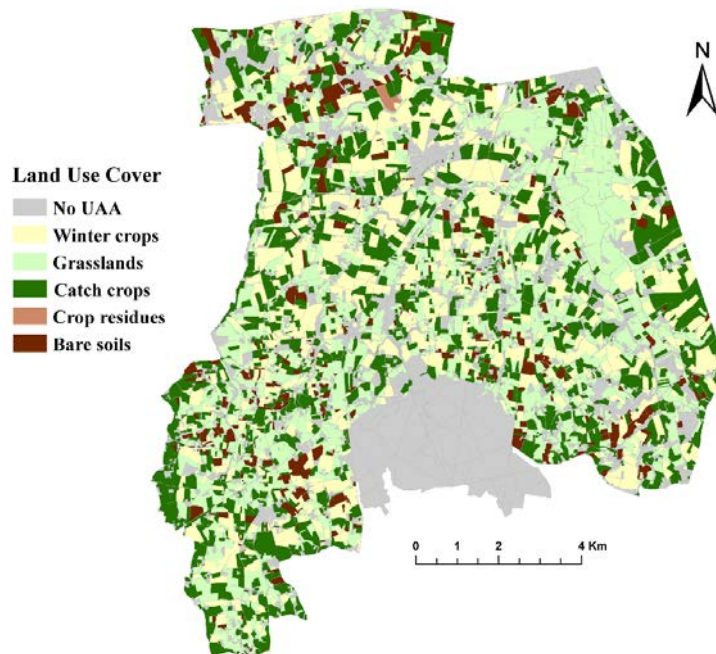


Figure II.11. Distribution of winter land use obtained using a parameter dataset derived from a combination of Sentinel-1 and -2 time-series. Classification was performed using a Random Forest algorithm.

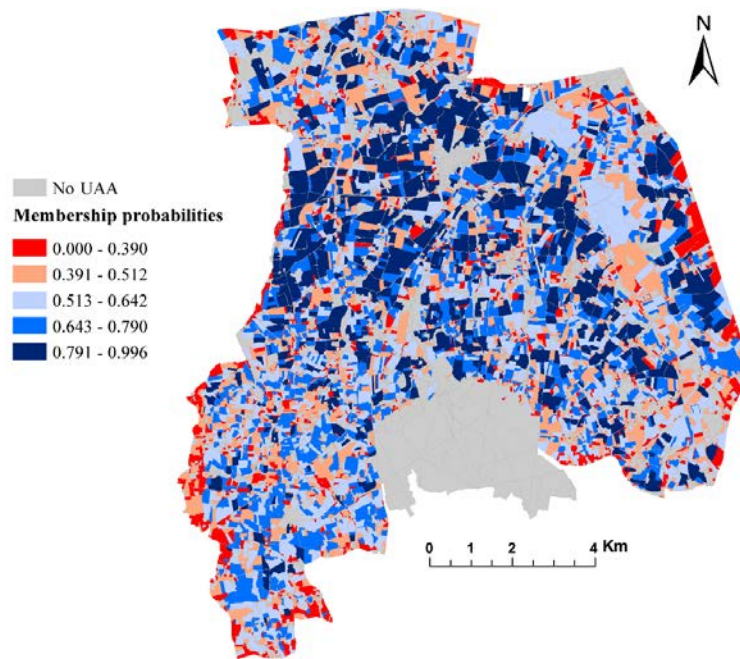


Figure II.12. Map of the distribution of winter land use membership probabilities obtained using the Random Forest algorithm.

V.4.3.2.2. Detailed winter land-use classification

Accuracy of the winter land-use classification obtained from the 82 selected parameters (43 SAR and 39 optical) using the RF algorithm varied significantly depending on the time-series dataset (i.e., Sentinel-1 dataset, Sentinel-2 dataset, or combination of both datasets). Optical data had higher classification accuracy (OA = 87%, Kappa index = 0.85) than SAR data (OA = 73%, Kappa index = 0.70) (**Table II.5**). Combining Sentinel-1 and -2 data decreased classification accuracy slightly (OA = 83%, Kappa index = 0.82), which indicates the superiority of Sentinel-2 time-series alone for mapping crops in winter. This result is inconsistent with those of studies (Carrasco et al., 2019; Inglada et al., 2016; Veloso et al., 2017) that demonstrated the potential of combining Sentinel-1 and -2 data to classify land use. In our study, however, the physical properties of winter land-use classes and weather conditions produced noise in the Sentinel-1 data, resulting in confusion between classes and lower accuracy of classification when used alone or in combination with Sentinel-2 data. Nonetheless, the results obtained using the SAR time-series are considered satisfactory and particularly useful for discriminating winter land-use in areas with high cloud cover. In addition to the superiority of optical images over SAR images, our study also confirmed the effectiveness of the RF classifier for mapping cropland already reported in the literature (Bargiel, 2017). The results highlight the importance of using key dates to classify winter land-use instead of using a temporal profile approach (Denize et al., 2019).

Table II.5. Mean accuracy (overall accuracy (OA) and Kappa index) of winter land-use classifications based on the most efficient Sentinel-1, Sentinel-2, and combined Sentinel-1 and -2 datasets using the Random Forest algorithm.

Dataset	OA (%)	Kappa
Sentinel-1	73	0.70
Sentinel-2	87	0.85
Sentinel-1 and -2	83	0.82

A confusion matrix derived from classification using the best Sentinel-2 parameters identified by the RF algorithm (**Table II.6**) showed that misclassification errors occurred mainly between winter barley and the other classes and between phacelia and winter wheat. The winter land-use map at 1:100 000 scale obtained from the Sentinel-2 image time-series (**Fig. II.13**) contained a few artifacts resulting from pixel-level classification. Crop residues covered less than 5% of the UAA, compared to 30% and 35% for grasslands and winter crops, respectively.

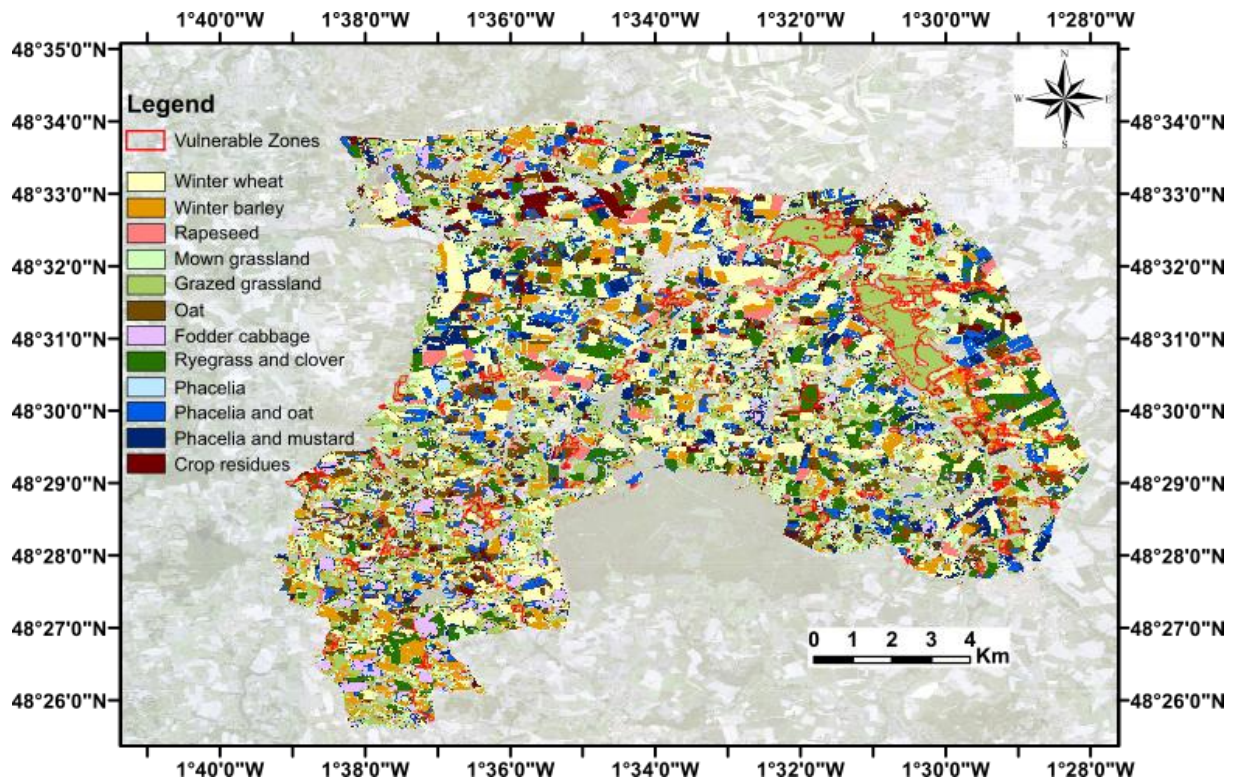


Figure II.13. Map of winter land-use obtained from the Sentinel-2 image time-series. A Random Forest algorithm classification was performed.

Our study benefited from the spatial and temporal resolution of Sentinel imagery for mapping winter land-use. The spatial resolution of the Sentinel sensor (10 and 20 m) successfully classified crops in the study site, except in areas with small fields, where the agricultural landscape is highly fragmented, for which misclassification errors and artifacts occurred more frequently (**Fig. II.13**). Other studies have reported advantages of the Sentinel spatial resolution for mapping cropland (Belgiu and Csillik, 2018; Vuolo et al., 2018) and for identifying and characterizing crop phenology (Bargiel, 2017; Minh et al., 2018; Veloso et al., 2017). The high temporal resolution of the freely available Sentinel imagery (5 days) increases the opportunity of finding cloud-free optical data, particularly when investigating land use in winter, when cloud cover is greater (Yan and Roy, 2015). Our results clearly demonstrate the value of Sentinel-2 time-series for mapping and monitoring land use in winter, and that Sentinel-1 data do not improve classification accuracy when the number of cloud-free optical images is sufficient. However, we suggest that SAR time-series can be especially useful in areas with high cloud cover.

Table II.6. Confusion matrix of the best winter land-use classification obtained using the Sentinel-2 time-series. Overall accuracy = 87%, Kappa index = 0.85.

	1	2	3	4	5	6	7	8	9	10	11	12	Commission Errors (%)
1: Winter wheat	45	5	2	0	0	0	8	0	0	0	0	0	75
2: Winter barley	0	39	0	1	0	0	0	0	0	0	0	0	97.5
3: Rapeseed	1	0	40	0	0	0	0	0	0	0	0	0	97.6
4: Mown grasslands	3	4	0	35	0	0	0	0	0	0	0	0	83.3
5: Grazed grasslands	2	3	0	1	37	0	0	1	0	0	5	0	75.5
6: Oat	0	0	0	1	0	49	3	0	0	0	0	1	90.7
7: Phacelia and oat	1	0	0	0	0	1	36	0	0	0	2	0	90
8: Fodder cabbage	0	0	0	0	0	0	1	45	0	3	0	0	91.8
9: Ryegrass and clover	1	0	0	0	0	0	0	3	38	2	0	0	86.4
10: Phacelia	0	0	0	0	0	1	1	0	0	41	0	0	95.3
11: Phacelia and mustard	0	0	0	2	0	2	3	0	0	0	36	0	83.7
12: Crop residues	0	0	0	0	0	0	0	0	0	0	1	50	98
Omission errors (%)	84.9	76.5	95.2	87.5	100	92.5	69.2	91.8	100	89.1	81.8	98	88.8

V.5. Conclusions

In this chapter, we evaluated the potential of Sentinel-1 and -2 time-series images for global and detailed mapping of winter land-use. Based on a methodological approach, the results highlighted the potential RF and SVM classifiers for the winter land-use classification with slightly better results for RF. The temporal profiles of Sentinel-1 and -2 parameters extracted from the time-series images were interpreted with the support of meteorological data. We demonstrated the ability of NDWI and NDVI derived from Sentinel-2 data to discriminate winter land-use classes. We also demonstrated that Sentinel-2 data had higher classification accuracy (OA = 87%, Kappa index = 0.85) than Sentinel-1 data (OA = 73%, Kappa index = 0.70). Also, inconsistent with other studies, combining Sentinel-1 and -2 data decreased classification accuracy slightly (OA = 83%, Kappa index = 0.82), which indicated that there is no need to combine Sentinel-1 and -2 datasets to improve the accuracy of discriminating crops in winter. Our results also indicate that SAR time-series are especially useful for discriminating land-use in winter in areas with high cloud cover, where cloud-free optical data are less available. While the Sentinel-1 and -2 time-series provided high classification accuracy, most misclassification errors and artifacts were located in small fields due to the spatial resolution of the Sentinel sensor (10 and 20 m), which was not suitable. Future research could assess the use of very high spatial resolution time-series from satellite images, such as ALOS-2 or RADARSAT-2 data, to improve the accuracy of mapping land use in winter.

V.6. References

- Bannari, A., Morin, D., Bonn, F., Huete, A.R., 1995. A review of vegetation indices. *Remote sensing reviews* 13, 95–120.
- Bargiel, D., 2017. A new method for crop classification combining time series of radar images and crop phenology information. *Remote sensing of environment* 198, 369–383.
- Beck, P.S., Atzberger, C., Høgda, K.A., Johansen, B., Skidmore, A.K., 2006. Improved monitoring of vegetation dynamics at very high latitudes: A new method using MODIS NDVI. *Remote sensing of Environment* 100, 321–334.
- Belgiu, M., Csillik, O., 2018. Sentinel-2 cropland mapping using pixel-based and object-based time-weighted dynamic time warping analysis. *Remote sensing of environment* 204, 509–523.
- Belgiu, M., Drăguț, L., 2016. Random forest in remote sensing: A review of applications and future directions. *ISPRS Journal of Photogrammetry and Remote Sensing* 114, 24–31.
- Betbeder, J., Fieuzal, R., Philippets, Y., Ferro-Famil, L., Baup, F., 2015. Estimation of crop parameters using multi-temporal optical and radar polarimetric satellite data, in: *Remote Sensing for Agriculture, Ecosystems, and Hydrology XVII*. International Society for Optics and Photonics, p. 963702.
- Breiman, L., 2001. Random forests. *Machine learning* 45, 5–32.
- Brown, S.C., Quegan, S., Morrison, K., Bennett, J.C., Cookmartin, G., 2003. High-resolution measurements of scattering in wheat canopies-Implications for crop parameter retrieval. *IEEE Transactions on Geoscience and Remote Sensing* 41, 1602–1610.
- Carrasco, L., O'Neil, A.W., Morton, R.D., Rowland, C.S., 2019. Evaluating combinations of temporally aggregated Sentinel-1, Sentinel-2 and Landsat 8 For land cover mapping with Google Earth Engine. *Remote Sensing* 11, 288.

Clay, D.E., Kim, K.-I., Chang, J., Clay, S.A., Dalsted, K., 2006. Characterizing water and nitrogen stress in corn using remote sensing. *Agronomy Journal* 98, 579–587.

Congalton, R.G., 1991. A review of assessing the accuracy of classifications of remotely sensed data. *Remote sensing of environment* 37, 35–46.

Cortes, C., Vapnik, V., 1995. Support-vector networks *Machine learning* (pp. 237–297), Vol. 20. Boston, MA: Kluwer Academic Publisher.

Dabney, S.M., McGregor, K.C., Wilson, G.V., Cullum, R.F., 2009. How management of grass hedges affects their erosion reduction potential. *Soil Science Society of America Journal* 73, 241–254.

Denize, J., Hubert-Moy, L., Betbeder, J., Corgne, S., Baudry, J., Pottier, E., 2019. Evaluation of using sentinel-1 and-2 time-series to identify winter land use in agricultural landscapes. *Remote Sensing* 11, 37.

Dimitriadou, E., Hornik, K., Leisch, F., Meyer, D., Weingessel, A., 2008. Misc functions of the Department of Statistics (e1071), TU Wien. R package 1, 5–24.

Duro, D.C., Franklin, S.E., Dubé, M.G., 2012. A comparison of pixel-based and object-based image analysis with selected machine learning algorithms for the classification of agricultural landscapes using SPOT-5 HRG imagery. *Remote sensing of environment* 118, 259–272.

Dusseux, P., Corpetti, T., Hubert-Moy, L., Corgne, S., 2014. Combined use of multi-temporal optical and radar satellite images for grassland monitoring. *Remote Sensing* 6, 6163–6182.

Fieuzal, R., Baup, F., Marais-Sicre, C., 2013. Monitoring wheat and rapeseed by using synchronous optical and radar satellite data—From temporal signatures to crop parameters estimation. *Advances in Remote Sensing* 2, 162.

Forkuor, G., Dimobe, K., Serme, I., Tondoh, J.E., 2018. Landsat-8 vs. Sentinel-2: examining the added value of sentinel-2's red-edge bands to land-use and land-cover mapping in Burkina Faso. *GIScience & remote sensing* 55, 331–354.

Galloway, J.N., Dentener, F.J., Capone, D.G., Boyer, E.W., Howarth, R.W., Seitzinger, S.P., Asner, G.P., Cleveland, C.C., Green, P.A., Holland, E.A., 2004. Nitrogen cycles: past, present, and future. *Biogeochemistry* 70, 153–226.

Gislason, P.O., Benediktsson, J.A., Sveinsson, J.R., 2006. Random forests for land cover classification. *Pattern Recognition Letters* 27, 294–300.

Gu, Y., Hunt, E., Wardlow, B., Basara, J.B., Brown, J.F., Verdin, J.P., 2008. Evaluation of MODIS NDVI and NDWI for vegetation drought monitoring using Oklahoma Mesonet soil moisture data. *Geophysical Research Letters* 35.

Haldar, D., Rana, P., Yadav, M., Hooda, R.S., Chakraborty, M., 2016. Time series analysis of co-polarization phase difference (PPD) for winter field crops using polarimetric C-band SAR data. *International Journal of Remote Sensing* 37, 3753–3770.

Inglada, J., Vincent, A., Arias, M., Marais-Sicre, C., 2016. Improved early crop type identification by joint use of high temporal resolution SAR and optical image time series. *Remote Sensing* 8, 362.

Jackson, T.J., Schmugge, T.J., 1991. Vegetation effects on the microwave emission of soils. *Remote Sensing of Environment* 36, 203–212.

Jacquemoud, S., Verhoef, W., Baret, F., Bacour, C., Zarco-Tejada, P.J., Asner, G.P., François, C., Ustin, S.L., 2009. PROSPECT+ SAIL models: A review of use for vegetation characterization. *Remote sensing of environment* 113, S56–S66.

Jakubauskas, M.E., Legates, D.R., Kastens, J.H., 2002. Crop identification using harmonic analysis of time-series AVHRR NDVI data. *Computers and electronics in agriculture* 37, 127–139.

Joshi, N., Baumann, M., Ehammer, A., Fensholt, R., Grogan, K., Hostert, P., Jepsen, M., Kuemmerle, T., Meyfroidt, P., Mitchard, E., 2016. A review of the application of optical and radar remote sensing data fusion to land use mapping and monitoring. *Remote Sensing* 8, 70.

Kostelich, E.J., Schreiber, T., 1993. Noise reduction in chaotic time-series data: A survey of common methods. *Physical Review E* 48, 1752.

Kuenzer, C., Dech, S., Wagner, W., 2015. Remote sensing time series revealing land surface dynamics: Status quo and the pathway ahead, in: *Remote Sensing Time Series*. Springer, pp. 1–24.

Lawrence, R.L., Wood, S.D., Sheley, R.L., 2006. Mapping invasive plants using hyperspectral imagery and Breiman Cutler classifications (RandomForest). *Remote Sensing of Environment* 100, 356–362.

Lecerf, R., Corpetti, T., Hubert-Moy, L., Dubreuil, V., 2005. Monitoring land use and land cover changes in oceanic and fragmented landscapes with reconstructed MODIS time series, in: *International Workshop on the Analysis of Multi-Temporal Remote Sensing Images, 2005*. IEEE, pp. 195–199.

Lee, J.-S., 1981. Speckle analysis and smoothing of synthetic aperture radar images. *Computer graphics and image processing* 17, 24–32.

Lee, J.-S., Wen, J.-H., Ainsworth, T.L., Chen, K.-S., Chen, A.J., 2008. Improved sigma filter for speckle filtering of SAR imagery. *IEEE Transactions on Geoscience and Remote Sensing* 47, 202–213.

Liaw, A., Wiener, M., 2002. Classification and regression by randomForest. *R news* 2, 18–22.

Lusch, D.P., 1999. Introduction to microwave remote sensing. Center for Remote Sensing and Geographic Information Science Michigan State University.

Maus, V., Câmara, G., Cartaxo, R., Sanchez, A., Ramos, F.M., de Queiroz, G.R., 2016. A time-weighted dynamic time warping method for land-use and land-cover mapping. *IEEE Journal of Selected Topics in Applied Earth Observations and Remote Sensing* 9, 3729–3739.

McNairn, H., Brisco, B., 2004. The application of C-band polarimetric SAR for agriculture: a review. *Canadian Journal of Remote Sensing* 30, 525–542.

Mercier, A., Betbeder, J., Rumiano, F., Baudry, J., Gond, V., Blanc, L., Bourgoïn, C., Cornu, G., Marchamalo, M., Pocard-Chapuis, R., 2019. Evaluation of Sentinel-1 and 2 Time Series for Land Cover Classification of Forest–Agriculture Mosaics in Temperate and Tropical Landscapes. *Remote Sensing* 11, 979.

Minh, D.H.T., Ienco, D., Gaetano, R., Lalande, N., Ndikumana, E., Osman, F., Maurel, P., 2018. Deep recurrent neural networks for winter vegetation quality mapping via multitemporal SAR Sentinel-1. *IEEE Geoscience and Remote Sensing Letters* 15, 464–468.

Mountrakis, G., Im, J., Ogole, C., 2011. Support vector machines in remote sensing: A review. *ISPRS Journal of Photogrammetry and Remote Sensing* 66, 247–259.

Myint, S.W., Gober, P., Brazel, A., Grossman-Clarke, S., Weng, Q., 2011. Per-pixel vs. object-based classification of urban land cover extraction using high spatial resolution imagery. *Remote sensing of environment* 115, 1145–1161.

Pacheco, A., McNairn, H., 2010. Evaluating multispectral remote sensing and spectral unmixing analysis for crop residue mapping. *Remote Sensing of Environment* 114, 2219–2228.

Pal, M., 2005. Random forest classifier for remote sensing classification. *International Journal of Remote Sensing* 26, 217–222.

Pohl, C., Van Genderen, J.L., 1998. Review article multisensor image fusion in remote sensing: concepts, methods and applications. *International journal of remote sensing* 19, 823–854.

Pottier, E., Ferro-Famil, L., 2012. PolSARPro V5. 0: An ESA educational toolbox used for self-education in the field of POLSAR and POL-INSAR data analysis, in: 2012 IEEE International Geoscience and Remote Sensing Symposium. IEEE, pp. 7377–7380.

Réfrégier, P., Morio, J., 2006. Shannon entropy of partially polarized and partially coherent light with Gaussian fluctuations. *JOSA A* 23, 3036–3044.

Satalino, G., Mattia, F., Le Toan, T., Rinaldi, M., 2009. Wheat crop mapping by using ASAR AP data. *IEEE Transactions on Geoscience and Remote Sensing* 47, 527–530.

Skakun, S., Kussul, N., Shelestov, A.Y., Lavreniuk, M., Kussul, O., 2015. Efficiency assessment of multitemporal C-band Radarsat-2 intensity and Landsat-8 surface reflectance satellite imagery for crop classification in Ukraine. *IEEE Journal of Selected Topics in Applied Earth Observations and Remote Sensing* 9, 3712–3719.

Smith, A.M., Major, D.J., 1996. Radar backscatter and crop residues. *Canadian journal of remote sensing* 22, 243–247.

Su, J.J., van Bochove, E., Thériault, G., Novotna, B., Khaldoune, J., Denault, J.T., Zhou, J., Nolin, M.C., Hu, C.X., Bernier, M., 2011. Effects of snowmelt on phosphorus and sediment losses from agricultural watersheds in Eastern Canada. *Agricultural water management* 98, 867–876.

Sun, C., Bian, Y., Zhou, T., Pan, J., 2019. Using of Multi-Source and Multi-Temporal Remote Sensing Data Improves Crop-Type Mapping in the Subtropical Agriculture Region. *Sensors* 19, 2401.

Torbick, N., Chowdhury, D., Salas, W., Qi, J., 2017. Monitoring rice agriculture across myanmar using time series Sentinel-1 assisted by Landsat-8 and PALSAR-2. *Remote Sensing* 9, 119.

Ulaby, F.T., Moore, R.K., Fung, A.K., 1986. *Microwave remote sensing: Active and passive. Volume 3-From theory to applications.*

Veloso, A., Mermoz, S., Bouvet, A., Le Toan, T., Planells, M., Dejoux, J.-F., Ceschia, E., 2017. Understanding the temporal behavior of crops using Sentinel-1 and Sentinel-2-like data for agricultural applications. *Remote sensing of environment* 199, 415–426.

Vuolo, F., Neuwirth, M., Immitzer, M., Atzberger, C., Ng, W.-T., 2018. How much does multi-temporal Sentinel-2 data improve crop type classification? *International journal of applied earth observation and geoinformation* 72, 122–130.

Wardlow, B.D., Egbert, S.L., 2008. Large-area crop mapping using time-series MODIS 250 m NDVI data: An assessment for the US Central Great Plains. *Remote sensing of environment* 112, 1096–1116.

Weiss, M., Baret, F., Smith, G.J., Jonckheere, I., Coppin, P., 2004. Review of methods for in situ leaf area index (LAI) determination: Part II. Estimation of LAI, errors and sampling. *Agricultural and forest meteorology* 121, 37–53.

Wiseman, G., McNairn, H., Homayouni, S., Shang, J., 2014. RADARSAT-2 polarimetric SAR response to crop biomass for agricultural production monitoring. *IEEE Journal of Selected Topics in Applied Earth Observations and Remote Sensing* 7, 4461–4471.

Yan, G., Mas, J.-F., Maathuis, B.H.P., Xiangmin, Z., Van Dijk, P.M., 2006. Comparison of pixel-based and object-oriented image classification approaches—a case study in a coal fire area, Wuda, Inner Mongolia, China. *International Journal of Remote Sensing* 27, 4039–4055.

Yan, L., Roy, D.P., 2015. Improved time series land cover classification by missing-observation-adaptive nonlinear dimensionality reduction. *Remote Sensing of Environment* 158, 478–491.

Yengoh, G.T., Dent, D., Olsson, L., Tengberg, A.E., Tucker III, C.J., 2015. *Use of the Normalized Difference Vegetation Index (NDVI) to Assess Land Degradation at Multiple Scales: Current Status, Future Trends, and Practical Considerations.* Springer.

Conclusion of the second part

In this second part, the approach implemented aimed to determine the most appropriate classification procedure to identify and characterize winter land-use as the main factor to prevent and reduce the agricultural pollutant transfers. In this context, three objectives have been set: i) Determine the most efficient classifiers to study winter land-use; ii) Identify an optimal winter land-use nomenclature iii) Assess the potential of optical (S2) et SAR (S1) time-series for winter land-use classification at a local scale.

Thus, at the local level, winter land-use was studied using time-series of optical Sentinel-2 and SAR Sentinel-1 images. The first objective was to determine by a comparative approach the most efficient classification algorithm to identify winter land-use classes using remote sensing data. The results obtained first demonstrated high variability in the algorithms accuracies to classify a similar sample of winter land-use classes. Afterwards, we established that the Random Forest and SVM classifiers were the most adapted for the studied problematic, either from Sentinel-2 optical data or from Sentinel-1 SAR data.

In a second step, we analyze and interpret the interactions that may occur between the optical or SAR signal and winter land-use classes. The results demonstrated the ability of remote sensing data to meet this objective. However, they also highlighted the limits of the Sentinel-1 data to discriminate some land-use classes such as catch crops. In contrast, the Sentinel-2 data proved their ability to discriminate finely land-use classes during winter. Thus, this first approach highlighted the potential of the Sentinel-2 data and in particular, the NDVI and NDWI ratios that obtain the best discrimination. In addition, the results allowed to readjust the land-use classification whose limits had been emphasized in the conclusion of the first step of this part.

Afterwards, feedbacks from the first step have led to a better appreciation of the potential of Sentinel-1 and -2 images. Thus, a new classification procedure adapted to the different points highlighted so far was developed. The results obtained then demonstrated the full potential of the Sentinel data and in particular of Sentinel-2 for which the classification accuracies remain significantly higher than those obtained during the second part of the manuscript with a Kappa index of 0.85 for a 12 winter land-use classes classification. These results have also presented, in contrast to the studies conducted to date, the limits of the combined Sentinel-1 and -2 approach, for which classification accuracy remains lower than those obtained with only Sentinel-2 data. In addition, they pointed out the limits of Sentinel-1 SAR data for the detailed identification and characterization of winter land-use. However, the Sentinel-1 time-series have shown some interest in discriminating between specific land-use classes, particularly when cloud cover becomes a limiting factor and prevents the acquisition of optical data. Thus, an extensive study on the potential of SAR satellite imagery will be presented in the fourth part in order to evaluate their potential to identify and characterize winter land-use.

3

SAR configuration for the study of winter land-use at a local scale

Contents

INTRODUCTION OF PART THREE	129
CHAPTER 6: IDENTIFICATION OF WINTER LAND-USE USING POLARIMETRIC SAR TIME-SERIES	131
CONCLUSION OF THE THREE PART	161

Introduction of part three

The third part of the manuscript presents the work conducted in order to evaluate the potential of SAR time-series images (Sentinel-1, RADARSAT-2, and ALOS-2) for the identification of winter land-use. This part attempts to meet the limits and perspectives of SAR data presented in the third part conclusion, which pointed out the limits of Sentinel-1 SAR images to study winter land-use classes. In order to achieve this issue, an objective was implemented. This objective aims to determine the most appropriate SAR configuration (polarization, frequency, the density of time-series) for the identification of winter land-use. The methodological framework of this part was developed in *Section IV.3*.

In chapter six, winter land-use classes will be studied at a local scale based on three SAR time-series of Sentinel-1, Radarsat-2 and Alos-2 acquired between August 2016 and May 2017 over the ZAA and presented in *Section III.3.1*. First, a pre-processing methodology will be developed to extract SAR parameter datasets from the quad-pol C-band, dual-pol C-band, and dual-pol L-band time-series. Secondly, a comparative approach will be performed based on a classification procedure using RF classifier in order to determine the most efficient SAR configuration for land-use classification during the winter season.

Chapter 6

Identification of winter land-use using polarimetric SAR time-series

Contents

VI.1. INTRODUCTION	ERREUR ! SIGNET NON DEFINI.
VI.2. MATERIALS AND METHODS	ERREUR ! SIGNET NON DEFINI.
VI.3. RESULTS	ERREUR ! SIGNET NON DEFINI.
VI.4. DISCUSSION	ERREUR ! SIGNET NON DEFINI.
VI.5. CONCLUSIONS	ERREUR ! SIGNET NON DEFINI.



This chapter was published in a peer-reviewed journal

Denize, J., Hubert-Moy, L., & Pottier, E. (2019). Polarimetric SAR Time-Series for Identification of Winter Land Use. *Sensors*, 19(24), 5574. and presented in two international conferences

Conference EUSAR (12th European Conference on Synthetic Aperture Radar), Aachen (Germany), 4-7 June 2018, Title: Identification and characterization of agricultural winter land-use based on Alos-2 and Radarsat-2 polarimetric SAR time-series images

Conference IGARSS (IEEE Geoscience and Remote Sensing Society), Valence (Spain), 22-27 July 2018, Title: Evaluation of the potentiality of polarimetric C- and L-SAR time-series images for the identification of winter land-use.



Article

Polarimetric SAR Time-Series for Identification of Winter Land Use

Julien Denize ^{1,2,*} Laurence Hubert-Moy ² and Eric Pottier ¹

¹ University of Rennes & IETR UMR 6164, 35 000, Rennes, France; eric.pottier@univ-rennes1.fr

² University of Rennes & LETG UMR 6554, 35 000, Rennes, France; laurence.moy@univ-rennes2.fr

* Correspondence: julien.denize@univ-rennes1.fr

Received: 3 October 2019; Accepted: 11 December; Published: date

Abstract: In the past decade, high spatial resolution Synthetic Aperture Radar (SAR) sensors have provided information that contributed significantly to cropland monitoring. However, the specific configurations of SAR sensors (e.g., band frequency, polarization mode) used to identify land-use types remains underexplored. This study investigates the contribution of C/L-Band frequency, dual/quad polarization and the density of image time-series to winter land-use identification in an agricultural area of approximately 130 km² located in northwestern France. First, SAR parameters were derived from RADARSAT-2, Sentinel-1 and Advanced Land Observing Satellite 2 (ALOS-2) time-series, and one quad-pol and six dual-pol datasets with different spatial resolutions and densities were calculated. Then, land use was classified using the Random Forest algorithm with each of these seven SAR datasets to determine the most suitable SAR configuration for identifying winter land-use. Results highlighted that (i) the C-Band (F1-score 0.70) outperformed the L-Band (F1-score 0.57), (ii) quad polarization (F1-score 0.69) outperformed dual polarization (F1-score 0.59) and (iii) a dense Sentinel-1 time-series (F1-score 0.70) outperformed RADARSAT-2 and ALOS-2 time-series (F1-score 0.69 and 0.29, respectively). In addition, Shannon Entropy and SPAN were the SAR parameters most important for discriminating winter land-use. Thus, the results of this study emphasize the interest of using Sentinel-1 time-series data for identifying winter land-use.

Keywords: crops; RADARSAT-2; sentinel-1; ALOS-2; C-band frequency; L-band frequency; dual-polarization; quad polarization; random forest classification

VI.1. Introduction

The importance of vegetation cover during winter to preserve soil quality and water resources is now well-recognized by scientists, decision makers and citizens, and land-use mapping is considered a relevant input into decision-making to implement appropriate policy responses (Fasona et al., 2005). However, although identifying land use in agricultural areas is a major environmental and scientific issue (Corgne, 2004), it remains challenging due to its high spatio-temporal dynamics (Denize et al., 2019). In this context, remotely sensed time-series data are a valuable tool to identify land use by providing precise and timely information about the phenological status and development of vegetation at different scales, from local to global extents (Duchemin et al., 2015; Veloso et al., 2017). In the past few decades, progress has been made with the development of high and very high spatial and temporal resolution optical (e.g., Satellite pour l'observation de la Terre (SPOT-6/7), Sentinel-2) and Synthetic Aperture Radar (SAR) (e.g., TerraSAR-X, RADARSAT-2, Advanced Land Observing Satellite 2 (ALOS-2), Sentinel-1) sensors (Morena et al., 2004; Potin et al., 2012; Drusch et al., 2012). However, using optical time-series to identify land use in winter is limited by cloud cover and/or low solar irradiance (Huang et al., 2017), and late winter is a critical period during which vegetation begins to grow (Denize et al., 2019). Conversely, SAR time-series provide a reliable solution to address the limitations of optical images because they are not sensitive to atmospheric conditions and can operate day and night (Smith, 1997).

These advantages, along with a sensitivity of microwave scattering to soil and vegetation characteristics (Ulaby, 1986; Hosseini et al., 2015), have led scientists to evaluate the potential of using SAR sensors to monitor agriculture (McNairn and Brisco, 2004; Mascolo, 2015; Hütt et al., 2016; Haldar et al., 2016). The potential of using SAR data to identify land use is based on the sensitivity of the radar signal to the dielectric constant of the objects and to their structure (i.e., the distribution of size shape and orientation of the scatterers) (Ulaby, 1986; Skriver, 2011). Thus, some studies have demonstrated the ability of SAR backscattering-coefficient and polarimetric data to classify land use using the dielectric properties of soil, surface roughness and vegetation canopy structure (Skriver et al., 1999; McNairn et al., 2001; Jiao et al., 2010; Nurtyawan et al., 1996). Most of these studies used the C-Band frequency rather than other frequencies (e.g., X- or L-Bands). Since microwave penetration depends on wavelength and incident angle, L-Band (~20 cm) wavelengths penetrate further into crop canopies than those of the C-Band (~5.5 cm). Consequently, C-Band wavelengths interact more with the upper canopy, while L-Band wavelength responses result from greater interaction with the soil/canopy and scattering directly from the soil (Ulaby, 1986; Hosseini et al., 2015). Thus, McNairn and Brisco (2004) demonstrated the potential of vertically (V) and horizontally (H) polarized C-Band microwaves to identify land use. Indeed, since V microwaves respond to predominantly vertical structure, they penetrate the canopy less. Conversely, H microwaves tend to penetrate the canopy more than V microwaves. Similarly, others (Skriver, 2012; Skriver et al., 1999) illustrated the ability of the L-Band and the combined use of C- and L-Bands to classify land use. Many studies have also shown the potential of radar data to map crop residues (McNairn and Brisco, 2004; Smith, 1996) or crop types during summer (Paris, 1983; Lee et al., 2001).

However, only a few studies have demonstrated the potential of SAR time-series to identify land-use types in winter. Haldar et al. (2016) illustrated the potential of polarimetric C-Band SAR time-series data to derive useful information, such as biophysical parameters,

from mustard (*Sinapis alba* L.) and wheat (*Triticum aestivum* L.) crops. Similarly, few studies have shown Sentinel-1's potential to identify and characterize land-cover and land-use dynamics. For example, some studies (Veloso et al., 2017; Abdikan et al., 2016; Dimov et al., 2016; Bargiel, 2017) have shown benefits of using Sentinel-1 time-series to understand crop behavior and dynamics and classify land use. Likewise, Minh et al. (2018) used Sentinel-1 time-series to produce a winter vegetation quality map with five classes ("bare soil" to "high quality") based on a deep-learning method, with an overall accuracy (OA) >98%. However, the specific configurations of SAR sensors (e.g., band frequency, polarization mode) used to identify land-use types remain underexplored, and even unexplored for winter land-use.

This study aimed to evaluate and compare the value of multi-temporal ALOS-2 (ALS-2), RADARSAT-2 (RST-2) and Sentinel-1 (S-1) data for monitoring winter land-use in agricultural areas. Specifically, we addressed the main question: What is the most appropriate SAR configuration (polarization, frequency, density of time-series) for characterizing winter land-use? To this end, we first calculated SAR parameters from quad-polarization (pol) C-Band, dual-pol C-Band and dual-pol L-Band time-series to generate several parameter datasets. We then applied a classification procedure using the Random Forest (RF) algorithm to determine the most discriminating SAR configuration for land-use monitoring in winter. Finally, we identified advantages and disadvantages of the method and its results.

VI.2. Materials and Methods

VI.2.1. Study Site

The study site is a relatively flat area located to the south of the Bay of Mont-Saint-Michel ($8^{\circ} 31' 0''$ N, $1^{\circ} 31' 30''$ W) in France and covers an area of ca. 130 km² (**Fig. III.1**). This site has been included in long-term ecological research (LTER) networks at the European (LTER-Europe) and international (ILTER) levels since 1993 to assess relationships between changes in farming activities, landscape dynamics and ecological processes related to biodiversity, water quality and climate (“ZA Armorique”, 2019). This study site is also referenced in the “Kalidéos program”, which is coordinated and managed by the CNES (French Space Agency) to promote and demonstrate the use of spatial data by supporting research and development, prototyping and user demonstration activities. The site is composed of ca. 7 000 agricultural fields ranging from 0.1–65 ha and is characterized by a fragmented agricultural landscape (from a hedgerow network to open fields). This temperate climate area is exposed to mean annual precipitation of 600–700 mm and mean average temperature $>12^{\circ}$ C. In summer, farming systems are based on one main crop per field: maize (*Zea mays* L.), wheat (*Triticum aestivum* L.), rapeseed (*Brassica napus* L.) or barley (*Hordeum vulgare* L.). In winter, in addition to grasslands, which play a major role in regulating water flows and nutrient cycling, catch crops are sown to decrease nitrogen leaching, as required by the European Union’s “Nitrates Directive” (2019).

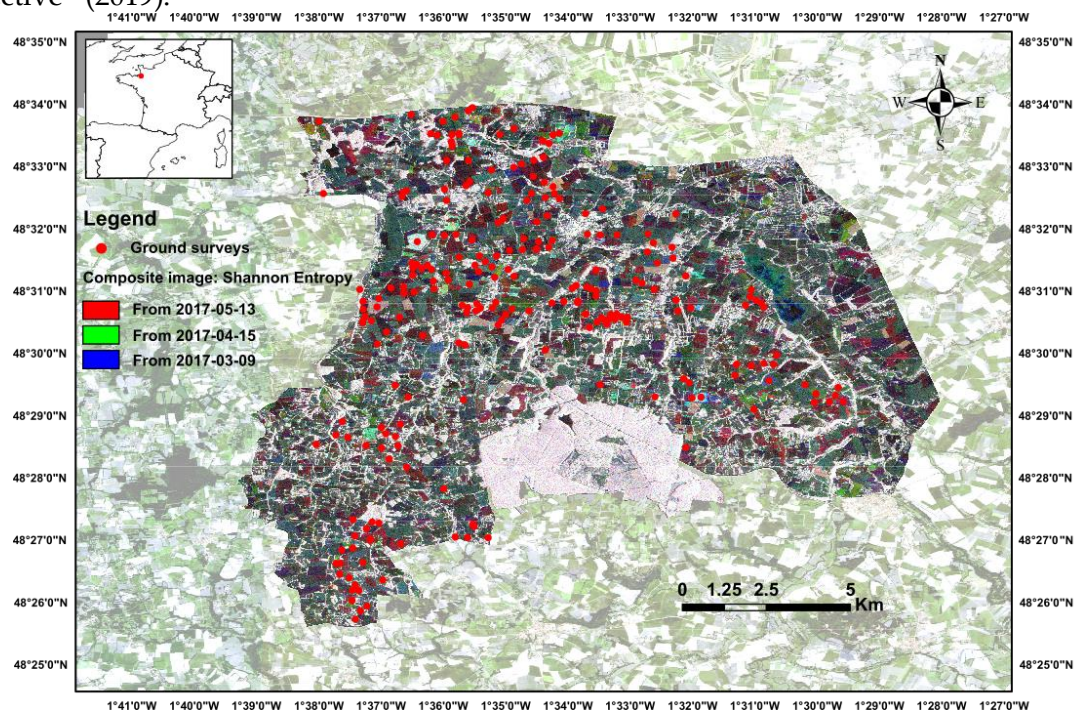


Figure III.1. Study site location, ground surveys (RGB composite image constructed from Shannon Entropy extracted from Advanced Land Observing Satellite 2 (ALOS-2) data for three dates: 03-09-2017, 04-15-2017 and 05-13-2017. ©Kalidéos data 2017 and JAXA data).

VI.2.2. Field Data

The mainland-use types encountered and investigated in winter in the study area (**Fig. III.2 and Table III.1**) are the following:

- Winter crops, which cover ca. 40% of the UAA (utilized agricultural area) and include three main annual crops: winter wheat, winter barley and rapeseed.
- Grasslands, which cover ca. 30% of the UAA and can be mown or grazed.
- Catch crops, which are sown after harvest of the main crop from August to October, cover ca. 25% of the UAA and include a wide variety of crops.
- Crop residues, which cover ca. 5% of the UAA and correspond to maize stalks that are left in fields when the maize is harvested after 1 November (Denize et al., 2019).



Figure III.2. The mainland-use types encountered in winter in the study area: (a) winter crops (winter barley), (b) catch crops (mustard), (c) grasslands and (d) crop residues (maize stalks).

Table III.1. Land-use classification.

Winter Land Use Type	Main Crops
Winter crops	Winter wheat
	Winter barley
	Rapeseed
Grasslands	Mown grasslands
	Grazed grasslands
Catch crops	Oat
	Fodder cabbage
	Ryegrass and clover
	Phacelia
	Phacelia and mustard
Crop residues	Phacelia and oat
	Maize stalks

Field observations were conducted in 231 crop fields monthly from November 2016 to February 2017 to calibrate and validate classification of remote sensing data (**Fig. III.1**). Samples were randomly distributed throughout the study site, with half of the fields (116) being used for training and the other half for validation. The fields inventoried ranged in size from 0.1–65 ha. The number of training samples of each winter land-use class inventoried was 54 for winter crops, 14 for grasslands, 42 for catch crops and 6 for crop residues.

VI.2.3. Satellite Data

VI.2.3.1. RADARSAT-2 Time-Series

A series of 10 RST-2 SAR images from October 2016 to May 2017 were acquired by MacDonald, Dettwiler and Associates and provided by the VIGISAT project managed by Collecte Localisation Satellites in the framework of the GIS Bretel (“Groupement Bretagne Télédétection”, Bretagne, France) (**Table III.2**). RST-2 images were acquired in Single Look Complex (SLC) mode (delivered in quad-pol mode: HH, HV, VH and VV polarization states) with an incidence angle of 35°. The range and azimuth spatial resolutions were 8.2 and 4.7 m, respectively.

VI.2.3.2. Sentinel-1 Time-Series

Two series of eight and twenty S-1 SAR images, respectively, from August 2016 to May 2017 were acquired by the European Space Agency and provided by its data hub (“Open Hub Access”, 2019) (**Table III.2**). S-1 images were acquired in SLC mode (delivered in dual-pol mode: VH and VV) with an incidence angle of 31° to 46° and an angle of 40° on the study area. The range and azimuth spatial resolutions were 2.3 and 13.9 m, respectively.

VI.2.3.3. ALOS-2 Time-Series

A series of six ALS-2 SAR images from January–June 2017 were acquired by the Japan Aerospace Exploration Agency and provided by the Kalidéos program (“Kalideos”, 2019) (**Table III.2**). ALS-2 images were acquired in SLC mode (delivered in dual-pol mode: HH and HV) with an incidence angle of 40° and range and azimuth spatial resolutions of 1.4 and 1.9 m, respectively.

Table III.2. Characteristics of the RADARSAT-2, Sentinel-1 and Advanced Land Observing Satellite 2 (ALOS-2) images used in the study. Dates in bold text for Sentinel-1 images indicate those with sparse time-series, while asterisks indicate those with dense time-series.

	RADARSAT-2	Sentinel-1	ALOS-2	
Dates (M-D-Y)		08-25-2016		
		09-18-2016*		
		09-30-2016*		
		10-12-2016*		
		10-24-2016*		
		11-05-2016*		
		11-17-2016*		
		11-29-2016*		
		12-11-2016*	01-04-2017	
		12-23-2016*	02-04-2017	
		01-03-2017	01-04-2017*	03-06-2017
		01-27-2017	01-16-2017*	04-15-2017
		02-20-2017	01-28-2017*	05-13-2017
		03-16-2017	02-09-2017*	06-10-2017
		04-09-2017	02-21-2017*	
		05-03-2017	03-05-2017*	
		05-27-2017	03-17-2017*	
		03-29-2017*		
		04-10-2017*		
		04-22-2017*		
		05-04-2017*		
		05-16-2017		
Ground Resolution	8.2 m	2.3 m	1.4 m	
Azimuth Resolution	4.7 m	13.9 m	1.9 m	
Polarization	Quad (HH-VV-HV-VH)	Dual (VV – VH)	Dual (HH-HV)	
Frequency	C-Band	C-Band	L-Band	
Mode	Fine Quad Polarization (SLC)	Interferometric wide (SLC)	Spotlight (SLC)	
Incidence Angle	35° (right descending)	31° to 46° (right descending)	40° (left ascending)	
Coverage	18 km × 25 km	>250 km × 100 km	25 km × 25 km	

VI.2.4. Extraction of SAR Parameters

SAR quad-pol and dual-pol parameters from the three sensor datasets (RST-2, S-1 and ALS-2) were calculated using Sentinel Application Platform (SNAP) v6.0 (Develop by Esa, Paris, France) and PolSARpro v5.1.3 software (Pottier et al., 2018) (Develop by IETR, Rennes, France).

VI.2.4.1. Quad-Pol Time-Series

- Backscattering coefficients ($\sigma^{0HH}, \sigma^{0HV}, \sigma^{0VH}, \sigma^{0VV}$) were calculated from the radiometrically calibrated RST-2 time-series using SNAP according to Eq. III.1 (“Radarsat-1 products”, 2017):

$$\sigma_j^o = \beta_j^o + 10 \times \log_{10}(\sin I_j) \quad (\text{III.1})$$

where β is the radar brightness and I_j is the incidence angle at the j^{th} range pixel.

Equation 1 assumes that the Earth is a smooth ellipsoid at sea level. A Lee Sigma filter (Lee et al., 2008) was applied with a window of 7×7 pixels and a sigma value of 0.8. RST-2 images were then geocoded at an 8-m resolution using Shuttle Radar Topography Mission 3s data to correct topographic deformations. The accuracy of geometric correction was less than 8 m per pixel. Next, two backscattering ratios were calculated ($\sigma^{0HH}:\sigma^{0VV}$, $\sigma^{0HH}:\sigma^{0HV}$) that highlight scattering mechanisms of each target.

- Polarimetric parameters were calculated from SLC RST-2 time-series. First, a 3×3 coherency matrix T_3 was extracted from the scattering matrix (S) of each image using PolSARpro. Next, a Lee Sigma filter was applied with a window of 7×7 pixels and a sigma value of 0.8. The elements of the matrix, which are independent of the polarimetric absolute phase (Lee and Pottier, 2009), were then geocoded directly using SNAP with an 8-m resolution.

Second, Cloude–Pottier decomposition (Cloude and Pottier, 1996) was then calculated based on the T_3 matrix. From the eigenvalues extracted, we calculated three independent parameters: (i) entropy (H), which expresses the randomness of the scatter; (ii) alpha angle (α), which describes the dominant scattering mechanism and (iii) anisotropy (A), which represents the relative power of the dominant mechanism. In addition, four parameters based on the Cloude–Pottier decomposition ($H \times A$; $H \times (1 - A)$; $(1 - H) \times A$; $(1 - H)(1 - A)$) were calculated because they can provide the number of scattering mechanisms in each resolution cell.

Third, Freeman–Durden decomposition (Freeman and Durden, 1998) was used to model the 3×3 covariance matrix (C_3) as the contribution of three scattering mechanisms for each pixel: volume, double-bounce and surface/single-bounce. Fourth, SPAN (total scattered power) and Shannon Entropy (SE), which equals the sum of two parameters related to the intensity (SE_i) and degree of polarization (SE_p) (Lee and Pottier, 2009), were calculated from the T_3 matrix. SE measures the disorder encountered in polarimetric SAR images.

Finally, two polarimetric parameters were extracted from the T_3 matrix: pedestal height and the Radar Vegetation Index (RVI). Pedestal height is the ratio of the maximum received intensity to the minimum received intensity; it indicates the presence of unpolarized scattering

and thus the degree of polarization of a scattered wave (Kim et al., 2012). RVI is a function of incidence angle, since the path length through the vegetation canopy will increase as the incidence angle increases (McNairn et al., 2004). Ranging from 0 to 1, RVI measures the randomness of the scatter according to **Equation III.2**:

$$RVI = \frac{8\sigma^{\circ HV}}{\sigma^{\circ HH} + \sigma^{\circ VV} + 2\sigma^{\circ HV}} \quad (\text{III.2})$$

A total of 25 quad-pol parameters were calculated for each of the 10 quad-pol 8-m RST-2 images, yielding a dataset with 250 variables.

VI.2.4.2. Dual-Pol Time-Series

The dual-polarization preprocessing step included (i) conversion of RST-2 time-series images from quad- to dual-polarization mode, (ii) resampling of RST-2 and ALS-2 time-series images at the spatial resolution of S-1 images and (iii) extraction of dual-pol C-Band and dual-pol L-Band SAR parameters.

- *Converting the RST-2 time-series polarization mode*: Each 3×3 coherency matrix T_3 extracted from RST-2 quad-polarization images was converted to a 2×2 covariance matrix C_2 using PolSARpro. The converted RST-2 images had the same polarizations (HH and HV) as ALS-2 images.
- *Calculating S-1 and ALS-2 covariance matrices*: A 2×2 covariance matrix (C_2) was extracted from the two polarizations of each ALS-2 2-m image and each S-1 image (for S-1 dense and sparse time-series).
- *Resampling RST-2 and ALS-2 time-series*: A multi-looking function was applied using a 2×1 pixel window for RST-2 images (i.e., 2×4.7 m and 1×8.2 m) and a 5×6 pixel window for ALS-2 images (i.e., 5×1.9 m and 6×1.4 m) using PolSARpro. Resampled RST-2 images had a resolution of 9.4×8.2 m, which was close to that of resampled ALS-2 images (9.5×8.4 m) and 10-m corrected S-1 images.
- *Calibrating backscattering coefficients*: Backscattering coefficients $\sigma^{\circ HH}$ and $\sigma^{\circ HV}$ were simultaneously calibrated radiometrically from dual-pol converted and resampled RST-2 images and original and resampled ALS-2 images using SNAP. Backscattering coefficients $\sigma^{\circ VV}$ and $\sigma^{\circ VH}$ were simultaneously calibrated radiometrically from dual-pol S-1 images. Then, a Lee Sigma filter (Lee et al., 2008) with a window of 7×7 pixels and a sigma value of 0.8 was applied to all images to attenuate speckle noise. Next, geometric correction was performed using the Shuttle radar topographic mission (SRTM) for each time-series dataset, with a 2-m resolution for original ALS-2 images; 8-m resolution for original RST-2 images and 10-m resolution for resampled ALS-2, resampled RST-2 and the two S-1 images. Finally, the $\sigma^{\circ HH}:\sigma^{\circ HV}$ ratio and $\sigma^{\circ HH} - \sigma^{\circ HV}$ difference were calculated from ALS-2 and RST-2 backscattering coefficients, and the $\sigma^{\circ VH}:\sigma^{\circ VV}$ ratio and $\sigma^{\circ VH} - \sigma^{\circ VV}$ difference were calculated from S-1 backscattering coefficients.

- *Extracting polarimetric parameters:* Dual-polarimetric parameters were simultaneously extracted from dual-pol S-1 images, converted and resampled RST-2 images and original and resampled ALS-2 images. To this end, the same Lee Sigma filter was applied to the C_2 matrices to filter out speckle noise. Then, geometric corrections were applied to all polarimetric parameters using the SRTM with the previously used 2-m, 8-m and 10-m resolutions. SPAN, SE, SEi, SEp, normalized SE, normalized SEi and normalized SEp were also extracted.

A total of 11 dual-pol parameters (2 backscattering coefficients, 1 ratio and 1 difference based on the backscattering coefficients, 1 SPAN, 2 SE, 2 SEi and 2 SEp) were calculated for each of the 10 RST-2, 6 ALS-2 and 8 or 20 S-1 images. Finally, six dual-pol datasets were created:

1. original RST-2 8-m dataset with 110 variables (11 parameters \times 10 dates)
2. resampled RST-2 10-m dataset with 110 variables (11 parameters \times 10 dates)
3. original ALS-2 2-m dataset with 66 variables (11 parameters \times 6 dates)
4. resampled ALS-2 10-m dataset with 66 variables (11 parameters \times 6 dates)
5. sparse S-1 10-m dataset with 88 variables (11 parameters \times 8 dates)
6. dense S-1 10-m dataset with 220 variables (11 parameters \times 20 dates)

VI.2.5. Classification of SAR Parameter Datasets

A two-step approach was performed to identify winter land-use using the seven SAR parameter datasets (one quad-pol and six dual-pol). First, parameter importance was analyzed for each SAR parameter dataset using the RF importance function. The RF importance function was performed to rank the features in order of importance based on the mean decrease in the Gini index (Breiman et al., 2001) repeated 100 times by changing the training sample, to identify the parameters most important for identifying winter land-use types. A measure of variable importance was provided for each candidate predictor and each classification using the heuristic method based on the Gini Index (Kostelich and Schreiber, 1993; Breiman et al., 2001; Pal, 2005).

Second, RF, as a supervised classification algorithm, was used to classify land-use during winter 2016–2017. The RF was chosen for its high performance and accurate classification of land use (Belgiu and Csillik, 2018). RF is an ensemble classifier that uses classification and regression trees to make predictions (Breiman et al., 2001). The trees are created by drawing a subset of training samples through replacement (a bagging approach). In this way, some samples may be selected several times, while other samples may not be selected at all. The “randomForest” package (v.4.6–14) developed by (Liaw and Wiener, 2002) and implemented in R software (v.3.5.1) (“R Project”, 2019) (Develop by Bell Laboratories, Murray Hill, New Jersey, United-Sates) was used to perform classifications. Two RF parameters were tuned using the “name” function in this package. The first, the number of trees randomly created using the training dataset, was set to 1000, since the number of errors decreases little with more than 1000 trees (Lawrence et al., 2006). The second parameter, the number of variables randomly sampled as candidates at each split node (mtry), was defined starting with a mtry equals the square root of the number of input variables, then searching for the optimal value to improve the quality of the model.

From each image (one per date), 1200 samples (pixels) were randomly selected. Half (600 “in-bag” samples) were used to train the trees, while the rest (600 “out-of-the-bag” samples)

were used to estimate the accuracy of the RF model (Belgiu and Drăgu, 2016). This process being repeated 100 times with replacement of samples, we can consider that bagging was used during the overall process (Denize et al., 2019). Classification accuracy was assessed using the F1-score and the Kappa index. The F1-score is a standard measure of classification accuracy defined as the weighted average of precision and recall (Audebert et al., 2018), while the Kappa index expresses the proportional decrease in error generated by the classification compared to the error of a completely random classification (Congalton, 1991).

A four-step classification procedure was performed to evaluate the potential of SAR time-series to identify winter land-use types:

1. RST-2 quad-pol, S-1 dense and ALS-2 2-m time-series datasets were classified to demonstrate the full potential of these SAR sensors
2. RST-2 10-m dual-pol, ALS-2 10-m and S-1 sparse time-series datasets were classified to identify the best band frequency
3. RST-2 quad-pol and RST-2 8-m dual-pol time-series datasets were classified to identify the best polarization mode
4. S-1 dense and sparse time-series datasets were classified to evaluate the influence of the number of images.

VI.3. Results

VI.3.1. Importance of SAR Parameters for Discriminating Winter Land-Use

The most important SAR parameters for discriminating winter land-use depended on the polarization mode and band frequency (**Fig. III.3 and III.4**). Concerning polarization mode, the most important parameters in the quad-pol data were SPAN (7.8%), SE (7.7%), normalized SE (7.5%) and, to a lesser extent, SE_i (5.9%) and the normalized SE_i (5.8%) (**Fig. III.3**). Conversely, the least important parameters were the Freeman–Durden double-bounce (2.1%) and anisotropy (2%). Parameters related to backscattering coefficients were less important (4.3% and 2.4% for VV backscattering and the HV:HH ratio, respectively). For the dual-pol data, the most important parameters were SE and normalized SE, with an importance of 11.5% for both for the ALS-2 L-Band; 13.1% and 12.5%, respectively, for RST-2 and 11.7% and 11.6%, respectively, for S-1. In addition, for the ALS-2 L-Band, SPAN was the most important parameter (11.7%). Conversely, the least important parameter was the HH:HV ratio for the ALS-2 L-Band and RST-2 C-Band (5.6% and 6.4%, respectively) and the difference VV – VH for the S-1 C-Band (6.7%).

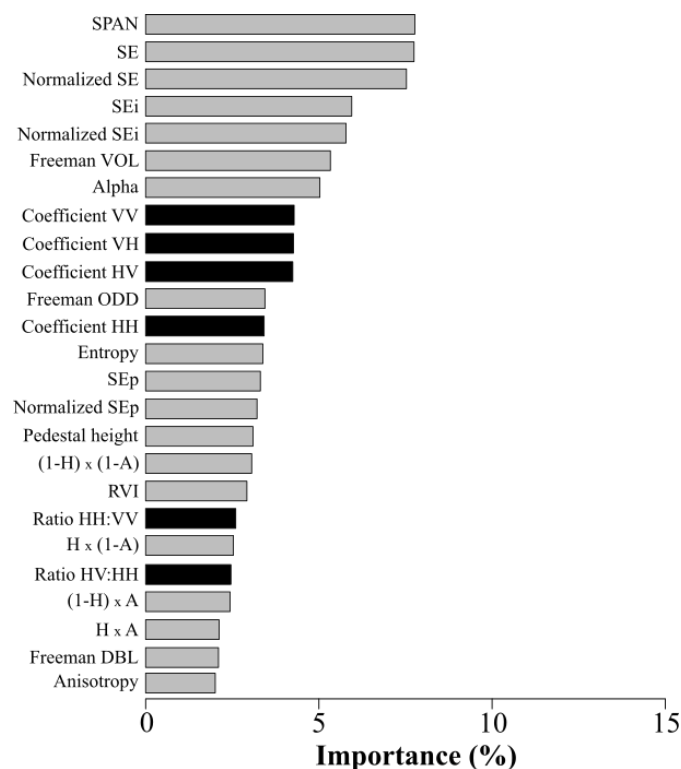


Figure III.3. Importance (in %) of quad-pol SAR parameters based on 100 random forest classifications. Parameters related to backscattering coefficients are in black, while polarimetric parameters are in gray. SE: Shannon Entropy.

Concerning band frequency, in the dual-pol L-Band (Dual-L) configuration, parameters related to backscattering coefficients were less important than polarimetric parameters (mean importance of 6.6% and 10.5%, respectively) (**Fig. III.4**). In the dual-pol C-Band (Dual-C) configuration, the ranks of the parameters related to backscattering coefficients were similar

for RST-2 and S-1 classification models. For each of them, a backscattering coefficient was important: the HV coefficient for RST-2 and VV coefficient for S-1 (10.4% and 10.7%, respectively). Similarly, the HH:HV and VV:VH ratios were less important (6.4% and 6.7%, respectively). The importance of polarimetric parameters was similar for Dual-C and Dual-L configurations, with SE and SE_i being the most important parameters. However, SPAN was the most important parameter for Dual-L but one of the least important for Dual-C.

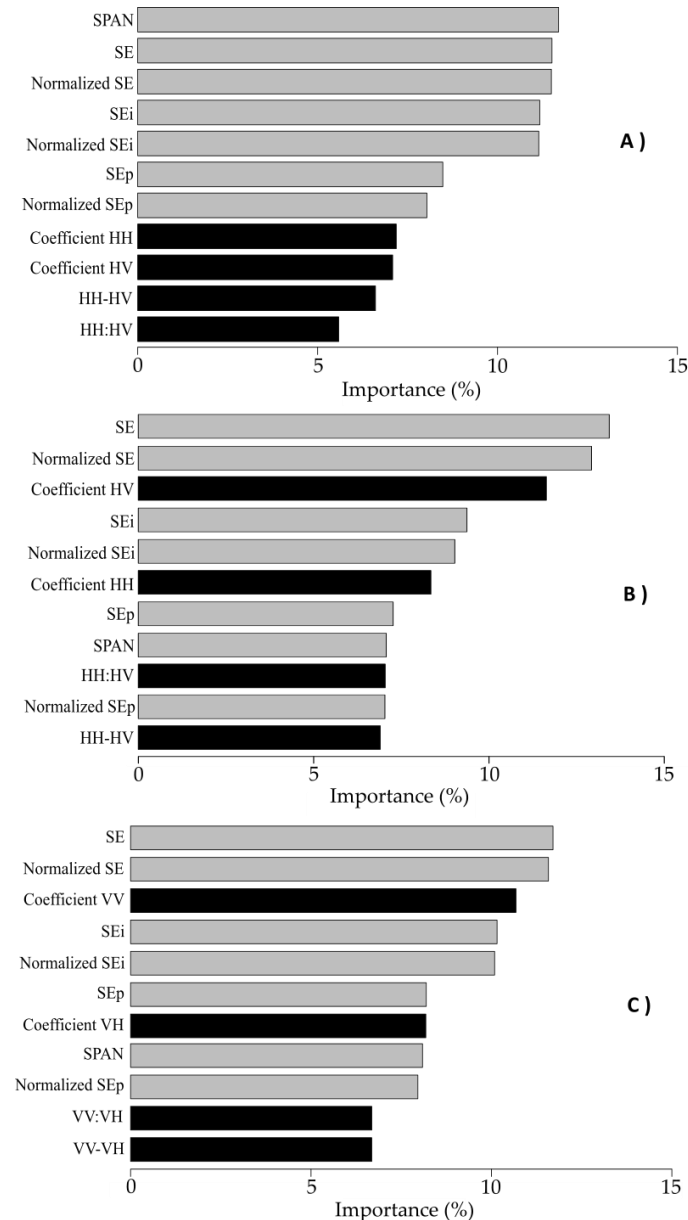


Figure III.4. Importance (in %) of dual-pol SAR parameters based on 100 random forest classifications using (A) ALOS-2 parameters, (B) RADARSAT-2 parameters and (C) Sentinel-1 parameters. Parameters related to backscattering coefficients are in black, while polarimetric parameters are in gray. SE: Shannon Entropy.

VI.3.2. Contribution of Polarization Mode to Accuracy of Winter Land-Use Classification

The F1-score of land-use classification was higher using the quad-pol dataset (median F1-score 0.69, standard deviation (SD) 0.05; median Kappa 0.68, SD 0.02;) than the dual-pol datasets (median F1-score 0.59, SD 0.05; median Kappa 0.54, SD 0.02) (**Fig. III.5**). The superiority of quad-pol mode over dual-pol mode was observed for all winter land-use classes (**Fig. III.5**). The largest differences in median F1-score between quad-pol and dual-pol mode concerned the oat (0.64 and 0.50, respectively), ryegrass and clover (0.60 and 0.46, respectively) and phacelia (0.75 and 0.66, respectively) classes. Conversely, the rapeseed class was discriminated slightly better using the quad-pol rather than dual-pol dataset (median F1-score 0.87 and 0.85, respectively). Moreover, Standard Deviation (SD) in F1-score accuracy was slightly lower using the quad-pol rather than dual-pol dataset for fodder cabbage (0.05 and 0.06, respectively) and crop residue (0.03 and 0.04, respectively) classes, but the opposite is true for other classes such as ryegrass and clover (0.05 and 0.04, respectively) (**Fig. III.5**).

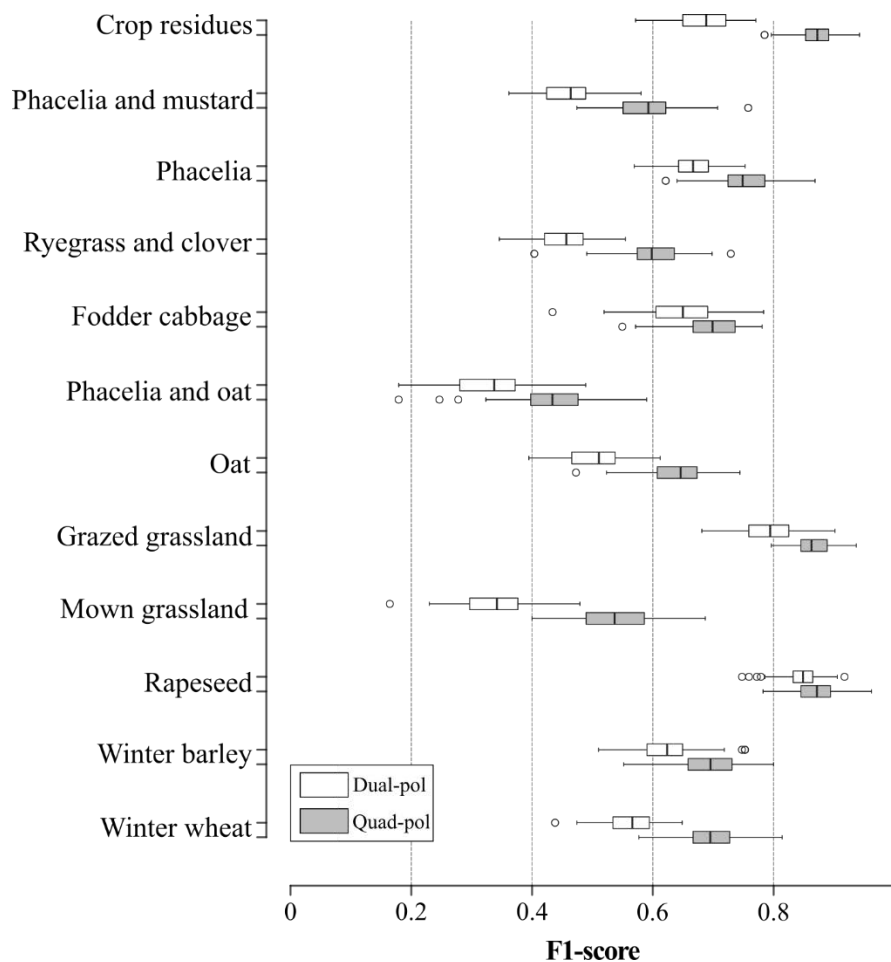


Figure III.5. Comparison of classification accuracy of each land-use class between dual and quad polarization (pol) modes. Box-and-whisker plots represent the variation in random forest classification accuracy based on 100 iterations. Whiskers indicate 1.5 times the interquartile range.

VI.3.3. Contribution of Band Frequency to Accuracy of Winter Land-Use Classification

The F1-score of land-use classification was slightly higher for the RST-2 C-Band frequency (median F1-score 0.64, SD 0.05; median Kappa 0.64, SD 0.02) than S-1 C-Band frequency (median F1-score 0.61, SD 0.05; median Kappa 0.59, SD 0.02) or the ALS-2 L-Band frequency (median F1-score 0.57, SD 0.05; median Kappa 0.60, SD 0.02) (**Fig. III.6**). More precisely, classification accuracy depended on the band frequency and land-use class (**Fig. III.6**). F1-score was highest for the C-Band frequency, except for the crop residue, phacelia, fodder cabbage and mown grassland classes, for which the ALS-2 L-Band frequency had the highest accuracy (median F1-score 0.89, 0.80, 0.77 and 0.49, respectively). Classification accuracy using the S-1 parameter dataset was highest for grazed grassland, winter wheat and oat classes (median F1-score 0.83, 0.65 and 0.57, respectively). For the other classes (phacelia and mustard, ryegrass and clover, phacelia and oat, rapeseed and winter barley), F1-score was highest using the RSR-2 parameter dataset. Regardless of the band frequency, the F1-score of the rapeseed, grazed grassland and crop residue classes was higher than those of the other classes (**Fig. III.6**). The Standard Deviation in classification accuracy of land-use classes was similar among the ALS-2, RST-2 and S-1 models (0.05, 0.049 and 0.05, respectively).

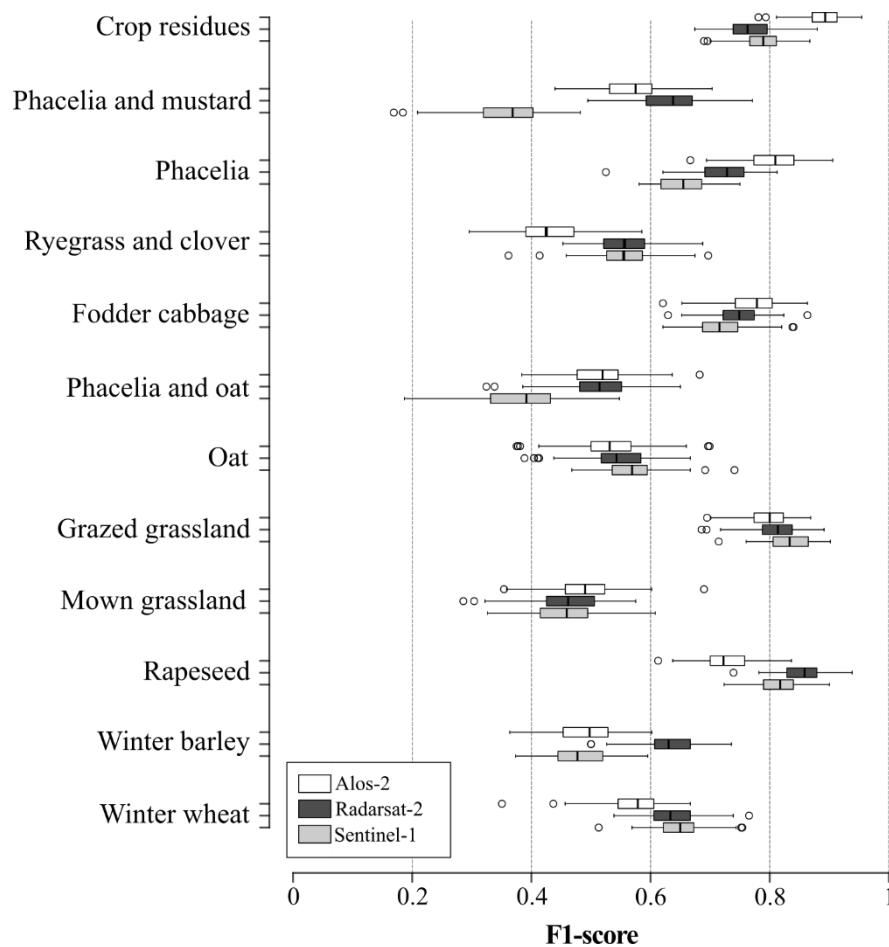


Figure III.6. Comparison of classification accuracy of each land-use class among band frequencies. Box-and-whisker plots represent the variation in random forest classification accuracy based on 100 iterations. Whiskers indicate 1.5 times the interquartile range.

VI.3.4. Contribution of Time-Series Density to Accuracy of Winter Land-Use Classification

The F1-score of land-use classification was higher for the dense S-1 time-series (median F1-score 0.70, SD 0.05; median Kappa 0.69, SD 0.02) than for the sparse S-1 time-series (median F1-score 0.61, SD 0.05; median Kappa 0.60, SD 0.02) (**Fig. III.7**). The largest differences between dense and sparse time-series concerned the phacelia and mustard (median F1-score 0.59 and 0.36, respectively), phacelia and oat (median F1-score 0.60 and 0.39, respectively) and phacelia (median F1-score 0.80 and 0.66, respectively) classes. Moreover, the variance in classification accuracy was slightly lower for the dense rather than sparse S-1 time-series of the phacelia and oat (SD 0.06 and 0.07, respectively) and grazed grassland (SD 0.03 and 0.04, respectively) classes (**Fig. III.7**). Conversely, the variance in classification accuracy in sparse and dense time-series of some winter land-use classes, such as winter wheat (SD 0.04 and 0.05, respectively) and winter barley (SD 0.05 and 0.06, respectively), was higher using the dense time-series.

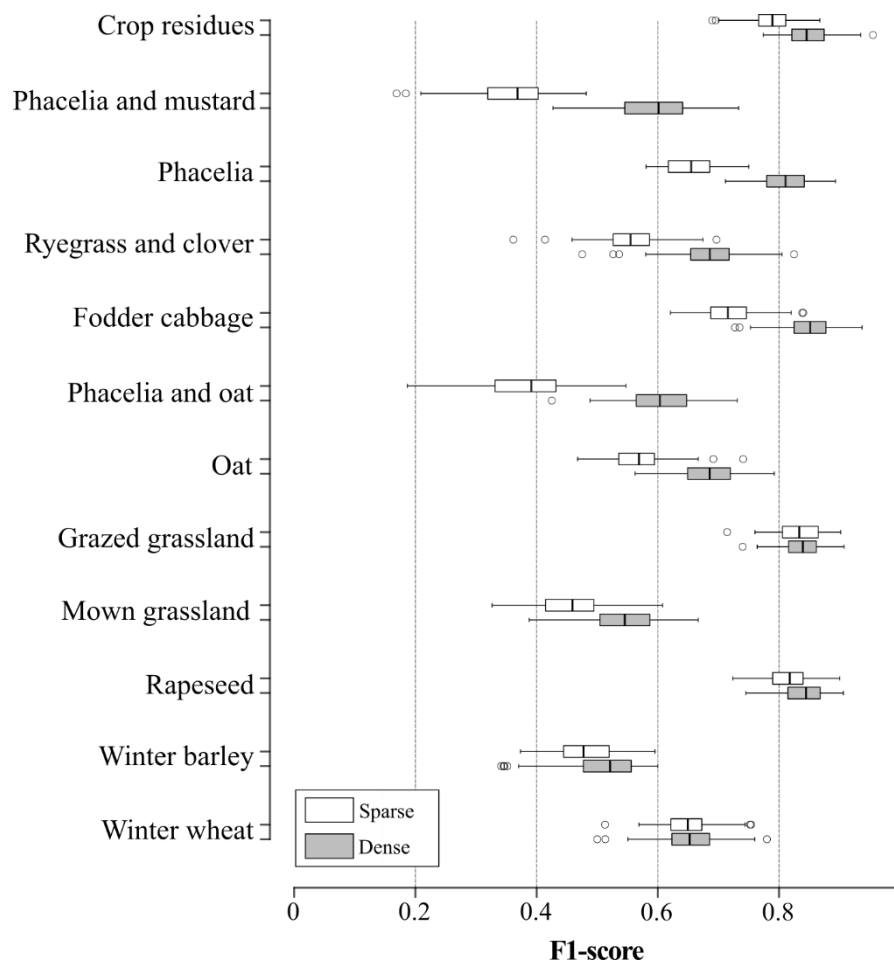


Figure III.7. Comparison of classification accuracy of each land-use class between sparse and dense Sentinel-1 time-series. Box-and-whisker plots represent the variation in random forest classification accuracy based on 100 iterations. Whiskers indicate 1.5 times the interquartile range.

VI.3.5. Definition of the Best SAR Configuration

The F1-score of land-use classification was slightly higher using the S-1 dense time-series (median F1-score 0.70, SD 0.00; median Kappa 0.69, SD 0.02) than using the RST-2 quad-pol (median F1-score 0.69, SD 0.05; median Kappa 0.68, SD 0.02) or ALS-2 original dual-pol (median F1-score 0.29, SD 0.05; median Kappa 0.32, SD 0.02) time-series (**Fig. III.8**). More precisely, classification accuracy depended on the sensor and land-use class (**Fig. III.8**). The F1-score was higher with the S-1 model, except for the winter wheat, winter barley, rapeseed, grazed grassland and crop residue classes, for which the RST-2 model had higher accuracy. The accuracy of the S-1 model was slightly higher (by 0.01 in the F1-score 1%) than that of RST-2 for the phacelia and mustard and mown grassland classes, while that of the ALS-2 model was always lower than those of S-1 and RST-2. Finally, the variance in classification accuracy was similar among the S-1, RST-2 and ALS-2 models (SD 0.05, 0.05 and 0.05, respectively).

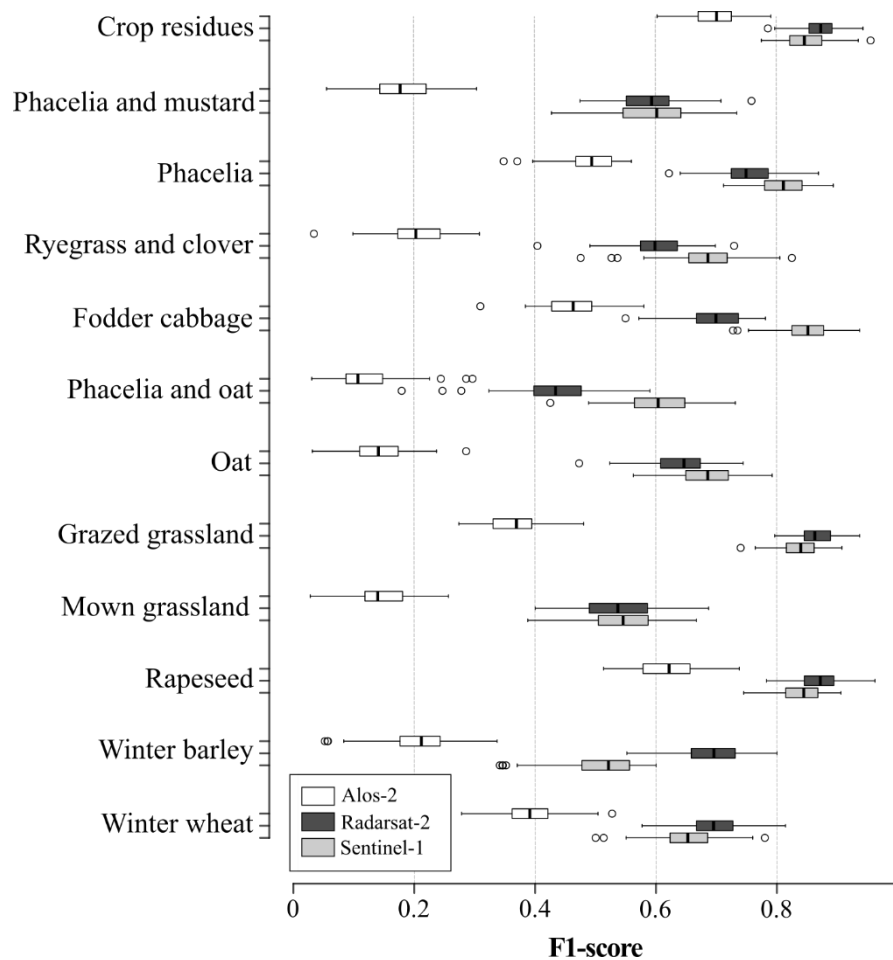


Figure III.8. Comparison of classification accuracy of each land-use class among SAR sensors. Box-and-whisker plots represent the variation in RF classification accuracy based on 100 iterations. Whiskers indicate 1.5 times the interquartile range.

VI.3.6. Spatial Distribution of Winter Land-Use Classes

Winter land-use classes were mapped at the 1:100 000 scale using the best classification model: the RF classification using the SAR parameter dataset extracted from S-1 dense time-series images. While grasslands were classified well (F1-score, 0.71), some misclassification errors and artifacts occurred, mainly between catch-crop classes, such as oat and phacelia and oat classes (**Table III.3**). In general, catch crops and winter crops were located on the largest fields, while grasslands were located on the smallest ones (**Fig. III.9**).

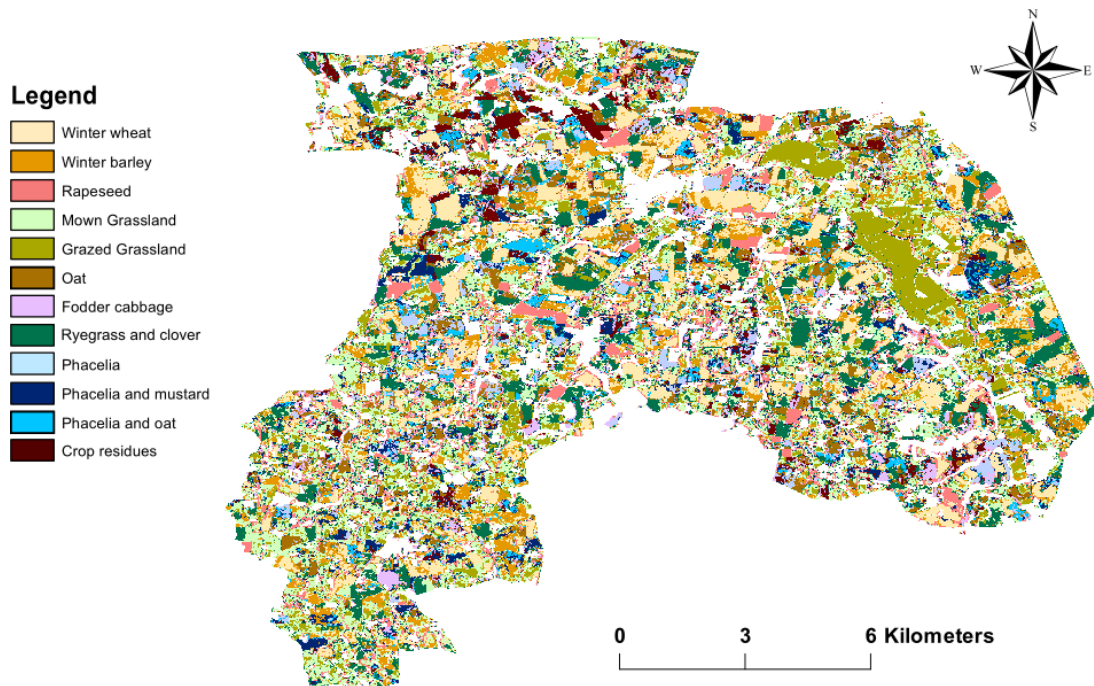


Figure III.9. Map of winter land-use classes obtained using a parameter dataset derived from the Sentinel-1 dense time-series. Classification was performed using the random forest algorithm.

Table III.3. Confusion matrix of winter land-use obtained from RF classification using the SAR parameter dataset extracted from the S-1 dense time-series dataset.

Land Use	1	2	3	4	5	6	7	8	9	10	11	12	Commission Error (%)
1: Winter wheat	32	1	4	1	0	0	2	0	1	0	2	0	74.4
2: Winter barley	11	22	0	6	2	2	4	0	1	0	5	0	41.5
3: Rapeseed	1	3	49	2	1	3	2	2	1	1	0	1	74.2
4: Mown grasslands	0	3	2	28	7	0	1	0	0	2	1	2	60.9
5: Grazed grasslands	0	0	0	0	44	0	1	2	1	0	0	0	91.7
6: Oat	0	2	0	5	0	33	8	0	1	4	2	1	58.9
7: Phacelia and oat	0	1	0	2	0	4	26	0	5	3	3	0	59.1
8: Fodder cabbage	1	0	1	3	0	1	1	41	2	0	2	1	77.4
9: Ryegrass and clover	1	1	1	1	2	2	0	4	36	0	1	0	73.5
10: Phacelia	0	0	1	0	0	1	5	0	0	41	4	0	78.9
11: Phacelia and mustard	1	0	0	0	0	1	0	0	0	0	34	1	91.9
12: Crop residues	0	0	0	0	0	3	0	0	2	0	4	44	83.0
Omission error (%)	68.1	66.7	84.5	58.3	78.6	66.0	52.0	83.7	72.0	80.4	58.6	88.0	71.7

VI.4. Discussion

This study aimed to evaluate and compare the value of multi-temporal ALS-2, RST-2 and S-1 data for monitoring winter land-use in agricultural areas. Winter land-use classes, which depend on vegetation characteristics and phenology, can be discriminated using the specific properties of SAR sensors to identify crops (Veloso et al., 2017; Jiao et al., 2014; Yusoff et al., 2017). A two-step method was applied to the study site. First, SAR parameters were derived from RST-2, S-1, and ALS-2 time-series, and one quad-pol and six dual-pol parameter datasets with different spatial resolutions and densities were calculated from these time-series. Then, land use was classified using the RF algorithm with each of these seven SAR parameter datasets to determine the most suitable SAR configuration for identifying winter land-use.

VI.4.1. Which SAR Configuration for Mapping Winter Land-Use?

Our study took advantage of the potential of SAR sensor characteristics to identify winter land-use types. The physical properties and specific resolutions (spatial, temporal and frequency) of ALS-2, RST-2 and S-1 sensors allowed us to discriminate winter land-use classes in our study area, including areas where the agricultural landscape was fragmented. However, some SAR configurations appear to be more effective than others.

Results highlight that the C-Band outperformed the L-Band, the quad-polarization mode outperformed the dual-polarization mode and S-1 dense time-series outperformed RST-2 and ALOS-2 time-series. Overall, the dense S-1 time-series was the most suitable SAR configuration data for winter land-use identification, with classification accuracy slightly higher than those of the others. This result is consistent with other studies that have reported the added value of S-1 data for mapping cropland (Belgiu and Csillik, 2018; Immitzer et al., 2016) or identifying and characterizing crop phenology (Bargiel, 2017). Nevertheless, the quad-pol C-Band RST-2 dataset also showed potential to identify winter land-use, with accuracies similar to those obtained using the dense dual-pol C-Band S-1 dataset. This result is consistent with the studies of (McNairn et al., 2009; Liu et al., 2012), which also showed the potential of polarimetric RST-2 data for monitoring and classifying crops. Conversely, the dual-pol L-Band ALS-2 dataset appeared to be of little use for identifying and mapping land-use in winter, except for certain classes such as crop residues or phacelia and mustard. These results add information to the research to date, which has demonstrated the ability of the L-Band to classify crops in summer (Skriver, 2011; Haldar et al., 2012). However, these results should be interpreted with caution because, as shown by the results obtained with S-1 images, time-series density has a significant impact on the identification of winter land-use classes, as shown by Blaes et al. (2005). Thus, if the classification score obtained with the ALS-2 time-series is lower than that obtained with the RST-2 and S-1 sparse time-series (F1-score 0.57 vs 0.61 and 0.64, respectively), it should be noted that the ALS-2 time-series had the least number of images (6 against 10 and 8 for RST-2 and S-1, respectively). In addition, the difference between the incidence angles of the images, although small (35° for RTS-2 and 40° for S-1 and ALS-2), can have an impact on the accuracy of the results, as noted by (Baghdadi et al., 2009; Inoue et al., 2012).

Results indicate that SE and SPAN were the most important parameters, while difference and ratio parameters had low importance. These results are consistent with the research conducted to date. Loosvelt et al. (2012) demonstrated the importance of SE in studying land use and land cover. Some studies also demonstrated the ability of SE to characterize the canopy

of vegetated areas (Dufour et al., 2013). Likewise, many studies (e.g., Hong et al., 2015; Zhang and Wu, 2011) have described the ability of SPAN parameters to classify crops.

The best accuracy, obtained using the dense dual-pol C-Band S-1 dataset (OA 72%), demonstrated the limits of using one SAR dataset alone to identify winter land-use accurately. Nevertheless, our results demonstrate the ability of other band frequencies to discriminate land-use classes. For example, ALS-2 data appear to be useful for classifying crop residue and phacelia and mustard classes. Similarly, RST-2 data appear to be useful for classifying rapeseed and grazed grassland classes. These results highlight the utility of combining SAR parameters. For example, Skriver et al. (2011) demonstrated the utility of combining C-Band and L-Band SAR data for classifying crops. Hence, use of combined ALS-2, RST-2 and S-1 SAR datasets should be considered to obtain a denser time-series to discriminate between land-use types better.

VI.4.2. Advantages and Disadvantages of the Classification Approach

Results demonstrated the potential of this classification approach based on the RF algorithm, although the highest F1-score achieved was 0.70. Some studies based on SAR data classified using the RF algorithm also highlighted this complexity in identifying winter crops, unlike for annual crops such as maize (Veloso et al., 2017; Bargiel, 2017). Moreover, the results also confirm the ability of SAR data to classify crop residues, as some previous studies have shown (McNairn et al., 2011; Adams et al., 2013).

Several other approaches can be considered. In this study, the term time-series refers to a set of images acquired during a given period, and each acquisition was processed as an independent image without capturing properties of time-series data. New approaches that take time explicitly into account such as TWDTW (Time-Weighted Dynamic Time Warping) algorithm have proven to be very effective in solving complex classification problems. Although few studies of winter land-use classification have been performed, Minh et al. (2018) for example showed the utility of deep learning for classifying vegetation quality (cover density) in winter using S-1 data, with preliminary results achieving a Kappa index of 0.98. However, these approaches require high-performance calculations and need to run hyperparameter searches, adjustments and tests, which need further investigations that will be done in future work. Furthermore, as mentioned, the results highlighted the value of specific radar parameters in the L- and C-Bands for discriminating winter land-use classes. These results highlight the utility of approaches that combine data to classify crops, as demonstrated in certain studies (Skriver, 2011; Skriver et al., 1999).

VI.5. Conclusion

This study evaluated advantages of using S-1, RST-2 and/or ALS-2 time-series to determine the best SAR configuration to identify winter land-use classes accurately using the RF algorithm. Several SAR configurations were tested to discriminate land-use types during winter using the RF algorithm; to our knowledge, this is the first time such a study has been undertaken. Results show that the best SAR configuration was the dense dual-pol C-Band S-1 time-series, although RST-2 and ALS-2 time-series provided useful information about vegetation cover. Finally, our results demonstrated the limits of using one SAR dataset alone to identify winter land use accurately, the highest F1-score reaching only 0.70. Thus, future research could study the utility of combining SAR parameters or using new classification approaches based on deep learning to improve the accuracy of classifying land-use types in winter. Better understanding of SAR signal behaviors of agricultural practices and environmental conditions could also help to identify winter land use, which has important implications for developing sustainable agriculture.

VI.6. Patents

Author Contributions: Conceptualization, J.D., E.P. and L.H.-M.; methodology, J.D., E.P. and L.H.-M.; software, E.P. and J.D.; validation, J.D.; resources, J.D.; data curation, J.D., writing—original draft preparation, J.D.; writing—review and editing, J.D., L. H.-M. and E.P.; visualization, J.D., E.P. and L.H.-M.; supervision, E.P. and L.H.-M.; project administration, E.P. and L.H.-M.; funding acquisition, E.P.

Funding: This research was funded by the French Ministry of Higher Education and Research, Ph.D. grant 2016

Acknowledgments: This study was supported by the Kalideos project, funded by the CNES (<https://www.kalideos.fr/drupal/>) and the Zone Atelier Armorique project. This study was also supported by public funds (Ministère de l'Éducation Nationale, de l'Enseignement Supérieur et de la Recherche, FEDER, Région Bretagne, Conseil Général du Finistère, Brest Métropole), VIGISAT project and the GIS Bretel ("Groupement Bretagne Télédétection"). We thank Napo N'Bohn and Marianne Balaesque for their help collecting field data.

Conflicts of Interest: "The authors declare no conflict of interest."

VI.7. References

Fasona, M.J.; Omojola, A.S. Climate change, human security and communal clashes in Nigeria. In Proceedings of the International Workshop on Human Security and Climate Change, Oslo, Norway, 21–23 June 2005; pp. 21–23.

Corgne, S. Hiérarchisation des facteurs structurant les dynamiques pluriannuelles des sols nus hivernaux. Application au bassin versant du Yar (Bretagne). *Norvis Environ. Aménagement. Société* **2004**, *193*, 17–29.

Denize, J.; Hubert-Moy, L.; Betbeder, J.; Corgne, S.; Baudry, J.; Pottier, E. Evaluation of using sentinel-1 and-2 time-series to identify winter land use in agricultural landscapes. *Remote Sens.* **2019**, *11*, 37.

Duchemin, B.; Fieuzal, R.; Rivera, M.A.; Ezzahar, J.; Jarlan, L.; Rodriguez, J.C.; Hagolle, O.; Watts, C. Impact of sowing date on yield and water use efficiency of wheat analyzed through spatial modeling and FORMOSAT-2 images. *Remote Sens.* **2015**, *7*, 5951–5979.

Veloso, A.; Mermoz, S.; Bouvet, A.; Le Toan, T.; Planells, M.; Dejoux, J.-F.; Ceschia, E. Understanding the temporal behavior of crops using Sentinel-1 and Sentinel-2-like data for agricultural applications. *Remote Sens. Environ.* **2017**, *199*, 415–426.

Morena, L.C.; James, K.V.; Beck, J. An introduction to the RADARSAT-2 mission. *Can. J. Remote Sens.* **2004**, *30*, 221–234.

Potin, P.; Bargellini, P.; Laur, H.; Rosich, B.; Schmuck, S. Sentinel-1 mission operations concept. In Proceedings of the 2012 IEEE International Geoscience and Remote Sensing Symposium; IEEE, Munich, Germany, 22–27 July 2012; pp. 1745–1748.

Drusch, M.; Del Bello, U.; Carlier, S.; Colin, O.; Fernandez, V.; Gascon, F.; Hoersch, B.; Isola, C.; Laberinti, P.; Martimort, P. Sentinel-2: ESA's optical high-resolution mission for GMES operational services. *Remote Sens. Environ.* **2012**, *120*, 25–36.

Huang, H.; Chen, Y.; Clinton, N.; Wang, J.; Wang, X.; Liu, C.; Gong, P.; Yang, J.; Bai, Y.; Zheng, Y. Mapping major land cover dynamics in Beijing using all Landsat images in Google Earth Engine. *Remote Sens. Environ.* **2017**, *202*, 166–176.

Smith, L.C. Satellite remote sensing of river inundation area, stage, and discharge: a review. *Hydrol. Process.* **1997**, *11*, 1427–1439.

Ulaby, F.T.; Moore, R.K.; Fung, A.K. Microwave remote sensing active and passive-volume III: From theory to applications. **1986**. <https://ntrs.nasa.gov/search.jsp?R=19860041708>.

Hosseini, M.; McNairn, H.; Merzouki, A.; Pacheco, A. Estimation of Leaf Area Index (LAI) in corn and soybeans using multi-polarization C-and L-band radar data. *Remote Sens. Environ.* **2015**, *170*, 77–89.

McNairn, H.; Brisco, B. The application of C-band polarimetric SAR for agriculture: a review. *Can. J. Remote Sens.* **2004**, *30*, 525–542.

Mascolo, L. Polarimetric SAR for the Monitoring of Agricultural Crops. Ph.D. Thesis, Università degli Studi di Cagliari, Cagliari, Italy, 2015.

Hütt, C.; Koppe, W.; Miao, Y.; Bareth, G. Best accuracy land use/land cover (LULC) classification to derive crop types using multitemporal, multisensor, and multi-polarization SAR satellite images. *Remote Sens.* **2016**, *8*, 684.

Haldar, D.; Rana, P.; Yadav, M.; Hooda, R.S.; Chakraborty, M. Time series analysis of co-polarization phase difference (PPD) for winter field crops using polarimetric C-band SAR data. *Int. J. Remote Sens.* **2016**, *37*, 3753–3770.

Skriver, H. Crop classification by multitemporal C-and L-band single-and dual-polarization and fully polarimetric SAR. *IEEE Trans. Geosci. Remote Sens.* **2012**, *50*, 2138–2149.

Skriver, H.; Svendsen, M.T.; Thomsen, A.G. Multitemporal C-and L-band polarimetric signatures of crops. *IEEE Trans. Geosci. Remote Sens.* **1999**, *37*, 2413–2429.

McNairn, H.; Duguay, C.; Boisvert, J.; Huffman, E.; Brisco, B. Defining the sensitivity of multi-frequency and multi-polarized radar backscatter to post-harvest crop residue. *Can. J. Remote Sens.* **2001**, *27*, 247–263.

Jiao, X.; McNairn, H.; Shang, J.; Liu, J. The sensitivity of multi-frequency (X, C and L-band) radar backscatter signatures to bio-physical variables (LAI) over corn and soybean fields. In Proceedings of the ISPRS TC VII Symposium — 100 Years ISPRS; Vienna, Austria, 5–7 July 2010; pp. 317–325.

Nurtyawan, R.; Saepuloh, A.; Budiharto, A.; Wikantika, K. Modeling Surface Roughness to Estimate Surface Moisture Using Radarsat-2 Quad Polarimetric SAR Data. In Proceedings of the Journal of Physics: Conference Series; IOP Publishing, Bandung, Indonesia, 19–20 August 2016, Volume 739; p. 012105.

Smith, A.M.; Major, D.J. Radar backscatter and crop residues. *Can. J. Remote Sens.* **1996**, *22*, 243–247.

Paris, J.F. Radar backscattering properties of corn and soybeans at frequencies of 1.6, 4.75, and 13.3 Ghz. *IEEE Trans. Geosci. Remote Sens.* **1983**, 392–400.

- Lee, J.-S.; Grunes, M.R.; Pottier, E. Quantitative comparison of classification capability: Fully polarimetric versus dual and single-polarization SAR. *IEEE Trans. Geosci. Remote Sens.* **2001**, *39*, 2343–2351.
- Abdikan, S.; Sanli, F.B.; Ustuner, M.; Calò, F. Land cover mapping using sentinel-1 SAR data. *Int. Arch. Photogramm. Remote Sens. Spat. Inf. Sci.* **2016**, *41*, 757.
- Dimov, D.; Löw, F.; Ibrakhimov, M.; Stulina, G.; Conrad, C. SAR and optical time series for crop classification. In Proceedings of the 2017 IEEE International Geoscience and Remote Sensing Symposium (IGARSS); IEEE, Fort Worth, TX, USA, 23–28 July 2017; pp. 811–814.
- Bargiel, D. A new method for crop classification combining time series of radar images and crop phenology information. *Remote Sens. Environ.* **2017**, *198*, 369–383.
- Minh, D.H.T.; Ienco, D.; Gaetano, R.; Lalande, N.; Ndikumana, E.; Osman, F.; Maurel, P. Deep recurrent neural networks for winter vegetation quality mapping via multitemporal SAR Sentinel-1. *IEEE Geosci. Remote Sens. Lett.* **2018**, *15*, 464–468.
- ZA Armorique. Available online: <https://osur.univ-rennes1.fr/za-armorique/> (accessed on 24 May 2019).
- Nitrates—Water Pollution—Environment—European Commission. Available online: http://ec.europa.eu/environment/water/water-nitrates/index_en.html (accessed on 24 May 2019).
- Open Access Hub. Available online: <https://scihub.copernicus.eu/> (accessed on 10 September 2019).
- Kalideos. Available online: <https://www.kalideos.fr/drupal/fr> (accessed on 24 May 2019).
- Pottier, E.; Ferro-Famil, L.; Fitzryk, M.; Desnos, Y.-L. PolSARpro-BIO: The new Scientific Toolbox for ESA & third party fully Polarimetric SAR Missions. In Proceedings of the EUSAR 2018; 12th European Conference on Synthetic Aperture Radar; VDE, Aachen, Germany, 4–7 June 2018; pp. 1–4.
- Radarsat 1 Products Image Resolution Geomatics. Available online: <https://www.scribd.com/document/73559622/Radarsat-1-Products> (accessed on 20 November 2017).
- Lee, J.-S.; Wen, J.-H.; Ainsworth, T.L.; Chen, K.-S.; Chen, A.J. Improved sigma filter for speckle filtering of SAR imagery. *IEEE Trans. Geosci. Remote Sens.* **2009**, *47*, 202–213.
- Lee, J.-S.; Pottier, E. *Polarimetric Radar Imaging: From Basics to Applications*; CRC Press: Boca Raton, FL, USA, 2009.
- Cloude, S.R.; Pottier, E. A review of target decomposition theorems in radar polarimetry. *IEEE Trans. Geosci. Remote Sens.* **1996**, *34*, 498–518.
- Freeman, A.; Durden, S.L. A three-component scattering model for polarimetric SAR data. *IEEE Trans. Geosci. Remote Sens.* **1998**, *36*, 963–973.
- Kim, Y.; Jackson, T.; Bindlish, R.; Lee, H.; Hong, S. Radar vegetation index for estimating the vegetation water content of rice and soybean. *IEEE Geosci. Remote Sens. Lett.* **2012**, *9*, 564–568.
- McNairn, H.; Hochheim, K.; Rabe, N. Applying polarimetric radar imagery for mapping the productivity of wheat crops. *Can. J. Remote Sens.* **2004**, *30*, 517–524.
- Kostelich, E.J.; Schreiber, T. Noise reduction in chaotic time-series data: A survey of common methods. *Phys. Rev. E* **1993**, *48*, 1752.
- Breiman, L. Random Forests. *Mach. Learn.* **2001**, *45*, 5–32.
- Pal, M. Random forest classifier for remote sensing classification. *Int. J. Remote Sens.* **2005**, *26*, 217–222.
- Belgiu, M.; Csillik, O. Sentinel-2 cropland mapping using pixel-based and object-based time-weighted dynamic time warping analysis. *Remote Sens. Environ.* **2018**, *204*, 509–523.

- Liaw, A.; Wiener, M. Classification and regression by randomForest. *R News* **2002**, *2*, 18–22.
- R: The R Project for Statistical Computing. Available online: <https://www.r-project.org/> (accessed on 10 September 2019).
- Lawrence, R.L.; Wood, S.D.; Sheley, R.L. Mapping invasive plants using hyperspectral imagery and Breiman Cutler classifications (RandomForest). *Remote Sens. Environ.* **2006**, *100*, 356–362.
- Belgiu, M.; Drăguț, L. Random forest in remote sensing: A review of applications and future directions. *ISPRS J. Photogramm. Remote Sens.* **2016**, *114*, 24–31.
- Audebert, N.; Le Saux, B.; Lefèvre, S. Beyond RGB: Very high resolution urban remote sensing with multimodal deep networks. *ISPRS J. Photogramm. Remote Sens.* **2018**, *140*, 20–32.
- Congalton, R.G. A review of assessing the accuracy of classifications of remotely sensed data. *Remote Sens. Environ.* **1991**, *37*, 35–46.
- Jiao, X.; Kovacs, J.M.; Shang, J.; McNairn, H.; Walters, D.; Ma, B.; Geng, X. Object-oriented crop mapping and monitoring using multi-temporal polarimetric RADARSAT-2 data. *ISPRS J. Photogramm. Remote Sens.* **2014**, *96*, 38–46.
- Yusoff, N.M.; Muharam, F.M.; Takeuchi, W.; Darmawan, S.; Abd Razak, M.H. Phenology and classification of abandoned agricultural land based on ALOS-1 and 2 PALSAR multi-temporal measurements. *Int. J. Digit. Earth* **2017**, *10*, 155–174.
- Immitzer, M.; Vuolo, F.; Atzberger, C. First experience with Sentinel-2 data for crop and tree species classifications in central Europe. *Remote Sens.* **2016**, *8*, 166.
- McNairn, H.; Shang, J.; Champagne, C.; Jiao, X. TerraSAR-X and RADARSAT-2 for crop classification and acreage estimation. In Proceedings of the 2009 IEEE International Geoscience and Remote Sensing Symposium; IEEE, Cape Town, South Africa, 12–17 July 2009; Volume 2, pp. 2–898.
- Liu, C.; Shang, J.; Vachon, P.W.; McNairn, H. Multiyear crop monitoring using polarimetric RADARSAT-2 data. *IEEE Trans. Geosci. Remote Sens.* **2012**, *51*, 2227–2240.
- Haldar, D.; Das, A.; Mohan, S.; Pal, O.; Hooda, R.S.; Chakraborty, M. Assessment of L-band SAR data at different polarization combinations for crop and other landuse classification. *Prog. Electromagn. Res.* **2012**, *36*, 303–321.
- Blaes, X.; Vanhalle, L.; Defourny, P. Efficiency of crop identification based on optical and SAR image time series. *Remote Sens. Environ.* **2005**, *96*, 352–365.
- Baghdadi, N.; Boyer, N.; Todoroff, P.; El Hajj, M.; Bégué, A. Potential of SAR sensors TerraSAR-X, ASAR/ENVISAT and PALSAR/ALOS for monitoring sugarcane crops on Reunion Island. *Remote Sens. Environ.* **2009**, *113*, 1724–1738.
- Inoue, Y.; Kurosu, T.; Maeno, H.; Uratsuka, S.; Kozu, T.; Dabrowska-Zielinska, K.; Qi, J. Season-long daily measurements of multifrequency (Ka, Ku, X, C, and L) and full-polarization backscatter signatures over paddy rice field and their relationship with biological variables. *Remote Sens. Environ.* **2002**, *81*, 194–204.
- Loosvelt, L.; Peters, J.; Skriver, H.; De Baets, B.; Verhoest, N.E. Impact of reducing polarimetric SAR input on the uncertainty of crop classifications based on the random forests algorithm. *IEEE Trans. Geosci. Remote Sens.* **2012**, *50*, 4185–4200.
- Dufour, S.; Bernez, I.; Betbeder, J.; Corgne, S.; Hubert-Moy, L.; Nabucet, J.; Rapinel, S.; Sawtschuk, J.; Trollé, C. Monitoring restored riparian vegetation: How can recent developments in remote sensing sciences help? *Knowl. Manag. Aquat. Ecosyst.* **2013**, *410*, 10.
- Hong, G.; Wang, S.; Li, J.; Huang, J. Fully polarimetric synthetic aperture radar (SAR) processing for crop type identification. *Photogramm. Eng. Remote Sens.* **2015**, *81*, 109–117.

Zhang, Y.; Wu, L. Crop classification by forward neural network with adaptive chaotic particle swarm optimization. *Sensors* **2011**, *11*, 4721–4743.

Adams, J.R.; Berg, A.A.; McNairn, H.; Merzouki, A. Sensitivity of C-band SAR polarimetric variables to unvegetated agricultural fields. *Can. J. Remote Sens.* **2013**, *39*, 1–16.



© 2019 by the authors. Submitted for possible open access publication under the terms and conditions of the Creative Commons Attribution (CC BY) license (<http://creativecommons.org/licenses/by/4.0/>).

Conclusion of the third part

In this third part, we identified the most appropriate SAR configuration for the identification of winter land-use. SAR time-series data has shown since several years its ability for identifying, characterizing and monitoring land use.

Thus, at the local scale of the "Pleine-fougères", a comparative methodology based on multi-temporal SAR Radarsat-2, Sentinel-1 and Alos-2 time-series images, has been developed to identify winter land-use classes. The first step of the methodology consisted of extracting SAR backscatter coefficients and polarimetric data. An analysis was then conducted using the RF algorithm to determine the importance of each SAR parameter for the identification of winter land-use classes. The results highlighted the main role of the Shannon Entropy for winter land-use classification in both quad and dual-polarization mode. Similarly, these results also presented the potential of the SPAN in a quad-pol configuration.

The second step of the developed methodology tried to define the most efficient SAR configuration for identifying winter land-use. A comparative approach has been implemented based on 6 SAR images datasets using the RF algorithm. The results pointed out four main points. *i)* The prevalence of quad-polarization mode versus dual-polarization mode. *ii)* The ability of the C-band compared to the L-band for this issue. *iii)* The importance of the density of time-series SAR images. *iv)* And finally the potential of Sentinel-1 best configuration compared to Radarsat-2 and Alos-2 data for identifying winter land-use classes.

The three successive approaches conducted in Parts 2 and 3 of this manuscript have demonstrated the interest of remote sensing data for the detailed identification and characterization of winter land-use at a local scale. In this context, the last part of this manuscript will attempt to define the potential of the best classification approach identified within these 2 parts for the identification and characterization of winter land-use on a regional scale (Brittany).

4

The study of winter land-use at a regional scale

Contents

INTRODUCTION OF THE FOURTH PART	165
CHAPTER 7: IDENTIFICATION OF WINTER LAND-USE AT A REGIONAL SCALE	167
CONCLUSION OF THE FOURTH PART	185

Introduction of the fourth part

The fourth part of the manuscript presents the researches carried out to evaluate the potential of time-series in order to identify winter land-use at a regional scale. The general framework of this approach has been developed in *Section IV.4* and will be presented below.

Chapter 7 is based on the synthesis of two previous parts in order to select both the best classification procedure and remote sensing data to identify winter land-use at a regional scale. To this end, a procedure using Sentinel-2 times-series with an RF algorithm was selected based on the results presented in the 2nd part of this document. From this perspective, Chapter 7 will aim to evaluate the ability of Sentinel-2 time-series to identify winter land-use classes in order to collect detailed information on UAA parcels (declared and not declared) to provide technical support to decision-makers.

In this context, winter land-use will be analyzed over a large agricultural area (Brittany, France), using a time-series of Level-2A Sentinel-2 images presented in *Section III.3.1*. First, a classification and temporal analysis will be performed to identify crop residues parcels (not declared to the Common Agriculture Policy) using a NDVI time-series images. Then, a classification procedure using Sentinel-2 time-series is realized at a regional scale to identify; *i*) winter land-use of declared parcels using RPG samples; *ii*) winter land-use of not declared parcels using “BD parcellaire” samples and crop residues parcels previously identified in order to provide detailed land-use information for the implementation of environmental measures by decision-makers.

Chapter 7

Identification of winter land-use at a regional scale

Contents

VII.1. INTRODUCTION	169
VII.2. STUDY SITE AND DATA	171
VII.3. METHODOLOGY	174
VII.4. RESULTS AND DISCUSSION	176
VII.6. CONCLUSIONS	181

This chapter will be submitted in a peer-reviewed journal

Article

Identification of winter land-use at regional scale using Sentinel-2 time-series: Technical support for environmental measures

Authors: Julien Denize^{1,2,*}, Laurence Hubert-Moy², Eric Pottier¹

¹ Institute of Electronics and Telecommunications of Rennes IETR, UMR CNRS 6164, University of Rennes, 35000 Rennes, France

² Littoral-Environnement-Téledétection-Géomatique LETG UMR 6554, University of Rennes, 35000 Rennes, France

* Corresponding author

Journal: International Journal of Applied Earth Observation

Highlights:

- Sentinel-2 time-series were used to identify winter land-use at the regional scale
- NDVI time-series were used to map crop-residue and surface-state changes
- Sentinel-2 parameter dataset were classified using Random Forest
- Parcel-based approach classified more accurately than pixel-based
- Overall winter land-use on undeclared parcels was successfully identified

Abstract:

Increasing pressure on agricultural areas, on which intensification and pesticide use have become fundamental practices to support an increasing world population, requires implementing environmental policies to ensure sustainable development of these areas. Acquiring detailed and spatialized information about winter land-use, which is recognized as an important factor in environmental change, is a major issue for scientific communities and decision-makers. In this context, this study evaluated the potential of Sentinel-2 optical images to identify winter land-use at the regional scale to provide technical support for making sustainability-oriented decisions. To this end, a time-series of NDVI extracted from Sentinel-2 data was first used to identify agricultural parcels vulnerable to pollutant transfers and the temporal dynamics of these parcels in the region of Brittany, France. Next, a set of Sentinel-2 parameters was extracted and classified with the Random Forest algorithm using an approach based on objects (parcels) or pixels. Classification results highlighted that the parcel-based approach (overall accuracy (OA) = 84%, Kappa = 0.77, F1-score = 0.85) was more accurate than the pixel-based approach (OA= 82%, Kappa = 0.73, F1-score = 0.83). This study demonstrates the potential of Sentinel-2 data to identify winter land-use at the regional scale, providing technical support to public and private decision-makers.

Keywords: Remote sensing, Sustainable agriculture, Optical time-series, NDVI, Random Forest algorithm, multi-temporal classification.

VII.1. Introduction

Implementing measures that promote sustainable development of agricultural systems must consider pressures exerted on the environment by global climate change, societies and their activities to manage these systems optimally. Fine-scale knowledge about agricultural systems and their practices thus remains a major issue for scientific communities and decision-makers. In this context, identifying and characterizing winter land-use, which is considered an important factor in environmental change, is required (Foley et al., 2005). In the European Union (EU) and particularly in France, this awareness of environmental issues, at small and large scales, has led authorities to establish legislation, such as the Nitrates Directive (Justes et al., 2012), enshrined in the Common Agricultural Policy (CAP), to maintain and improve the quality of environment, in particular for the quality of surface water impacted by transfer of agricultural pollutants (Buckley and Carney, 2013). These regulations mandate establishment of vegetative cover in winter to decrease transfer of agricultural pollutants to the environment and are supported by subsidies given to farmers by the CAP. In France, these subsidies are provided through an annual procedure of field declaration, which is summarized in the "Registre Parcellaire Graphique" (RPG) ("Graphical Field Register" in French), a geographical information system for agricultural parcels in France ("RPG IGN," 2019). However, because farmers do not declare parcels not supported by the CAP, these parcels are ignored by decision-makers, which complicates implementation of sustainable measures. In this context, remotely sensed images have emerged in the past few decades as a valuable tool to identify and characterize land use and provide detailed and timely information about the phenological status and development of vegetation cover at different scales (Bégué et al., 2018; Zadbagher et al., 2018).

Despite development in the late 1990s of optical sensors with medium spatial resolution such as MODIS or SPOT-Vegetation (250 m and 1 km, respectively), providing new opportunities for monitoring vegetation cover at the global scale, only a few studies have demonstrated the potential of these remotely sensed data for studying winter land-use. Most studies have investigated the potential of these optical data for identifying and characterizing land use. For example, (Jakubauskas et al., 2002) and (Sakamoto et al., 2005) demonstrated the ability of MODIS to characterize and monitor crop areas and their temporal dynamics. Similarly, (Kamthonkiat et al., 2005) and (Verbeiren et al., 2008) illustrated the ability of SPOT-Vegetation data to discriminate and classify crop areas with accuracy (R^2) greater than 85%. According to (Lecerf et al., 2005), few studies address winter land-use because the resolution of MODIS-like sensors is too low to identify and characterize winter land-use classes finely. The emergence of high and very-high spatial resolution optical sensors in the mid-1990s was unable to provide more detailed information because of the sensors' low temporal resolution (several tens of days) and sensitivity to meteorological conditions, both of which limit land-use monitoring during winter. The launch in 2015 and 2017 of a new generation of optical sensors with high spatial (10 m) and very high temporal resolution (every 6 days for the Sentinel constellation) has opened opportunities for identifying and characterizing winter land-use over large areas. In this context, (Denize et al., 2019) highlighted the potential of Sentinel-2 data to identify and characterize winter land-use at the local scale with an overall accuracy (OA) of 75%. Except for their study, studies performed to date have focused on land use during the vegetative-growth period (Delalay et al., 2019; Forkuor et al., 2018). In this context, no detailed information about winter land-use is available to date to support development of sustainable measures to manage these agricultural systems optimally over

large areas. Thus, this study aimed to evaluate the ability of Sentinel-2 time-series to identify and monitor winter land-use classes at the regional scale by collecting detailed information about the utilized agricultural area (UAA) of fields (declared and undeclared) to provide technical support to decision-makers.

VII.2. Study site and data

VII.2.1. Study site

Brittany, an area of 27,209 km² located in western France (**Fig. IV.1**), is exposed to an oceanic temperate climate, with an annual mean temperature above 12°C, a minimum mean for the coldest year above 8°C, a maximum mean above 16°C and mean annual rainfall of 600-700 mm. Brittany is the second-largest agricultural region in France, with 1.7 million ha of UAA, representing 53% of its area, in four administrative departments (“CCI Bretagne,” 2017). The UAA can be divided into two types of fields: “declared”, which can be declared and registered in the RPG to receive CAP subsidies, and “undeclared”, which are neither declared nor registered. The UAA of Brittany is covered by a variety of agricultural systems that in summer produce four main types of crops, most of which are used for livestock feed (“Agreste,” 2017):

- Forages, mainly forage maize and temporary or permanent grasslands, which covered nearly 63% of the UAA in 2015 (ca. 1,827,000 ha)
- Cereals, mainly wheat, barley, and triticale, which covered ca. 580,000 ha (ca. 20% of the UAA) in 2015
- Vegetables, mainly tomatoes, cauliflower, and artichokes, which make Brittany the leading region of vegetable production in France and covered 406,000 ha (ca. 14% of the UAA) in 2015
- Oilseed and protein crops, mainly (88%) rapeseed, which covered ca. 45,000 ha (< 3% of the UAA) in 2015

In winter, the agricultural systems have a high cover of grasslands and of two types of secondary annual crops (**Fig. IV.2**): winter crops (winter wheat, winter barley, and rapeseed) or intermediate crops (i.e. “catch crops”). With 98% of Brittany’s area (“Agreste,” 2017) designated as nitrate vulnerable zones, establishing vegetation cover during winter has become mandatory and highly regulated and controlled by EU authorities within the framework of the Nitrates Directive to prevent transfer of agricultural pollutants (“Nitrates Directive,” 2019). In this context, establishment of winter soil cover is supported by subsidies granted by the CAP to farmers. However, some exemptions are possible for parcels harvested after 1 November, which may remain as crop residues without winter cover (**Fig. IV.2**). These parcels, as well as parcels not subsidized by the CAP, are not subject to an annual declaration. As a result, no information about these parcels is available for state services or decision-makers, although they are considered areas potentially vulnerable to the transfer of agricultural pollutants. Thus, it is important to evaluate the potential of Sentinel-2 data to determine winter land-use in these fields.

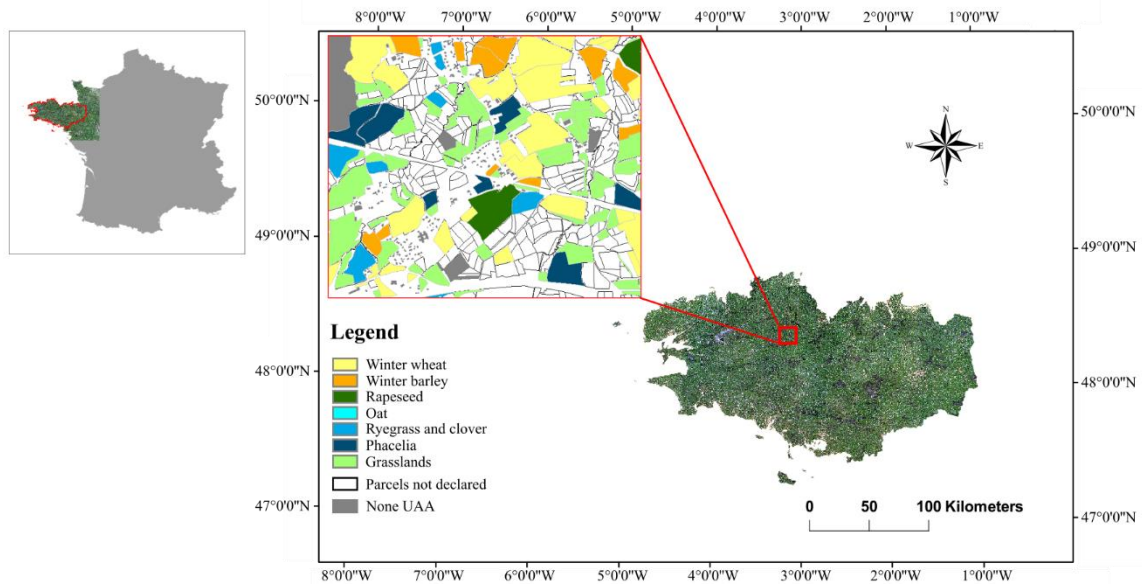


Figure IV.1. Location of the study site, Brittany, in France (RGB composite image from Sentinel-2 data, 2017, ©Copernicus data 2017) and representation of the utilized agricultural area (UAA) of fields declared and undeclared under the Common Agricultural Policy.



Figure IV.2. The main land-use types encountered in winter in the study area of Brittany, France: a) winter crops (winter barley), b) catch crops (phacelia), c) crop residues (maize stalks) and d) grasslands.

VII.2.2. Field data

VII.2.2.1. Land use data

External data were retrieved from the following sources to calibrate and validate the classification models.

- “Registre Parcellaire Graphique”

The RPG is managed by the French Service and Payment Agency. It is created from farmers' annual declarations of parcels to the EU as part of the CAP. The data provide information about land use at the parcel scale. The parcels declared in year N indicate their situation as of 1 January of year N+1 (“RPG IGN,” 2019). Several versions of the RPG are available, ranging from an “anonymized” RPG, with only land-use information, to an “un-anonymized” RPG that also includes information such as the name of the parcel’s farmer. We selected the latter for this study. Precautions should be taken with these data because they have some uncertainties: some farm areas are missing (e.g. farms not receiving subsidies), missing farm areas vary among years depending on how subsidies evolve, and farmers can change the boundaries of their parcels. The RPG for 2016 and 2017 were retrieved in the Lambert-93 projection system (RGF93, EPSG: 2154) from the National Institute for Geographic and Forest Information (IGN)

(“IGN,” 2019) to obtain complete information about vegetation cover during winter 2016-2017. The nomenclature of RPG crops was divided into two levels based on an approach developed by (Denize et al., 2019) (**Table IV.1**).

Table IV.1. The land-use classes included in two classification levels. Asterisks indicate classes not included in the “Registre Parcellaire Graphique”.

Level 1	Level 2
Winter crops	Winter wheat Winter barley Rapeseed
Catch crops	Oat Ryegrass and clover Phacelia
<i>Crop residues*</i>	<i>Maize stalks*</i>
Grasslands	Grasslands

✓ « BD Parcellaire »

The "BD Parcellaire" ("Field Database" in French) is a database of the IGN established in the context of the "Référéntiel géographique à Grande Échelle", mandated by French regulations in 2005 ("BD Parcellaire," 2019). By compiling digital cadastral maps, it provides geo-referenced and continuous cadastral information for the whole of France. Its data are accurate and offer many advantages, especially information about all agricultural fields in the UAA of France (whether declared or not). For this study, the BD Parcellaire was retrieved for Brittany in vector format (Shapefile ESRI) with a Lambert-93 geographical projection (RGF93, EPSG: 2154) from the IGN website, which provides free access to these data for scientific research ("BD Parcellaire," 2019).

VII.2.3. Satellite data

A series of 51 optical Sentinel-2 images, acquired by the European Space Agency (ESA) from September 2016 to May 2017, was obtained for the whole of Brittany from the Theia Data and Services Center ("Theia," 2019). Sentinel-2 images were acquired in level 2A (i.e. corrected for geometric and atmospheric effects) with a spatial resolution ranging from 10-20 m and a spectral resolution of 10 bands. Atmospheric corrections made to reach level 2A were performed using the MACCS ATCOR Joint Algorithm (MAJA) pre-processing chain developed by the Centre d'Etudes Spatiales de la BIOsphère (CESBIO). MAJA is a chain for cloud detection and atmospheric correction that is suitable for processing time-series of high spatial resolution images acquired from constant or almost constant angles of view ("MAJA," 2019). Moreover, a set of Sentinel-2 mask images calculated with MAJA was retrieved to mask potential cloud cover.

VII.3. Methodology

VII.3.1 Pre-processing of Sentinel-2 time-series

The Sentinel-2 time-series images acquired from Theia had been orthorectified and georeferenced using MAJA based on the UTM (area 30N) reference system and corrected for atmospheric perturbations. First, the corrections calculated with MAJA were evaluated, and then the cloud masks were applied to the 51 images. Finally, 12 optical parameters were extracted from each image using SNAP software (v.6.0) (**Table IV.2**): (i) the 10 corrected Sentinel-2 bands, (ii) the Normalized Difference Vegetation Index (NDVI, (Rouse Jr et al., 1974)), and (iii) the Normalized Difference Water Index (NDWI, (Gao, 1996)), the latter two derived for their ability to highlight processes related to vegetation, such as water stress, peak growth, and phenological stage (Mishra and Singh, 2010; Xue and Su, 2017). In total, 612 parameters (12 parameters \times 51 dates) were extracted from Sentinel-2 corrected time-series.

Table IV.2. Parameters derived from Sentinel-2 image time-series

Sentinel-2 optical parameters
Band 2 – blue
Band 3 – green
Band 4 – red
Band 5 – vegetation red edge
Band 6 – vegetation red edge
Band 7 – vegetation red edge
Band 8 – near-infrared (NIR)
Band 8a – narrow NIR
Band 11 – shortwave infrared (SWIR)
Band 12 – SWIR
Normalized Difference Vegetation Index ($NDVI = \frac{(Band\ 8 - Band\ 4)}{(Band\ 8 + Band\ 4)}$)
Normalized Difference Water Index ($NDWI = \frac{(Band\ 8 - Band\ 12)}{(Band\ 8 + Band\ 12)}$)

VII.3.2 Sentinel-2 time-series processing

VII.3.2.1. Extraction of crop residues parcels using NDVI Time-series

First, using the NDVI time-series previously extracted from corrected Sentinel-2 images, thresholds were defined to identify fields with or without vegetation cover from September 2016 to May 2017. The NDVI images were then reclassified into 51 binary images (one per date) by assigning 0 to pixels with $NDVI > 0.25$ (i.e. vegetation cover) and 1 to pixels with $NDVI < 0.25$ (i.e. little or no coverage). The threshold of 0.25 was defined based on results of (Denize et al., 2019), who identified and characterized crop-residue fields in winter by

analyzing the optical signal and winter land-use. Then, threshold images and the BD Parcellaire were cross-checked and summarized to identify crop-residue fields from 1 November 2016 to 1 February 2017. This period was defined based on Nitrates Directive legislation and temporal dynamics of crop residues identified by (Denize et al., 2019). A value of 1 was assigned to BD Parcellaire fields identified as uncovered at least twice from November 2016-October 2017, while 0 was assigned to the others. Next, the crop-residue fields were analyzed temporally to determine the date when their surface state changed (i.e. when they became covered by crop residues). Finally, a map of crop-residue parcels and a map of the date when the state of the surface changed were created for Brittany at 1:300,000 scale.

VII.3.2.2. Winter Land Use classification

To classify winter land-use, the dataset of 612 optical parameters extracted previously was first divided into 10 km ×10 km tiles using the "Create a grid" function of QGIS software (v.3.4.6) (Madeira) to parallelize processing and reduce the size and processing time. Next, features were extracted using R software (v.3.5.1) ("R Core Team, 2019," 2019) at the field and pixel level by overlaying RPG polygons on the Sentinel-2 parameter tiles. A set of 1,280 samples (corresponding to 30% of the most underrepresented class) was randomly selected for a 3-class and 7-class model of winter land-use in Brittany (i.e. one model per classification level). In total, 3,840 samples (1,280 samples × 3 classes) or 8,960 samples (1,280 samples × 7 classes) were extracted.

The Random Forest (RF) classifier was then chosen for its consistently strong performance and classification accuracy of winter land-use, as demonstrated by (Denize et al., 2019). RF collects classification algorithms using classification and regression trees to predict (Breiman, 2001). From a random selection of a training-sample subset, RF uses a series of trees for classification. For the 3- and 7-class classification model, 60% of the samples (2,304 and 5,376, respectively) were used to train the trees and the remaining 40% (1,536 and 3,584, respectively) were used in an internal cross-validation technique to estimate accuracy of the RF model (Belgiu and Drăguț, 2016). The randomForest package (v 4.6-14) (Liaw and Wiener, 2002) of R software was used to classify land use. Two RF parameters were tuned using the package's "tune" function. The number of trees (ntree) randomly created using samples from the training dataset was set to 1,000, which was identified as an optimal number to minimize the percentage of errors (Lawrence et al., 2006). The number of variables used to split tree nodes (mtry) was tuned and set randomly. Classification accuracy was assessed with the validation dataset by calculating OA, the Kappa index and F1-score, the last of which is a statistical measure of classification accuracy calculated as a weighted average of precision and recall (Audebert et al., 2018) (Eq.IV.1):

$$F1_i = 2 \times \frac{\text{precision}_i \times \text{recall}_i}{\text{precision}_i + \text{recall}_i} \quad (\text{Eq. IV.1})$$

The classification procedure was repeated 100 times by changing the training and validation subsamples. A declared winter land-use map was then generated for Brittany at 1:300,000 scale using the RF model with the highest OA. Finally, the best classification model was applied to fields in BD Parcellaire to identify winter land-use of all undeclared fields in Brittany's UAA. Classification accuracy was assessed by comparing results to RPG field samples.

VII.4. Results and Discussion

VII.4.1. Identification of crop-residue parcels

The process classified ca. 5,000 parcels as containing crop residues, which covered less than 1% of Brittany's UAA, as demonstrated at the local scale by (Denize et al., 2019). When mapped, crop-residue parcels had a homogeneous distribution in Brittany (**Fig. IV.3**).

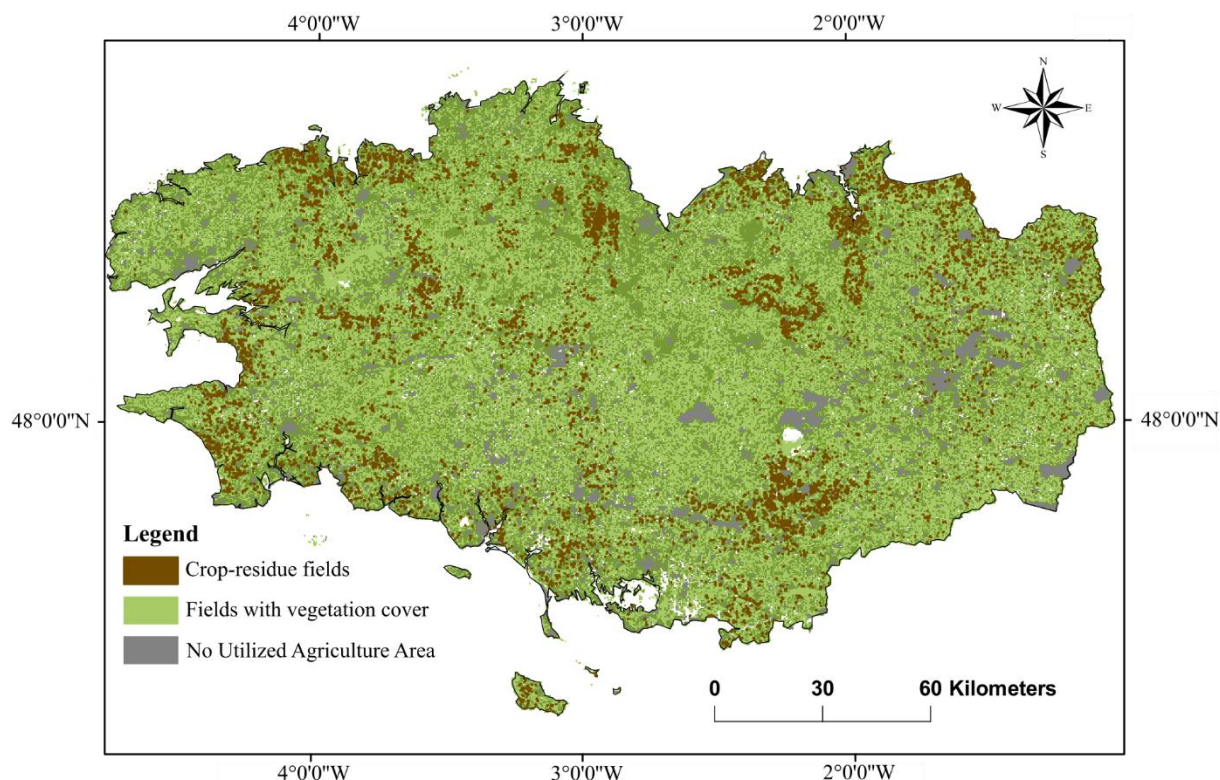


Figure IV.3. Map of crop-residue parcels obtained from Sentinel-2 NDVI time-series using a threshold of 0.25.

The map showing the dates when parcels became crop-residue parcels identified three areas in Brittany: (i) the east, where most changes occurred around 3 November 2016, (ii) the southwest, where most changes occurred around 6 November and (iii) the northwest, where changes occurred from 6-13 November (**Fig. IV.4**). These differences can be explained by differences in meteorological conditions ("Quand récolter," 2018), with a milder oceanic climate in the west and a warmer combination of oceanic and continental climates in the east, which influenced differently crop growth and the optimal harvest date (i.e. when the ratio of dry matter to grain value is optimal) (Ferreira et al., 2006).

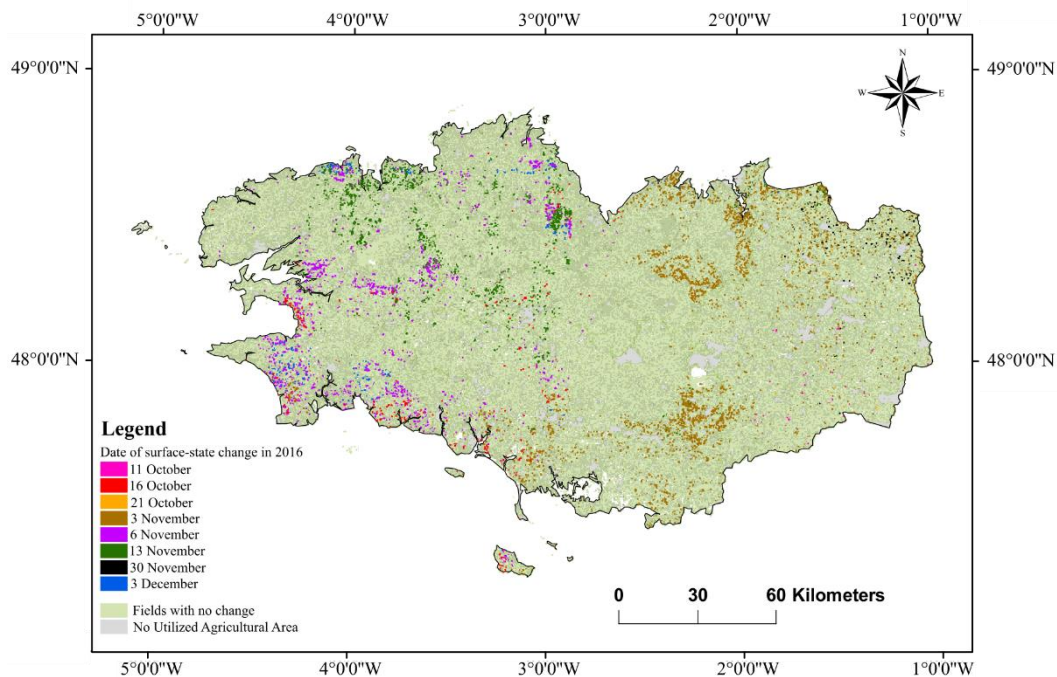


Figure IV.4. Map of the date when parcels became covered by crop residues, obtained from Sentinel-2 NDVI time-series images using a threshold of 0.25.

VII.4.2. Overall winter land-use classification accuracy

The accuracy of winter land-use classifications obtained from Sentinel-2 time-series parameters varied significantly depending on (i) the number of classes and (ii) the classification approach (i.e. parcel-based or pixel-based) used for the classification model. First, the 3-class model was more accurate (mean F1-score = 0.85, Kappa index = 0.77, OA = 84%) than the 7-class model (mean F1-score = 0.64, Kappa index = 0.59, OA = 65%) (**Table IV.3**). These results highlight limits of Sentinel-2 data for detailed identification of winter land-use at a large scale, in contrast to a recent study that demonstrated the ability of Sentinel-2 images to classify winter land-use at the local scale (Denize et al., 2019). The difference in accuracy between these two approaches, performed at different scales, is probably due to specific characteristics of the region or the number of exploitable images, which has less influence at the local scale. Although Sentinel-2 data are more adapted for studying winter land-use at the local scale (Denize et al., 2019), combining them with Sentinel-1 SAR data could provide additional information at the regional scale and thus overcome image-acquisition problems, as shown in studies of land-use in summer (Bargiel, 2017; Belgiu and Csillik, 2018; Immitzer et al., 2016).

Second, the parcel-based approach outperformed the pixel-based approach for both models (3 and 7 classes), with a mean F1-score of 0.84 and 0.83, respectively, for the 3-class model and 0.64 and 0.63, respectively, for the 7-class model (**Table IV.3**). These results are consistent with those in the literature, which have demonstrated the potential of the object-based approach for identifying and classifying land use using Sentinel-2 data (Belgiu and Csillik, 2018; Denize et al., 2019).

Table IV.3. Mean classification accuracy of 3 or 7 classes of winter land-use obtained for the best Sentinel-2 parameters using the Random Forest algorithm and a pixel-based or parcel-based approach. OA: overall accuracy.

Metric	Dataset			
	3 classes		7 classes	
	Pixel-based	parcel-based	Pixel-based	Parcel-based
OA (%)	82.3	84.4	64.1	65
Kappa index	0.73	0.77	0.58	0.59
F1-score	0.83	0.85	0.63	0.64

VII.4.3. Classification accuracy of winter land-use classes

For the 3-class model, accuracy of the catch crops class (mean F1-score = 0.86) was higher than those of the winter crops or grasslands classes (mean F1-score = 0.83 and 0.84, respectively) (**Fig. IV.5A**). For the 7-class model, the rapeseed class was the most accurate (mean F1-score = 0.87), while the oat, ryegrass, and clover and phacelia classes (which represent the catch crops class) were least accurate (mean F1-score = 0.45, 0.55 and 0.47 respectively) (**Fig. IV.5B**). The other three classes (winter wheat, grasslands and winter barley) had a mean F1-score of 0.76, 0.70 and 0.67, respectively. These results suggest high confusion between catch-crop classes and the other winter land-use classes, which leads to misclassification errors due to similar vegetative cycles (e.g. winter barley and oat). Moreover, they are consistent with several studies that have demonstrated the limits of characterizing land use using remote sensing data due to complex conditions such as cloud cover (Khalidouni et al., 2011).

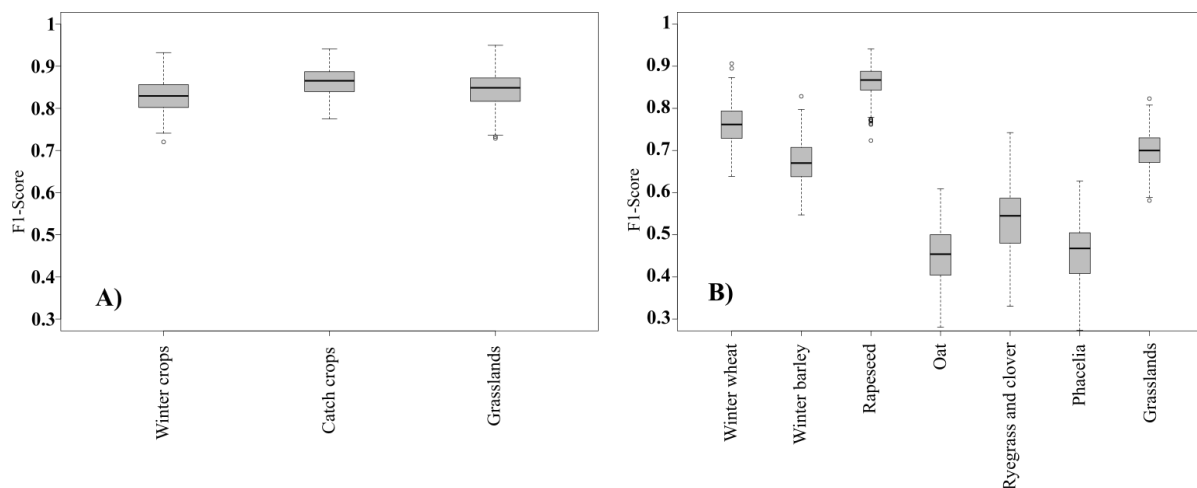


Figure IV.5. Boxplots of classification accuracies of (A) three or (B) seven land-use classes based on 100 Random Forest iterations. Whiskers indicate 1.5 times the interquartile range.

VII.4.4. Declared winter land-use mapping

The confusion matrix derived from the best classification model using Sentinel-2 time-series parameters (**Table IV.4**) showed that misclassification errors occurred mainly between winter crops and the other classes. The associated map showed a high prevalence of the grasslands class throughout Brittany (ca. 56% of the declared UAA) (**Fig. IV.6**), which was consistent with the regional statistics. In contrast, the catch crops class was the least prevalent (ca. 14% of the declared UAA). The winter crops class covered 30% of the declared UAA.

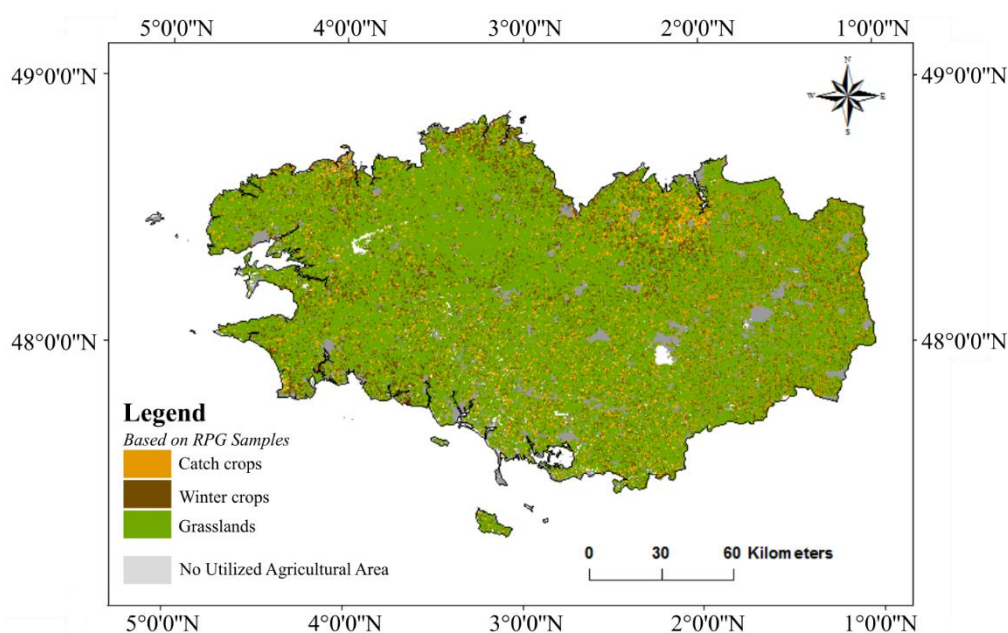


Figure IV.6. Map of declared winter land-use based on Sentinel-2 time-series images. The classification was performed using the Random Forest algorithm and the “Registre Parcellaire Graphique” (RPG) samples.

Table IV.4. Confusion matrix of the best winter land-use classification of declared fields obtained using the Sentinel-2 time-series. Kappa index = 0.77.

Land-use class	Winter crops	Catch crops	Grasslands	Commission errors (%)
Winter crops	406	43	32	84.41
Catch crops	40	448	26	87.16
Grasslands	57	32	452	83.55
Omission errors (%)	80.72	85.66	88.63	85.0

VII.4.5. Undeclared winter land-use mapping

The confusion matrix derived from the classification of undeclared parcels based on the best Sentinel-2 parameters with the 3-class model RF (**Table IV.5**) showed that misclassification errors occurred mainly for the catch crops class and between the winter crops and grasslands classes, as observed for the declared UAA. The associated map (ca. 345,000 fields covering 40% of the UAA) highlighted a high prevalence of the grasslands class throughout Brittany (68% of the undeclared UAA) (**Fig. IV.7**). In contrast, the crop residues class was predicted the

least (1% of the undeclared UAA). The winter crops and catch crops classes covered 19% and 12% of the undeclared UAA, respectively.

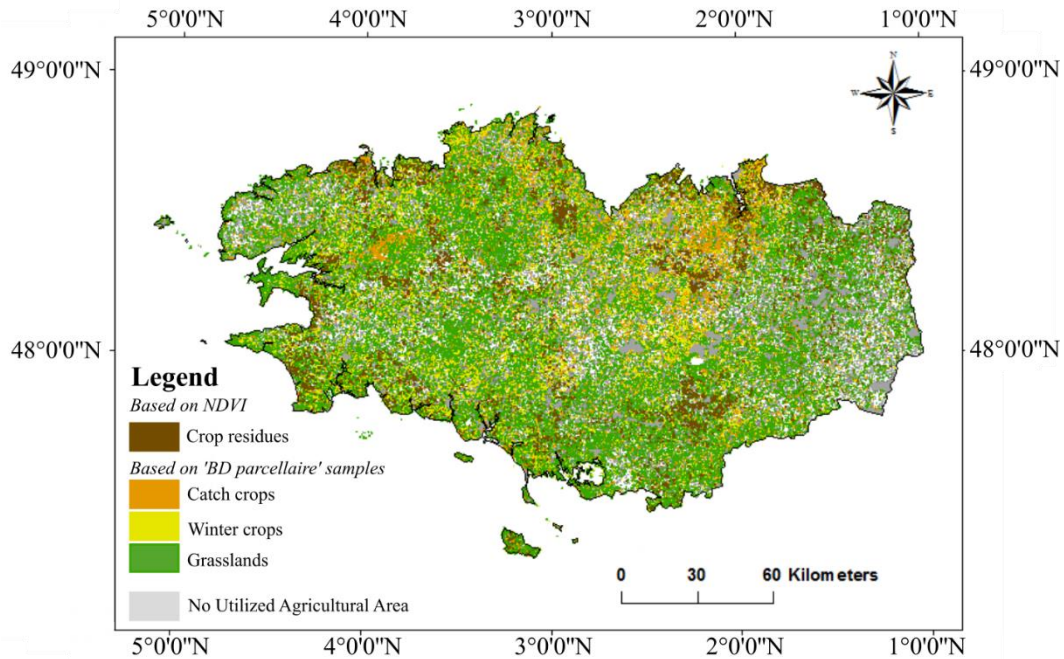


Figure IV.7. Map of undeclared winter land-use fields based on Sentinel-2 image time-series. Fields were classified by applying a Random Forest algorithm to “BD Parcellaire” samples.

Table IV.5. Confusion matrix of the best winter land-use classification of undeclared fields obtained using the Sentinel-2 time-series.

Land-use class	Winter crops	Catch crops	Grasslands	Commission errors (%)
Winter crops	130 309	24 520	81 073	55.2
Catch crops	23 472	78 634	34 458	57.6
Grasslands	88 173	39 200	270 963	68
Omission errors (%)	53.9	55.2	70.1	62.3

This study took advantage of the spatial and temporal resolution of Sentinel-2 images to identify winter land-use with good accuracy. Results were consistent with the literature, which highlights the potential of Sentinel-2 data for classifying land use over large areas (Forkuor et al., 2018; Immitzer et al., 2016) but with less accuracy than that obtained at the local scale (Denize et al., 2019). In addition, these results show the difficulty in monitoring winter land-use over large areas using Sentinel-2 data, mainly due to meteorological conditions that limit acquisition of optical images, but also because of the variety of winter land-use. From this perspective, establishing an adapted and standardized nomenclature throughout France remains an important issue to decrease confusion and optimize winter land-use monitoring. Nonetheless, the research performed in this study remains innovative and provides new opportunities to monitor winter land-use accurately at a scale as large as that of Brittany, or even France.

VII.6. Conclusions

This study evaluated the ability of Sentinel-2 time-series images to identify winter land-use at the regional scale to provide technical support for environmental measures. In this context, a method using NDVI time-series was applied to identify crop-residue fields, considered vulnerable to pollutant transfers, and then to classify winter land-use in Brittany's UAA to obtain information about the surface state of fields declared or undeclared to the CAP. Results demonstrated the ability of Sentinel-2 data to identify crop-residue fields and their temporal dynamics but also to classify winter land-use classes over large areas with a Kappa index of 0.77.

However, the results also identified limits of this approach related to the precision of the classification nomenclature. Meteorological conditions, combined with specific characteristics of agricultural areas, decrease classification accuracy at the regional level. Thus, although SAR data have shown some limits for detailed identification and characterization of winter land-use at the local scale, the contribution of accurate and detailed data could be an interesting alternative for future studies. Similarly, the use of new 3A-level Sentinel-2 corrected images could help obtain accurate and continuous information throughout a region.

VII.7. Patents

Acknowledgements

This research was funded by the French Ministry of Higher Education and Research, Ph.D. grant 2016, and was supported by the Kalideos project, funded by the CNES and the Zone Atelier Armorique project ("ZAA," 2019).

References

- Audebert, N., Le Saux, B., Lefèvre, S., 2018. Beyond RGB: Very high resolution urban remote sensing with multimodal deep networks. *ISPRS J. Photogramm. Remote Sens.* 140, 20–32.
- Bargiel, D., 2017. A new method for crop classification combining time series of radar images and crop phenology information. *Remote Sens. Environ.* 198, 369–383.
- BD PARCELLAIRE® | IGN - Espace professionnel [WWW Document], 2019. URL <http://professionnels.ign.fr/bdparcellaire#tab-1> (accessed 9.18.19).
- Bégué, A., Arvor, D., Bellon, B., Betbeder, J., De Aballeyra, D., PD Ferraz, R., Lebourgeois, V., Lelong, C., Simões, M., R Verón, S., 2018. Remote sensing and cropping practices: A review. *Remote Sens.* 10, 99.
- Belgiu, M., Csillik, O., 2018. Sentinel-2 cropland mapping using pixel-based and object-based time-weighted dynamic time warping analysis. *Remote Sens. Environ.* 204, 509–523.
- Belgiu, M., Drăguț, L., 2016. Random forest in remote sensing: A review of applications and future directions. *ISPRS J. Photogramm. Remote Sens.* 114, 24–31.
- Breiman, L., 2001. Random forests. *Mach. Learn.* 45, 5–32.
- Buckley, C., Carney, P., 2013. The potential to reduce the risk of diffuse pollution from agriculture while improving economic performance at farm level. *Environ. Sci. Policy* 25, 118–126.
- Chiffres Clés Bretagne 2017 | Chambre de commerce et d'industrie de région Bretagne [WWW Document], 2017. URL <https://www.bretagne.cci.fr/actualites/chiffres-cles-bretagne-2017> (accessed 9.18.19).

- Delalay, M., Tiwari, V., Ziegler, A.D., Gopal, V., Passy, P., 2019. Land-use and land-cover classification using Sentinel-2 data and machine-learning algorithms: operational method and its implementation for a mountainous area of Nepal. *J. Appl. Remote Sens.* 13, 014530.
- Denize, J., Hubert-Moy, L., Betbeder, J., Corgne, S., Baudry, J., Pottier, E., 2019. Evaluation of using sentinel-1 and-2 time-series to identify winter land use in agricultural landscapes. *Remote Sens.* 11, 37.
- Ferreira, M.E., De Varennes, A., de Melo-Abreu, J.P., Vieira, M.I., 2006. Predicting pod quality of green beans for processing. *Sci. Hortic.* 109, 207–211.
- Foley, J.A., DeFries, R., Asner, G.P., Barford, C., Bonan, G., Carpenter, S.R., Chapin, F.S., Coe, M.T., Daily, G.C., Gibbs, H.K., 2005. Global consequences of land use. *science* 309, 570–574.
- Forkuor, G., Dimobe, K., Serme, I., Tondoh, J.E., 2018. Landsat-8 vs. Sentinel-2: examining the added value of sentinel-2's red-edge bands to land-use and land-cover mapping in Burkina Faso. *GIScience Remote Sens.* 55, 331–354.
- Gao, B.-C., 1996. NDWI—A normalized difference water index for remote sensing of vegetation liquid water from space. *Remote Sens. Environ.* 58, 257–266.
- Immitzer, M., Vuolo, F., Atzberger, C., 2016. First experience with Sentinel-2 data for crop and tree species classifications in central Europe. *Remote Sens.* 8, 166.
- Jakubauskas, M.E., Legates, D.R., Kastens, J.H., 2002. Crop identification using harmonic analysis of time-series AVHRR NDVI data. *Comput. Electron. Agric.* 37, 127–139.
- Justes, E., Beaudoin, N., Bertuzzi, P., Charles, R., Constantin, J., Durr, C., Hermon, C., Joannon, A., Le Bas, C., Mary, B., 2012. Réduire les fuites de nitrate au moyen de cultures intermédiaires: conséquences sur les bilans d'eau et d'azote, autres services écosystémiques.
- Kamthonkiat, D., Honda, K., Turrall, H., Tripathi, N.K., Wuwongse, V., 2005. Discrimination of irrigated and rainfed rice in a tropical agricultural system using SPOT VEGETATION NDVI and rainfall data. *Int. J. Remote Sens.* 26, 2527–2547.
- Khalidoune, J., Van Bochove, E., Bernier, M., Nolin, M.C., 2011. Mapping agricultural frozen soil on the watershed scale using remote sensing data. *Appl. Environ. Soil Sci.* 2011.
- Lawrence, R.L., Wood, S.D., Sheley, R.L., 2006. Mapping invasive plants using hyperspectral imagery and Breiman Cutler classifications (RandomForest). *Remote Sens. Environ.* 100, 356–362.
- Lecerf, R., Corpetti, T., Hubert-Moy, L., Dubreuil, V., 2005. Monitoring land use and land cover changes in oceanic and fragmented landscapes with reconstructed MODIS time series, in: *International Workshop on the Analysis of Multi-Temporal Remote Sensing Images, 2005.* IEEE, pp. 195–199.
- Liaw, A., Wiener, M., 2002. Classification and regression by randomForest. *R News* 2, 18–22.
- MAJA | LOGICIELS CNES [WWW Document], 2019. URL <https://logiciels.cnes.fr/fr/content/maja> (accessed 9.18.19).
- Ministère de l'agriculture et de l'alimentation - agreste - La statistique, l'évaluation et la prospective agricole - Bretagne [WWW Document], 2017. URL <http://agreste.agriculture.gouv.fr/en-region/bretagne/> (accessed 9.18.19).
- Mishra, A.K., Singh, V.P., 2010. A review of drought concepts. *J. Hydrol.* 391, 202–216.
- Nitrates - Water pollution - Environment - European Commission [WWW Document], 2019. URL http://ec.europa.eu/environment/water/water-nitrates/index_en.html (accessed 5.24.19).
- Pôle Theia – THEIA-LAND, 2019. URL <https://www.theia-land.fr/pole-theia-2/> (accessed 9.18.19).
- Portail IGN | L'information grandeur nature [WWW Document], 2019. URL <http://www.ign.fr/> (accessed 9.18.19).

Quand récolter le maïs fourrage en 2018 ? [WWW Document], 2018. URL <https://www.arvalis-infos.fr/premiers-chantiers-prevus-autour-du-15-ao-t-@/view-27995-arvarticle.html> (accessed 9.15.19).

R: The R Project for Statistical Computing [WWW Document], 2019. URL <https://www.r-project.org/> (accessed 9.10.19).

Rouse Jr, J., Haas, R.H., Schell, J.A., Deering, D.W., 1974. Monitoring vegetation systems in the Great Plains with ERTS.

RPG | IGN - Espace professionnel [WWW Document], 2019. URL <http://professionnels.ign.fr/rpg> (accessed 9.18.19).

Sakamoto, T., Yokozawa, M., Toritani, H., Shibayama, M., Ishitsuka, N., Ohno, H., 2005. A crop phenology detection method using time-series MODIS data. *Remote Sens. Environ.* 96, 366–374.

Verbeiren, S., Eerens, H., Piccard, I., Bauwens, I., Van Orshoven, J., 2008. Sub-pixel classification of SPOT-VEGETATION time series for the assessment of regional crop areas in Belgium. *Int. J. Appl. Earth Obs. Geoinformation* 10, 486–497.

Xue, J., Su, B., 2017. Significant remote sensing vegetation indices: A review of developments and applications. *J. Sens.* 2017.

ZA Armorique [WWW Document], 2019. URL <https://osur.univ-rennes1.fr/za-armorique/> (accessed 5.24.19).

Zadbagher, E., Becek, K., Berberoglu, S., 2018. Modeling land use/land cover change using remote sensing and geographic information systems: case study of the Seyhan Basin, Turkey. *Environ. Monit. Assess.* 190, 494.

Conclusion of the fourth part

In this fourth part, we have attempted to highlight the potential of Sentinel-2 images for the identification of winter land-use classes at a regional scale.

Considered as one of the main factors of environmental change, the acquisition of winter land-use detailed and spatialized information over large areas have emerged in recent years as a main issue for the scientific communities and decision-makers. From this perspective, remote sensing data has appeared to be an interesting instrument to address this issue. However, despite the development of increasingly efficient remote sensing sensors, to date, only a few studies have been able to identify and characterize winter land-use over large areas. In this context, the purpose of this fifth part was based on the evaluation of Sentinel-2 time-series to identify winter land-use on all UAA parcels.

Thus, at the Brittany scale (France), a methodology was established based on the best classification procedure and remote sensing data elaborated in the last three parts in order to identify winter land-use. In this context, Sentinel-2 data were selected to identify winter land-use at a regional scale. The first step of this methodology aimed to identify not declared crop residues parcels. To this end, a time-series of NDVI images extracted from Sentinel-2 data is used. First results have identified crop residues parcels, but also highlighted a time shift in the surface state change of these parcels, which corresponds to the shift in the harvesting date. Afterwards, a classification procedure is performed using a re-adapted nomenclature at 3 or 7 classes. On the one hand, this procedure emphasized the potential of Sentinel-2 data for a global classification of winter land-use (3 classes) with a kappa index of 0.77 and an overall accuracy of 84%. On the other hand, the results pointed out the limits of the procedure in order to perform a detailed winter land-use classification (with 7 classes), which presents a kappa index of 0.59 and an overall accuracy of 65%. Finally, the best classification procedure is selected and extended over the not declared parcels at the Brittany scale.

Globally, the last part of this manuscript highlighted the potential of Sentinel-2 time-series for the identification of winter land-use at the regional scale. However, this part also pointed out the limits of Sentinel-2 optical data for a detailed winter land-use classification (7 classes) and leads us to re-examine the value of Sentinel-1 data for future works, which could provide reliable information at a regional scale when meteorological conditions limit the acquisition of optical images.

General conclusion and perspectives

The winter land-use was studied in this manuscript at local and regional scales based on satellite time-series images from optical and SAR sensors. More specifically, it aimed to evaluate the potential of Sentinel data (optical and SAR) but also Radarsat-2 and Alos-2 SAR sensors.

For that purpose, we were looking for (1) determining the most suitable classification method to identify land use in winter, both at the level of the classification itself and the classification approach (pixel or object-oriented); (2) comparing Sentinel-1 SAR images and Sentinel-2 optics; and (3) defining the most suitable SAR configuration by comparing three image time-series (Alos-2, Radarsat-2 and Sentinel-1)

First, we evaluated the respective contribution of optical and SAR time-series by comparing classification algorithms to identify winter land use. To do this, Sentinel-1 and 2 images acquired over the period August 2016-May 2017 were classified using the Support Vector Machine (SVM) and Random Forest (RF) algorithms applied with pixel and object-oriented approaches in a 130 km² agricultural zone, whose plot sizes range from 0.1 to 65 ha, with an average of 2.1 ha. Overall, the results show that winter land-use can be accurately identified using the Sentinel-1 and Sentinel-2 time-series combined with a pixel-based approach using an RF algorithm. In detail, they highlighted the value of the RF classification algorithm compared to the SVM algorithm. The results show the superiority of Sentinel-2 over Sentinel-1, with the accuracy of the classification obtained with the first being greater than 5% compared to that obtained with the second. They also point out that classification accuracy improves when using a combination of the Sentinel-1 and 2 time-series, with winter land cover identified with an overall accuracy of 81% (kappa index 0.77) compared to 75% (Kappa index 0.70) for the Sentinel-2 time-series used alone. In addition, the analysis of the Sentinel-1 and Sentinel-2 parameters used to identify winter land use led to recommendations for feature extraction when mapping winter land use, with the results revealing the advantage of using backscatter coefficients alone or combined with the NDVI index. Our results also showed the limitations of this approach to identifying winter land use: On the one hand, the nomenclature defined in this first study was not optimal for identifying and fine-tuning winter land use as it includes a "bare soil" class that only corresponds to a temporary soil surface condition during the winter period and includes crops with different spectral signatures in a single "winter crop" class, which leads to misclassification. On the other hand, classification errors are located in small plots due to the spatial resolution of the Sentinel sensors.

We then sought to assess the potential of the Sentinel-1 and 2 data to identify winter land use, but with a more detailed nomenclature that takes into account the diversity of winter land-use types and without determining a specific class for bare soils. To do this, the methodology that was implemented at the same study site consists of two steps: (1) A detailed analysis of winter signal/crop interactions based on optical or SAR parameters extracted from the Sentinel-1 and 2 time-series images; (2) A detailed classification of winter land use types using the RF algorithm. The results show that optical data classify winter land-use types with greater accuracy than SAR data (overall accuracy of 87% and Kappa index of 0.85 for Sentinel-2 versus 73% and 0.70 for Sentinel-1). The results also indicate that the combination of Sentinel-1 and Sentinel-2 data slightly reduces the accuracy of the classification (overall accuracy = 83%, Kappa index = 0.82). This study also shows the potential and parameters NDVI and NDWI derived from Sentinel-2 imagery to finely discriminate winter land use classes. While

highlighting the value of optical time-series, this study also highlights that SAR time-series can be useful in areas with high cloud cover.

Then, we focused on the assessment of SAR imagery to identify winter land-use. Specifically, we studied the contribution of frequency (C/L bands), polarization (double/quad polarization) and image time-series density at the same study site. First, SAR parameters were derived from Radarsat-2, Sentinel-1 and Alos-2 time-series, and a set of quad-pol parameters and six bi-pol data sets were calculated with different spatial resolutions and density. Then, a Random Forest classification was performed for each of the 7 sets of SAR parameter data that had previously been generated to determine the most appropriate SAR configuration to identify winter land-use patterns. The results highlight that (1) the C-band (overall accuracy of 72%) is higher than the L-band (overall accuracy of 63%), (2) the quad-pol mode (overall accuracy of 70%) exceeds the double-pol mode (overall accuracy of 58%) and (3) the dense Sentinel-1 time-series (overall accuracy of 72%) is higher than the Radarsat-2 and Alos-2 time-series (overall accuracy of 70% and 38% respectively). In addition, the results indicate that Shannon entropy and SPAN (total power of the coherence matrix) whether in full or dual-polarization are the most discriminating parameters. This study selects the most appropriate SAR configurations for identifying winter land use, namely the Sentinel-1 (C-band) time-series in dual-polarization, and dense for this study.

Based on the results obtained in the three previous studies, we then selected the most appropriate data and classification algorithm to identify winter land-use in a region. The objective of this study was to test the reproducibility of the approach initially developed at a local level. More precisely, the Sentinel-2 data were selected in order to determine, for the whole of Brittany, the winter land-use, knowing that this is only known for the parcels declared to the CAP system in the graphic parcel census (RPG), i.e. the parcels eligible for EU aid. First, Sentinel-2 time-series were classified on the parcels reported in the RPG using the RF algorithm, after having adapted the nomenclature used at the local level to the regional level into two nested levels. The results obtained at level 1, which includes 3 classes (winter crops, grassland intercrops), highlighted the value of this approach in discriminating land-use types, with an overall accuracy of 84% and a kappa index of 0.77. Conversely, these results highlighted the limitations of the approach for a more detailed classification, since the overall accuracy and kappa index reach 65% and 0.59 respectively with the level 2 classification which includes 7 classes. The classification model established at level 1 was then applied to undeclared plots covered by crop residues, which had previously been identified from an NDVI time-series derived from Sentinel-2 images. The map produced on winter land use at the parcel scale and over an entire region is new information.

In general, this thesis has demonstrated the potential of high spatial resolution remote sensing time-series, both optical (Sentinel-2) and radar (Sentinel-1, Radarsat-2, and Alos-2) for identifying and characterizing winter land use. While this thesis has shown that Sentinel-2 data are the most suitable for studying winter land use, SAR images are of great interest in regions where cloud cover is high, with the dense Sentinel-1 time-series defined as the most efficient.

The originality of this thesis lies in the study of winter land-use using optical and radar remote sensing data. Although winter land-use is recognized as a significant issue for scientific

communities and public or private decision-makers, to date only a few studies have attempted to precisely identify and characterize winter land-use based on remote sensing data. In this context, this manuscript develops a methodological approach based on optical and SAR sensors to provide detailed information about winter land-use at a local and regional scale. This information is essential in order to provide technical support to public and private decision-makers for the implementation of environmental measures that promote the sustainable development of agricultural areas and limit the impacts on climate change. In addition, this thesis work allowed an evaluation of optical and SAR remote sensing data for a thematic study on land-use. Although many results have been presented in this manuscript, some perspectives have emerged, which are the following:

The first perspective should be investigating the potential of the fusion process, between optical and SAR data but also between two SAR datasets. Indeed, the second part of the thesis showed interesting possibilities regarding the combined use of Sentinel-1 and -2 data, but these results were not concretized afterward. However, a higher-level of fusion such as the Dempster-Shafer method could exploit the ability to discriminate vegetation from optical data and the physical capacities of SAR data to characterize the plant structure. Similarly, the fusion of several frequency bands of SAR data could provide additional information to defined targets.

The second perspective would rely on the implementation of new classification methods such as Deep-Learning techniques, which have demonstrated their potential in recent years to analyze and classify time-series of remote sensing data. Furthermore, an attempt to readjust the TWDTW algorithm used in the second part of this thesis would be interesting. This algorithm, which was originally developed to identify vegetation patterns over several years, was probably limited by the small temporal dimension proposed by the samples sampling set. So it might be interesting to extend the sampling over several years in order to test the current model or to readjust the classification algorithm currently in place to increase its robustness with a more limited time-series.

The third perspective would be identifying a broader set of landscape elements. As we have mentioned several times in this thesis, winter land-use is based on two legislative instruments that define the authorized agricultural practices but also the types of coverage. For this thesis, we focused our study only on the landscape elements integrated within the agricultural fields. The point is to extend the classification approach to landscape elements included in the GAEC Rules, such as grassed strips, which play the same important role in regulating agricultural pollutant transfers and whose information remains limited. This information is needed not only by decision-makers but also by scientific communities such as ecologists in order to implement effective action programs.

The identification and characterization of winter land-use were carried out for this thesis by considering only a limited range of land-use classes sampled at the scale of France. Indeed, we have focused our research on a diversified agricultural landscape, ranging from open fields to dense hedged farmland, allowing the reproduction of the main French landscape dynamics. In this context, we opted for a nomenclature representing the optimal number of winter land-use classes, i. e. which is represented heterogeneously on the ZAA but which also represents a viable statistical sampling (with a minimum number of individuals). However, it is evident

that a large number of land-use classes existing in the French agricultural system were not included in the nomenclature implemented, such as bare soil class. Nevertheless, the methods developed during this thesis were developed using generic approaches allowing to consider potential extensions and readjustments to other areas of French territory.

In this manuscript, we have demonstrated that satellite time-series images of optical and SAR sensors allowed the identification and characterization of winter land-use on a local and regional scale. To conclude this thesis, we would like to make some suggestions regarding the identification and characterization of winter land-use. Thus, a consistent Sentinel-2 time-series is recommended in order to finely identify and characterize winter land-use at fine-scale. On a larger scale, notwithstanding the potential of optical data, the persistent absence of data restricting the creation of a consistent time-series leads us to recommend a combined or even a merged approach of optical and SAR data in order to ensure optimal discrimination between winter land-use classes and those despite unfavorable meteorological conditions.

References

- Abdikan, S., Sanli, F.B., Ustuner, M., Calò, F., 2016. Land cover mapping using sentinel-1 SAR data. *The International Archives of Photogrammetry, Remote Sensing and Spatial Information Sciences* 41, 757.
- Abkar, A.A., 1999. Likelihood-base segmentation and classification of remotely sensed images: a bayesian optimization approach for combining RS and GIS.
- Adams, J.R., Berg, A.A., McNairn, H., Merzouki, A., 2013. Sensitivity of C-band SAR polarimetric variables to unvegetated agricultural fields. *Canadian Journal of Remote Sensing* 39, 1–16.
- Addink, E.A., Van Coillie, F.M., De Jong, S.M., 2012. Introduction to the GEOBIA 2010 special issue: From pixels to geographic objects in remote sensing image analysis. Elsevier.
- Anderson, J.R., 1976. A land use and land cover classification system for use with remote sensor data. US Government Printing Office.
- Araya, Y.H., Hergarten, C., 2008. A comparison of pixel and object-based land cover classification: a case study of the Asmara region, Eritrea. *WIT Transactions on The Built Environment* 100, 233–243.
- Atmospheric Absorption & Transmission [WWW Document], 2019. URL http://gsp.humboldt.edu/OLM/Courses/GSP_216_Online/lesson2-1/atmosphere.html (accessed 9.18.19).
- Audebert, N., Le Saux, B., Lefèvre, S., 2018. Beyond RGB: Very high resolution urban remote sensing with multimodal deep networks. *ISPRS Journal of Photogrammetry and Remote Sensing* 140, 20–32.
- Baghdadi, N., Boyer, N., Todoroff, P., El Hajj, M., Bégué, A., 2009. Potential of SAR sensors TerraSAR-X, ASAR/ENVISAT and PALSAR/ALOS for monitoring sugarcane crops on Reunion Island. *Remote Sensing of Environment* 113, 1724–1738.
- Baghdadi, N., Zribi, M., 2016. Observation des surfaces continentales par télédétection I: Agriculture et forêt. ISTE Group.
- Baghdadi, N., Zribi, M., Loumagne, C., Ansart, P., Anguela, T.P., 2008. Analysis of TerraSAR-X data and their sensitivity to soil surface parameters over bare agricultural fields. *Remote Sensing of Environment* 112, 4370–4379.
- Bannari, A., Morin, D., Bonn, F., Huete, A.R., 1995. A review of vegetation indices. *Remote sensing reviews* 13, 95–120.
- Bargiel, D., 2017. A new method for crop classification combining time series of radar images and crop phenology information. *Remote sensing of environment* 198, 369–383.
- BD PARCELLAIRE® | IGN - Espace professionnel [WWW Document], 2019. URL <http://professionnels.ign.fr/bdparcellaire#tab-1> (accessed 9.18.19).
- Beck, P.S., Atzberger, C., Høgda, K.A., Johansen, B., Skidmore, A.K., 2006. Improved monitoring of vegetation dynamics at very high latitudes: A new method using MODIS NDVI. *Remote sensing of Environment* 100, 321–334.
- Bégué, A., Arvor, D., Bellon, B., Betbeder, J., De Abelleira, D., PD Ferraz, R., Lebourgeois, V., Lelong, C., Simões, M., R Verón, S., 2018. Remote sensing and cropping practices: A review. *Remote Sensing* 10, 99.

- Belgiu, M., Csillik, O., 2018. Sentinel-2 cropland mapping using pixel-based and object-based time-weighted dynamic time warping analysis. *Remote sensing of environment* 204, 509–523.
- Belgiu, M., Drăguț, L., 2016. Random forest in remote sensing: A review of applications and future directions. *ISPRS Journal of Photogrammetry and Remote Sensing* 114, 24–31.
- Betbeder, J., 2015. Evaluation des données de télédétection pour l'identification et la caractérisation des continuités écologiques (PhD Thesis).
- Betbeder, J., Fieuzal, R., Philippets, Y., Ferro-Famil, L., Baup, F., 2015. Estimation of crop parameters using multi-temporal optical and radar polarimetric satellite data, in: *Remote Sensing for Agriculture, Ecosystems, and Hydrology XVII*. International Society for Optics and Photonics, p. 963702.
- Blaes, X., Vanhalle, L., Defourny, P., 2005. Efficiency of crop identification based on optical and SAR image time series. *Remote sensing of environment* 96, 352–365.
- Boyd, D.S., Foody, G.M., 2011. An overview of recent remote sensing and GIS based research in ecological informatics. *Ecological Informatics* 6, 25–36.
- Breiman, L., 2001. Random forests. *Machine learning* 45, 5–32.
- Breiman, L., 1996. Bagging predictors. *Machine learning* 24, 123–140.
- Brown, D.G., Duh, J.-D., 2004. Spatial simulation for translating from land use to land cover. *International Journal of Geographical Information Science* 18, 35–60.
- Brown, S.C., Quegan, S., Morrison, K., Bennett, J.C., Cookmartin, G., 2003. High-resolution measurements of scattering in wheat canopies-Implications for crop parameter retrieval. *IEEE Transactions on Geoscience and Remote Sensing* 41, 1602–1610.
- Buckley, C., Carney, P., 2013. The potential to reduce the risk of diffuse pollution from agriculture while improving economic performance at farm level. *Environmental science & policy* 25, 118–126.
- Burges, C.J., 1998. A tutorial on support vector machines for pattern recognition. *Data mining and knowledge discovery* 2, 121–167.
- Caloz, R., Collet, C., 2001. Précis de télédétection-: Traitements numériques d'images de télédétection. PUQ.
- Campbell, J.B., Wynne, R.H., 2011. *Introduction to remote sensing*. Guilford Press.
- Canada, R. naturelles, 2008. Notions fondamentales de télédétection - Introduction [WWW Document]. URL <https://www.rncan.gc.ca/cartes-outils-publications/imagerie-satellitaire-photos-aer/tutoriels-sur-la-teledetection/notions-fondamentales-de-teledetection-introduction/9364> (accessed 9.18.19).
- Carrasco, L., O'Neil, A.W., Morton, R.D., Rowland, C.S., 2019. Evaluating combinations of temporally aggregated Sentinel-1, Sentinel-2 and Landsat 8 For land cover mapping with Google Earth Engine. *Remote Sensing* 11, 288.
- Chi, M., Feng, R., Bruzzone, L., 2008. Classification of hyperspectral remote-sensing data with primal SVM for small-sized training dataset problem. *Advances in space research* 41, 1793–1799.

- Chiffres Clés Bretagne 2017 | Chambre de commerce et d'industrie de région Bretagne [WWW Document], 2017. URL <https://www.bretagne.cci.fr/actualites/chiffres-cles-bretagne-2017> (accessed 9.18.19).
- CIPAN : quand l'outil réglementaire devient un atout agronomique et faunistique - PDF [WWW Document], 2008. URL <https://docplayer.fr/21149047-Cipan-quand-l-outil-reglementaire-devient-un-atout-agronomique-et-faunistique.html> (accessed 9.18.19).
- Clark, M.L., Aide, T.M., Grau, H.R., Riner, G., 2010. A scalable approach to mapping annual land cover at 250 m using MODIS time series data: A case study in the Dry Chaco ecoregion of South America. *Remote Sensing of Environment* 114, 2816–2832.
- Clay, D.E., Kim, K.-I., Chang, J., Clay, S.A., Dalsted, K., 2006. Characterizing water and nitrogen stress in corn using remote sensing. *Agronomy Journal* 98, 579–587.
- Cloude, S.R., Pottier, E., 1996. A review of target decomposition theorems in radar polarimetry. *IEEE transactions on geoscience and remote sensing* 34, 498–518.
- Comber, A., Fisher, P., Brunson, C., Khmag, A., 2012. Spatial analysis of remote sensing image classification accuracy. *Remote Sensing of Environment* 127, 237–246.
- Comber, A., Fisher, P., Wadsworth, R., 2005. What is land cover? *Environment and Planning B: Planning and Design* 32, 199–209.
- Comber, A., Fisher, P., Wadsworth, R., 2003. Actor–network theory: a suitable framework to understand how land cover mapping projects develop? *Land Use Policy* 20, 299–309.
- Comber, A.J., 2008. *Land use or land cover?* Taylor & Francis.
- Congalton, R.G., 1991. A review of assessing the accuracy of classifications of remotely sensed data. *Remote sensing of environment* 37, 35–46.
- Corcoran, J., Knight, J., Gallant, A., 2013. Influence of multi-source and multi-temporal remotely sensed and ancillary data on the accuracy of random forest classification of wetlands in Northern Minnesota. *Remote Sensing* 5, 3212–3238.
- Corgne, S., 2004. Hiérarchisation des facteurs structurant les dynamiques pluriannuelles des sols nus hivernaux. Application au bassin versant du Yar (Bretagne). *Norois. Environnement, aménagement, société* 17–29.
- Cortes, C., Vapnik, V., 1995. Support-vector networks *Machine learning* (pp. 237–297), Vol. 20. Boston, MA: Kluwer Academic Publisher.
- Cracknell, A.P., 2007. *Introduction to remote sensing*. CRC press.
- Dabney, S.M., 1998. Cover crop impacts on watershed hydrology. *Journal of Soil and Water Conservation* 53, 207–213.
- Dabney, S.M., McGregor, K.C., Wilson, G.V., Cullum, R.F., 2009. How management of grass hedges affects their erosion reduction potential. *Soil Science Society of America Journal* 73, 241–254.
- Davranche, A., Lefebvre, G., Poulin, B., 2010. Wetland monitoring using classification trees and SPOT-5 seasonal time series. *Remote sensing of environment* 114, 552–562.
- Decau, J., Pujol, B., 1992. [Contribution of cultivation techniques for controlling nitrogen pollution of ground water]. [French]. *Dossiers de l'Environnement de l'INRA (France)*. no. 4.

- DeFries, R.S., Townshend, J.R.G., Hansen, M.C., 1999. Continuous fields of vegetation characteristics at the global scale at 1-km resolution. *Journal of Geophysical Research: Atmospheres* 104, 16911–16923.
- Delalay, M., Tiwari, V., Ziegler, A.D., Gopal, V., Passy, P., 2019. Land-use and land-cover classification using Sentinel-2 data and machine-learning algorithms: operational method and its implementation for a mountainous area of Nepal. *Journal of Applied Remote Sensing* 13, 014530.
- Denize, J., Hubert-Moy, L., Betbeder, J., Corgne, S., Baudry, J., Pottier, E., 2019. Evaluation of using sentinel-1 and-2 time-series to identify winter land use in agricultural landscapes. *Remote Sensing* 11, 37.
- Dimitriadou, E., Hornik, K., Leisch, F., Meyer, D., Weingessel, A., 2008. Misc functions of the Department of Statistics (e1071), TU Wien. R package 1, 5–24.
- Dimov, D., Löw, F., Ibrakhimov, M., Stulina, G., Conrad, C., 2017. SAR and optical time series for crop classification, in: 2017 IEEE International Geoscience and Remote Sensing Symposium (IGARSS). IEEE, pp. 811–814.
- Drusch, M., Del Bello, U., Carlier, S., Colin, O., Fernandez, V., Gascon, F., Hoersch, B., Isola, C., Laberinti, P., Martimort, P., 2012. Sentinel-2: ESA's optical high-resolution mission for GMES operational services. *Remote sensing of Environment* 120, 25–36.
- Duchemin, B., Fieuzal, R., Rivera, M., Ezzahar, J., Jarlan, L., Rodriguez, J., Hagolle, O., Watts, C., 2015. Impact of sowing date on yield and water use efficiency of wheat analyzed through spatial modeling and FORMOSAT-2 images. *Remote Sensing* 7, 5951–5979.
- Dufour, S., Bernez, I., Betbeder, J., Corgne, S., Hubert-Moy, L., Nabucet, J., Rapinel, S., Sawtschuk, J., Trollé, C., 2013. Monitoring restored riparian vegetation: how can recent developments in remote sensing sciences help? *Knowledge and Management of Aquatic Ecosystems* 10.
- Duro, D.C., Franklin, S.E., Dubé, M.G., 2012. A comparison of pixel-based and object-based image analysis with selected machine learning algorithms for the classification of agricultural landscapes using SPOT-5 HRG imagery. *Remote sensing of environment* 118, 259–272.
- Dusseux, P., Corpetti, T., Hubert-Moy, L., Corgne, S., 2014. Combined use of multi-temporal optical and radar satellite images for grassland monitoring. *Remote Sensing* 6, 6163–6182.
- Duveiller, G., Defourny, P., 2010. A conceptual framework to define the spatial resolution requirements for agricultural monitoring using remote sensing. *Remote Sensing of Environment* 114, 2637–2650.
- El Hajj, M., Bégué, A., Guillaume, S., Martiné, J.-F., 2009. Integrating SPOT-5 time series, crop growth modeling and expert knowledge for monitoring agricultural practices—The case of sugarcane harvest on Reunion Island. *Remote Sensing of Environment* 113, 2052–2061.
- Erb, K.-H., Haberl, H., Jepsen, M.R., Kuemmerle, T., Lindner, M., Müller, D., Verburg, P.H., Reenberg, A., 2013. A conceptual framework for analysing and measuring land-use intensity. *Current opinion in environmental sustainability* 5, 464–470.
- Fasona, M.J., Omojola, A.S., 2005. Climate change, human security and communal clashes in Nigeria, in: *International Workshop on Human Security and Climate Change*, Oslo, Norway. June. pp. 21–23.

- Ferreira, M.E., De Varennes, A., de Melo-Abreu, J.P., Vieira, M.I., 2006. Predicting pod quality of green beans for processing. *Scientia horticultrae* 109, 207–211.
- Fieuzal, R., Baup, F., Marais-Sicre, C., 2013. Monitoring wheat and rapeseed by using synchronous optical and radar satellite data—From temporal signatures to crop parameters estimation. *Advances in Remote Sensing* 2, 162.
- Fisher, P., 1997. The pixel: a snare and a delusion. *International Journal of Remote Sensing* 18, 679–685.
- Foley, J.A., DeFries, R., Asner, G.P., Barford, C., Bonan, G., Carpenter, S.R., Chapin, F.S., Coe, M.T., Daily, G.C., Gibbs, H.K., 2005. Global consequences of land use. *science* 309, 570–574.
- Forkuor, G., Dimobe, K., Serme, I., Tondoh, J.E., 2018. Landsat-8 vs. Sentinel-2: examining the added value of sentinel-2's red-edge bands to land-use and land-cover mapping in Burkina Faso. *GIScience & remote sensing* 55, 331–354.
- Forshaw, M.R.B., Haskell, A., Miller, P.F., Stanley, D.J., Townshend, J.R.G., 1983. Spatial resolution of remotely sensed imagery A review paper. *International Journal of Remote Sensing* 4, 497–520.
- Freeman, A., Durden, S.L., 1998. A three-component scattering model for polarimetric SAR data. *IEEE Transactions on Geoscience and Remote Sensing* 36, 963–973.
- Galloway, J.N., Dentener, F.J., Capone, D.G., Boyer, E.W., Howarth, R.W., Seitzinger, S.P., Asner, G.P., Cleveland, C.C., Green, P.A., Holland, E.A., 2004. Nitrogen cycles: past, present, and future. *Biogeochemistry* 70, 153–226.
- Galloway, J.N., Townsend, A.R., Erisman, J.W., Bekunda, M., Cai, Z., Freney, J.R., Martinelli, L.A., Seitzinger, S.P., Sutton, M.A., 2008. Transformation of the nitrogen cycle: recent trends, questions, and potential solutions. *Science* 320, 889–892.
- Gao, B.-C., 1996. NDWI—A normalized difference water index for remote sensing of vegetation liquid water from space. *Remote sensing of environment* 58, 257–266.
- Gibson, D.J., 2009. *Grasses and grassland ecology*. Oxford University Press.
- Girard, M.-C., Walter, C., Rémy, J.-C., Berthelin, J., Morel, J.-L., 2011. *Sols et environnement-2e édition-Cours, exercices et études de cas-Livre+ compléments en ligne: Cours, exercices corrigés et études de cas*. Dunod.
- GIS BreTel, 2017. . Institut InSpace. URL <http://inspace-institute.com/adherents/gis-bretel/> (accessed 9.26.19).
- Gislason, P.O., Benediktsson, J.A., Sveinsson, J.R., 2006. Random forests for land cover classification. *Pattern Recognition Letters* 27, 294–300.
- Gómez, C., White, J.C., Wulder, M.A., 2016. Optical remotely sensed time series data for land cover classification: A review. *ISPRS Journal of Photogrammetry and Remote Sensing* 116, 55–72.
- Good Agricultural and Environmental Conditions (GAEC) - Wikicap - European Commission [WWW Document], 2019. URL https://marswiki.jrc.ec.europa.eu/wikicap/index.php/Good_Agricultural_and_Environmental_Conditions_%28GAEC%29 (accessed 9.18.19).
- Gressin, A., Mallet, C., Paparoditis, N., Vincent, N., 2014. MISE À JOUR D'UNE BASE DE DONNÉES D'OCCUPATION DU SOL À PARTIR D'UNE IMAGE SA^{TELLITE} TRÈS HAUTE

- RÉSOLUTION: APPLICATION AUX DONNÉES PLÉIADES. *Revue française de photogrammétrie et de télédétection* 11–18.
- Gu, Y., Hunt, E., Wardlow, B., Basara, J.B., Brown, J.F., Verdin, J.P., 2008. Evaluation of MODIS NDVI and NDWI for vegetation drought monitoring using Oklahoma Mesonet soil moisture data. *Geophysical Research Letters* 35.
- Guerschman, J.P., Scarth, P.F., McVicar, T.R., Renzullo, L.J., Malthus, T.J., Stewart, J.B., Rickards, J.E., Trevithick, R., 2015. Assessing the effects of site heterogeneity and soil properties when unmixing photosynthetic vegetation, non-photosynthetic vegetation and bare soil fractions from Landsat and MODIS data. *Remote Sensing of Environment* 161, 12–26.
- Haldar, D., Das, A., Mohan, S., Pal, O., Hooda, R.S., Chakraborty, M., 2012. Assessment of L-band SAR data at different polarization combinations for crop and other landuse classification. *Progress In Electromagnetics Research* 36, 303–321.
- Haldar, D., Rana, P., Yadav, M., Hooda, R.S., Chakraborty, M., 2016. Time series analysis of co-polarization phase difference (PPD) for winter field crops using polarimetric C-band SAR data. *International Journal of Remote Sensing* 37, 3753–3770.
- Haygarth, P.M., Jarvis, S.C., 2002. *Agriculture, hydrology, and water quality*. CABI Pub.
- Herrmann, S.M., Tappan, G.G., 2013. Vegetation impoverishment despite greening: A case study from central Senegal. *Journal of Arid Environments* 90, 55–66.
- Hong, G., Wang, S., Li, J., Huang, J., 2015. Fully polarimetric synthetic aperture radar (SAR) processing for crop type identification. *Photogrammetric Engineering & Remote Sensing* 81, 109–117.
- Hosseini, M., McNairn, H., Merzouki, A., Pacheco, A., 2015. Estimation of Leaf Area Index (LAI) in corn and soybeans using multi-polarization C-and L-band radar data. *Remote Sensing of Environment* 170, 77–89.
- Hu, T., Yang, J., Li, X., Gong, P., 2016. Mapping urban land use by using landsat images and open social data. *Remote Sensing* 8, 151.
- Huang, H., Chen, Y., Clinton, N., Wang, J., Wang, X., Liu, C., Gong, P., Yang, J., Bai, Y., Zheng, Y., 2017. Mapping major land cover dynamics in Beijing using all Landsat images in Google Earth Engine. *Remote Sensing of Environment* 202, 166–176.
- Huete, A.R., 1988. A soil-adjusted vegetation index (SAVI). *Remote sensing of environment* 25, 295–309.
- Hussain, M., Chen, D., Cheng, A., Wei, H., Stanley, D., 2013. Change detection from remotely sensed images: From pixel-based to object-based approaches. *ISPRS Journal of photogrammetry and remote sensing* 80, 91–106.
- Hütt, C., Koppe, W., Miao, Y., Bareth, G., 2016. Best accuracy land use/land cover (LULC) classification to derive crop types using multitemporal, multisensor, and multi-polarization SAR satellite images. *Remote sensing* 8, 684.
- Huynen, J.R., 1970. Phenomenological theory of radar targets.
- i Canals, L.M., Bauer, C., Depestele, J., Dubreuil, A., Knuchel, R.F., Gaillard, G., Michelsen, O., Müller-Wenk, R., Rydgren, B., 2007. Key elements in a framework for land use impact assessment within LCA (11 pp). *The International Journal of Life Cycle Assessment* 12, 5–15.

- Immitzer, M., Vuolo, F., Atzberger, C., 2016. First experience with Sentinel-2 data for crop and tree species classifications in central Europe. *Remote Sensing* 8, 166.
- Inglada, J., Vincent, A., Arias, M., Marais-Sicre, C., 2016. Improved early crop type identification by joint use of high temporal resolution SAR and optical image time series. *Remote Sensing* 8, 362.
- Inoue, Y., Kurosu, T., Maeno, H., Uratsuka, S., Kozu, T., Dabrowska-Zielinska, K., Qi, J., 2002. Season-long daily measurements of multifrequency (Ka, Ku, X, C, and L) and full-polarization backscatter signatures over paddy rice field and their relationship with biological variables. *Remote Sensing of Environment* 81, 194–204.
- Jackson, T.J., Schmugge, T.J., 1991. Vegetation effects on the microwave emission of soils. *Remote Sensing of Environment* 36, 203–212.
- Jacquemoud, S., Verhoef, W., Baret, F., Bacour, C., Zarco-Tejada, P.J., Asner, G.P., François, C., Ustin, S.L., 2009. PROSPECT+ SAIL models: A review of use for vegetation characterization. *Remote sensing of environment* 113, S56–S66.
- Jakubauskas, M.E., Legates, D.R., Kastens, J.H., 2002. Crop identification using harmonic analysis of time-series AVHRR NDVI data. *Computers and electronics in agriculture* 37, 127–139.
- Jetz, W., Wilcove, D.S., Dobson, A.P., 2007. Projected impacts of climate and land-use change on the global diversity of birds. *PLoS biology* 5, e157.
- Jianya, G., Haigang, S., Guorui, M., Qiming, Z., 2008. A review of multi-temporal remote sensing data change detection algorithms. *The International Archives of the Photogrammetry, Remote Sensing and Spatial Information Sciences* 37, 757–762.
- Jiao, X., McNairn, H., Shang, J., Liu, J., 2010. The sensitivity of multi-frequency (X, C and L-band) radar backscatter signatures to bio-physical variables (LAI) over corn and soybean fields, in: *ISPRS TC VII Symposium – 100 Years ISPRS*. pp. 317–325.
- Johansen, K., Arroyo, L.A., Phinn, S., Witte, C., 2010. Comparison of geo-object based and pixel-based change detection of riparian environments using high spatial resolution multi-spectral imagery. *Photogrammetric Engineering & Remote Sensing* 76, 123–136.
- Joshi, N., Baumann, M., Ehammer, A., Fensholt, R., Grogan, K., Hostert, P., Jepsen, M., Kuemmerle, T., Meyfroidt, P., Mitchard, E., 2016. A review of the application of optical and radar remote sensing data fusion to land use mapping and monitoring. *Remote Sensing* 8, 70.
- Joshi, N., Mitchard, E.T., Woo, N., Torres, J., Moll-Rocek, J., Ehammer, A., Collins, M., Jepsen, M.R., Fensholt, R., 2015. Mapping dynamics of deforestation and forest degradation in tropical forests using radar satellite data. *Environmental Research Letters* 10, 034014.
- Justes, E., Beaudoin, N., Bertuzzi, P., Charles, R., Constantin, J., Durr, C., Hermon, C., Joannon, A., Le Bas, C., Mary, B., 2012. Réduire les fuites de nitrate au moyen de cultures intermédiaires: conséquences sur les bilans d'eau et d'azote, autres services écosystémiques.
- Kalideos [WWW Document], 2019. . Kalideos. URL <https://www.kalideos.fr/drupal/fr> (accessed 5.24.19).
- Kamthonkiat, D., Honda, K., Turrall, H., Tripathi, N.K., Wuwongse, V., 2005. Discrimination of irrigated and rainfed rice in a tropical agricultural system using SPOT VEGETATION NDVI and rainfall data. *International Journal of Remote Sensing* 26, 2527–2547.

- Kemp, J., Burns, J., 2016. Agricultural monitoring using pursuit monostatic TanDEM-X coherence in the Western Cape, South Africa, in: Proceedings of EUSAR 2016: 11th European Conference on Synthetic Aperture Radar. VDE, pp. 1–4.
- Khaldoune, J., Van Bochove, E., Bernier, M., Nolin, M.C., 2011. Mapping agricultural frozen soil on the watershed scale using remote sensing data. *Applied and Environmental Soil Science* 2011.
- Khan, M.R., De Bie, C.A., Van Keulen, H., Smaling, E.M.A., Real, R., 2010. Disaggregating and mapping crop statistics using hypertemporal remote sensing. *International Journal of Applied Earth Observation and Geoinformation* 12, 36–46.
- Kim, Y., Jackson, T., Bindlish, R., Lee, H., Hong, S., 2011. Radar vegetation index for estimating the vegetation water content of rice and soybean. *IEEE Geoscience and Remote Sensing Letters* 9, 564–568.
- Kostelich, E.J., Schreiber, T., 1993. Noise reduction in chaotic time-series data: A survey of common methods. *Physical Review E* 48, 1752.
- Kuenzer, C., Dech, S., Wagner, W., 2015. Remote sensing time series revealing land surface dynamics: Status quo and the pathway ahead, in: *Remote Sensing Time Series*. Springer, pp. 1–24.
- Lacroix, A., 1995. Les solutions agronomiques à la pollution azotée.
- Lambin, E.F., Meyfroidt, P., 2011. Global land use change, economic globalization, and the looming land scarcity. *Proceedings of the National Academy of Sciences* 108, 3465–3472.
- Larrañaga, A., Álvarez-Mozos, J., 2016. On the added value of Quad-Pol Data in a multi-temporal crop classification framework based on RADARSAT-2 imagery. *Remote Sensing* 8, 335.
- Lavalle, M., Wright, T., 2009. Absolute radiometric and polarimetric calibration of ALOS PALSAR products. Document Issue (1), Revision (3).
- Lawrence, R.L., Wood, S.D., Sheley, R.L., 2006. Mapping invasive plants using hyperspectral imagery and Breiman Cutler classifications (RandomForest). *Remote Sensing of Environment* 100, 356–362.
- Lecerf, R., Corpetti, T., Hubert-Moy, L., Dubreuil, V., 2005. Monitoring land use and land cover changes in oceanic and fragmented landscapes with reconstructed MODIS time series, in: *International Workshop on the Analysis of Multi-Temporal Remote Sensing Images, 2005*. IEEE, pp. 195–199.
- Lee, J.-S., 1981. Speckle analysis and smoothing of synthetic aperture radar images. *Computer graphics and image processing* 17, 24–32.
- Lee, J.-S., Grunes, M.R., Pottier, E., 2001. Quantitative comparison of classification capability: Fully polarimetric versus dual and single-polarization SAR. *IEEE Transactions on Geoscience and Remote Sensing* 39, 2343–2351.
- Lee, J.-S., Pottier, E., 2009. *Polarimetric radar imaging: from basics to applications*. CRC press.
- Lee, J.-S., Wen, J.-H., Ainsworth, T.L., Chen, K.-S., Chen, A.J., 2008. Improved sigma filter for speckle filtering of SAR imagery. *IEEE Transactions on Geoscience and Remote Sensing* 47, 202–213.
- Les Zones Ateliers | www.za-inee.org [WWW Document], 2019. URL <http://www.za-inee.org/fr/ateliers> (accessed 9.18.19).

- Liaw, A., Wiener, M., 2002. Classification and regression by randomForest. *R news* 2, 18–22.
- Lillesand, T., Kiefer, R.W., Chipman, J., 2015. Remote sensing and image interpretation. John Wiley & Sons.
- Liu, C., Shang, J., Vachon, P.W., McNairn, H., 2012. Multiyear crop monitoring using polarimetric RADARSAT-2 data. *IEEE Transactions on Geoscience and Remote sensing* 51, 2227–2240.
- Liu, K., Shi, W., Zhang, H., 2011. A fuzzy topology-based maximum likelihood classification. *ISPRS Journal of Photogrammetry and Remote Sensing* 66, 103–114.
- Loosvelt, L., Peters, J., Skriver, H., De Baets, B., Verhoest, N.E., 2012. Impact of reducing polarimetric SAR input on the uncertainty of crop classifications based on the random forests algorithm. *IEEE Transactions on Geoscience and Remote Sensing* 50, 4185–4200.
- Louis, J., Debaecker, V., Pflug, B., Main-Knorn, M., Bieniarz, J., Mueller-Wilm, U., Cadau, E., Gascon, F., 2016. Sentinel-2 SEN2COR: L2A processor for users, in: *Proceedings of the Living Planet Symposium, Prague, Czech Republic*. pp. 9–13.
- Lu, D., Weng, Q., 2007. A survey of image classification methods and techniques for improving classification performance. *International journal of Remote sensing* 28, 823–870.
- Lusch, D.P., 1999. Introduction to microwave remote sensing. Center for Remote Sensing and Geographic Information Science Michigan State University.
- MAJA | LOGICIELS CNES [WWW Document], 2019. URL <https://logiciels.cnes.fr/fr/content/maja> (accessed 9.18.19).
- Mantero, P., Moser, G., Serpico, S.B., 2005. Partially supervised classification of remote sensing images through SVM-based probability density estimation. *IEEE Transactions on Geoscience and Remote Sensing* 43, 559–570.
- Martínez-Casasnovas, J.A., Martín-Montero, A., Casterad, M.A., 2005. Mapping multi-year cropping patterns in small irrigation districts from time-series analysis of Landsat TM images. *European Journal of Agronomy* 23, 159–169.
- Mascolo, L., 2015. Polarimetric SAR for the monitoring of agricultural crops (PhD Thesis). Università degli Studi di Cagliari.
- Maus, V., Câmara, G., Cartaxo, R., Sanchez, A., Ramos, F.M., de Queiroz, G.R., 2016. A time-weighted dynamic time warping method for land-use and land-cover mapping. *IEEE Journal of Selected Topics in Applied Earth Observations and Remote Sensing* 9, 3729–3739.
- McNairn, H., Brisco, B., 2004. The application of C-band polarimetric SAR for agriculture: a review. *Canadian Journal of Remote Sensing* 30, 525–542.
- McNairn, H., Duguay, C., Boisvert, J., Huffman, E., Brisco, B., 2001. Defining the sensitivity of multi-frequency and multi-polarized radar backscatter to post-harvest crop residue. *Canadian Journal of Remote Sensing* 27, 247–263.
- McNairn, H., Hochheim, K., Rabe, N., 2004. Applying polarimetric radar imagery for mapping the productivity of wheat crops. *Canadian Journal of Remote Sensing* 30, 517–524.
- McNairn, H., Shang, J., Champagne, C., Jiao, X., 2009. TerraSAR-X and RADARSAT-2 for crop classification and acreage estimation, in: *2009 IEEE International Geoscience and Remote Sensing Symposium*. IEEE, pp. II–898.

- Mercier, A., Betbeder, J., Rumiano, F., Baudry, J., Gond, V., Blanc, L., Bourgoin, C., Cornu, G., Marchamalo, M., Poccard-Chapuis, R., 2019. Evaluation of Sentinel-1 and 2 Time Series for Land Cover Classification of Forest–Agriculture Mosaics in Temperate and Tropical Landscapes. *Remote Sensing* 11, 979.
- Meyer, W.B., Turner, B.L., 1992. Human population growth and global land-use/cover change. *Annual review of ecology and systematics* 23, 39–61.
- Minh, D.H.T., Ienco, D., Gaetano, R., Lalande, N., Ndikumana, E., Osman, F., Maurel, P., 2018. Deep recurrent neural networks for winter vegetation quality mapping via multitemporal SAR Sentinel-1. *IEEE Geoscience and Remote Sensing Letters* 15, 464–468.
- Ministère de l’agriculture et de l’alimentation - agreste - La statistique, l’évaluation et la prospective agricole - Bretagne [WWW Document], 2017. URL <http://agreste.agriculture.gouv.fr/en-region/bretagne/> (accessed 9.18.19).
- Miranda, N., Meadows, P.J., 2015. Radiometric Calibration of S-1 Level-1 Products Generated by the S-1 IPF. Technical note. European Space Agency.
- Mishra, A.K., Singh, V.P., 2010. A review of drought concepts. *Journal of hydrology* 391, 202–216.
- Morena, L.C., James, K.V., Beck, J., 2004. An introduction to the RADARSAT-2 mission. *Canadian Journal of Remote Sensing* 30, 221–234.
- Mott, H., 2006. Remote sensing with polarimetric radar. John Wiley & Sons.
- Mountrakis, G., Im, J., Ogole, C., 2011. Support vector machines in remote sensing: A review. *ISPRS Journal of Photogrammetry and Remote Sensing* 66, 247–259.
- Müller, M., 2007. Dynamic time warping. *Information retrieval for music and motion* 69–84.
- Myint, S.W., Gober, P., Brazel, A., Grossman-Clarke, S., Weng, Q., 2011. Per-pixel vs. object-based classification of urban land cover extraction using high spatial resolution imagery. *Remote sensing of environment* 115, 1145–1161.
- Newbold, T., Hudson, L.N., Hill, S.L., Contu, S., Lysenko, I., Senior, R.A., Börger, L., Bennett, D.J., Choimes, A., Collen, B., 2015. Global effects of land use on local terrestrial biodiversity. *Nature* 520, 45.
- Nicholls, C.I., Altieri, M.A., 2013. Plant biodiversity enhances bees and other insect pollinators in agroecosystems. A review. *Agronomy for Sustainable development* 33, 257–274.
- Nitrates - Water pollution - Environment - European Commission [WWW Document], 2019. URL http://ec.europa.eu/environment/water/water-nitrates/index_en.html (accessed 5.24.19).
- Nurtyawan, R., Saepuloh, A., Budiharto, A., Wikantika, K., 2016. Modeling Surface Roughness to Estimate Surface Moisture Using Radarsat-2 Quad Polarimetric SAR Data, in: *Journal of Physics: Conference Series*. IOP Publishing, p. 012105.
- Open Access Hub [WWW Document], 2019. URL <https://scihub.copernicus.eu/> (accessed 9.10.19).
- Ouma, G., Jeruto, P., 2010. Sustainable horticultural crop production through intercropping: The case of fruits and vegetable crops: A review. *Agriculture and Biology Journal of North America* 1, 1098–1105.
- Ozdogan, M., 2010. The spatial distribution of crop types from MODIS data: Temporal unmixing using Independent Component Analysis. *Remote Sensing of Environment* 114, 1190–1204.

- Pacheco, A., McNairn, H., 2010. Evaluating multispectral remote sensing and spectral unmixing analysis for crop residue mapping. *Remote Sensing of Environment* 114, 2219–2228.
- Pal, M., 2005. Random forest classifier for remote sensing classification. *International Journal of Remote Sensing* 26, 217–222.
- Paloscia, S., Pettinato, S., Santi, E., Notarnicola, C., Greifeneder, F., Cuzzo, G., Nicolini, I., Demir, B., Bruzzone, L., 2015. Cosmo-SkyMed and RADARSAT2 image investigation for the monitoring of agricultural areas, in: *SAR Image Analysis, Modeling, and Techniques XV*. International Society for Optics and Photonics, p. 964206.
- Panda, S.S., Ames, D.P., Panigrahi, S., 2010. Application of vegetation indices for agricultural crop yield prediction using neural network techniques. *Remote Sensing* 2, 673–696.
- Paris, J.F., 1983. Radar backscattering properties of corn and soybeans at frequencies of 1.6, 4.75, and 13.3 Ghz. *IEEE transactions on geoscience and remote sensing* 392–400.
- Pedergrana, M., Marpu, P.R., Dalla Mura, M., Benediktsson, J.A., Bruzzone, L., 2013. A novel technique for optimal feature selection in attribute profiles based on genetic algorithms. *IEEE Transactions on Geoscience and Remote Sensing* 51, 3514–3528.
- Peeters, A., 2009. Importance, evolution, environmental impact and future challenges of grasslands and grassland-based systems in Europe. *Grassland Science* 55, 113–125.
- Pereira, L. de O., Freitas, C. da C., Sant'Anna, S.J.S., Lu, D., Moran, E.F., 2013. Optical and radar data integration for land use and land cover mapping in the Brazilian Amazon. *GIScience & Remote Sensing* 50, 301–321.
- Petitjean, F., Inglada, J., Gançarski, P., 2012. Satellite image time series analysis under time warping. *IEEE transactions on geoscience and remote sensing* 50, 3081–3095.
- Pohl, C., Van Genderen, J.L., 1998. Review article multisensor image fusion in remote sensing: concepts, methods and applications. *International journal of remote sensing* 19, 823–854.
- Pôle Theia – THEIA-LAND, 2019. URL <https://www.theia-land.fr/pole-theia-2/> (accessed 9.18.19).
- Potin, P., Bargellini, P., Laur, H., Rosich, B., Schmuck, S., 2012. Sentinel-1 mission operations concept, in: *2012 IEEE International Geoscience and Remote Sensing Symposium*. IEEE, pp. 1745–1748.
- Pottier, E., Ferro-Famil, L., 2012. PolSARPro V5. 0: An ESA educational toolbox used for self-education in the field of POLSAR and POL-INSAR data analysis, in: *2012 IEEE International Geoscience and Remote Sensing Symposium*. IEEE, pp. 7377–7380.
- Pottier, E., Ferro-Famil, L., Fitrzyk, M., Desnos, Y.-L., 2018. PolSARpro-BIO: The new Scientific Toolbox for ESA & third party fully Polarimetric SAR Missions, in: *EUSAR 2018; 12th European Conference on Synthetic Aperture Radar*. VDE, pp. 1–4.
- Quand récolter le maïs fourrage en 2018 ? [WWW Document], 2018. URL <https://www.arvalis-infos.fr/premiers-chantiers-prevus-autour-du-15-ao-t-@/view-27995-arvarticle.html> (accessed 9.15.19).
- R: The R Project for Statistical Computing [WWW Document], 2019. URL <https://www.r-project.org/> (accessed 9.10.19).
- Radarsat 1 Products | Image Resolution | Geomatics [WWW Document], 2019. . Scribd. URL <https://www.scribd.com/document/73559622/Radarsat-1-Products> (accessed 5.24.19).

- Radoux, J., Chomé, G., Jacques, D., Waldner, F., Bellemans, N., Matton, N., Lamarche, C., d'Andrimont, R., Defourny, P., 2016. Sentinel-2's potential for sub-pixel landscape feature detection. *Remote Sensing* 8, 488.
- Ratanamahatana, C.A., Keogh, E., 2004. Making time-series classification more accurate using learned constraints, in: *Proceedings of the 2004 SIAM International Conference on Data Mining*. SIAM, pp. 11–22.
- Réfrégier, P., Morio, J., 2006. Shannon entropy of partially polarized and partially coherent light with Gaussian fluctuations. *JOSA A* 23, 3036–3044.
- Richards, J.A., 2009. *Remote sensing with imaging radar*. Springer.
- Rouse Jr, J., Haas, R.H., Schell, J.A., Deering, D.W., 1974. Monitoring vegetation systems in the Great Plains with ERTS.
- RPG | IGN - Espace professionnel [WWW Document], 2019. URL <http://professionnels.ign.fr/rpg> (accessed 9.18.19).
- Sakamoto, T., Yokozawa, M., Toritani, H., Shibayama, M., Ishitsuka, N., Ohno, H., 2005. A crop phenology detection method using time-series MODIS data. *Remote sensing of environment* 96, 366–374.
- Sakoe, H., Chiba, S., 1978. Dynamic programming algorithm optimization for spoken word recognition. *IEEE transactions on acoustics, speech, and signal processing* 26, 43–49.
- Sanderson, M.A., Wedin, D., Tracy, B., Wedin, W.F., Fales, S.L., 2009. Grassland: Definition, origins, extent, and future. *Grassland Quietness and Strength for a New American Agriculture*, Madison, WI: Crop Science Society of America 57–74.
- Satalino, G., Mattia, F., Le Toan, T., Rinaldi, M., 2009. Wheat crop mapping by using ASAR AP data. *IEEE Transactions on Geoscience and Remote Sensing* 47, 527–530.
- Skakun, S., Kussul, N., Shelestov, A.Y., Lavreniuk, M., Kussul, O., 2015. Efficiency assessment of multitemporal C-band Radarsat-2 intensity and Landsat-8 surface reflectance satellite imagery for crop classification in Ukraine. *IEEE Journal of Selected Topics in Applied Earth Observations and Remote Sensing* 9, 3712–3719.
- Skriver, H., 2011. Crop classification by multitemporal C-and L-band single-and dual-polarization and fully polarimetric SAR. *IEEE Transactions on Geoscience and Remote Sensing* 50, 2138–2149.
- Skriver, H., Svendsen, M.T., Thomsen, A.G., 1999. Multitemporal C-and L-band polarimetric signatures of crops. *IEEE Transactions on Geoscience and Remote Sensing* 37, 2413–2429.
- Smith, A.M., Major, D.J., 1996. Radar backscatter and crop residues. *Canadian journal of remote sensing* 22, 243–247.
- Smith, L.C., 1997. Satellite remote sensing of river inundation area, stage, and discharge: A review. *Hydrological processes* 11, 1427–1439.
- Soria-Ruiz, J., Fernandez-Ordonez, Y., Woodhouse, I.H., 2010. Land-cover classification using radar and optical images: a case study in Central Mexico. *International Journal of Remote Sensing* 31, 3291–3305.
- Soussana, J.-F., Lüscher, A., 2007. Temperate grasslands and global atmospheric change: a review. *Grass and Forage Science* 62, 127–134.

- Steinhausen, M.J., Wagner, P.D., Narasimhan, B., Waske, B., 2018. Combining Sentinel-1 and Sentinel-2 data for improved land use and land cover mapping of monsoon regions. *International journal of applied earth observation and geoinformation* 73, 595–604.
- Su, J.J., van Bochove, E., Thériault, G., Novotna, B., Khaldoune, J., Denault, J.T., Zhou, J., Nolin, M.C., Hu, C.X., Bernier, M., 2011. Effects of snowmelt on phosphorus and sediment losses from agricultural watersheds in Eastern Canada. *Agricultural water management* 98, 867–876.
- Sun, C., Bian, Y., Zhou, T., Pan, J., 2019. Using of Multi-Source and Multi-Temporal Remote Sensing Data Improves Crop-Type Mapping in the Subtropical Agriculture Region. *Sensors* 19, 2401.
- Tarn, site des S. de l'Etat du département du, 2015. Les surfaces d'intérêt écologique [WWW Document]. URL <http://www.tarn.gouv.fr/les-surfaces-d-interet-ecologique-a3063.html> (accessed 9.18.19).
- The difference between “land use” and “land cover” [WWW Document], 2019. . MSU Extension. URL https://www.canr.msu.edu/news/the_difference_between_land_use_and_land_cover (accessed 9.18.19).
- Torbick, N., Chowdhury, D., Salas, W., Qi, J., 2017. Monitoring rice agriculture across myanmar using time series Sentinel-1 assisted by Landsat-8 and PALSAR-2. *Remote Sensing* 9, 119.
- Tottrup, C., Rasmussen, M.S., 2004. Mapping long-term changes in savannah crop productivity in Senegal through trend analysis of time series of remote sensing data. *Agriculture, Ecosystems & Environment* 103, 545–560.
- Ulaby, F.T., Elachi, C., 1990. Radar polarimetry for geoscience applications.
- Ulaby, F.T., Moore, R.K., Fung, A.K., 1986. Microwave remote sensing: Active and passive. Volume 3-From theory to applications.
- UMR AGIR AGroécologie, Innovations et TerRitoires - Réduire les fuites de nitrate au moyen de cultures intermédiaires [WWW Document], 2012. URL <https://www6.toulouse.inra.fr/agir/Les-productions/Expertises/Reduire-les-fuites-de-nitrate-au-moyen-de-cultures-intermediaires> (accessed 9.18.19).
- US Department of Commerce, N.O. and A.A., 2019. What is the difference between land cover and land use? [WWW Document]. URL <https://oceanservice.noaa.gov/facts/lclu.html> (accessed 9.18.19).
- Van Tricht, K., Gobin, A., Gilliams, S., Piccard, I., 2018. Synergistic use of radar Sentinel-1 and optical Sentinel-2 imagery for crop mapping: a case study for Belgium. *Remote Sensing* 10, 1642.
- Vapnik, V., 1979. Estimation of Dependences Based on Empirical Data Nauka. Moscow: Nauka.(in Russian).
- Vaudour, E., Noirot-Cosson, P.E., Membrive, O., 2015. Early-season mapping of crops and cultural operations using very high spatial resolution Pléiades images. *International Journal of Applied Earth Observation and Geoinformation* 42, 128–141.
- Veloso, A., Mermoz, S., Bouvet, A., Le Toan, T., Planells, M., Dejoux, J.-F., Ceschia, E., 2017. Understanding the temporal behavior of crops using Sentinel-1 and Sentinel-2-like data for agricultural applications. *Remote sensing of environment* 199, 415–426.

- Verbeiren, S., Eerens, H., Piccard, I., Bauwens, I., Van Orshoven, J., 2008. Sub-pixel classification of SPOT-VEGETATION time series for the assessment of regional crop areas in Belgium. *International Journal of Applied Earth Observation and Geoinformation* 10, 486–497.
- Verburg, P.H., Neumann, K., Nol, L., 2011. Challenges in using land use and land cover data for global change studies. *Global change biology* 17, 974–989.
- VIGISAT - CLS place l'océan sous haute surveillance [WWW Document], 2019. URL <http://www.vigisat.eu/> (accessed 9.26.19).
- Vuolo, F., Neuwirth, M., Immitzer, M., Atzberger, C., Ng, W.-T., 2018. How much does multi-temporal Sentinel-2 data improve crop type classification? *International journal of applied earth observation and geoinformation* 72, 122–130.
- Wagger, M.G., Cabrera, M.L., Ranells, N.N., 1998. Nitrogen and carbon cycling in relation to cover crop residue quality. *Journal of Soil and Water Conservation* 53, 214–218.
- Wang, H., Allain-Bailhache, S., Méric, S., Pottier, E., 2016. Soil parameter retrievals over bare agricultural fields using multiangular RADARSAT-2 dataset. *IEEE Journal of Selected Topics in Applied Earth Observations and Remote Sensing* 9, 5666–5676.
- Wardlow, B.D., Egbert, S.L., 2008. Large-area crop mapping using time-series MODIS 250 m NDVI data: An assessment for the US Central Great Plains. *Remote sensing of environment* 112, 1096–1116.
- Wardlow, B.D., Egbert, S.L., Kastens, J.H., 2007. Analysis of time-series MODIS 250 m vegetation index data for crop classification in the US Central Great Plains. *Remote Sensing of Environment* 108, 290–310.
- Weiss, M., Baret, F., Smith, G.J., Jonckheere, I., Coppin, P., 2004. Review of methods for in situ leaf area index (LAI) determination: Part II. Estimation of LAI, errors and sampling. *Agricultural and forest meteorology* 121, 37–53.
- Wiseman, G., McNairn, H., Homayouni, S., Shang, J., 2014. RADARSAT-2 polarimetric SAR response to crop biomass for agricultural production monitoring. *IEEE Journal of Selected Topics in Applied Earth Observations and Remote Sensing* 7, 4461–4471.
- Withers, P., Neal, C., Jarvie, H., Doody, D., 2014. Agriculture and eutrophication: where do we go from here? *Sustainability* 6, 5853–5875.
- Xu, D., Guo, X., 2014. Compare NDVI extracted from Landsat 8 imagery with that from Landsat 7 imagery. *American Journal of Remote Sensing* 2, 10–14.
- Xue, J., Su, B., 2017. Significant remote sensing vegetation indices: A review of developments and applications. *Journal of Sensors* 2017.
- Yan, G., Mas, J.-F., Maathuis, B.H.P., Xiangmin, Z., Van Dijk, P.M., 2006. Comparison of pixel-based and object-oriented image classification approaches—a case study in a coal fire area, Wuda, Inner Mongolia, China. *International Journal of Remote Sensing* 27, 4039–4055.
- Yan, L., Roy, D.P., 2015. Improved time series land cover classification by missing-observation-adaptive nonlinear dimensionality reduction. *Remote Sensing of Environment* 158, 478–491.
- Yang, M.-S., 1993. On a class of fuzzy classification maximum likelihood procedures. *Fuzzy Sets and Systems* 57, 365–375.

- Yang, Z., Shao, Y., Li, K., Liu, Q., Liu, L., Brisco, B., 2017. An improved scheme for rice phenology estimation based on time-series multispectral HJ-1A/B and polarimetric RADARSAT-2 data. *Remote sensing of environment* 195, 184–201.
- Yengoh, G.T., Dent, D., Olsson, L., Tengberg, A.E., Tucker III, C.J., 2015. *Use of the Normalized Difference Vegetation Index (NDVI) to Assess Land Degradation at Multiple Scales: Current Status, Future Trends, and Practical Considerations*. Springer.
- Yusoff, N.M., Muharam, F.M., Takeuchi, W., Darmawan, S., Abd Razak, M.H., 2017. Phenology and classification of abandoned agricultural land based on ALOS-1 and 2 PALSAR multi-temporal measurements. *International journal of digital earth* 10, 155–174.
- ZA Armorique [WWW Document], 2019. URL <https://osur.univ-rennes1.fr/za-armorique/> (accessed 5.24.19).
- Zadbagher, E., Becek, K., Berberoglu, S., 2018. Modeling land use/land cover change using remote sensing and geographic information systems: case study of the Seyhan Basin, Turkey. *Environmental monitoring and assessment* 190, 494.
- Zaks, D.P., Kucharik, C.J., 2011. Data and monitoring needs for a more ecological agriculture. *Environmental Research Letters* 6, 014017.
- Zhang, X., Friedl, M.A., Schaaf, C.B., Strahler, A.H., Hodges, J.C., Gao, F., Reed, B.C., Huete, A., 2003. Monitoring vegetation phenology using MODIS. *Remote sensing of environment* 84, 471–475.
- Zhang, Y., Wu, L., 2011. Crop classification by forward neural network with adaptive chaotic particle swarm optimization. *Sensors* 11, 4721–4743.
- Zhu, G., Blumberg, D.G., 2002. Classification using ASTER data and SVM algorithms;: The case study of Beer Sheva, Israel. *Remote sensing of Environment* 80, 233–240.

Appendices



APPENDIX 1. Directive n° 91/676/CEE

Directive n° 91/676/CEE du 12/12/91 concernant la protection des eaux contre la pollution par les nitrates à partir de sources agricoles

- Type : Directive
- Date de signature : 12/12/1991
- Date de publication : 31/12/1991
- Etat : en vigueur

(JOCE n° L 375 du 31 décembre 1991)

Texte modifié par :

Règlement (CE) n° 1137/2008 du Parlement européen et du Conseil du 22 octobre 2008 (JOUE n° L 311 du 21 novembre 2008).

Règlement (CE) n° 1882/2003 du Parlement européen et du Conseil du 29 septembre 2003 (JOUE n° L 284 du 31 octobre 2003).

Vus

Vu le traité instituant la Communauté économique européenne, et notamment son article 130 S,

Vu la proposition de la Commission (1),

Vu l'avis du Parlement européen (2),

Vu l'avis du Comité économique et social (3),

(1) JOCE n° C 54 du 3 mars 1989, p.4, JOCE n° C 51 du 2 mars 1990, p. 12.

(2) JOCE n° C 158 du 26 juin 1989, p. 487.

(3) JOCE n° C 159 du 26 juin 1989, p. 1.

Considérants

Considérant que le teneur en nitrates de l'eau dans certaines régions des Etats membres est en augmentation et atteint déjà un niveau élevé par rapport aux normes fixées par la directive 75/440/CEE du Conseil, du 16 juin 1975, concernant la qualité requise des eaux superficielles destinées à la production d'eaux alimentaires dans les Etats membres (4), modifiée par la directive 79/869/CEE (5), et la directive 80/778/CEE du Conseil, du 15 juillet 1980, relative à la qualité des eaux destinées à la consommation humaine (6), modifiée par l'acte d'adhésion de 1985;

Considérant que le quatrième programme d'action des Communautés européennes en matière d'environnement (7) indique que la Commission a l'intention de présenter une proposition de directive concernant la lutte contre la pollution des eaux résultant de l'épandage ou des rejets de déjections animales et de l'utilisation excessive d'engrais, ainsi que la réduction de celle-ci;

Considérant qu'il est indiqué dans le "Livre vert" de la Commission intitulé "Perspectives de la politique agricole commune", définissant la réforme de la politique agricole commune que l'utilisation d'engrais et de fumiers contenant de l'azote est nécessaire à l'agriculture de la Communauté, mais que l'utilisation excessive d'engrais constitue un danger pour l'environnement ; qu'il est nécessaire de prendre des mesures communes pour résoudre les problèmes découlant de l'élevage intensif de bétail et que la politique agricole doit prendre davantage en considération la politique en matière d'environnement;

Considérant que la résolution du Conseil, du 28 juin 1988, sur la protection de la mer du Nord et d'autres eaux de la Communauté (8) invite la Commission à présenter des propositions de mesures communautaires ;

Considérant que les nitrates d'origine agricole sont la cause principale de la pollution provenant de sources diffuses, qui affecte les eaux de la Communauté ;

Considérant qu'il est dès lors nécessaire, pour protéger la santé humaine, les ressources vivantes et les écosystèmes aquatiques et pour garantir d'autres usages légitimes des eaux, de réduire la pollution directe ou indirecte des eaux par les nitrates provenant de l'agriculture et d'en prévenir l'extension ; que, à cet effet, il importe de prendre des mesures concernant le stockage et l'épandage sur les sols de composés azotés et concernant certaines pratiques de gestion des terres ;

Considérant que la pollution des eaux par les nitrates dans un Etat membre peut affecter les eaux d'autres Etats membres, et qu'une action est donc nécessaire au niveau communautaire conformément à l'article 130 R ;

Considérant que les Etats membres, en encourageant de bonnes pratiques agricoles, peuvent assurer à l'avenir un certain niveau de protection de l'ensemble des eaux contre la pollution ;

Considérant qu'il convient de prévoir une protection spéciale pour certaines zones dont les bassins versants alimentent des eaux susceptibles d'être polluées par des composés azotés ;

Considérant qu'il convient que les Etats membres définissent les zones vulnérables, qu'ils élaborent et mettent en œuvre des programmes d'action visant à réduire la pollution des eaux par les composés azotés dans ces zones ;

Considérant que de tels programmes doivent comporter des mesures visant à limiter l'épandage sur les sols de tout engrais contenant de l'azote et, en particulier, à fixer des limites spécifiques pour l'épandage d'effluents d'élevage ;

Considérant qu'il convient, pour assurer l'efficacité des actions, de surveiller la qualité des eaux et d'appliquer des méthodes de référence pour les dosages des composés azotés ;

Considérant qu'il est admis que les conditions hydrogéologiques dans certains Etats membres sont telles qu'il faudra peut-être de nombreuses années pour que les mesures de protection entraînent une amélioration de la qualité des eaux ;

Considérant qu'il convient d'instituer un comité chargé d'assister la Commission dans l'application de la présente directive et son adaptation au progrès scientifique et technique ;

Considérant que les Etats membres doivent établir et présenter à la Commission des rapports sur l'application de la présente directive ;

Considérant que la Commission doit régulièrement rendre compte de l'application de la présente directive par les Etats membres ;

A arrêté la présente directive :

- (4) *JOCE n° L 194 du 25 juillet 1975, p. 26.,*
- (5) *JOCE n° L 271 du 29 octobre 1979, p. 44.*
- (6) *JOCE n° L 229 du 30 août 1980, p. 11.*
- (7) *JOCE n° C 328 du 7 décembre 1987, p. 1.*
- (8) *JOCE n° C 209 du 9 août 1988, p. 3.*

Article 1er de la directive du 12 décembre 1991

La présente directive vise à :

Réduire la pollution des eaux provoquée ou induite par les nitrates à partir de sources agricoles, prévenir toute nouvelle pollution de ce type.

Article 2 de la directive du 12 décembre 1991

Aux fins de la présente directive, on entend par :

- a) "eaux souterraines" : toutes les eaux se trouvant sous la surface du sol dans la zone de saturation et qui sont en contact avec le sol ou le sous-sol ;
- b) "eaux douces" : les eaux qui se présentent à l'Etat naturel avec une faible teneur en sels et généralement considérées comme pouvant être captées et traitées en vue de la production d'eau potable ;
- c) "composé azoté" : toute substance contenant de l'azote, à l'exception de l'azote moléculaire gazeux ;
- d) "animaux" : tous les animaux élevés à des fins d'exploitation ou à des fins lucratives ;
- e) "fertilisant" : toute substance contenant un ou des composés azotés épanchée sur les sols afin d'améliorer la croissance de la végétation, y compris les effluents d'élevage, les résidus des élevages piscicoles et les boues d'épuration ;
- f) "engrais chimique" : tout fertilisant fabriqué selon un procédé industriel ;
- g) "effluent d'élevage" : les déjections d'animaux ou un mélange de litière et de déjections d'animaux, même s'ils ont subi une transformation ;
- h) "épandage" : l'apport au sol de matières par projection à la surface du sol, injection, enfouissement ou brassage avec les couches superficielles du sol ;

- i) "eutrophisation" : l'entrichissement de l'eau en composés azotés, provoquant un développement accéléré des algues et des végétaux d'espèces supérieures qui perturbe l'équilibre des organismes présents dans l'eau et entraîne une dégradation de la qualité de l'eau en question ;
- j) "pollution" : le rejet de composés azotés de sources agricoles dans le milieu aquatique, directement ou indirectement, ayant des conséquences de nature à mettre en danger la santé humaine, à nuire aux ressources vivantes et au système écologique aquatique, à porter atteinte aux agréments ou à gêner d'autres utilisations légitimes des eaux ;
- k) "zone vulnérable" : les terres désignées conformément à l'article 3 paragraphe 2.

Article 3 de la directive du 12 décembre 1991

1. Les eaux atteintes par la pollution et celles qui sont susceptibles de l'être si les mesures prévues à l'article 5 ne sont pas prises sont définies par les Etats membres en fonction des critères fixés à l'annexe I.
2. Dans un délai de deux ans à compter de la notification de la présente directive, les Etats membres désignent comme zones vulnérables toutes les zones connues sur leur territoire qui alimentent les eaux définies conformément au paragraphe 1 et qui contribuent à la pollution. Ils notifient cette désignation initiale à la Commission dans un délai de six mois.
3. Lorsque des eaux définies par un Etat membre conformément au paragraphe 1 sont touchées par la pollution des eaux d'un autre Etat membre qui y sont drainées directement ou indirectement, l'Etat membre dont les eaux sont touchées peut notifier les faits à l'autre Etat membre ainsi qu'à la Commission. Les Etats membres concernés procèdent, le cas échéant avec la Commission, à la concertation nécessaire pour identifier les sources concernées et les mesures à prendre en faveur des eaux touchées afin d'en assurer la conformité avec la présente directive.
4. Les Etats membres réexaminent et, au besoin, révisent ou complètent en temps opportun, au moins tous les quatre ans, la liste des zones vulnérables désignées, afin de tenir compte des changements et des facteurs imprévisibles au moment de la désignation précédente. Ils notifient à la Commission, dans un délai de six mois, toute révision ou ajout apporté à la liste des désignations.
5. Les Etats membres sont exemptés de l'obligation de désigner des zones vulnérables spécifiques lorsqu'ils établissent et appliquent à l'ensemble de leur territoire national les programmes d'action visés à l'article 5 conformément à la présente directive.

Article 4 de la directive du 12 décembre 1991

1. En vue d'assurer, pour toutes les eaux, un niveau général de protection contre la pollution, les Etats membres, dans un délai de deux ans à compter de la notification de la présente directive :

a) établissement un ou des codes de bonne pratique agricole, qui seront mis en œuvre volontairement par les agriculteurs et qui devraient contenir au moins les éléments énumérés au point A de l'annexe II ;

b) élaborent au besoin un programme prévoyant la formation et l'information des agriculteurs en vue de promouvoir l'application du ou des codes de bonne pratique agricole.

2. Les Etats membres présentent à la Commission les modalités de leurs codes de bonne pratique agricole et celle-ci inclut des informations sur ces codes dans le rapport visé à l'article 11. A la lumière des informations reçues, la Commission peut, si elle l'estime nécessaire, faire des propositions appropriées au Conseil.

Article 5 de la directive du 12 décembre 1991

1. Pour les besoins des objectifs visés à l'article 1er et dans un délai de deux ans à compter de la désignation initiale visée à l'article 3 paragraphe 2 ou d'un an après chaque nouvelle désignation visée à l'article 3 paragraphe 4, les Etats membres établissent des programmes d'action portant sur les zones vulnérables désignées.

2. Un programme d'action peut porter sur toutes les zones vulnérables situées sur le territoire d'un Etat membre ou, si cet Etat l'estime approprié, des programmes différents peuvent être établis pour diverses zones ou parties de zones vulnérables.

3. Les programmes d'action tiennent compte :

a) des données scientifiques et techniques disponibles concernant essentiellement les quantités respectives d'azote d'origine agricole ou provenant d'autres sources ;

b) des conditions de l'environnement dans les régions concernées de l'Etat membre en question.

4. Les programmes d'action sont mis en œuvre dans un délai de quatre ans à compter de leur élaboration et ils contiennent les mesures obligatoires suivantes :

a) les mesures visées à l'annexe III ;

b) les mesures que les Etats membres ont arrêtées dans le(s) code(s) de bonne pratique agricole élaboré(s) conformément à l'article 4, à l'exception de celles qui ont été remplacées par les mesures énoncées à l'annexe III.

5. En outre, les Etats membres prennent, dans le cadre des programmes d'action, toutes les mesures supplémentaires ou actions renforcées qu'ils estiment nécessaires, s'il s'avère, dès le début ou à la lumière de l'expérience acquise lors de la mise en œuvre des programmes d'action, que les mesures visées au paragraphe 4 ne suffiront pas pour atteindre les objectifs définis à l'article 1er. Dans le choix de ces mesures ou actions, les Etats membres tiennent compte de leur efficacité et de leur coût par rapport à d'autres mesures préventives envisageables.

6. Les Etats membres élaborent et mettent en œuvre des programmes de surveillance adéquats pour évaluer l'efficacité des programmes d'action établis en vertu du présent article.

Les Etats membres qui appliquent les dispositions de l'article 5 à l'ensemble de leur territoire national surveillent la teneur en nitrates des eaux (eaux de surface et eaux souterraines) à des points de mesure sélectionnés, qui permettent de déterminer l'étendue de la pollution des eaux par les nitrates à partir de sources agricoles.

7. Les Etats membres réexaminent et, le cas échéant, révisent leurs programmes d'action, y compris toute mesure supplémentaire prise en vertu du paragraphe 5, tous les quatre ans au moins. Ils informent la Commission de toute modification apportée aux programmes d'action.

Article 6 de la directive du 12 décembre 1991

1. Aux fins de désigner les zones vulnérables et de réviser la liste établie, les Etats membres :

a) dans un délai de deux ans à compter de la notification de la présente directive, surveillent pendant une période d'un an la concentration de nitrates dans les eaux douces :

i) au niveau des stations de prélèvement des eaux superficielles prévues à l'article 5 paragraphe 4 de la directive 75/440/CEE et /ou d'autres stations de prélèvement représentatives des eaux superficielles des Etats membres, au moins une fois par mois et plus fréquemment durant les périodes de crues ;

ii) au niveau des stations de prélèvement représentatives des nappes phréatiques des Etats membres, à intervalles réguliers, compte tenu des dispositions de la directive 80/778/CEE ;

b) reprennent le programme de surveillance décrit au point a) tous les quatre ans au moins, sauf dans le cas des stations de prélèvement où la concentration de nitrates de tous les échantillons précédents s'est révélée inférieure à 25 milligrammes par litre et où aucun facteur nouveau susceptible d'accroître la teneur en nitrates n'a été constaté ; en ce cas, le programme de surveillance ne doit être mis en œuvre que tous les huit ans ;

c) réexaminent tous les quatre ans l'état d'eutrophisation des eaux douces superficielles, des eaux côtières et d'estuaires.

2. Les méthodes de mesure de référence définies à l'annexe IV sont utilisées.

Article 7 de la directive du 12 décembre 1991

(Règlement (CE) n° 1137/2008 du 22 octobre 2008)

La Commission peut formuler des recommandations pour la surveillance visée aux articles 5 et 6 conformément à la procédure de réglementation visée à l'article 9, paragraphe 2.

Article 8 de la directive du 12 décembre 1991

Les annexes de la présente directive peuvent être adaptées au progrès scientifique et technique, conformément à la procédure prévue à l'article 9.

Article 9 de la directive du 12 décembre 1991

(Règlement (CE) n° 1882/2003 du 29 septembre 2003 et Règlement (CE) n° 1137/2008 du 22 octobre 2008).

1. La Commission est assistée par un comité.

2. Dans le cas où il est fait référence au présent article, les articles 5 et 7 de la décision 1999/468/CE (1) s'appliquent, dans le respect des dispositions de l'article 8 de celle-ci.

La période prévue à l'article 5, paragraphe 6, de la décision 1999/468/CE est fixée à trois mois.

3. Dans le cas où il est fait référence au présent paragraphe, l'article 5 bis, paragraphes 1 à 4, et l'article 7 de la décision 1999/468/CE s'appliquent, dans le respect des dispositions de l'article 8 de celle-ci.

(1) Décision 1999/468/CE du Conseil du 28 juin 1999 fixant les modalités de l'exercice des compétences d'exécution conférées à la Commission (JO L 184 du 17.7.1999, p. 23).

Article 10 de la directive du 12 décembre 1991

1. Les Etats membres soumettent à la Commission, pour la période de quatre ans qui suit la notification de la présente directive et pour chaque période ultérieure de quatre ans, un rapport contenant les informations visées à l'annexe V.

2. Ils soumettent à la Commission un rapport, en vertu du présent article, dans un délai de six mois après l'expiration de la période sur laquelle il porte.

Article 11 de la directive du 12 décembre 1991

A partir des informations reçues en vertu de l'article 10, la Commission publie des rapports de synthèse dans un délai de six mois après la réception des rapports des Etats membres et elle les communique au Parlement européen et au Conseil. À la lumière de la mise en oeuvre de la présente directive, et notamment des dispositions de l'annexe III, la Commission soumet au Conseil, d'ici le 1er janvier 1998, un rapport assorti, le cas échéant, de propositions de révision de la présente directive.

Article 12 de la directive du 12 décembre 1991

1. Les Etats membres mettent en vigueur les dispositions législatives, réglementaires et administratives nécessaires pour se conformer à la présente directive dans un délai de deux ans à compter de sa notification (9). Ils en informent immédiatement la Commission.

2. Lorsque les Etats membres adoptent ces dispositions, celles-ci contiennent une référence à la présente directive ou sont accompagnées d'une telle référence lors de leur publication officielle. Les modalités de cette référence sont arrêtées par les Etats membres.

3. Les Etats membres communiquent à la Commission le texte des dispositions essentielles de droit interne qu'ils adoptent dans le domaine régi par la présente directive.

(9) La présente directive a été notifiée aux Etats membres le 19 décembre 1991.

Annexe I : Critères de définition des eaux visés à l'article 3 paragraphe 1

A. Les eaux visées à l'article 3 paragraphe 1 sont définies en fonction, entre autres, des critères suivants :

1) si les eaux douces superficielles, notamment celles servant ou destinées au captage d'eau potable, contiennent ou risquent de contenir, si les mesures prévues à l'article 5 ne sont pas prises, une concentration de nitrates supérieure à celle prévue par la directive 75/440/CEE;

2) si les eaux souterraines ont, ou risquent d'avoir, une teneur en nitrate supérieure à 50 milligrammes par litre si les mesures prévues à l'article 5 ne sont pas prises ;

3) si les lacs naturels d'eau douce, les autres masses d'eau douce, les estuaires, les eaux côtières et marines ont subi ou risquent dans un avenir proche de subir une eutrophisation si les mesures prévues à l'article 5 ne sont pas prises.

B. Dans l'application de ces critères, les Etats membres tiennent également compte :

1) des caractéristiques physiques et environnementales des eaux et des terres ;

2) des connaissances actuelles concernant le comportement des composés azotés dans l'environnement (eaux et sols) ;

3) des connaissances actuelles concernant l'incidence des mesures prises conformément à l'article 5.

Annexe II : Code(s) de bonne pratique agricole

A. Un ou des codes de bonne pratique agricole visant à réduire la pollution par les nitrates et tenant compte des conditions prévalant dans les différentes régions de la Communauté devraient contenir des règles couvrant les éléments ci-après, pour autant qu'ils soient pertinents :

1) les périodes pendant lesquelles l'épandage de fertilisants est inapproprié ;

2) les conditions d'épandage des fertilisants sur les sols en forte pente ;

3) les conditions d'épandage des fertilisants sur les sols détremés, inondés, gelés ou couverts de neige ;

4) les conditions d'épandage des fertilisants près des cours d'eau ;

5) la capacité et la construction des cuves destinées au stockage des effluents d'élevage, notamment les mesures visant à empêcher la pollution des eaux par ruissellement et infiltration dans le sol ou écoulement dans les eaux superficielles de liquides contenant des effluents d'élevage et des effluents de matières végétales telles que le fourrage ensilé ;

6) les modes d'épandage des engrais chimiques et des effluents d'élevage, notamment son niveau et son uniformité, pour pouvoir maintenir à un niveau acceptable la fuite dans les eaux d'éléments nutritifs.

B. Les Etats membres peuvent également inclure les éléments ci-après dans leur(s) code(s) de bonne pratique agricole :

7) la gestion des terres, notamment l'utilisation d'un système de rotation des cultures et la proportion des terres consacrées aux cultures permanentes par rapport aux cultures annuelles ;

8) le maintien d'une quantité minimale de couverture végétale au cours des périodes (pluvieuses) destinée à absorber l'azote du sol qui, en l'absence d'une telle couverture végétale, provoquerait une pollution des eaux par les nitrates ;

9) l'élaboration de plans de fertilisation en fonction de chaque exploitation et la tenue de registres d'utilisation des fertilisants ;

10) la prévention de la pollution des eaux par ruissellement et percolation d'eau hors d'atteinte du système racinaire dans le cas des cultures irriguées.

Annexe III : Mesures à inclure dans les programmes d'action conformément à l'article 5 paragraphe 4 point a)

(Règlement (CE) n° 1137/2008 du 22 octobre 2008)

1. Les mesures comportent des règles concernant :

1) les périodes durant lesquelles l'épandage de certains types de fertilisants est interdit ;

2) la capacité des cuves destinées au stockage des effluents d'élevage ; celle-ci doit dépasser la capacité nécessaire au stockage durant la plus longue des périodes d'interdiction d'épandage dans la zone vulnérable, sauf s'il peut être démontré à l'autorité compétente que le volume d'effluents d'élevage qui dépasse la capacité de stockage réelle sera évacué d'une manière inoffensive pour l'environnement ;

3) la limitation de l'épandage des fertilisants, conformément aux bonnes pratiques agricoles et compte tenu des caractéristiques de la zone vulnérable concernée, notamment :

a) de l'état des sols, de leur composition et de leur pente ;

b) des conditions climatiques, des précipitations et de l'irrigation ;

c) de l'utilisation des sols et des pratiques agricoles, notamment des systèmes de rotation des cultures ; et fondée sur un équilibre entre :

- i) les besoins prévisibles en azote des cultures et
- ii) l'azote apporté aux cultures par le sol et les fertilisants correspondant à :
 - La quantité d'azote présente dans le sol au moment où les cultures commencent à l'utiliser dans des proportions importantes (quantités restant à la fin de l'hiver),
 - L'apport d'azote par la minéralisation nette des réserves d'azote organique dans le sol, les apports de composés azotés provenant des effluents d'élevage,
 - Les apports de composés azotés provenant des engrais chimiques et autres composés.

2. Ces mesures assurent que, pour chaque exploitation ou élevage, la quantité d'effluents d'élevage épandue annuellement, y compris par les animaux eux-mêmes, ne dépasse pas une quantité donnée par hectare.

Cette quantité donnée par hectare correspond à la quantité d'effluents contenant 170 kilogrammes d'azote. Toutefois :

a) pour le premier programme d'action quadriennal, les Etats membres peuvent autoriser une quantité d'effluents contenant jusqu'à 210 kilogrammes d'azote ;

b) pendant le premier programme d'action quadriennal et à l'issue de ce programme, les Etats membres peuvent fixer des quantités différentes de celles indiquées ci-avant. Ces quantités doivent être déterminées de sorte à ne pas compromettre la réalisation des objectifs visés à l'article 1er et doivent se justifier par des critères objectifs, tels que :

- Des périodes de végétation longues,
- Des cultures à forte absorption d'azote,
- Des précipitations nettes élevées dans la zone vulnérable,
- Des sols présentant une capacité de dénitrification exceptionnellement élevée.

Si un État membre autorise une quantité différente en vertu du deuxième alinéa, point b), il en informe la Commission qui examine sa justification conformément à la procédure de réglementation visée à l'article 9, paragraphe 2.

3. Les Etats membres peuvent calculer les quantités visées au point 2 en fonction du nombre d'animaux.

4. Les Etats membres informent la Commission de la manière dont ils appliquent le point 2. A la lumière des informations reçues, la Commission peut, si elle l'estime nécessaire, présenter au Conseil des propositions appropriées, conformément à l'article 11.

Annexe IV : Méthodes de mesure de référence

Engrais chimiques

Les composés azotés sont mesurés selon la méthode décrite dans la directive 77/535/CEE de la Commission, du 22 juin 1977, concernant le rapprochement des législations des Etats membres

relatives aux méthodes d'échantillonnage et d'analyse des engrais (10), telle que modifiée par la directive 89/519/CEE (11).

Eaux douces, eaux côtières et marines

La concentration de nitrates est mesurée conformément à l'article 4 bis paragraphe 3 de la décision 77/795/CEE du Conseil, du 12 décembre 1977, instituant une procédure commune d'échange d'informations relative à la qualité des eaux douces superficielles dans la Communauté (12), telle que modifiée par la décision 86/574/CEE (13).

(10) JOCE n° L. 213 du 22 août 1977, p. 1.

(11) JOCE n° L 265 du 12 septembre 1989, p. 30.

(12) JOCE n° L. 334 du 24 décembre 1977, p. 29.

(13) JOCE n° L. 335 du 28 novembre 1986, p. 44.

Annexe V : Informations devant figurer dans les rapports visés à l'article 10

1. Un compte rendu des actions de prévention menées en vertu de l'article 4.

2. Une carte :

a) des eaux identifiées conformément à l'article 3 paragraphe 1 et à l'annexe I indiquant, dans chaque cas, lequel de critères mentionnés à l'annexe I a été utilisé en vue de cette identification ;

b) des zones identifiées désignées faisant apparaître de manière distincte les zones anciennes et les zones désignées depuis le dernier rapport.

3. Un résumé des résultats de la surveillance exercée en vertu de l'article 6, comprenant un exposé des considérations qui ont conduit à la désignation de chaque zone vulnérable et à toute révision ou ajout apporté à la désignation.

4. Un résumé des programmes d'action élaborés en vertu de l'article 5 et, en particulier :

a) les mesures requises en vertu de l'article 5 paragraphe 4 points a) et b) ;

b) les informations requises en vertu du point 4 de l'annexe III ;

c) toute mesure supplémentaire ou action renforcée prise en vertu de l'article 5 paragraphe 5 ;

d) un résumé des résultats des programmes de surveillance mise en œuvre au titre de l'article 5 paragraphe 6 ;

e) les estimations des Etats membres concernant les délais approximatifs dans lesquels on peut s'attendre à ce que les eaux définies conformément à l'article 3 paragraphe 1 réagissent aux mesures prévues dans le programme d'action, ainsi qu'une indication du niveau d'incertitude que présentent ces estimations.

B

APPENDIX 2. The rules of Good Agricultural and Environmental Conditions (GAEC)

DOMAINE « ENVIRONNEMENT, CHANGEMENT CLIMATIQUE ET BONNES CONDITIONS AGRICOLES DES TERRES »

SOUS-DOMAINE « BCAE » Fiche I

BANDE TAMPON LE LONG DES COURS D'EAU

Quel est l'objectif ?

Les bandes tampons localisées le long des cours d'eau protègent les sols des risques érosifs, améliorent leur structure et contribuent à la protection des eaux courantes en limitant les risques de pollutions diffuses. D'une façon générale, elles favorisent les auxiliaires de culture et la biodiversité.

Qui est concerné ?

Tous les exploitants agricoles demandeurs d'aides soumises à la conditionnalité ¹ qui disposent de terres agricoles localisées à moins de 5 mètres de la bordure d'un cours d'eau défini par arrêté ministériel relatif aux règles BCAE.

Que vérifie-t-on ?

Il est vérifié que sur l'exploitation contrôlée, il existe une « bande tampon » de 5 mètres de large au minimum sans traitement phyto-pharmaceutique ni fertilisation implantée le long de tous les cours d'eau définis par arrêté ministériel relatif aux règles BCAE. Lorsque la réglementation s'appliquant aux parcelles en zones vulnérables aux pollutions par les nitrates fixe une largeur supérieure, c'est cette largeur supérieure qu'il convient de respecter.

1 – La largeur de la bande tampon le long des cours d'eau *Définition des cours d'eau à border*

Les cours d'eau à border ² sont définis par l'arrêté ministériel relatif aux règles BCAE. Ils concernent notamment les cours d'eau représentés en trait bleu plein voire certains en trait bleu pointillé sur les cartes les plus récemment éditées au 1/25 000^e par l'Institut national de l'information géographique et forestière.

La largeur de la bande tampon

Il est vérifié la largeur de la bande tampon. Elle doit être d'au moins 5 mètres (lorsque la réglementation s'appliquant aux parcelles en zones vulnérables aux pollutions par les nitrates fixe une largeur supérieure, c'est cette largeur supérieure qu'il convient de respecter) à partir du bord du cours d'eau, là où la berge est accessible à partir d'un semoir. Il n'y a pas de limite maximale à cette largeur. Il n'y a pas non plus de surface minimale.

Cette largeur prend en compte, le cas échéant, la largeur des chemins ou des ripisylves longeant le cours d'eau. Ainsi un chemin ou des ripisylves d'une largeur inférieure à la largeur minimale depuis le bord du cours d'eau doit être complétés par une bande tampon afin d'atteindre la largeur minimale depuis le bord du cours d'eau.

Les dispositifs tampons en sortie de réseau de drainage peuvent empiéter sur la bande tampon si ces dispositifs sont végétalisés, sont éloignés d'au moins un mètre de la berge et respectent le cas échéant les dispositions de l'article L. 214-1 du code de l'environnement.

2 – La validité et la présence du couvert Il est vérifié que le couvert est :

- Herbacé, arbustif ou arboré (les friches, les espèces invasives listées en annexe de l'arrêté ministériel relatif aux règles BCAE et le miscanthus ne sont pas retenus comme couverts autorisés) ;
- couvrant ;
- permanent.

Les sols nus ne sont pas autorisés (sauf pour les chemins longeant le cours d'eau).

Le couvert (herbacé, arbustif ou arboré) peut être implanté ou spontané. Dans tous les cas, l'objectif est d'arriver à un couvert répondant aux objectifs de permanence de la bande tampon, donc plurispécifique et semi-naturel.

En cas d'implantation du couvert, de préférence à l'automne et au plus tard le 31 mai :

- L'implantation d'espèces considérées comme invasives n'est pas autorisée ;
- Le mélange d'espèces est conseillé mais l'implantation d'une seule espèce reste autorisée à l'exception de l'implantation de légumineuses « pures » qui est interdite mais les légumineuses en mélange avec des graminées sont autorisées.

En cas de couverts spontanés ou implantés déjà existant, le maintien est recommandé (sauf le miscanthus qui devra être détruit) avec, le cas échéant, des modalités de gestion favorisant une évolution vers une couverture permanente et diversifiée :

- Les cultures pérennes déjà implantées devront faire l'objet d'un enherbement complet sur 5 mètres de large au minimum ;
- Les implantations en légumineuses pures seront conservées pour éviter les émissions d'azote lors du retournement et gérées pour permettre une évolution vers un couvert autochtone diversifié ;
- Les couverts comportant une espèce invasive autre que celles mentionnées en annexe de l'arrêté ministériel relatif aux règles BCAE seront maintenus (sauf le miscanthus qui devra être détruit) avec un entretien approprié pour limiter la diffusion et favoriser la diversité botanique.

¹ Les aides soumises à la conditionnalité couvrent les paiements directs au titre du règlement (UE) n° 1307/2013 (paiements de base, paiement redistributif, paiements au titre du verdissement, paiements pour les jeunes agriculteurs, soutiens couplés facultatifs), les paiements au titre des articles 46 et 47 du règlement (UE) n° 1308/2013 (re-structuration et reconversion des vignobles, vendange en vert) et les primes annuelles en vertu de l'article 21, paragraphe 1, points a) et b), des articles 28 à 31, et des articles 33 et 34, du règlement (UE) n° 1305/2013 (aide au boisement et à la création de surfaces boisées, aide pour la mise en place de systèmes agroforestiers, mesures agroenvironnementales et climatiques, soutien à l'agriculture biologique, paiements au titre de Natura 2000 et de la directive-cadre sur l'eau, paiements en faveur des zones soumises à des contraintes naturelles ou à d'autres contraintes spécifiques, paiements en faveur du bien-être des animaux, aides correspondant à des engagements forestiers, environnementaux et climatiques).

3 – L'entretien du couvert

Des obligations spécifiques s'imposent aux bandes tampons :

- Le couvert de la bande tampon doit rester en place toute l'année,
- L'utilisation de fertilisants minéraux ou organiques et de traitements phytopharmaceutiques est interdite sur les bandes tampon (sauf dans le cadre de la lutte contre les nuisibles prévue par un arrêté préfectoral pris en application de l'article L.251-8 du code rural et de la pêche maritime),
- La surface consacrée à la bande tampon ne peut être utilisée pour l'entreposage de matériel agricole ou d'irrigation, pour le stockage des produits ou des sous-produits de récolte ou des déchets (fumier),
- Le labour est interdit mais le travail superficiel du sol est autorisé,
- Le pâturage est autorisé sous réserve du respect des règles d'usage pour l'accès des animaux au cours d'eau,
- La fauche ou le broyage sont autorisés sur une largeur maximale de 20 mètres,
- Les amendements alcalins (calciques et magnésiens) sont autorisés.

GRILLE « BCAE » - « BANDE TAMPON LE LONG DES COURS D'EAU (MÉTROPOLE) »

Points vérifiés	Anomalies	Système d'avertissement précoce		Réduction
		Applicable ?	Délai de remise en conformité	
Réalisation de la bande tampon	Absence totale de bande tampon : <ul style="list-style-type: none"> • sur une portion de cours d'eau BCAE traversant l'exploitation • le long de tous les cours d'eau BCAE traversant l'exploitation 	non		5%
		non		intentionnelle
	Pratique d'entretien interdite sur la bande tampon le long du ou des cours d'eau BCAE traversant l'exploitation.	non		3%
	Bande tampon de largeur insuffisante le long d'une partie du ou des cours d'eau BCAE traversant l'exploitation.	non		3%

DOMAINE « ENVIRONNEMENT, CHANGEMENT CLIMATIQUE ET BONNES CONDITIONS AGRICOLES DES TERRES »

SOUS-DOMAINE « BCAA »

Fiche II

PRÉLÈVEMENTS POUR L'IRRIGATION

Quel est l'objectif ?

La maîtrise de l'irrigation améliore la gestion de la ressource en eau. Elle permet également de conserver la structure des sols en évitant les effets de tassement et d'entraînement des couches supérieures.

Qui est concerné ?

Tous les exploitants agricoles demandeurs d'aides soumises à la conditionnalité ¹ qui prélèvent de l'eau à usage non domestique dans les masses d'eaux superficielles ou souterraines par le biais d'installations ou d'ouvrages soumis à autorisation ou à déclaration au titre de la police de l'eau, sont concernés. Depuis 2010, toute la sole irriguée est concernée par cette BCAA.

Remarque : pour satisfaire aux deux exigences de la grille, les exploitants irriguant en structure collective ou s'approvisionnant auprès d'un fournisseur d'eau devront présenter un bulletin d'adhésion à jour ou un contrat de fourniture pour l'année en cours.

Que vérifie-t-on ?

1. La détention du récépissé de la déclaration ou de l'arrêté d'autorisation de prélèvements d'eau destinée à l'irrigation ².
2. L'existence d'un moyen d'évaluation approprié des volumes prélevés conforme aux arrêtés du 11 septembre 2003 ³.

En cas de pompage, le compteur volumétrique est obligatoire :

- Le choix et les conditions de montage du compteur doivent permettre de garantir la précision des volumes mesurés ;
- Les compteurs volumétriques équipés d'un système de remise à zéro sont interdits. Par ailleurs, le compteur doit permettre d'afficher le volume en permanence ou, en cas de pompage, pendant toute la période de prélèvement ⁴.

Dans une retenue collinaire : soit un compteur est installé sur la pompe de reprise quand elle est nécessaire, soit il existe une échelle graduée sur la retenue et d'une courbe de correspondance entre le volume de la retenue et la hauteur du plan d'eau.

En cas d'irrigation par submersion : un enregistrement volumétrique à la source de tout mètre cube par seconde est nécessaire.

GRILLE « BCAA » - « PRÉLÈVEMENTS POUR L'IRRIGATION »

Points vérifiés	Anomalies	Système d'avertissement précoce		Réduction
		Applicable ?	Délai de remise en conformité	
Détention du récépissé de déclaration ou de l'arrêté d'autorisation de prélèvement et présence de moyen d'évaluation des volumes	Non-détention du récépissé de la déclaration ou de l'arrêté d'autorisation de prélèvement d'eau.	non		5%
	Absence de moyens appropriés de mesure des volumes d'eau prélevés.	non		3%

¹ Les aides soumises à la conditionnalité couvrent les paiements directs au titre du règlement (UE) n° 1307/2013 (paiements de base, paiement redistributif, paiements au titre du verdissement, paiements pour les jeunes agriculteurs, soutiens couplés facultatifs), les paiements au titre des articles 46 et 47 du règlement (UE) n° 1308/2013 (re-structuration et reconversion des vignobles, vendange en vert) et les primes annuelles en vertu de l'article 21, paragraphe 1, points a) et b), des articles 28 à 31, et des articles 33 et 34, du règlement (UE) n° 1305/2013 (aide au boisement et à la création de surfaces boisées, aide pour la mise en place de systèmes agroforestiers, mesures agroenvironnementales et climatiques, soutien à l'agriculture biologique, paiements au titre de Natura 2000 et de la directive-cadre sur l'eau, paiements en faveur des zones soumises à des contraintes naturelles ou à d'autres contraintes spécifiques, paiements en faveur du bien-être des animaux, aides correspondant à des engagements forestiers, environnementaux et climatiques).

² Articles L 214.1 à L. 214.6 du code de l'environnement

³ Arrêtés du 11 septembre 2003 portant application du décret n° 96-102 du 2 février 1996 et fixant les prescriptions générales applicables aux prélèvements soumis à auto-risation ou à déclaration en application des articles L. 214-1 à L. 214-3 du code de l'environnement et relevant des rubriques 1.1.2.0, 1.2.1.0, 1.2.2.0 ou 1.3.1.0 de la nomenclature annexée au décret n° 93-743 du 29 mars 1993 modifié.

⁴ En cas de non-utilisation de compteur, un autre dispositif de mesure en continu doit être présenté assurant la même garantie qu'un compteur volumétrique en termes de précision, de stabilité et de représentativité des volumes d'eau prélevés.



DOMAINE « ENVIRONNEMENT, CHANGEMENT CLIMATIQUE ET BONNES CONDITIONS AGRICOLES DES TERRES »

SOUS-DOMAINE « BCAA »

Fiche III

PROTECTION DES EAUX SOUTERRAINES CONTRE LA POLLUTION CAUSÉE PAR DES SUBSTANCES DANGEREUSES

Quel est l'objectif ?

Les eaux souterraines fournissent 75 % de l'eau potable. Afin de préserver leur qualité, les rejets dans l'environnement de certaines substances visées à l'annexe de la directive européenne sur la protection des eaux souterraines ¹ dans la version en vigueur le dernier jour de son application pour ce qui concerne l'activité agricole sont interdits ou réglementés. Cette directive ayant été abrogée, les exigences minimales qu'elle prévoyait concernant les listes de familles et groupes de substances ont été reprises en 2014 ² au titre d'une nouvelle BCAA, sans modification de contenu

Qui est concerné ?

Tous les exploitants agricoles, en particulier les exploitants demandeurs d'aides soumises à la conditionnalité ³, sont concernés dans la mesure où ils utilisent des produits comportant des substances visées par la directive, notamment les produits phytopharmaceutiques, carburants et lubrifiants, produits de désinfection et de santé animale, fertilisants.

Que vérifie-t-on ?

Deux points de contrôle ont été définis et sont vérifiés.

Point de contrôle 1. Absence de pollution des eaux souterraines Le contrôle porte sur l'existence d'un rejet dans les sols, imputable à l'agriculteur, d'une substance interdite.

Il est vérifié visuellement le jour du contrôle sur l'exploitation ⁴ l'absence de rejet dans les sols de substances présentant un risque de toxicité, de persistance et de bioaccumulation (par exemple : composés organophosphorés, huiles minérales et hydrocarbures, etc.).

Point de contrôle 2. Stockage des effluents d'élevage dans le respect des distances d'éloignement par rapport aux points d'eaux souterraines. Le contrôle concerne les exploitations qui stockent des effluents d'élevage.

La distance minimum d'éloignement à respecter par rapport aux points d'eau souterraine est de 35 mètres.

GRILLE « BCAA » - « PROTECTION DES EAUX SOUTERRAINES »

Points vérifiés	Anomalies	Système d'avertissement précoce		Réduction
		Applicable ?	Délai de remise en conformité	
Absence de pollution des eaux souterraines	Existence d'un rejet dans les sols (imputable à l'agriculteur) d'une substance interdite	non		5%
Stockage des effluents d'élevage dans le respect des distances d'éloignement par rapport aux points d'eaux souterraines	Non-respect des distances de stockage des effluents d'élevage	non		3%

¹ Directive 80/68/CEE du Conseil du 17 décembre 1979 concernant la protection des eaux souterraines contre la pollution causée par certaines substances dangereuses (JOCE L 20 du 26.1.1980, p. 43).

² Règlement (UE) n°1310/2013 du Parlement européen et du Conseil du 17/12/2013

³ Les aides soumises à la conditionnalité couvrent les paiements directs au titre du règlement (UE) n° 1307/2013 (paiements de base, paiement redistributif, paiements au titre du verdissement, paiements pour les jeunes agriculteurs, soutiens couplés facultatifs), les paiements au titre des articles 46 et 47 du règlement (UE) n° 1308/2013 (restructuration et reconversion des vignobles, vendange en vert) et les primes annuelles en vertu de l'article 21, paragraphe 1, points a) et b), des articles 28 à 31, et des articles 33 et 34, du règlement (UE) n° 1305/2013 (aide au boisement et à la création de surfaces boisées, aide pour la mise en place de systèmes agroforestiers, mesures agroenvironnementales et climatiques, soutien à l'agriculture biologique, paiements au titre de Natura 2000 et de la directive-cadre sur l'eau, paiements en faveur des zones soumises à des contraintes naturelles ou à d'autres contraintes spécifiques, paiements en faveur du bien-être des animaux, aides correspondant à des engagements forestiers, environnementaux et climatiques).

⁴ Cette obligation s'applique sur les terres agricoles et sur les terres boisées aidées (aide au boisement des terres agricoles, aide à la mise en place de systèmes agroforestiers).

DOMAINE « ENVIRONNEMENT, CHANGEMENT CLIMATIQUE ET BONNES CONDITIONS AGRICOLES DES TERRES »

SOUS-DOMAINE « BCAA »

Fiche IV

COUVERTURE MINIMALE DES SOLS

Quel est l'objectif ?

La couverture minimale des sols vise à favoriser le stockage du carbone.

Qui est concerné ?

Tous les exploitants agricoles demandeurs d'aides soumises à la conditionnalité¹ qui disposent de terres agricoles sont concernés. Cependant, les points de contrôle sont sans objet pour les terres arables soumises à l'obligation de maintien en jachère noire ou les terres arables entièrement consacrées à des cultures sous eau (riz).

Que vérifie-t-on ?

Il est vérifié :

- Sur les terres arables, l'existence d'un semis ou d'un couvert au 31 mai,
- Sur les surfaces restées agricoles après arrachage de vignobles, de vergers ou de houblonnières, la présence d'un couvert végétal, implanté ou spontané au 31 mai.

GRILLE « BCAA » - « COUVERTURE MINIMALE DES SOLS »

Points vérifiés	Anomalies	Système d'avertissement précoce		Réduction
		Applicable ?	Délai de remise en conformité	
Terres arables (en production ou en jachère)	Absence de couvert sur les surfaces mises en culture (y compris les surfaces en herbe) ou les surfaces en jachère	non		5 %
	Non-respect de la date limite de semis sur les surfaces mises en culture (y compris les surfaces en herbe) ou les surfaces en jachère	non		3%
	Absence d'un couvert végétal entre les phases d'arrachage et de réimplantation des cultures fruitières, viticoles ou de houblon	non		5%

¹ Les aides soumises à la conditionnalité couvrent les paiements directs au titre du règlement (UE) n° 1307/2013 (paiements de base, paiement redistributif, paiements au titre du verdissement, paiements pour les jeunes agriculteurs, soutiens couplés facultatifs), les paiements au titre des articles 46 et 47 du règlement (UE) n° 1308/2013 (re-structuration et reconversion des vignobles, vendange en vert) et les primes annuelles en vertu de l'article 21, paragraphe 1, points a) et b), des articles 28 à 31, et des articles 33 et 34, du règlement (UE) n° 1305/2013 (aide au boisement et à la création de surfaces boisées, aide pour la mise en place de systèmes agroforestiers, mesures agroenvironnementales et climatiques, soutien à l'agriculture biologique, paiements au titre de Natura 2000 et de la directive-cadre sur l'eau, paiements en faveur des zones soumises à des contraintes naturelles ou à d'autres contraintes spécifiques, paiements en faveur du bien-être des animaux, aides correspondant à des engagements forestiers, environnementaux et climatiques).



DOMAINE « ENVIRONNEMENT, CHANGEMENT CLIMATIQUE ET BONNES CONDITIONS AGRICOLES DES TERRES »

SOUS-DOMAINE « BCAE »

Fiche V

LIMITATION DE L'ÉROSION

Quel est l'objectif ?

La limitation de l'érosion vise à favoriser le maintien de la structure des sols.

Que vérifie-t-on ?

Il est vérifié l'absence de travail des sols (labour, travail superficiel, semis direct...) sur une parcelle gorgée d'eau ou inondée.

Qui est concerné ?

Tous les exploitants agricoles demandeurs d'aides soumises à la conditionnalité¹ qui disposent de terres agricoles sont concernés. Cependant, le point de contrôle est sans objet pour les terres arables entièrement consacrées à des cultures sous eau (riz).

GRILLE « BCAE » - « LIMITATION DE L'ÉROSION »

Points vérifiés	Anomalies	Système d'avertissement précoce		Réduction
		Applicable ?	Délai de remise en conformité	
Limitation de l'érosion	Non-respect de l'interdiction de travail des sols gorgés d'eau ou inondés	non		3 %

¹ Les aides soumises à la conditionnalité couvrent les paiements directs au titre du règlement (UE) n° 1307/2013 (paiements de base, paiement redistributif, paiements au titre du verdissement, paiements pour les jeunes agriculteurs, soutiens couplés facultatifs), les paiements au titre des articles 46 et 47 du règlement (UE) n° 1308/2013 (re-structuration et reconversion des vignobles, vendange en vert) et les primes annuelles en vertu de l'article 21, paragraphe 1, points a) et b), des articles 28 à 31, et des articles 33 et 34, du règlement (UE) n° 1305/2013 (aide au boisement et à la création de surfaces boisées, aide pour la mise en place de systèmes agroforestiers, mesures agroenvironnementales et climatiques, soutien à l'agriculture biologique, paiements au titre de Natura 2000 et de la directive-cadre sur l'eau, paiements en faveur des zones soumises à des contraintes naturelles ou à d'autres contraintes spécifiques, paiements en faveur du bien-être des animaux, aides correspondant à des engagements forestiers, environnementaux et climatiques).



DOMAINE « ENVIRONNEMENT, CHANGEMENT CLIMATIQUE ET BONNES CONDITIONS AGRICOLES DES TERRES »

SOUS-DOMAINE « BCAE »

Fiche VI

NON-BRÛLAGE DES RÉSIDUS DE CULTURE

Quel est l'objectif ?

Le non-brûlage des résidus de culture permet de préserver la matière organique des sols et d'éviter leur appauvrissement.

Qui est concerné ?

Tous les exploitants agricoles demandeurs d'aides soumises à la conditionnalité¹ qui disposent de surfaces en céréales, oléagineux et protéagineux, sont concernés, à l'exception des exploitants bénéficiant d'une dérogation nationale (surfaces en riz) ou individuelle (par décision motivée du préfet pour des raisons agronomiques ou sanitaires).

Que vérifie-t-on ?

L'absence de traces de brûlage intentionnel des résidus de culture sur les sols de l'exploitation ou l'existence d'une dérogation qui permet de pratiquer le brûlage des résidus de culture.

Aucune réduction n'est appliquée en cas de brûlage accidentel ne relevant pas de la responsabilité de l'exploitant.

L'écobuage sur prairies est autorisé.

GRILLE « BCAE » - « NON-BRÛLAGE DES RÉSIDUS DE CULTURE »

Points vérifiés	Anomalies	Système d'avertissement précoce		Réduction
		Applicable ?	Délai de remise en conformité	
Non-brûlage des résidus de cultures sauf dérogation	Constat de brûlage en absence de dérogation à l'interdiction.	non		3%

¹ Les aides soumises à la conditionnalité couvrent les paiements directs au titre du règlement (UE) n° 1307/2013 (paiements de base, paiement redistributif, paiements au titre du verdissement, paiements pour les jeunes agriculteurs, soutiens couplés facultatifs), les paiements au titre des articles 46 et 47 du règlement (UE) n° 1308/2013 (re-structuration et reconversion des vignobles, vendange en vert) et les primes annuelles en vertu de l'article 21, paragraphe 1, points a) et b), des articles 28 à 31, et des articles 33 et 34, du règlement (UE) n° 1305/2013 (aide au boisement et à la création de surfaces boisées, aide pour la mise en place de systèmes agroforestiers, mesures agroenvironnementales et climatiques, soutien à l'agriculture biologique, paiements au titre de Natura 2000 et de la directive-cadre sur l'eau, paiements en faveur des zones soumises à des contraintes naturelles ou à d'autres contraintes spécifiques, paiements en faveur du bien-être des animaux, aides correspondant à des engagements forestiers, environnementaux et climatiques).



DOMAINE « ENVIRONNEMENT, CHANGEMENT CLIMATIQUE ET BONNES CONDITIONS AGRICOLES DES TERRES »

SOUS-DOMAINE « BCAE »

Fiche VII

MAINTIEN DES PARTICULARITÉS TOPOGRAPHIQUES

Quel est l'objectif ?

Les particularités topographiques sont des éléments pérennes du paysage (haies, bosquets, mares). Ces milieux semi-naturels, essentiels à la mise en œuvre d'une politique de développement durable, constituent des habitats, des zones de transition et des milieux de déplacement favorables à la diversité des espèces végétales et animales.

Qui est concerné ?

Tous les exploitants agricoles demandeurs d'aides soumises à la conditionnalité¹ qui disposent de terres agricoles sont concernés.

Que vérifie-t-on ?

Point de contrôle n°1 – Le maintien des particularités topographiques

Le maintien des haies

Une haie est une unité linéaire de végétation ligneuse, implantée à plat, sur talus ou sur creux, avec :

- Présence d'arbustes, et, le cas échéant, présence d'arbres et/ou d'autres ligneux (ronces, genêts, ajoncs...);
- Ou présence d'arbres et d'autres ligneux (ronces, genêts, ajoncs...).

Ne sont pas inclus dans les haies :

- Les alignements d'arbres caractérisés par la présence d'une unité linéaire de végétation ligneuse composée uniquement d'arbres (ni arbustes, ni autres ligneux);
- Les bosquets : constitués d'un élément non linéaire d'arbres ou d'arbustes : si un élément n'est pas clairement linéaire, il ne sera pas classé comme haie (ou alignement d'arbres).

Toutes les haies d'une largeur inférieure ou égale à 10 mètres et qui sont à la disposition de l'agriculteur (c'est à dire qu'il en a le « contrôle ») doivent être maintenues.

Il n'est pas exigé de hauteur minimale ni maximale de la haie.

NB : une haie ne peut pas présenter de discontinuité (« trou ») de plus de 5 mètres.

Lors d'un contrôle, le maintien des haies est établi par la vérification de l'absence de suppression d'une haie, sur tout ou partie de son linéaire. Il faut noter que l'exploitation du bois et la coupe à blanc sont autorisées, ainsi que le recépage. Par ailleurs, la suppression est possible, suite à une déclaration préalable auprès de la DDT, dans les cas suivants.

• Cas de suppression définitive d'une haie ou partie de haie sans replantation d'un linéaire équivalent sur l'exploitation (« destruction ») :

- Création d'un nouveau chemin d'accès rendu nécessaire pour l'accès et l'exploitation de la parcelle, la largeur du chemin n'excédant pas 10 mètres,
- Création ou agrandissement d'un bâtiment d'exploitation justifié par un permis de construire,
- Gestion sanitaire de la haie décidée par l'autorité administrative (éradication d'une maladie de la haie);
- Défense de la forêt contre les incendies (décision administrative),
- Réhabilitation d'un fossé dans un objectif de rétablissement d'une circulation hydraulique,
- Travaux déclarés d'utilité publique (DUP),
- Opération d'aménagement foncier avec consultation du public, en lien avec des travaux déclarés d'utilité publique; l'opération doit faire l'objet d'un conseil environnemental par un organisme reconnu dans l'arrêté ministériel relatif aux règles BCAE.

• Cas de suppression définitive d'une haie ou partie de haie avec replantation d'un linéaire équivalent sur l'exploitation (« déplacement »), sans exigence quant à la nature ou la composition de la haie :

- Déplacement dans la limite de 2 % du linéaire de l'exploitation ou de 5 mètres par campagne; dans ce cas uniquement, il n'est pas attendu de déclaration préalable auprès de la DDT,
- Déplacement pour un meilleur emplacement environnemental de la haie, justifié sur la base d'une prescription dispensée par un organisme reconnu dans l'arrêté ministériel relatif aux règles BCAE,
- déplacement de haies ou parties de haies présentes sur (ou en bordure de) parcelles ayant fait l'objet d'un transfert de parcelles entre l'exploitation concernée et une autre exploitation (par exemple : agrandissement de l'exploitation, installation d'un nouvel agriculteur reprenant partiellement ou totalement une exploitation existante, échanges parcellaires...), avec réimplantation sur (ou en bordure de) la (ou l'une des) parcelle(s) portant initialement la (ou les) haie(s), ou ailleurs sur l'exploitation s'il s'agit de déplacer une haie formant une séparation de deux parcelles contigües pour regrouper ces deux parcelles en une seule nouvelle parcelle.

• Cas de destruction suivie d'une réimplantation d'une nouvelle haie au même endroit (« remplacement »), afin de remplacer des éléments morts ou de changer d'espèces.

Le contrôle vise à vérifier que les haies sont présentes sur le terrain conformément à ce qui a été identifié sur le RPG :

¹ Les aides soumises à la conditionnalité couvrent les paiements directs au titre du règlement (UE) n° 1307/2013 (paiements de base, paiement redistributif, paiements au titre du verdissement, paiements pour les jeunes agriculteurs, soutiens couplés facultatifs), les paiements au titre des articles 46 et 47 du règlement (UE) n° 1308/2013 (re-structuration et reconversion des vignobles, vendange en vert) et les primes annuelles en vertu de l'article 21, paragraphe 1, points a) et b), des articles 28 à 31, et des articles 33 et 34, du règlement (UE) n° 1305/2013 (aide au boisement et à la création de surfaces boisées, aide pour la mise en place de systèmes agroforestiers, mesures agroenvironnementales et climatiques, soutien à l'agriculture biologique, paiements au titre de Natura 2000 et de la directive-cadre sur l'eau, paiements en faveur des zones soumises à des contraintes naturelles ou à d'autres contraintes spécifiques, paiements en faveur du bien-être des animaux, aides correspondant à des engagements forestiers, environnementaux et climatiques).

- Si aucune destruction (y compris en vue d'un remplacement) n'est constatée, il n'y aura pas, sauf en cas de doute, de mesure sur place de la longueur de la haie,
- Dans le cas où une partie de haies n'est pas présente sur le terrain alors qu'elle était identifiée sur le RPG, le contrôleur mesurera systématiquement la longueur de haie supprimée,
- En cas de déplacement, il mesurera également la longueur de haie implantée en remplacement.

Lorsqu'un cas de destruction, de déplacement ou de remplacement d'une haie nécessitant une déclaration préalable auprès de la DDT sera identifié lors d'un contrôle, la présence et la date de la déclaration seront vérifiées.

Conditions et délai de remise en conformité des anomalies prises en compte dans le cadre du système d'avertissement précoce
Rappel : aucune réduction n'est appliquée pour ces anomalies, sauf en cas de nouveau contrôle sur l'une des deux campagnes suivantes établissant l'absence de réalisation d'une action corrective dans les délais prescrits.

Lorsque la non-conformité « Non-respect de l'obligation de maintien d'une haie, et ce pour un linéaire inférieur ou égal à 1 % du linéaire total » est constatée, les conditions de remise en conformité seront considérées remplies, dans le cadre d'une vérification lors d'un deuxième contrôle (non systématique) au cours de l'une des deux campagnes suivantes, lorsque l'exploitant aura déclaré dans sa déclaration PAC de la campagne suivant le contrôle initial, au plus tard avant le 15 mai, un linéaire de haies égal ou supérieur au linéaire initial.

Le maintien des mares et bosquets

Il est vérifié le maintien sur l'exploitation des mares d'une surface strictement supérieure à 10 ares et inférieure ou égale à 50 ares et des bosquets d'une surface strictement supérieure à 10 ares et inférieure ou égale à 50 ares.

Conditions et délai de remise en conformité des anomalies prises en compte dans le cadre du système d'avertissement précoce
Rappel : aucune réduction n'est appliquée pour ces anomalies, sauf en cas de nouveau contrôle sur l'une des deux campagnes suivantes établissant l'absence de réalisation d'une action corrective dans les délais prescrits

Lorsque la non-conformité « Non-respect de l'obligation de maintien d'un élément surfacique (mare ou bosquet), et ce pour une surface inférieure ou égal à 1 % de la surface totale pour chaque catégorie » est constatée, les conditions de remise en conformité seront considérées remplies, dans le cadre d'une vérification lors d'un deuxième contrôle (non systématique) au cours de l'une des deux campagnes suivantes, lorsque l'exploitant aura déclaré dans sa déclaration PAC de la campagne suivant le contrôle initial, au plus tard avant le 15 mai de cette campagne, une surface de bosquet et de mares égale ou supérieure à la surface initiale pour chaque catégorie.

Point de contrôle n° 2 – La taille des haies et des arbres

Il est vérifié l'absence de taille des haies et des arbres entre le 1^{er} avril et le 31 juillet inclus.

GRILLE « BCAA » - « MAINTIEN DES PARTICULARITÉS TOPOGRAPHIQUES »

Points vérifiés	Anomalies	Système d'avertissement précoce		Réduction
		Applicable ?	Délai de remise en conformité	
Maintien des particularités topographiques	Non-respect de l'obligation de maintien d'une haie : <ul style="list-style-type: none"> inférieur ou égal à 3 % du linéaire (ou inférieur ou égal à 2 mètres) 	oui, si non-respect inférieur ou égal à 1 % du linéaire	campagne suivante (15 mai N+1)	1 %
	<ul style="list-style-type: none"> plus de 3 % et inférieur ou égal à 10 % du linéaire (ou plus de 2 mètres et inférieur ou égal à 6 mètres) 	non		3 %
	<ul style="list-style-type: none"> plus de 10 % et inférieur ou égal à 20 % du linéaire (ou plus de 6 mètres et inférieur ou égal à 15 mètres) plus de 20 % du linéaire (et plus de 15 mètres) 	non		5 %
	<p><i>NB :</i></p> <ul style="list-style-type: none"> <i>on entend par « linéaire » le linéaire total de l'exploitation</i> <i>le déplacement, le remplacement ou la destruction d'une haie dans le cadre dérogatoire réglementaire ne sont pas considérés comme des cas de non-respect</i> 			intentionnelle
	Non-respect de l'obligation de déclaration préalable pour effectuer un déplacement, un remplacement ou une destruction de haie	non		1 %
	Non-respect de l'obligation de maintien d'un élément surfacique (mare ou bosquet) : <ul style="list-style-type: none"> inférieur ou égal à 3 % de la surface (ou inférieur ou égal à 1 are) pour chaque catégorie 	oui, si non-respect inférieur ou égal à 1 % de la surface pour chaque catégorie	campagne suivante (15 mai N+1)	1 %
	<ul style="list-style-type: none"> plus de 3 % et inférieur ou égal à 10 % de la surface (ou plus de 1 are et inférieur ou égal à 5 ares) pour au moins une catégorie 	non		3 %
	<ul style="list-style-type: none"> plus de 10 % et inférieur ou égal à 20 % de la surface (ou plus de 5 ares et inférieur ou égal à 10 ares) pour au moins une catégorie 	non		5 %
	<ul style="list-style-type: none"> plus de 20 % de la surface (et plus de 10 ares) pour au moins une catégorie 	non		intentionnelle
Taille des haies et des arbres	Non-respect de l'interdiction de taille des haies et des arbres entre le 1 ^{er} avril et le 31 juillet	non		3 %



APPENDIX 3. Land-use survey example

Information on farmers

Survey Number: 1

Last name:

First name:

Address: **La Lande de Montomblay**

City: **Sains**

Phone number: XX

Information on the exploitation

Installation date: 18/10/2011 (actual farmer); Creation dates of exploitation → 1983-1984

Total surface area exploited: 227 hectares

% UAA in ownership: 223 hectares

% of spreadable UAA: 209 hectares

Breeding: YES NO

Type of breeding: Cattle Pork Chicken Other:

Does effluent management have an impact on catch crops management? If yes, on which interventions (location, nature of the cover, destruction) and why?

Yes, use of the Ryegrass and clover and rapeseed in September to empty the pits. Equally for cornfield but the date of spreading authorized on corn is increasingly far away (March 1 currently).

N° /Parcel	Crops 2015-16	Harvest date	Crops 2016-17	Sowing date	Catch crops	Date and sowing practice	Date and destruction mode	Other interventions
1 - 1	Grass	Grazing land	Corn	Mid-April 2017 (20)	Ryegrass	Beginning September 2016	Grazing and mechanics	Catch crops: Cover crop + ploughing
2 - 2	Winter Wheat	End July (20)	Winter barley	18/10/2016				
3 - 3	Winter Wheat	End July (20)	Maize	Mid-April 2017 (20)	Oat + Phacelia	Beginning September 2016	Mechanical with plough	
4 - 4	Winter Wheat	End July (20)	Winter barley	18/10/2016				
5 - 5	Winter Wheat	End July (20)	Maize	Mid-April 2017 (20)	Oat + Phacelia	Beginning September 2016	Mechanical with plough	
6 - 6	Rapeseed	Beginning July	Maize	20-25/10/2016				
7 - 7	Winter Wheat	End July (20)	Winter barley	18/10/2016				
8 - 8	Barley	End June / Beginning July	Corn	Mid-April 2017 (20)	Oat + Phacelia	Beginning September 2016	Mechanical with plough	
9 - 9	Fodder Maize	Mid-September	Winter Wheat	20-25/10/2016				
10 - 10	Colza	Beginning July	Winter Wheat	20-25/10/2016				
11 - 11	Fodder Maize	Mid-September	Maize	Mid-April 2017 (20)	Oat + Phacelia	Beginning September 2016	Mechanical with plough	

12 - 12	Winter Wheat	End July (20)	Maize	Mid-April 2017 (20)	Oat + Phacelia	Beginning September 2016	Mechanical with plough
13 - 13	Rapeseed	Beginning July	Winter Wheat	20-25/10/2016			
14 - 14	Winter Wheat	End July (20))	Rapeseed	8-9/09/2016			
15 - 15	Winter Wheat	End July (20)	Fodder Maize	Mid-April 2017 (20)	Oat + Phacelia	Beginning September 2016	Mechanical with plough
16 - 16	Corn	Beginning October	Winter Wheat	20-25/10/2016			
17 - 17	Winter Wheat	End July (20)	Maize	Mid-April 2017 (20)	Oat + Phacelia	Beginning September 2016	Mechanical with plough
18 - 18	Winter Wheat	End July (20)	Maize	Mid-April 2017 (20)	Ryegrass	Beginning September 2016	Grazing/ Mechanical with plough
19 - 19	Winter Wheat	End July (20)	Colza	8-9/09/2016			
20 - 20	Winter Wheat	End July (20)	Maize	Mid-April 2017 (20))	Ryegrass	Beginning September 2016	Grazing/ Mechanical with plough
21 - 21	Winter Wheat	End July (20)	Colza	8-9/09/2016			
22 - 22	Winter Wheat	End July (20)	Maize	Mid-April 2017 (20)	Oat + Phacelia	Beginning September 2016	Mechanical with plough
23 - 23	Fodder Maize	Mid-September	Winter Wheat	20-25/10/2016			
24 - 24	Winter Wheat	End July (20))	Rapeseed	8-9/09/2016			

25 - 25	Winter Wheat	End July (20)	Winter barley	18/10/2016			
26 - 26	Winter Wheat	End July (20)	Winter barley	18/10/2016			
27 - 27	Winter barley	End June/ Beginning July	Linen	Mid-March 2017	Oat + Phacelia	Beginning September 2016	Mechanical with plough
28 - 28	Winter barley	End June / Beginning July	Rapeseed	8-9/09/2016			
29 - 29	Fodder Maize	Mid-September	Maize	Mid-April 2017 (20)	Oat + Phacelia	Beginning September 2016	Mechanical with plough
30 - 30	Corn	Beginning October	Winter Wheat	20-25/10/2016			
31 - 31	Fodder corn	Mid-September	Maize	Mid-April 2017 (20)	Oat + Phacelia	Beginning September 2016	Mechanical with plough
32 - 32	Winter barley	End June / Beginning July	Rapeseed	8-9/09/2016			
33 - 33	Grasslands		Grasslands				
34 - 34	Fodder Maize	Mid-September	Winter Wheat	20-25/10/2016			
35 - 35	Corn	Beginning October	Winter Wheat	20-25/10/2016			
36 - 36	Fodder Maize	Mid-September	Winter Wheat	20-25/10/2016			

Additional information provided by the farmer:

- ✓ Total cereal area: 35 hectares
- ✓ The majority of his corn and cereals are destined to be sold (very little fodder)
- ✓ He plans to plant his maize around April 20, or even earlier depending on the weather conditions
- ✓ For linseed, he plans to sow it in mid-March and beat it around mid-September
- ✓ Regarding the treatments
 - On wheat, for seeds, gaucho treatment
 - Nitrate + sulfur treatment with a first pass planned for mid-March
 - Weeding carried out so early in the sowing season, otherwise in February-March

List of figures

Figure I.1: Mapping demonstrating the confusion between land use and land cover (Hu et al., 2016).	14
Figure I.2: illustration of two types of winter crops. A) Winter wheat, B) Winter barley and C) Rapeseed.	16
Figure I.3: Illustration of grassland types.	17
Figure I.4: Illustration of catch crops no used. A) Phacelia; B) Mustard.	18
Figure I.5: Illustration of catch crops used. A) Ryegrass; B) Fodder cabbage.	19
Figure I.6: Illustration of a crop residues parcel.	20
Figure I.7: Illustration of a temporary bare soil.	20
Figure I.8: Electromagnetic spectrum (“Electromagnetic Spectrum,” 2016).	27
Figure I.9: Illustration of vegetation indexes derived from a Sentinel-2 image from May 2017 using a Red Green Blue (RGB) color composition. NDVI in Red (R); NDWI in Green (G); SAVI in Blue (B).	30
Figure I.10: Atmospheric absorption bands in relation to radar wavelengths (“HUMBOLDT State university,” 2019).	31
Figure I.11: SAR image property (Lee and Pottier, 2009).	32
Figure I.12: SAR images geometric distortions (Lusch, 1999).	33
Figure I.13: Illustration of HV backscattering coefficient parameter derived from a Radarsat-2 images using a RGB color composition. HV from 10 December 2016 in Red (R); HV from 20 February 2017 in Green (G); HV from 03 May 2017 in Blue (B).	35
Figure I.14: Illustration of SPAN parameter derived from a Radarsat-2 images using a RGB color composition. SPAN from 10 December 2016 in Red (R); SPAN from 20 February 2017 in Green (G); SPAN from 03 May 2017 in Blue (B).	37
Figure I.15: The dominant scattering mechanisms (a) single bounce, (b) double bounce and (c) diffuse scattering (Lee and Pottier, 2009).	37
Figure I.16: The three main scattering mechanisms.	39

Figure I.17: Illustration of Cloude and Pottier decomposition derived from a Radarsat-2 image of April 2017 using a RGB color composition. Alpha in Red (R); Anisotropy in Green (G); Entropy in Blue (B).	40
Figure I.18: Illustration of Freeman and Durden decomposition derived from a Radarsat-2 image of April 2017 using a RGB color composition. Double-bounce in Red (R); Surface in Green (G); Volume in Blue (B).	41
Figure I.19: Illustration of Shannon Entropy (SE) parameter derived from a Radarsat-2 images using a RGB color composition. SE from 10 December 2016 in Red (R); SE from 20 February 2017 in Green (G); SE from 03 May 2017 in Blue (B).	42
Figure I.20: Illustration of Radar Vegetation Index (RVI) parameter derived from a Radarsat-2 images using a RGB color composition. RVI from 10 December 2016 in Red (R); RVI from 20 February 2017 in Green (G); RVI from 03 May 2017 in Blue (B).	43
Figure I.21: Illustration of Pedestal Height (PED) parameter derived from a Radarsat-2 images using a RGB color composition. PED from 10 December 2016 in Red (R); PED from 20 February 2017 in Green (G); PED from 03 May 2017 in Blue (B).	43
Figure I.22: Location of the « Zone Atelier Armorique », sub-site of « Pleine Fougères ».	52
Figure I.23: Location of the regional study site, Brittany.	54
Figure I.24: Test results performed on Radarsat-2 images with different filters and window sizes.	59
Figure I.25: Localization and illustration of land-use records.	62
Figure I.26: Localization and illustration of land-use surveys.	63
Figure I.27: Localization of weather stations and illustration of weather records.	63
Figure I.28: Main crops in A) summer 2016, B) summer 2017.	65
Figure I.29: Winter land-use established during winter 2016-2017.	65
Figure I.30: Catch crops established during winter 2016-2017, with catch crops no used in blue and catch crops used in grey. RGI: Italian Ryegrass.	66
Figure I.31: Umbrothermal diagram over the period September 2016 - July 2017.	66
Figure I.32: General methodology implemented in this thesis.	70
Figure I.33: Maximum Likelihood conceptual example.	72
Figure I.34: Mechanism of Support Vectors Machines adapted of (Burges, 1998).	73
Figure I.35: Random forest algorithm example.	74
Figure I.36: Time-Weighted Dynamic Time Wrapping conceptual example.	75
Figure II.1: The five main winter land-use types in the study area.	93

- Figure II.2:** Winter land-use classification accuracy according to classification algorithms. Box-and-whisker plots represent the variation in classification accuracy based on 100 iterations. 102
- Figure II.3:** Temporal profiles of SAR parameters VH and VV, optical parameters NDWI and NDVI (the central line corresponds to the median of each class and the profile limits correspond to the interquartile, 1st (lower) and 3rd (upper)), rainfall, and temperature for winter crops at the study site from September 2016 to May 2017. 104
- Figure II.4:** Temporal profiles of SAR parameters VH and VV, optical parameters NDWI and NDVI (the central line corresponds to the median of each class and the profile limits correspond to the interquartile, 1st (lower) and 3rd (upper)), rainfall, and temperature for catch crops at the study site from September 2016 to May 2017. 106
- Figure II.5:** Temporal profiles of SAR parameters VH and VV, optical parameters NDWI and NDVI (the central line corresponds to the median of each class and the profile limits correspond to the interquartile, 1st (lower) and 3rd (upper)), rainfall, and temperature for crop residue at the study site from September 2016 to May 2017. 108
- Figure II.6:** Temporal profiles of SAR parameters VH and VV, optical parameters NDWI and NDVI (the central line corresponds to the median of each class and the profile limits correspond to the interquartile, 1st (lower) and 3rd (upper)), rainfall, and temperature for grasslands at the study site from September 2016 to May 2017. 110
- Figure II.7:** Parameters that contributed the most to land use classifications, ranked by importance for (a) optical and (b) Synthetic-Aperture Radar image time-series from August 2016 to May 2017. See Table 3 for the definition of abbreviations. 111
- Figure II.8:** Distribution of (a) the Soil Adjusted Vegetation Index (SAVI) and (b) the ratio VH/VV parameters for winter land use classes calculated from May 2017 images. 112
- Figure II.9:** Most contributing parameters to land-use classifications, ranked by importance for (a) SAR and (b) optical image time-series from August 2016 to May 2017. The most important parameters are in bold. The red lines indicate the break in each histogram used as the threshold for selecting the most important parameters. 113
- Figure II.10:** Overall accuracy of (a) object-based and (b) pixel-based image classifications of winter land use, for the best Sentinel-1, Sentinel-2 and combined Sentinel-1 and -2 parameters using the Random Forest (RF) and Support Vector Machine (SVM) algorithms. 115
- Figure II.11:** Distribution of winter land use obtained using a parameter dataset derived from a combination of Sentinel-1 and -2 time-series. Classification was performed using a Random Forest algorithm. 116
- Figure II.12:** Map of the distribution of winter land use membership probabilities obtained using the Random Forest algorithm. 117
- Figure II.13:** Map of winter land-use obtained from the Sentinel-2 image time-series. A Random Forest algorithm classification was performed. 118

- Figure III.1:** Study site location, ground surveys (RGB composite image constructed from Shannon Entropy extracted from ALOS-2 data for three dates: 03-09-2017, 04-15-2017 and 05-13-2017. ©Kalidéos data 2017 and JAXA data). 136
- Figure III.2:** The main land-use types encountered in winter in the study area: a) winter crops (winter barley), b) catch crops (mustard), c) grasslands and d) crop residues (maize stalks). 137
- Figure III.3:** Importance (in %) of quad-pol SAR parameters based on 100 Random Forest classifications. Parameters related to backscattering coefficients are in black, while polarimetric parameters are in gray. SE: Shannon Entropy. 144
- Figure III.4:** Importance (in %) of dual-pol SAR parameters based on 100 Random Forest classifications using (A) ALOS-2 parameters, B) RADARSAT-2 parameters and C) Sentinel-1 parameters). Parameters related to backscattering coefficients are in black, while polarimetric parameters are in gray. SE: Shannon Entropy. 145
- Figure III.5:** Comparison of classification accuracy of each land-use class between dual and quad polarization (pol) modes. Box-and-whisker plots represent the variation in Random Forest classification accuracy based on 100 iterations. Whiskers indicate 1.5 times the interquartile range. 146
- Figure III.6:** Comparison of classification accuracy of each land-use class among band frequencies. Box-and-whisker plots represent the variation in Random Forest classification accuracy based on 100 iterations. Whiskers indicate 1.5 times the interquartile range. 147
- Figure III.7:** Comparison of classification accuracy of each land-use class between adjusted and dense Sentinel-1 time-series. Box-and-whisker plots represent the variation in Random Forest classification accuracy based on 100 iterations. Whiskers indicate 1.5 times the interquartile range. 148
- Figure III.8:** Comparison of classification accuracy of each land-use class among SAR sensors. Box-and-whisker plots represent the variation in RF classification accuracy based on 100 iterations. Whiskers indicate 1.5 times the interquartile range. 149
- Figure III.9:** Map of winter land-use classes obtained using a parameter dataset derived from the Sentinel-1 dense time-series. Classification was performed using the Random Forest algorithm. 150
- Figure IV.1:** Location of the study site, Brittany, in France (RGB composite image from Sentinel-2 data, 2017, ©Copernicus data 2017) and representation of the utilized agricultural area (UAA) of fields declared and undeclared under the Common Agricultural Policy. 172
- Figure IV.2:** The main land-use types encountered in winter in the study area of Brittany, France: a) winter crops (winter barley), b) catch crops (phacelia), c) crop residues (maize stalks) and d) grasslands. 172
- Figure IV.3:** Map of crop-residue parcels obtained from Sentinel-2 NDVI time-series using a threshold of 0.25. 176
- Figure IV.4:** Map of the date when parcels became covered by crop residues, obtained from Sentinel-2 NDVI time-series images using a threshold of 0.25. 177

Figure IV.5. Boxplots of classification accuracies of (A) three or (B) seven land-use classes based on 100 Random Forest iterations. Whiskers indicate 1.5 times the interquartile range. **178**

Figure IV.6. Map of declared winter land-use based on Sentinel-2 time-series images. The classification was performed using the Random Forest algorithm and the “Registre Parcellaire Graphique” (RPG) samples. **179**

Figure IV.7. Map of undeclared winter land-use fields based on Sentinel-2 image time-series. Fields were classified by applying a Random Forest algorithm to “BD Parcellaire” samples. **180**

List of tables

Table I.1: Catch crops no use authorized during the winter season.	18
Table I.2: Microwave frequency of SAR sensors.	31
Table I.3: Geometric and matrix representations of canonical targets adapted from (Lee and Pottier, 2009).	39
Table I.4: Winter land-use classification.	52
Table I.5: Sentinel-2 images. NIR: Near-infrared, SWIR: Shortwave-infrared.	55
Table I.6: Characteristics of the RADARSAT-2, Alos-2, and Sentinel-1 SAR images.	57
Table II.1. Types and sub-types of winter land-use classified in the study.	94
Table II.2. Characteristics of Sentinel-1 and Sentinel-2 images. Dates in bold text for Sentinel-1 images indicate those with sparse time-series, while asterisks indicate those with dense time-series.	95
Table II.3. Median accuracy of winter land use classifications obtained for the best Sentinel-1, Sentinel-2 and combined Sentinel-1 and -2 parameters using the Random Forest (RF) and Support Vector Machine (SVM) algorithms. OA: overall accuracy, Kappa: Kappa index.	115
Table II.4. Confusion matrix of the best winter land use classification obtained using a parameter dataset derived from a combination of Sentinel-1 and -2 time-series. Overall accuracy = 81%, Kappa index = 0.77.	116
Table II.5. Mean accuracy (overall accuracy (OA) and Kappa index) of winter land-use classifications based on the most efficient Sentinel-1, Sentinel-2, and combined Sentinel-1 and -2 datasets using the Random Forest algorithm.	117
Table II.6. Confusion matrix of the best winter land-use classification obtained using the Sentinel-2 time-series. Overall accuracy = 87%, Kappa index = 0.85.	119
Table III.1. Land-use classification	137
Table III.2: Characteristics of the RADARSAT-2, Sentinel-1 and ALOS-2 images used in the study. Dates in bold text for Sentinel-1 images indicate those with adjusted time-series, while asterisks indicate those with dense time-series.	139

Table III.3. Confusion matrix of winter land-use obtained from RF classification using the SAR parameter dataset extracted from the S-1 dense time-series dataset.	151
Table IV.1. The land-use classes included in two classification levels. Asterisks indicate classes not included in the “Registre Parcellaire Graphique”.	173
Table IV.2. Parameters derived from Sentinel-2 image time-series	174
Table IV.3. Mean classification accuracy of 3 or 7 classes of winter land-use obtained for the best Sentinel-2 parameters using the Random Forest algorithm and a pixel-based or parcel-based approach. OA: overall accuracy.	178
Table IV.4. Confusion matrix of the best winter land-use classification of declared fields obtained using the Sentinel-2 time-series. Kappa index = 0.77.	179
Table IV.5. Confusion matrix of the best winter land-use classification of undeclared fields obtained using the Sentinel-2 time-series.	180

Résumé étendu

Les surfaces agricoles occupent actuellement plus d'un tiers des terres émergées à l'échelle du globe et doivent permettre à l'horizon 2030 de nourrir plus de 8,5 milliards d'êtres humains. Face à l'augmentation constante de la population mondiale et dans le cadre du réchauffement climatique planétaire, un des enjeux majeurs de ce siècle réside dans notre capacité à produire suffisamment de nourriture et de manière durable, tout en préservant les ressources naturelles et en limitant les pressions exercées par nos sociétés sur l'environnement. Dans ce contexte, de nombreux travaux scientifiques ont montré les impacts négatifs de l'intensification et des changements de l'usage des sols (progression de la monoculture, suppression de haies bocagères, développement de l'usage d'intrants tels que l'azote, les pesticides et le phosphore...) sur l'environnement à travers l'observation de la dégradation de la qualité de l'eau, des sols, de l'air, et de la santé des populations (Lambin and Meyfroidt, 2011; Newbold et al., 2015). Ceci est particulièrement visible dans les régions telles que la Bretagne où l'agriculture intensive domine, et où les changements des pratiques agricoles, la fragmentation des paysages, les bouleversements de l'utilisation des sols qui se sont produits depuis plusieurs décennies ont entraîné des perturbations profondes de l'environnement. Pour pallier ces impacts, des législations et des programmes européens nationaux et locaux ont été élaborés à partir des années 90, entraînant la mise en place d'opérations d'aménagement du territoire et d'actions permettant de modifier les pratiques agricoles. Ainsi, une nouvelle série de mesures environnementales a été initiée au début des années 2000 par les instances européennes imposant l'implantation de couverts végétaux et d'éléments paysagers durant la période hivernale qui est déterminante dans le transfert de flux polluants ("Nitrates Directive," 2019).

Le suivi du couvert végétal en hiver est un enjeu environnemental et scientifique majeur en milieu agricole. D'un point de vue environnemental, la présence et le type de couverture végétale en hiver influencent le transport des polluants vers les cours d'eau en réduisant les pertes de nitrates, de nutriments, de pesticides ou de sédiments des champs agricoles (Galloway et al., 2008; Withers et al., 2014). L'absence de couverture végétale agit comme un accélérateur lorsque les sols sont dénudés après une culture principale (maïs, colza, etc.), tandis que les cultures dérobées agissent comme un obstacle aux transferts de flux et de matières (Dabney, 1998). Dans ce contexte, l'identification et la caractérisation de l'utilisation hivernale des terres est une composante majeure de la restauration de la qualité de l'eau et de la gestion durable dans les paysages agricoles (Corgne, 2004). **Cependant la connaissance des dynamiques spatio-temporelles associées à l'utilisation du sol en période hivernale demeure aujourd'hui encore un défi pour la communauté scientifique.** En effet, d'un point de vue méthodologique, la caractérisation de la dynamique spatio-temporelle de l'utilisation et de l'occupation du sol (UTCL) à l'échelle de la parcelle agricole est difficile en raison de la diversité des stratégies et pratiques agricoles en hiver. L'identification de l'utilisation des terres en hiver demeure un défi scientifique majeur pour la communauté de la télédétection.

Dans ce contexte, la télédétection spatiale est apparue comme un outil privilégié afin de mettre en place des suivis et des méthodes d'identification de l'utilisation du sol à large échelle. Au début des années 2000, un certain nombre de travaux scientifiques ont montré l'intérêt de la télédétection optique à moyenne résolution spatiale (de 250 m à 1km) pour répondre à cet enjeu. Les travaux de Clark et al., (2010) et Zhang et al., (2003) ont ainsi permis d'élaborer les premières méthodes de discrimination de grands ensembles cultureux sur de grandes surfaces. Néanmoins, les limites de ces capteurs optiques à moyenne résolution ont

été rapidement atteintes pour étudier l'usage des sols au cours de la période hivernale, en particulier dans les régions où les parcelles sont de petite taille, seuls les îlots parcellaires à dominante de sols nus ayant pu être identifiés (Lecerf et al., 2005). Par la suite, des données de télédétection spatiale optique à très haute résolution ont été évaluées afin d'effectuer une cartographie annuelle de l'utilisation du sol intégrant les cultures hivernales. Toutefois, la limite de ce type de données réside dans le faible nombre d'images exploitables pendant la période hivernale au cours de laquelle le couvert nuageux peut être fréquent (Guerschman et al., 2015; Lillesand et al., 2015; Xu and Guo, 2014). Dans ce contexte, la télédétection spatiale active permet de lever cette contrainte dans la mesure où elle permet de s'affranchir des conditions météorologiques, atmosphériques et d'illumination. Le développement, depuis une vingtaine d'années, de capteurs RSO tels que Radarsat-2 permettant l'acquisition de séries temporelles plus denses à haute résolution spatiale a conforté l'intérêt de ces derniers pour l'identification et la caractérisation de l'utilisation du sol en période hivernale. Jiao et al., (2010); McNairn et al., (2001) et Skriver, (2011) ont ainsi souligné l'intérêt de ces données pour la classification de l'utilisation du sol grâce à l'utilisation des propriétés diélectriques du sol, de la rugosité de surface et de la structure du couvert végétal. Le lancement à partir des années 2014-2015 des satellites RSO et optique Sentinel-1 et -2 permet d'envisager de nouvelles possibilités quant à l'étude de l'utilisation hivernale du sol. Ainsi, Belgiu and Csillik, (2018) et Vuolo et al., (2018) ont démontré le potentiel des images Sentinel-2 afin de cartographier l'utilisation du sol durant la période végétative. De leur côté, Bargiel, (2017) et Veloso et al., (2017) ont illustré l'intérêt des données Sentinel-1 pour l'étude et la classification des cultures annuelles. Cependant, jusqu'à présent très peu de recherches ont su démontrer l'intérêt de l'imagerie RSO pour l'identification et la caractérisation de l'utilisation hivernale des sols, les principaux travaux effectués portant sur la détermination du taux de couverture des sols (Minh et al., 2018).

C'est dans ce contexte que s'inscrivent ces travaux de thèse dont l'objectif est d'évaluer le potentiel de séries temporelles d'images optiques et radar à synthèse d'ouverture (RSO) à haute résolution spatiale pour l'étude de l'utilisation des sols en période hivernale à une échelle locale et régionale. Plus précisément, elle consiste à développer, à partir de ces séries temporelles, des méthodes afin de (1) déterminer la méthode de classification la plus adaptée pour identifier l'usage des sols en hiver, tant au niveau du classifieur lui-même que de l'approche de classification (pixel ou orientée-objet); (2) comparer des images RSO Sentinel-1 et optiques Sentinel-2 et (3) définir la configuration RSO la plus adaptée en comparant trois séries temporelles d'images (Alos-2, Radarsat-2 et Sentinel-1).

Nous avons tout d'abord évalué la contribution respective des séries temporelles optiques et RSO en comparant des algorithmes de classification pour identifier l'utilisation des terres en hiver. Pour ce faire, des images Sentinel-1 et 2 acquises sur la période août 2016-mai 2017 ont été classées à l'aide des algorithmes Séparateurs à Vastes Marges (SVM) et Random Forest (RF) appliqués avec des approches pixel et orientée objet dans une zone agricole de 130 km² localisée en France, au Sud-ouest de la baie du Mont-Saint-Michel, dont la taille des parcelles varie de 0,1 à 65 ha, avec une moyenne de 2,1 ha. Globalement, les résultats montrent que l'utilisation des terres en hiver peut être identifiée avec précision à l'aide des séries chronologiques Sentinel-1 et Sentinel-2 combinées avec une approche basée sur les pixels utilisant un algorithme RF. Dans le détail, ils ont mis en évidence l'intérêt de l'algorithme de classification RF comparativement à l'algorithme SVM. Les résultats montrent la supériorité

de Sentinel-2 sur Sentinel-1, la précision de la classification obtenue avec le premier étant supérieure à 5% par rapport à celle obtenue avec le second. Ils soulignent également que la précision de la classification s'améliore lorsqu'on utilise une combinaison des séries temporelles Sentinel-1 et 2, la couverture hivernale des sols étant identifiée avec une précision globale de 81 % (indice kappa de 0,77) contre 75 % (indice Kappa de 0,70) pour la série temporelle Sentinel-2 utilisée seule. En outre, l'analyse des paramètres Sentinel-1 et Sentinel-2 utilisés pour identifier l'utilisation des terres en hiver a conduit à des recommandations pour l'extraction de caractéristiques lors de la cartographie de l'utilisation des terres en hiver, les résultats révélant l'avantage d'utiliser les coefficients de rétrodiffusion seuls ou combinés avec l'indice NDVI. Nos résultats ont également montré les limites de cette approche pour identifier l'utilisation des terres d'hiver : D'une part, la nomenclature définie lors de cette première étude n'était pas optimale pour identifier et caractériser finement l'utilisation hivernale du sol dans la mesure où elle comprend une classe « Sols nus » qui ne correspond qu'à un état de surface des sols temporaire au cours de la période hivernale et où elle inclue dans une seule classe « cultures d'hiver » des cultures aux signatures spectrales différentes, ce qui entraîne des erreurs de classification. D'autre part, des erreurs de classification sont localisées dans les petites parcelles, en raison de la résolution spatiale des capteurs Sentinel.

Nous avons ensuite cherché à évaluer le potentiel des données Sentinel-1 et 2 pour identifier l'utilisation hivernale du sol, mais avec une nomenclature plus détaillée qui prend en compte la diversité des types d'utilisation des sols en hiver et sans déterminer une classe spécifique aux sols nus. Pour se faire, la méthodologie qui a été mise en œuvre sur le même site d'étude comprend deux étapes : (1) Une analyse détaillée des interactions signaux/cultures hivernales à partir de paramètres optiques ou RSO extraits des séries temporelles d'images Sentinel-1 et 2 ; (2) Une classification fine des types d'utilisation hivernale des sols en utilisant l'algorithme RF. Les résultats montrent que les données optiques permettent de classer les types d'utilisation hivernale des sols avec une plus grande précision que les données RSO (précision globale de 87 % et indice Kappa de 0,85 pour Sentinel-2 contre 73 % et 0,70 pour Sentinel-1). Les résultats indiquent également que la combinaison des données Sentinel-1 et Sentinel-2 réduit légèrement la précision de la classification (précision globale = 83 %, indice Kappa = 0,82). Cette étude montre aussi le potentiel et des paramètres NDVI et NDWI dérivés de l'imagerie Sentinel-2 pour discriminer finement les classes d'utilisation hivernale du sol. Bien qu'elle souligne l'intérêt des séries temporelles optiques, cette étude met aussi en évidence que les séries chronologiques SAR peuvent être utiles dans les régions à forte couverture nuageuse.

Ensuite, nous nous sommes focalisés sur l'évaluation de l'imagerie RSO pour identifier l'utilisation du sol en période hivernale. Plus précisément, nous avons étudié la contribution de la fréquence (bandes C/L), de la polarisation (double/quad polarisation) et de la densité des séries chronologiques d'images sur le même site d'étude. Tout d'abord, des paramètres RSO ont été dérivés de séries temporelles Radarsat-2, Sentinel-1 et Alos-2, et un ensemble de paramètres quad-pol et six ensembles de données bi-pol ont été calculés avec différentes résolutions spatiales et densités. Ensuite, une classification Random Forest a été effectuée pour chacun des 7 ensembles de données de paramètres SAR qui avaient été générés auparavant afin de déterminer la configuration RSO la plus appropriée pour identifier les modes d'usage des terres en hiver. Les résultats soulignent que (1) la bande C (précision globale de 72 %) est supérieure à la bande L (précision globale de 63 %), (2) le mode quad-pol (précision globale de

70 %) surpasse le mode double-pol (précision globale de 58 %) et (3) la série temporelle dense Sentinel-1 (précision globale de 72 %) est supérieure aux séries temporelles Radarsat-2 et Alos-2 (précision globale de respectivement 70 et 38 %). De plus, les résultats indiquent que l'entropie de Shannon et le SPAN (puissance totale de la matrice de cohérence) que soit en pleine polarisation ou en double-polarisation sont les paramètres les plus discriminants. Cette étude permet de choisir les configurations RSO les plus appropriées pour l'identification de l'utilisation hivernale des terres, soit la série temporelle Sentinel-1 (bande C,) en polarisation double, et dense dans le cas de cette étude.

Sur la base des résultats obtenus dans les trois études précédentes, nous avons alors retenu les données et l'algorithme de classification les plus adaptés pour identifier l'utilisation hivernale du sol à une régionale. L'objectif de cette étude était de tester la reproductibilité de l'approche développée initialement à une échelle locale. Plus précisément, les données Sentinel-2 ont été sélectionnées afin de déterminer, sur l'ensemble de la région Bretagne, l'utilisation hivernale du sol, sachant que celle-ci n'est connue que pour les parcelles déclarées au système PAC dans le recensement parcellaire graphique (RPG), à savoir les parcelles susceptibles de recevoir des aides de l'Union Européenne. Dans un premier temps, des séries temporelles Sentinel-2 ont été classées sur les parcelles déclarées dans le RPG en utilisant l'algorithme RF, après avoir adapté la nomenclature utilisée à l'échelle locale au niveau régional en deux niveaux emboîtés. Les résultats obtenus au niveau 1 qui comprend 3 classes (cultures d'hiver, intercultures prairies) ont souligné l'intérêt de cette approche pour discriminer les types d'utilisation des sols, avec une précision globale de 84% et un indice de kappa de 0,77. A l'inverse, ces résultats ont souligné les limites de l'approche pour une classification plus détaillée, puisque la précision globale et l'indice de kappa atteignent respectivement 65% et 0.59 avec la nomenclature de niveau 2 qui comprend 7 classes. Le modèle de classification établi au niveau 1 a alors été appliqué aux parcelles non déclarées et couvertes par des résidus de cultures, ces parcelles ayant été préalablement identifiées partir d'une série temporelle de NDVI dérivée des images Sentinel-2. La cartographie produite sur l'usage des sols en hiver à l'échelle parcellaire et sur toute une région constitue une information inédite.

De manière générale, cette thèse a permis de montrer le potentiel des séries temporelles de données de télédétection à haute résolution spatiale, quelles soit optiques (Sentinel-2) ou radar (Sentinel-1, Radarsat-2 et Alos-2) pour l'identification et la caractérisation de l'utilisation du sol en hiver. Si cette thèse a permis de montrer que les données Sentinel-2 sont les plus adaptées pour étudier l'utilisation du sol en période hivernale, les images RSO ont tout leur intérêt dans les régions où le couvert nuageux est important, les séries temporelles denses Sentinel-1 ayant été définies comme les plus performantes. Les résultats obtenus, tant à l'échelle locale qu'à l'échelle régionale, permettent d'ouvrir de nouvelles perspectives en termes de développements méthodologiques, telles que la fusion des données ou la classification basée sur le deep learning. En outre, l'information produite au sein de cette thèse pourra être utilisée pour effectuer des diagnostics environnementaux et mettre en place des actions permettant de limiter les risques liés aux transferts de flux polluants au sein des hydrosystèmes.

Titre : Evaluation de séries temporelles d'images RSO et optiques pour l'étude de l'utilisation des sols en période hivernale.

Mots clés : Télédétection, Agriculture, Sentinel-1 and -2, Radarsat-2, Alos-2, Classification.

Résumé : L'étude de l'utilisation hivernale du sol représente un enjeu majeur afin de préserver et d'améliorer la qualité des sols et des eaux de surfaces. Cependant la connaissance des dynamiques spatio-temporelles associées à l'utilisation du sol en période hivernale demeure aujourd'hui encore un défi pour la communauté scientifique. C'est dans ce contexte que s'inscrivent ces travaux de thèse dont l'objectif est d'évaluer le potentiel de séries temporelles d'images optiques et RSO à haute résolution spatiale pour l'étude de l'utilisation des sols en période hivernale à une échelle locale et régionale. Pour se faire, une méthodologie a été établie afin : (i) de déterminer la méthode de classification la plus adaptée pour identifier l'usage des sols en hiver; (ii) de comparer des images RSO Sentinel-1 et optiques Sentinel-2; (iii) de définir la configuration RSO la plus adaptée en comparant trois séries temporelles d'images (Alos-2, Radarsat-2 et Sentinel-1).

Les résultats ont tout d'abord mis en évidence l'intérêt de l'algorithme de classification Random Forest pour discriminer à une échelle fine les types d'usage des sols en hiver qui sont très variés. Dans un second temps, ils ont souligné l'intérêt des données Sentinel-2 pour cartographier l'utilisation hivernale des sols à une échelle locale et régionale. Enfin, ils ont permis de déterminer qu'une série temporelle dense d'images Sentinel-1 était la configuration RSO la plus adaptée afin d'identifier l'utilisation hivernale du sol. De manière générale, si cette thèse a permis de montrer que les données Sentinel-2 sont les plus adaptées pour étudier l'utilisation du sol en période hivernale, les images RSO ont tout leur intérêt dans les régions où le couvert nuageux est important, les séries temporelles denses Sentinel-1 ayant été définies comme les plus performantes.

Title : Evaluation of time-series SAR and optical images for the study of winter land-use.

Keywords: Remote sensing, Agriculture, Sentinel-1 and -2, Radarsat-2, Alos-2, Classification.

Abstract : The study of winter land-use is a major challenge in order to preserve and improve the quality of soils and surface water. However, knowledge of the spatio-temporal dynamics associated with winter land-use remains a challenge for the scientific community. In this context, the objective of this study is to evaluate the potential of time series of high spatial resolution optical and SAR images for the study of winter land-use at a local and regional scale. For that purpose, a methodology has been established to: (i) determine the most suitable classification method for identifying winter land-use; (ii) compare Sentinel-1 SAR and Sentinel-2 optical images; (iii) define the most suitable SAR configuration by comparing three image time-series (Alos-2, Radarsat-2 and Sentinel-1).

The results first of all highlighted the interest of the Random Forest classification algorithm to discriminate at a fine scale the different types of land use in winter. Secondly, they showed the value of Sentinel-2 data for mapping winter land-use at a local and regional scale. Finally, they determined that a dense time series of Sentinel-1 images was the most appropriate SAR configuration to identify winter land-use. In general, while this thesis has shown that Sentinel-2 data are best suited to studying land use in winter, SAR images are of great interest in regions with significant cloud cover, dense Sentinel-1 time-series having been defined as the most efficient.